Optimal Coordination of Chassis Systems for Vehicle Motion Control

Moad Kissai

université PARIS-SACLAY

NNT : 2019SACLY004

Thèse de doctorat

OPTIMAL COORDINATION OF CHASSIS SYSTEMS FOR VEHICLE MOTION CONTROL

Thèse de doctorat de l'Université Paris-Saclay
préparée à l'École Nationale Supérieure de Techniques Avancées
et au Groupe Renault

École doctorale n°573 INTERFACES (EDI)
Spécialité de doctorat: Automatique

Thèse présentée et soutenue à Palaiseau, le 17/06/2019, par

MOAD KISSAI

Composition du Jury :

Tarek Raïssi Professeur, Conservatoire National des Arts et Métiers (Cedric-Lab)	Président
Valentin Ivanov Privatdozent, Technische Universität Ilmenau (Department of Mechanical Engineering)	Rapporteur
Olivier Sename Professeur, Institut polytechnique de Grenoble - Grenoble INP (GIPSA-lab)	Rapporteur
Barys Shyrokau Professeur Assistant, Delft University of Technology (Intelligent Vehicles Group - Department of Cognitive Robotics)	Examinateur
Bruno Monsuez Professeur, ENSTA ParisTech (U2IS)	Directeur de thèse
Adriana Tapus Professeur, ENSTA ParisTech (U2IS)	Co-directrice de thèse
Xavier Mouton Docteur, Renault (Systèmes Châssis)	Invité
Didier Martinez Docteur, Renault (Systèmes Châssis)	Invité

Declaration of Authorship

I, Moad KISSAI, declare that this thesis titled, “OPTIMAL COORDINATION OF CHASSIS SYSTEMS FOR VEHICLE MOTION CONTROL” and the work presented in it are my own. I confirm that:

- This work was done wholly or mainly while in candidature for a research degree at this University.
- Where any part of this thesis has previously been submitted for a degree or any other qualification at this University or any other institution, this has been clearly stated.
- Where I have consulted the published work of others, this is always clearly attributed.
- Where I have quoted from the work of others, the source is always given. With the exception of such quotations, this thesis is entirely my own work.
- I have acknowledged all main sources of help.
- Where the thesis is based on work done by myself jointly with others, I have made clear exactly what was done by others and what I have contributed myself.

Signed:

Date:

"*We cannot solve our problems with the same thinking we used when we created them.*"

Albert Einstein

Acknowledgements

The work presented in this thesis would not have been possible without the close collaboration of many people.

I would like to express my deep gratitude to my research guide, my main research supervisor, Professor Bruno Monsuez, for his patient guidance, enthusiastic encouragement and useful critiques of this research work. I have learnt extensively from him, including how to explore new possibilities, how to change the problem perspective and how to approach it methodically.

My special words of thanks should also go to Professor Adriana Tapus, my second research supervisor, for her valuable and constructive suggestions during the planning and development of every research paper and every step of this work. Her willingness to give her time so generously has been very much appreciated.

My heartfelt thanks to Dr. Xavier Mouton, for believing in my ideas and his assistance for pushing the envelope within the teams of Renault while keeping our ego in check. He has been a great mentor these past years.

My grateful thanks go also to Dr. Didier Martinez for his priceless tips in control engineering, and for his help in carrying the experimentations and data post-processing and analysis.

I would also like to extend my thanks to every member of the chassis systems department of Renault for their help in offering the necessary resources in pursuing this research.

I gratefully acknowledge the Group Renault for providing the financial support for this work.

My warmest thanks go to my uncle Abdelbasset and his wife Zakia for keeping the family ties tight and attending every big event despite their busy schedule.

A special thanks to my source of joy, my younger brother that knows always how to put a smile on my face.

Last, but by no means least, I wish to thank my parents for their encouragement throughout my study. Their unconditional moral support helped me to stay always positive and motivated.

Contents

List of Figures

List of Tables

List of Abbreviations

4WD	4-Wheel Drive
4WS	4-Wheel Steering
ABS	Anti-lock Braking System
ACC	Active Cruise Control
ADAS	Advanced Driver Assistance Systems
ADS	Active Differential System
AFS	Active Front Steering
AI	Artificial Intelligence
APF	Auxiliary Particle Filter
ARC	Active Roll Control
ARS	Active Rear Steering
AS	Adaptive Suspension
ASA	Active Set Algorithms
CA	Control Allocation
CAN	Controller Area Network
CGI	Cascading Generalized Inverses
CoG	Center of Gravity
DOF	Degrees Of Freedom
DYC	Dynamic Yaw Control
ECUs	Electronic Control Units
EPAS	Electric Power-Assisted Steering
ESP	Electronic Stability Program
FEM	Finite Element Methods
FPI	Fixed-Point Iteration
GCC	Global Chassis Control
HIL	Hardware-In-the-Loop
ICC	Integrated Chassis Control
IEKF	Iterated Extended Kalman Filter
IP	Interior Point
IPR	Intellectual Property Rights
LIDAR	Laser Imaging Detection And Ranging
LMI	Linear Matrix Inequality
LP	Linear Programming
LPV	Linear with Parameters Varying
MBD	Model Based Design
MIMO	Multi-Inputs Multi-Outputs
MPC	Model Predictive Control
OEMs	Original Equipment Manufacturers
PID	Proportional-Integral-Derivative
QP	Quadratic Programming
RADAR	RAdio Detection And Ranging
RGA	Relative Gain Array
RMSE	Root Mean Squared Error

RTV	Rear Torque Vectoring
SAS	Semi-Active Suspension
SBW	Steer-By-Wire
SISO	Single-Input Single-Output
SLS	Sequential Least Squares
SMC	Sliding Mode Control
SQP	Sequential Quadratic Programming
TV	Torque Vectoring
VDC	Vehicle Dynamics Control
WLS	Weighted Least Squares
WPI	Weighted Pseudo-Inverse

List of Symbols

α	the side-slip
α_f	front equivalent side-slip
α_r	rear equivalent side-slip
β	side-slip angle of the vehicle
Γ	the general acceleration
δ	the general dynamic moment
δ_f	front wheel angle
δ_r	rear wheel angle
ϵ	tracking error
ζ	the damping ratio of the vehicle
θ	pitch angle of the sprung mass
κ	longitudinal slip
μ	resulting friction coefficient
μ_k	kinetic friction coefficient
μ_s	static friction coefficient
μ_x	longitudinal friction coefficient
μ_y	lateral friction coefficient
σ	the general angular moment
Σ	the overall vehicle system
σ_0	rubber longitudinal lumped stiffness (LuGre's parameter)
σ_1	rubber longitudinal lumped damping (LuGre's parameter)
σ_2	viscous relative damping (LuGre's parameter)
σ_x	theoretical longitudinal slip
σ_y	theoretical lateral slip
ϕ	roll angle of the sprung mass
ψ	yaw angle of the vehicle
ω	wheel's angular velocity
Ω_c	the overall vehicle's angular velocity
ω_n	the natural frequency of the vehicle
a_x	longitudinal acceleration of the vehicle
a_y	lateral acceleration of the vehicle
$\mathbf{B}$	control effectiveness matrix
$\mathbf{B}^\sharp$	pseudo inverse of $\mathbf{B}$
B	stiffness factor (Pacejka's parameter)
C	shape factor (Pacejka's parameter)
C_α	cornering stiffness of the tire
C_α^*	tire varying cornering stiffness with respect to κ, μ, and the vertical load F_z
c_p	tread element stiffness
C_s	longitudinal stiffness of the tire
C_s^*	tire varying longitudinal stiffness with respect to α, μ, and F_z
C_{s_p}	equivalent overall pitch suspension damping
C_{s_r}	equivalent overall roll suspension damping

$c_{s_{i,j}}$	suspension's damping
D	peak value (Pacejka's parameter)
E	curvature factor (Pacejka's parameter)
$F_{i_{tot}}$	combination of tire forces projected at the axis "i"
$F_{x_{i,j}}$	$i-j$ longitudinal tire force Where "i" is front or rear, and "j" is right or left
$F_{y_{i,j}}$	$i-j$ lateral tire force
F_{y_f}	equivalent lateral force at the front axle
F_{y_r}	equivalent lateral force at the rear axle
$F_{z_{i,j}}$	vertical load on the $i-j$ tire
g	standard gravity
G	Center of Gravity of the overall vehicle
G_s	Center of Gravity of the sprung mass
G_{uf}	Center of Gravity of the front unsprung mass of a mass
G_{ur}	Center of Gravity of the rear unsprung mass
h_f	the vertical distances between O and G
h_g	the horizontal distance between O and G
h_G	height of the Center of Gravity (CoG) with respect to the ground
h_O	height of the center of the roll/pitch axis
h_s	the vertical distance between G_s and O
I_{i_k}	inertia moment in the direction i of the mass S_k with respect to its CoG
I_{ij_k}	inertia moment in the plan ij of the mass S_k with respect to its CoG
I_{uf}	the inertia tonsor of the mass S_{uf}
$I_{x_{uf}}$	the inertia moment in the longitudinal direction with respect to G_{uf}
$I_{y_{uf}}$	the inertia moment in the lateral direction with respect to G_{uf}
$I_{z_{uf}}$	the inertia moment in the vertical direction with respect to G_{uf}
I_z	yaw inertia moment of the overall vehicle with respect to its CoG
K	controller
k_{ϕ_f}	the front anti-roll bar stiffness
k_{ϕ_r}	the rear anti-roll bar stiffness
K_p	equivalent overall pitch suspension stiffness
K_r	equivalent overall antiroll bar stiffness
$k_{s_{i,j}}$	suspension's stiffness
L	vehicle's wheelbase
l_f	distance between the front axle and the vehicle's center of gravity
l_r	distance between the rear axle and the vehicle's center of gravity
l_s	the horizontal distance between G_s and O
O	the roll center of the vehicle
M	mass of the overall vehicle
$M_{i_{tot}}$	combination of moments generated by tire forces with respect to the axis "i"
M_s	mass of the sprung mass
M_{uf}	mass of the front unsprung mass
M_{ur}	mass of the rear unsprung mass
M_{vdc}	yaw moment generated by the VDC system
$\sum M_z$	self-aligning moments of the tires
q_z	distribution of the vertical load
R	wheel's dynamic radius
$\mathcal{R}_c$	the vehicle's body frame
$\mathcal{R}_g$	the inertial frame of reference
s	Laplace operator
S_H	horizontal shift (Pacejka's parameter)

S_s	the sprung mass
S_{uf}	the front unsprung mass
S_{ur}	the rear unsprung mass
S_V	vertical shift (Pacejka's parameter)
t	vehicle's track in case of $t_f = t_r$
T_b	brake torque
T_d	driving torque
t_f	front rear track of the vehicle
t_r	rear track of the vehicle
$u_{s_{i,j}}$	control forces of the active suspensions
V	vehicle's resulting speed
v_s	sliding speed
v_{st}	stribeck velocity
v_{wx}	the longitudinal component of the tire velocity at the tire/road interface
v_{wy}	the lateral component of the tire velocity at the tire/road interface
V_x	longitudinal velocity of the vehicle
V_y	lateral velocity of the vehicle
V_z	vertical velocity of the sprung mass
$\mathbf{W_u}$	non-singular weighting matrix affecting control distribution among the actuators
$\mathbf{W_v}$	non-singular weighting matrix affecting the prioritization among the virtual control components
$x_{r_{i,j}}$	vertical profile of the road
$x_{s_{i,j}}$	vertical travel of suspensions
$x_{t_{i,j}}$	vertical travel of tires
z	vertical travel of the sprung mass

To my life-coaches, my role models, my both late grandfathers.

1 General Introduction

In today's automotive sector, driving experience, vehicle safety, and environmental protection are key competitive criteria. Original Equipment Manufacturers (OEMs) propose constantly new attractive subsystems to stand out from their competitors. Recently, a large interest has been given, to autonomous vehicles in particular. These vehicles are gathering different stakeholders that were formerly far from mobility problems. Automation promises indeed safer and smarter vehicles. Several researches has been carried out in robotic vision, sensor fusion, decision algorithms, big data management, and others. However, a full autonomous vehicle requires the ability to make its own decision like a human would do. Car manufacturers, taxi companies, and car-sharing services rely on Artificial Intelligence (AI) to overcome this complexity. The main philosophy is saying that most of accidents are caused by human factors, such as the lack of attention or fatigue of the driver, so we should replace this driver by an intelligence that is tireless and always attentive. The problem is that validating a complex autonomous system accurately and efficiently is non-trivial (due to the large number of internal and external, predictable and unpredictable parameters). Any visual perception system based on machine learning cannot be 100 % accurate (Shi et al., 2017). Hence, the system may fail for a specific input pattern and accurately estimating its failure rate can be extremely time-consuming (Shi et al., 2016). One can affirm in this case that the AI will not be necessarily better than humans are, and could induce accidents that humans could have avoided.

A complementary solution that car manufacturers are working on is the over-actuation of the vehicle itself (Shyrokau and Wang, 2012) (Soltani, 2014), (Bhat, 2016). Giving the vehicle new features such as the ability of steering the rear wheels (Yim, S., 2015), distributing the brake torques or/and the engine torques differently between left and right tires (Siampis, Massaro, and Velenis, 2013) and so on, can expand the vehicle's performance and generate new motion possibilities and car behaviors. As soon as the vehicle is "aware" of its environment and a trajectory is planned, chassis systems should be actuated in a way to ensure reference[1] tracking with the desired behavior dynamics. To do so, the vehicle has in fact more than one subsystem per control axis (Soltani, 2014). These subsystems cannot be controlled by the human driver directly. Therefore, an over-actuated vehicle that can control each one of its subsystems in harmony may exceed the human driver capabilities (Kuisma, 2001).

In addition, advances in Electronic Control Units (ECUs) make the cost of vehicle embedded systems constantly decreasing. Subsequently, the number of chassis systems and Advanced Driver Assistance Systems (ADAS) implemented within a single vehicle grows rapidly (Heißing and Ersoy, 2011). These embedded systems may influence differently the same physical variable of the vehicle to be controlled. For example, an Electronic Stability Program (ESP) (Liebemann et al., 2004) generating a yaw moment through differential braking in emergency situations acts on the vehicle's yaw rate. At the same time, the Electric Power-Assisted Steering (EPAS)

[1] Here, it is the trajectory planned.

that generates an additional torque at the steering column to help the driver steer (Soltani, 2014), also influence the vehicle's yaw rate. In this simple situation, one can suggest that each system should be activated in a specific scenario. The ESP can be only activated in emergency situations, shutting down the EPAS assist. The EPAS should be always activated in the rest of the situations, without the ESP being involved. First of all, this limits the potential of the vehicle as only one system is activated at a time, and therefore, the vehicle would not cope with specific situations that might be handled if both systems are superposed. Secondly, this strategy can be only conceivable if few subsystems are involved. According to the growing number of embedded systems into a single passenger car, we believe that the over-actuation problem should be tackled differently.

The over-actuation problem exists already in today's passenger cars. Ground vehicles integrate more than a single chassis system (Soltani, 2014). Because these subsystems act on the same vehicle, interactions arise. The complexity of these interactions increases as the number of subsystems increases. We can already see the difficulties that this would induce regarding autonomous vehicles. These vehicles require a large amount of subsystems to operate at the same time. Conflicts would be more numerous and more complex to handle, and it would be hard for automotive engineers to foresee all the possible scenarios. The problem is that each vehicle subsystem comes from a different supplier and therefore has an independent control logic in order to satisfy a specific objective. Due to financial competition matters, car manufacturers tend to vary their suppliers to ride shotgun on the automotive market. Unfortunately, in this case, the objectives intended to be fulfilled by each subsystem might compete and induce contradictory logic: if a braking-based yaw control is used to reduce over-steer or under-steer, the longitudinal acceleration demand in a cornering operation will deteriorate. Rather than feeling supported, the driver might get the feeling of being under-ruled.

Since implementing a new hardware is always expensive, improvements must be provided by the synergies that already exist between subsystems (Coelingh, Chaumette, and Andersson, 2002). If instead of implementing competing systems, subsystems get coordinated, over-actuation would offer new opportunities to improve the overall system's safety and performance (Zhang and Jiang, 2008). This could be done by developing a supervised global chassis control system, where information is shared by many subsystems. In this case, less resources are required, and computational costs are decreased avoiding unnecessary duplication (Coelingh, Chaumette, and Andersson, 2002), and achieving what is commonly known as *interoperability* (Gordon, Howell, and Brandao, 2003). Since this will influence the vehicle's overall behavior, the high-level control architecture should be designed by car manufacturers. And as long as different suppliers are concerned, a standardization of actuators, sensors, and software components interfaces is crucial. The development of this architecture requires a close collaboration between vehicle manufacturers and their suppliers. Any proposed solution should respect the Intellectual Property Rights (IPR) of both sides (Navet and Simonot-Lion, 2008).

Aside from the performance and safety improvement, the coordination of several systems may lead to the use of the same sensors, a central ECU and so on (Selby, 2003). An obvious example is the integration of the 4WS and the ESP. Both system can control the yaw rate of the vehicle, and therefore, both of them need the yaw rate response signal. Implementing these systems separately may lead to a duplication of sensors increasing the cost of the overall system. For good measure, when the systems integrated influence the same physical variable, a degree of tuning is provided through software (Selby, 2003). The same car may therefore perform more

comfortable riding behavior, or in contrast, a sporty setting. A coordinated chassis can then reach a broader range of people and a larger market.

1.1 Research purposes

The main purpose of this work is to propose a new classification of integrated control architectures, compare them in order to speculate about what would be the best coordination approach for future vehicles, and propose the necessary guidelines to develop it. We expect to sensitize the different stakeholders about the necessity of reinventing the chassis systems coordination architecture. This would have a large impact on the way car manufacturers collaborate with their suppliers. Indeed, changing the position of the different subsystems in the control architecture would have a direct influence on the inputs/outputs of each subsystem. New constraints are to be expected for controllers design. This would not be the first try, as in (Gordon, Howell, and Brandao, 2003) a classification of integrated control methodologies for road vehicles has been proposed. The architectures have been differentiated as *centralized*, *supervisory*, *hierarchical*, and *coordinated control*. However, no discussion is provided so as to assign an architecture to a specific goal. Another recent classification was proposed by (Ivanov and Savitski, 2015), where the classification has been simplified to affect the architectures to the desired goals. Two classes were proposed: *single-criterion* and *multi-criterion* integration motion control. In the single-criterion integration motion control approach, the integrated systems are combined to improve one single aspect of the vehicle. In the multi-criterion integration motion control approach, the combined systems aim to manage different concurrent vehicle dynamics. However, for each class, we can find different combination methodologies depending on the problem's complexity.

The new classification should enable a fast positioning for car manufacturers to adopt a specific approach. In addition, the comparison of the different approaches should make possible speculations about the right architecture to be adopted by future vehicles, and provide few guidelines regarding its development. More specifically, the new architecture should be (Kissai, Monsuez, and Tapus, 2017):

- *adaptive* to face environmental changes and drivers' preferences,
- *fault-tolerant* and propose some degraded modes to best achieve control objectives even in case of one or more actuators failures,
- *reconfigurable* to provide a soft transition from one set of available actuators to another configuration without penalizing the vehicle's stability,
- *flexible* so the control architecture would not be specific to any control design method,
- *extensible* to incorporate rapidly new systems and technologies without redesigning the overall architecture,
- *modular* so each component of the architecture can be developed independently and rapidly,
- and offer some degree of *openness* to support different control logics without jeopardizing the intellectual property rights of the different automotive stakeholders.

Car stakeholders should then show some flexibility in sharing their products to accelerate autonomous vehicles development. Consequently, there is a huge need for standardization and benchmarking of this type of architectures.

We expect that by coordinating integrated automotive systems, we can improve the vehicle handling, maneuverability, and stability, especially through optimum utilization of each subsystem. The goal is then to develop different coordinated control architectures, for different systems combination in order to compare them. That is to say that we want to prove that a modular coordinated control architecture do not depend on a specific combination of systems but can be easily broaden to a large set of chassis systems and ADAS.

This should come with the satisfaction of specific objectives. Mainly, we focus on the vehicle's safety, performance and passenger's comfort. As in some cases not all the objectives can be satisfied at the same time, one objective should be prioritized over another and the control strategy should at least satisfy the most prior objective. For example, an ideal situation would be a vehicle operating in a safe and comfortable manner. The vehicle should detect fast enough a pedestrian crossing the road for example, decelerate slowly without inducing any discomfort, until complete stoppage if necessary. However, in some unpredictable situations, like a falling package from a truck in front of the ego-vehicle, the latter should steer as quickly as possible to avoid the obstacle. Comfort in this case may be sacrificed in order to ensure passengers' safety. Moreover, this control strategy should be executable in real-time with low computational cost. One of our goals is also to implement successfully the control logic in a real vehicle.

Many coordination architectures have been proposed in the literature without a clear justification of their choice. To the best of our knowledge, this is mainly due to the fact that no references, standards or benchmarks exist to lead automotive engineers to favor one strategy over another. That is why this thesis will focus on first defining different approaches to tackle the problem of system coordination, and then detail the development of the most suitable one for future vehicles.

1.2 Research Contribution

A main difference if not the main difference that we distinguished from the different architectures reviewed, is the position of the coordination layer in the control flow. Two main approaches could be adopted to deal with subsystems combination problem: The first one consists in treating the interactions and the eventual conflicts after the subsystems' operations. The idea of the second one is to control the commands distribution to the different subsystems before their operations in order to generate the desired synergies and avoid conflicts. We call the first approach *systems downstream coordination*, and the second, *systems upstream coordination*. Both approaches have been developed and compared through different embedded systems combinations. Our research enabled us to evaluate the pros and cons of each approach and their relevance for future vehicles. This thesis questions the current coordination approach to face future challenges of over-actuated vehicles. The simplicity of today's approaches comes with a lack of potential to solve problems that are more complex. An alternative approach is then developed and detailed to serve as a reference to be followed by automotive control engineers in the future. The contributions of this research can be summarized in the following:

1. Classifying integrated vehicle dynamics control into only two main categories,

2. Giving the general guidelines of the downstream approach development adopted by industrials nowadays,
3. Proposing a structured development of the future multi-layered upstream approach that should be adopted by car manufacturers,
4. Development of a new linear tire model with varying parameters to take into account the combined slip phenomenon in the control synthesis stage,
5. Development of a general yet simple full-body vehicle model that can be used for high-level global chassis control design,
6. Proposing a simple new method to estimate the friction coefficient,
7. Adaptation of both approaches into different systems combination to give few insights about the strength and performance of every approach in the context of practical applications,
8. Comparison of both approaches by co-simulation procedure for more realistic results,
9. Utilization of the optimization-based Control Allocation (CA) algorithms for fault-tolerance features to show the benefits in the safety context,
10. Utilization of qualitative objectives in the CA scheme in order to improve the passengers' comfort,
11. Primary in-vehicle experimentation of both architectures to give an idea about the real world challenges.

1.3 Development process

The development of both architecture are based on the well-accepted "V" development process. This approach is well-accepted for mechatronic systems development although it originates from system engineering and software development (Soltani, 2014). This method consists of feedback steps starting from requirement definition and ending up with in-vehicle validation. As the control architecture differs from a coordination approach to another, the "V" development process slightly differs to fit every architecture requirements. This is detailed in Part III where we expose the development of each architecture in different scenarios. We recall the general concept of the "V" development process in Figure 1.1 (Holtmann, Meyer, and Meyer, 2011).

As the Figure 1.1 shows, the system should be decomposed before its implementation. This goes along the same line as developing a modular architecture. In this research, two different architectures are developed to compare between a downstream coordination approach and an upstream one. At the design stage, several methodologies can be adopted. Here, a Model Based Design (MBD) methodology is selected as it has proven its effectiveness along with the "V" development process in control system development (Nicolescu and Mosterman, 2010). Even if both approaches differ at the architectural level, the main steps remain:

- System Modeling: here the physical representations of the system dynamics are mathematically described. This a the key step in an MBD design methodology due to the fact that the control logic developed is closely related to the model itself,

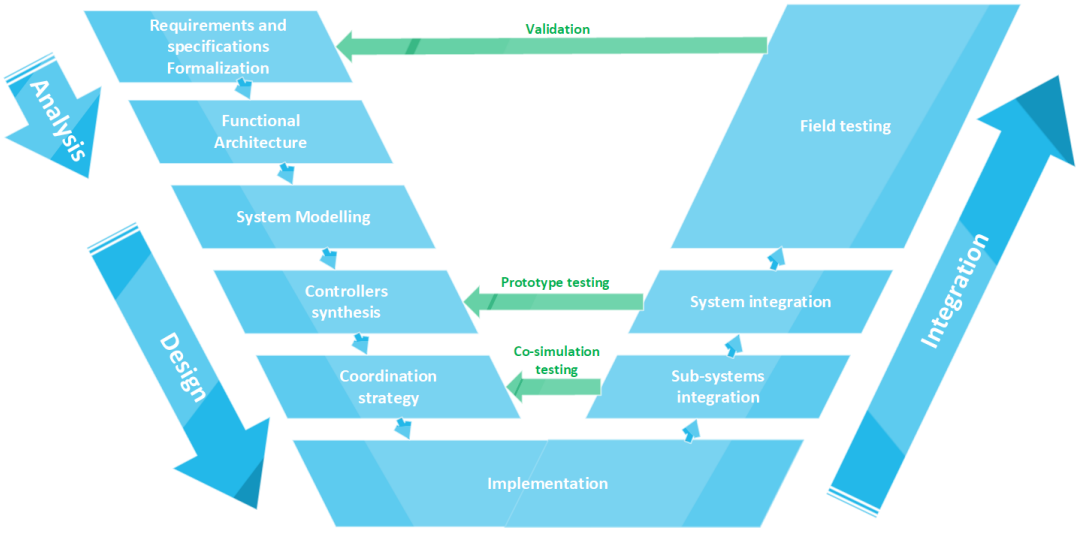

FIGURE 1.1: V-model for over-actuated control system design.

- Controllers Synthesis: here the different algorithms required to control the vehicle dynamics are developed based on the system modeling,
- Coordination Strategy Development: as the overall system is over-actuated, coordination between subsystems should be ensured in order to satisfy the high-level requirements. This is done differently depending on the approach adopted.

After the design step, the overall architecture should be implemented in such a way to be executed in real-time. Several requirements at the software level should be fulfilled. The global system can be integrated within the vehicle for field testing afterwards. The "V" development process goes in several loops as the Figure 1.1 shows. That means that in the ascending part of the V cycle, we do not proceed to the next step unless we validate the needs of the corresponding bloc at the descending part. This dissertation follows this development process for both approaches.

1.4 Dissertation Outline

In order to bring the necessary answers for the issues listed above, this thesis is arranged as follows:

- **Part I** presents the current approach adopted by most of car manufacturers today.
  - **Chapter 2** gives first a global state of art about coordination strategies and modeling limitations that led to specific control synthesis choices.
  - **Chapter 3** presents the downstream coordination approach. The control architecture is illustrated, the vehicle modeling usually used in this approach is described, and the control synthesis is outlined.
- **Part II** introduces our proposal regarding chassis systems coordination: the upstream approach.
  - **Chapter 4** details the control architecture that should be adopted.

  - **Chapter 5** exposes our development of a global vehicle model.
  - **Chapter 6** gives an overview on tire modeling and shed light on the need of a new tire model, especially when several subsystems are activated at the same time.
  - **Chapter 7** proposes a simple method of estimating the necessary states needed for friction circle estimation.
  - **Chapter 8** gives general guidelines on the robust controllers synthesis procedure adopted in this thesis.
  - **Chapter 9** explains the main concept of the upstream approach: CA.

- In **Part III** several systems combination examples are exposed where both approaches are applied and compared.

  - **Chapter 10** presents the case of the integration of both the 4WS system and the VDC system.
  - **Chapter 11** documents the development of the integration of the 4WS system, the VDC system and a Rear Torque Vectoring (RTV) system. Here, focus is put more on the ability of the upstream distribution approach to handle such a complex system. Additional features as friction estimation are tested through co-simulation in this chapter.
  - **Chapter 12** details the design of a 4-Wheel Drive (4WD) system with Torque Vectoring capabilities as well as VDC in an autonomous driving context. More importantly, we show how the upstream approach can be beneficial for future autonomous vehicles using qualitative objectives.
  - **Chapter 13** describes few experimental results in case of the implementation of both of the already available 4WS and VDC systems in Renault's cars.

- **Chapter 14** summarizes the benefits of each approach. We specifically speculate about the relevance of optimal CA for future over-actuated vehicles.

- **Chapter 15** presents an overview of this work and identifies the key conclusions to be drawn. Based on the outcomes of this thesis, future areas of research are highlighted at the end.

Part I

THE CURRENT APPROACH

Before getting into the heart of this thesis, we will first look at the current approach and see why it was adopted until these days. As mentioned before, today's vehicles are already over-actuated. While a single passenger car may incorporate several embedded systems, few of them can act on the same physical variable. In the example of the integration of both the 4WS system and the VDC system, which is the case of the prototype presented in Chapter 13, both systems can influence the vehicle's yaw rate. Without any planned coordination strategy, conflicts may arise and jeopardize the stability of the vehicle and the safety of the passengers.

Nevertheless, chassis systems can be very different. In the case of the 4WS-VDC integration, the first system is based on the lateral force of tires while the second is based on the longitudinal force of tires using the vehicle's brakes. The 4WS enables steering the rear wheels and acts directly on the lateral motion of the car. The VDC creates a yaw moment through a differential braking between right and left tires. This influence not only the yaw rate of the vehicle but also its longitudinal speed. The two systems can then be activated in different situations to satisfy different requirements. For example, the 4WS can be activated in a comfort mode to make the vehicle more maneuverable, and the VDC can be activated only in emergency situations as obstacle avoidance where the vehicle needs also to decelerate in order to stay controllable.

These rule-based strategies can be very simple to develop without generating any large additional costs. This is very attractive from an industrial point of view, which probably was the reason behind adopting it in most passenger cars. In this part, we describe a state-of-the-art not only of the coordination strategies but also of the modeling and the simplifications adopted in order to design rapidly the current control approach. We after give the general guidelines of developing this approach from the general architecture to the control synthesis.

2 State of Art

For ground vehicles, safety is not the only concern. Passenger cars have always been subject to people's fascination. From the very beginning, passenger cars were not considered as only a transportation device, but also an object of luxury and pleasure. Car manufacturers and equipment suppliers are always racing to propose new technologies in order to improve the cars' performances while keeping an acceptable level of safety. This competition is about to become fiercer with the upcoming autonomous vehicles. Not only every car manufacturer and every equipment supplier is working on this new generation of passenger cars, but also additional stakeholders are taking part in the race. This is mainly due to the fact that autonomous vehicles would require additional knowledge as artificial intelligence, sensor fusion, cyber-security, and so on, which was not included in the know-how of the automotive industry. Several experimental researches are published in the literature showing that these advanced vehicles are close than never to invade public roads.

The development of chassis systems has been ongoing since the late 1970's (Selby, 2003). Before the 1970's, passive safety systems were sufficient to ensure passengers' security. With the increasing number of vehicles on the roads, more complex situations have arisen. Active systems made their entry into the automotive market to help the driver control its vehicle when these complex situations are encountered. These situations are the main reason of fatal accidents and a significant number of them can be avoided thanks to active safety systems (Liebemann et al., 2004). An overview of the ADAS proposed in the last three decades is shown in Figure 2.1.

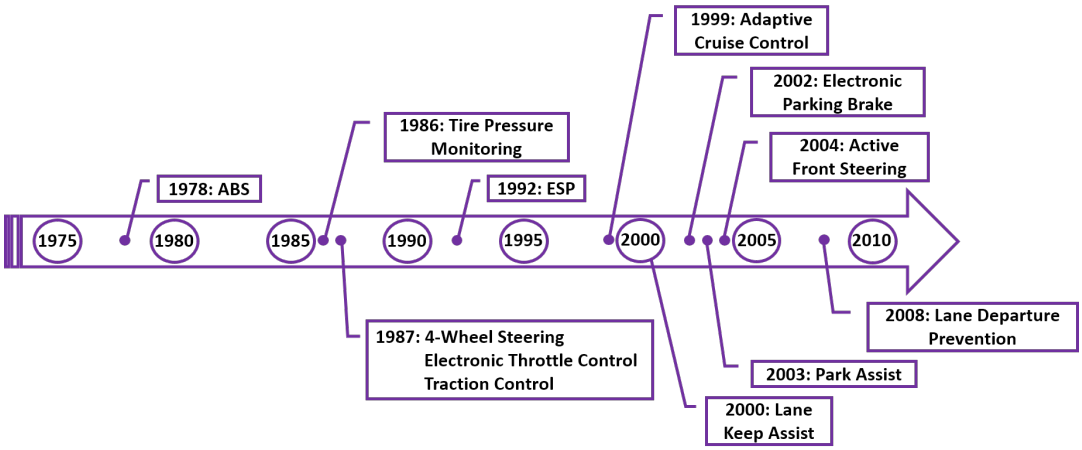

FIGURE 2.1: Time-line of active safety systems introduction in passenger cars (Gerard, 2011).

Active systems have been introduced gradually as a luxury option to become a standard in all passenger cars. A fully autonomous system is thus a natural evolution towards safer and more comfortable vehicles. At first, systems based on longitudinal tire forces were used for vehicle's longitudinal control, and systems based on lateral

tire forces were used for vehicle's lateral control. It started with the Anti-lock Braking System (ABS) in 1978 (Gerard, 2011). This system consists of relaxing the brakes to retrieve adherence capabilities and then braking again to decelerate the vehicle. The major goal of ABS was to reduce the distance of braking for better longitudinal control. With the appearance of systems such as the ESP (Liebemann et al., 2004), the previous approach was no longer valid. This system consists of a differential braking between right and left tires to provide a yaw moment and control the yaw rate. This is also the case for any system that uses different right longitudinal tire forces than left ones as the Torque Vectoring (TV) system (Velardocchia, 2013). In other words, systems based on longitudinal tire forces can be used for vehicle lateral control. When several subsystems control the same physical quantity, the overall system becomes over-actuated. If no coordination is ensured, conflicts may occur causing the vehicle's loss of control. In Figure 2.1, we can also see that the integrated systems are designed for single-objective performances. For example, the ESP uses the brake to generate a yaw moment and stabilize the vehicle (Liebemann et al., 2004), Active Cruise Control (ACC) controls the throttle to keep regulatory safe distance between vehicles (Moon, Moon, and Yi, 2009), EPAS generates an additional torque at the steering column to help the driver steer (Soltani, 2014) and so on. This is about to change with the arrival of autonomous vehicles. The virtual pilot has to handle combined operations. For example, let us consider the high speed cornering maneuver. In the present situation, the human pilot controls the longitudinal motion, and unconsciously, its interaction with the lateral motion. Active steering systems (for example the 4WS system (Brennan and Alleyne, 2001)) or, in hazardous situations, brake-based yaw control systems (for example the ESP (Velardocchia, 2013)) control the lateral dynamics to ensure the vehicle stability. In contrast, the virtual pilot has to handle multi-objective control problems. Both longitudinal and lateral motions should be controlled at the same time. The dynamic couplings between these physical variables should be taken into account.

2.1 Coordination Strategies

In the coordination context, one common industrial practice is to study the influence of each subsystem on the overall vehicle off-line, then to develop rule-based algorithms to prioritize the most influencing subsystem or the least consuming one depending on the prior objective (Selby, 2003), (Ivanov and Savitski, 2015), (Kissai, Monsuez, and Tapus, 2017). This requires a deep understanding and an expert knowledge on vehicle dynamics to predict the influence of each actuator over an another, and foresee the possible conflicts. For example, the work in (Velardocchia, 2013) used Active Differential System (ADS), ESP, and TV to improve the vehicle lateral performances. A simple method based on prioritizing one system over another has been used. A more complex method based on *Artificial Neural Network* had been adopted in (Nwagboso, Ouyang, and Morgan, 2002). This method consists of simple averaging via non-linear interpolation function weights. These functions could be chosen to ensure smooth transitions between coordination modes. A larger review can be found in (Kissai, Monsuez, and Tapus, 2017).

These rules or prioritizing strategies are based on a deep understanding of the vehicle dynamics. The automotive engineer has to foresee the possible conflicting scenarios, and then elaborate strategies to overcome them. Over the years, car manufacturers have in fact developed an expertise and a certain know-how that allow them to counter some hazardous situations. As long as a low number of chassis

systems is concerned, rule-based approaches might be sufficient to handle most conflicting situations (Selby, 2003). However, the more we get closer to autonomous driving, the more chassis systems are added, the higher the complexity gets. As broad as an expert knowledge could be, it cannot foresee all the possible situations. Automotive engineers can only hope to avoid the scenarios imagined in pre-studies. As long as optimization is not explicitly formalized, we cannot prove that any rule-based approach is the best existing solution. That is why most of the time only a single objective is targeted (Ivanov and Savitski, 2015). Using only a limited amount of subsystems in a rule-based approach, or in some cases, prioritize one system over another, limit the potential of the overall vehicle. Conflicted scenarios that could be avoided might happen and objectives that could be fulfilled might be abandoned. Since the vehicle is over-actuated, secondary objectives could be achieved. Control objectives should be then mathematically formalized to enable optimization of chassis systems coordination. A search for an optimal solution, or at least a sub-optimal one, should be carried out to ensure a "state of play" of existing solutions, and whether or not an additional subsystem is needed to ensure specific performances. This can only be ensured if we act differently on the subsystems references. Interactions should be mathematically formalized and managed before allocating the commands. Because of the over-actuation, the system of equations to be solved has more unknowns than equations. To top it all off, each actuator has its own position and speed limits. Command vectors are then constrained. This problem has been already encountered in flight-control systems. While ganging has been used in many of these systems, optimization-based methods have become necessary regarding advanced aircraft with more numerous actuators (Bodson, 2002). This is called *the CA problem*. In an over-actuation context, where various solutions can be found and secondary objectives can be fulfilled, not only conflicts could be handled, but also better performances could be achieved and secondary objectives can be fulfilled. Unlike a rule-based approach, the conflicts here are prevented rather than mitigated.

In the automotive sector, optimization methods are considered too complex and too time-consuming to be implemented in a passenger car (Ivanov and Savitski, 2015). Yet, dramatic increases in computing speed and algorithms efficiency have been elaborated. We believe that it is high time for optimization-based methods to be implemented in passenger cars. Better solutions can be provided, secondary objectives can be ensured, and the overall performance can be enhanced.

In addition, in the CA framework, fault-tolerance is naturally managed and reconfiguration strategies are softer (Johansen and Fossen, 2013). These characteristics constitute a major aspect for autonomous vehicles' safety. In this context, the common industrial practice is making critical safety systems redundant. In (Anwar and Chen, 2007) a redundancy-based fault detection and isolation regarding the Steer-By-Wire (SBW) system has been proposed. The goal was to reduce the total number of redundant road-wheel angle sensors while maintaining a high level of reliability. Authors of (Bishop and Spong, 1998) used a switched control scheme in order to control redundant planar robotic manipulators. An example has also been given in (Zhang and Jiang, 2008) to demonstrate the effectiveness of a fault-tolerant control against partial actuator failures. However, several expensive systems cannot be redundant in commercial ground vehicles. As different systems can influence the same physical quantity in an over-actuation context, we should take benefit from the existing synergies between different chassis systems (Coelingh, Chaumette, and Andersson, 2002). This can ensure some sort of complementarity between systems with different natures. So if a system fails, another completely different system can

take over. Techniques used to solve the redundancy problem can be used to solve over-actuation problems. But caution should be taken in the control technique to employ, as in this case, the control should switch from a system with a given behavior to another one with a different behavior. For this reason, CA methods are more relevant, as contrary to the existing reconfiguration methods that modify controllers to tolerate faults, CA methods only change allocation laws. On one hand, this is advantageous in a way that allocation laws take account of systems with different natures, and on the other hand, stability of the closed-loop system after reconfiguration is guaranteed (Yang, Kim, and Lee, 2010).

2.2 Tire Couplings

As far as combined maneuvers are concerned, dynamic couplings should be taken into consideration. Since the tire is the only effector between the vehicle and the road (Soltani, 2014), one of the most important couplings is the combined slip. Several accidents are triggered by a poor managing of tire forces. A more precise tire model is needed for an effective coordination of chassis systems. In this context, two major approaches are adopted: empirical methods or theoretical methods. Figure 2.2 depicts the various differences between the two approaches (Pacejka, 2005).

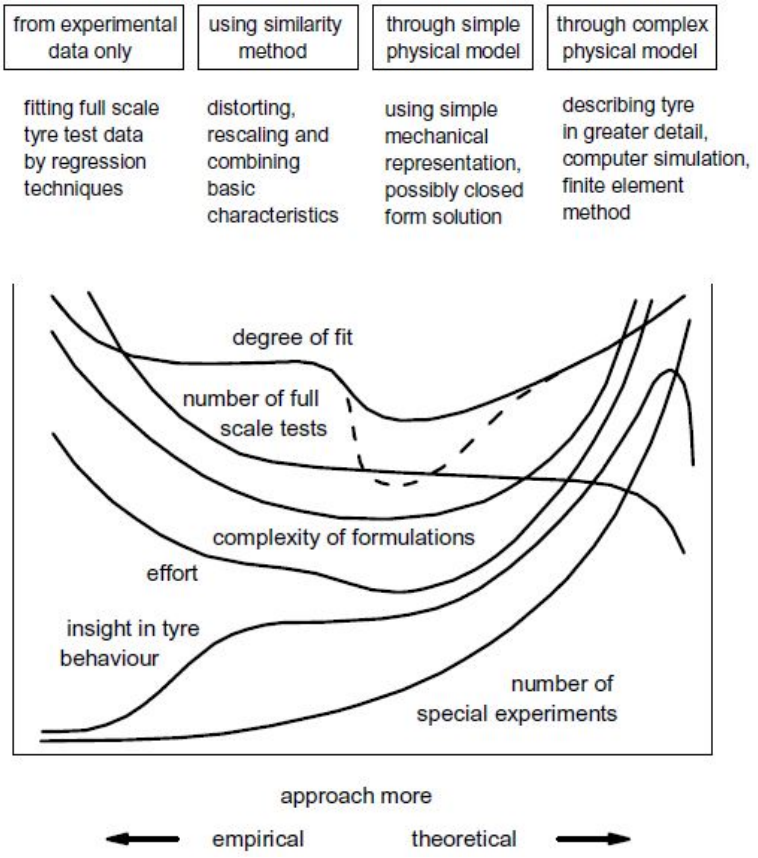

FIGURE 2.2: Possible categories of tire modeling approaches (taken from (Pacejka, 2005)).

Six parameters are considered in (Pacejka, 2005):

- *Degree of fit*: model's accuracy with respect to the design objective,

- *Number of full scale tests*: amount of tests required to validate the model,
- *Complexity of formulations*,
- *Effort* required to design the model,
- *Insight in tire behavior*: model's ability of predicting the tire behavior,
- *Number of special experiments*: amount of experiments required to develop the model.

As expected, empirical approaches require a huge amount of full scale tests with respect to theoretical approaches. These latter are more based on the tire's physical structure theory. Four categories are distinguished in (Pacejka, 2005): "*from experimental data only*", "*using similarity method*", "*through simple physical model*", "*through complex physical model*". The first category at the extreme left uses regression procedures to develop mathematical formulations whose parameters fit best the measured data. A well-known empirical model is the Magic Formula (Pacejka, 2005). This model provides an excellent fit for tire's efforts curves, which makes it more suitable for vehicle motion simulations. The similarity approach uses rather simple distortion and re-scaling methods to develop simpler empirical models. This method is particularly useful when fast computations are needed (Pacejka, 2005). A good example would be Dugoff's model, which uses a simpler representation of tire deformation while keeping a good representation of combined slip (Dugoff, Fancher, and Segel, 1969). But these two categories provide less insight in tire behavior. The relatively simple physical models of the third category are more useful to get better understandings about the tire behavior. The "brush model" represents a good illustration in this context (Svendenius, 2003), (Svendenius and Wittenmark, 2003), (Pacejka, 2005). Regarding the fourth category, interest is given to tire performances related to its construction. More detailed analysis is required and complex finite element based models are usually adopted (Pacejka, 2005). On one hand, empirical models rely on experimental measures to make simulation more accurate, and on the other hand, theoretical models rely on physical models to give more insight about the tire behavior and improve its construction. No model however is designed for control synthesis. Physical models are too complex to be implemented in real-time operations, and empirical models are based on numerous parameters with poor physical meaning, which make them hard to measure or estimate in real time. A new tire model should be designed to fit control synthesis requirements, especially in a global chassis control framework. This model should accurately represent the combined slip behavior in a sufficiently simple way using only online measurable or estimable parameters.

Be that as it may, the performance of the tire to tract the vehicle still depends on the surface condition. If the friction changes, the overall behavior of the vehicle changes. The tire model should depict this phenomenon by explicitly expressing the relationship with the friction coefficient. Subsequently, this latter should be estimated. However, as the friction coefficient is a representative ratio between the tire force and the vertical load (Majdoub et al., 2012), it cannot be directly measured. Even the costly sensors equipped at the tire rubber blocks are usually used for tire force measurement, e.g. a wireless piezoelectric tire sensor for the measurements of tire deformations (Erdogan, 2009). Important efforts have been carried out in order to provide an estimate of the friction coefficient. In (Zhao et al., 2017), an attempt to estimate the road friction is presented which is based on vehicle braking dynamics. Simulation results showed the ability of the observer to provide a good

estimation when braking. However, in combined maneuvers, when the vehicle is accelerating and steering at the same time for example, combined slip dynamics should be taken into account (Pacejka, 2005). This is mainly due to the ellipse of friction (Pacejka, 2005) that shows that the lateral tire force penalize the longitudinal one, and vice-versa. Not taking into account the influence of the lateral force may prevent a good diagnosis of longitudinal tire force penalization. One cannot tell if it is due to a combined slip or a friction variation. In (Patra and Datta, 2012) a more complicated sliding mode observer have been designed based on Dugoff tire model (Dugoff, Fancher, and Segel, 1969). This latter showed good precision in the linear zone of tire force while braking only. Recently, data-based techniques have received more attention. For example, an Auxiliary Particle Filter (APF) have been combined with the Iterated Extended Kalman Filter (IEKF) in (Liu et al., 2017) based rather on the lateral dynamics only. Data-based techniques are used to correct the errors generated by the non-modeled dynamics, and fit the signals values to the real ones. Experimental tests showed promising results. We believe however that the initial modeling should be precise enough to limit the number of errors to be corrected by data-based techniques. This can give an initial estimator good enough for most use-cases, and can be trained afterwards using Artificial Neural Networks to handle more difficult situations. Our investigations showed that particularly the vertical dynamics have important influence in some variables estimation, but are neglected in most research papers. This pertains also in the case of autonomous vehicles. In (Funke and Gerdes, 2015), trajectories have been calculated using simple clothoids for lane change. What is interesting about this research in our context, is the fact that both the trajectory planning and the velocity profile generation are closely related to friction constraints. Authors however suppose that friction values are available and no estimation method is provided. The same methods have been detailed in (Kritayakirana, 2012) to test an autonomous vehicle at the limits of handling. Here, the controller uses a priori knowledge about the friction. This shows the importance of estimating the friction coefficient, but also the lack of robust methods to do so.

2.3 Vehicle Modeling

Similar limitations stand also for the chosen vehicle model. In the current downstream approach, engineers settled on using standalone subsystems based on a reduced vehicle model where only a single controllable variable is targeted.

For example, the ACC controls only the longitudinal velocity to keep regulatory safe distance between vehicles (Moon, Moon, and Yi, 2009), the ESP uses the brake to control the yaw rate and stabilize the vehicle (Liebemann et al., 2004), the Adaptive Suspension (AS) controls vertical motions to improve passenger comfort (Gaspar, Szabo, and Bokor, 2009) and so on. These physical variables are actually coupled as the vehicle's equations of motion prove (Dukkipati, 2010). No matter how efficient assistance systems can be, when put in the same vehicle, one system will compromise the performance of the other. The car manufacturer is therefore obliged to develop an overall chassis systems coordination architecture to benefit from a maximum performance without jeopardizing passengers' safety. This requires a more complete vehicle model taking into account the dynamic couplings for better coordination. The optimization-based approach takes account of the dynamic couplings to find the best commands distribution. These couplings are generally non-linear. This makes the present approach less complex but very limited, and

the eventual future approach more complex but very promising. Additionally, vehicle parameters, as the overall mass (Reinold and Traechtler, 2013) or the tires' cornering stiffness (Chebly, Talj, and Charara, 2017), are uncertain. Motion control performances should stay acceptable whether there is only the driver in the car or with other passengers, and in different type of roads. Robust control is an important requirement to be fulfilled by active chassis systems. Design of robust controllers depends on the augmented plant model. For example, in the conventional $\mathcal{H}_\infty$ design, the order of the controller resulting is equal to the number of states in the plant plus the number of states in the requirements weights plus twice the number of states in feed-through matrix (Skogestad and Postlethwaite, 2005). For high-order plants, the controller generated by such design procedures is difficult to implement. The common practice is to then consider a reduced plant model that depicts only the important dynamics. In this context, in (Soltani, 2014), a Relative Gain Array (RGA) study has been conducted to evaluate the system couplings near the crossover frequency using a simplified four-wheeled vehicle equipped by an ESP and an EPAS. Authors concluded that the system can be decoupled for high frequencies. Youla parameterization has been used then for each Single-Input Single-Output (SISO) transfer function. Results were acceptable for each variable only when the throttle was on, which means with the presence of a driver to control the longitudinal speed. Authors in (Yim, S., 2015) proposed an Sliding Mode Control (SMC) to coordinate the ESP and active steering devices, both in front and rear. The bicycle model has been chosen to design the controller. Two objectives has been pursued: maneuverability by means of yaw rate tracking, and lateral stability by minimizing the side-slip angle. A four-wheeled vehicle model has been considered afterwards in the low-level control for the ESP. Couplings were not managed at the high-level control as two different vehicle model have been considered. Moreover, no lateral velocity control have been ensured whereas a vehicle equipped by an Active Front Steering (AFS) & ARS can ensure a lateral transitional motion to avoid an obstacle for example. SMC was used also in (Feng et al., 2014) to control an electric vehicle equipped by a 4WS system and a 4WD system. A four-wheeled vehicle model was considered, but only to control the lateral dynamics of the vehicle. Couplings with the longitudinal dynamics were then ignored. In (Doumiati et al., 2013), a Linear with Parameters Varying (LPV)/$\mathcal{H}_\infty$ controller has been chosen as the high-level controller for a vehicle equipped by an AFS and rear braking. Although good robustness is ensured, again, only a bicycle model was considered to design the controller. A 14-Degrees Of Freedom (DOF) full vehicle model equipped by an AFS, an ABS, and Semi-Active Suspension (SAS) has been used in (Zhao, Li, and Qu, 2014) and then simplified for control synthesis. A high-level controller based on SMC has been chosen. As the authors noted, the SMC procedure suffers from high-frequency chattering. The sign function can be used instead of the saturation function (Zhao, Li, and Qu, 2014) to reduce the effect of chattering. We believe that this method is more suited for electronic devices, but in contrast, could accelerate mechanical actuators aging or tire wear. The state of art shows that either we employ complex robust controllers based on simplified vehicle models, or we decouple the vehicle model to use simplified controllers. In Part II of this research, we privilege neither the first nor the second approach. We rather investigate the use of a robust high-level controller based on a global vehicle model. The goal is to evaluate the dynamic couplings at the vehicle level to justify the structure of the high-level controller. A full vehicle model is first developed, and a pre-study is then carried out to evaluate the dynamic couplings and what can be simplified.

2.4 Secondary Objectives

Regarding autonomous vehicles, qualitative objectives could be required. When a driver has its hands off the steering wheel, if an unexpected motion is generated, he/she could be tempted to regain control of the vehicle. In case of a vehicle equipped with an EPAS system, this may present few risks for drivers' hands due to the important amount of steering wheel torque (Soltani, 2014). One way to prevent this is to tune the vehicle motion in a way to generate expected motions like a human being would do. To the best of our knowledge, there exist two methods to tune the vehicle behavior. We either act on motion references to be followed by the vehicle so the controllers impose different commands to actuators, or we modify the CA strategy so the commands are distributed differently. CA techniques have been tested to handle various multi-objectives problems. In (Shyrokau and Wang, 2012), the Fixed-Point Iteration (FPI) has been used to handle the CA problem and tested in a Hardware-In-the-Loop procedure. The FPI is particularly suitable for real-time applications (Wang and Longoria, 2009). Energy consumption and energy losses have been selected as performance criteria. The choice of these criteria is more relevant for electrical vehicles (Shyrokau et al., 2013). Authors of (Chen and Wang, 2011) have also focused on energy-efficient CA in the context of electric vehicles by adding a cost function. Stability has been added to energy optimization in (Jing et al., 2017). A two-step optimal CA has been developed: a pre-allocation for energy efficiency optimization assuming that the vehicle is stable, then a reallocation in case of wheels skidding or locking using Model Predictive Control (MPC). Generally, the literature has been more interested in power consumption and tire energy dissipation (Shyrokau et al., 2015). The driving pleasure and comfort have always been ensured by the driver itself. Each driver corrects the vehicle behavior gradually until it fits its comfort and confidence requirements. To the best of our knowledge, chassis systems coordination taking into account the feelings generated has been ignored in the literature. By motion feelings, we mean the accelerations that the chassis systems may generate, and not for example the relationship of the driver with his steering wheel. In an autonomous driving context, coordination should be made especially in such a way to avoid the generation of unexpected car behavior.

Furthermore, to expand the performance of the vehicle, car manufacturers tend to implement additional subsystems. One common practice to validate a new system, is to test it at its limits. In this context, researches in (Funke and Gerdes, 2015) use simple clothoids to generate the trajectory that should be followed while respecting the friction constraints considered as the major limitation (Pacejka, 2005). This work originates from the thesis of (Kritayakirana, 2012) where methods to test an autonomous vehicle at the limits of handling have been exposed. Results showed good performance by using an a priori knowledge of friction and a robust controller to deal with surface variations. However, these results remains far from the real potential of ground vehicles. One of the reasons of these limitations is the use of only the front steering capability of the vehicle to turn. Today's vehicles are already equipped by various chassis systems and ADAS. For example, The ESP detects an avoidance situation and use a differential braking between left and right wheels to create a yaw moment and steer back the vehicle lest its loss of control. This technology showed the relevance of making use of the four tires to handle severe scenarios as obstacle avoidance. While the ESP activates only in specific scenarios, one could think of using differential braking in more additional hazardous situations. In this thesis,

we will call this the VDC system[1]. However, using the brakes repetitively while the driver does not ask for them could be annoying and would deteriorate the tires faster. Another way to take advantage from the potential of the four tires is TV. Here, it is the drive torque that is split between right and left wheels. Several researches focus on the TV system in the literature. In (Siampis, Massaro, and Velenis, 2013), combined yaw stability and velocity regulation are proposed by means of an electric rear axle TV. The controller consists of an LQR (linear–quadratic regulator), and the drive torque is split between left and right rear wheels using a limited slip differential calculated at steady-states conditions. As long as tires are not used longitudinally and laterally at the same time, no combined slip phenomena are considered at the tire level. But, in order to expand the vehicle potential, we believe that TV should be used also at the front tires by taking into account the combined slip for a better coordination. In (Wang et al., 2017), authors tackled the problem of the four-wheel independently actuated electric vehicle. A hierarchical control architecture is adopted to enhance the vehicle stability. As a high-level controller, a SMC scheme is adopted to determine the desired longitudinal and lateral forces and yaw moment. In the low-level control, an optimization algorithm is adopted to allocate the driving/braking torques to each in-wheel motor by means of the Sequential Quadratic Programming (SQP). Good performances are exhibited in few standardized scenarios. The longitudinal velocity however is not very high and do not vary in the middle of the maneuvers. Moreover, the SMC uses only the sign function as the reaching law, which causes chattering and may accelerate tire wear. In order to represent a real life situation and attract the different stakeholders, different severe scenarios should be tested.

[1] This is actually the commercial name given by Renault for this system.

3 The Downstream Coordination Approach

As mentioned before, car manufacturers often vary their suppliers for competition strategies matters. Subsystems are then based on different vehicle models, have different control strategies, and act independently. Nevertheless, car manufacturers integrate directly chassis systems provided by equipment suppliers. This is actually cheaper as manufacturers can proceed to bulk purchasing and benefit from the economy of scale advantages. To mitigate possible conflicts, car manufacturers use rule-based coordination strategies downstream the subsystems by prioritizing one system over another (Velardocchia, 2013). Next, this downstream coordination approach is described.

3.1 Control Architecture

Chassis systems internal functioning is usually provided as a black box so the supplier can preserve its intellectual property. In addition, these subsystems need a direct feedback from the vehicle states as they are developed individually. With this configuration, the car manufacturer can only act downstream the subsystems, at their outputs. We choose the appellation "*Downstream Coordination Approach*" because of the position of the coordination layer with respect to the subsystems standalone controllers. Figure 3.1 schematize this approach. The control here is *decen-*

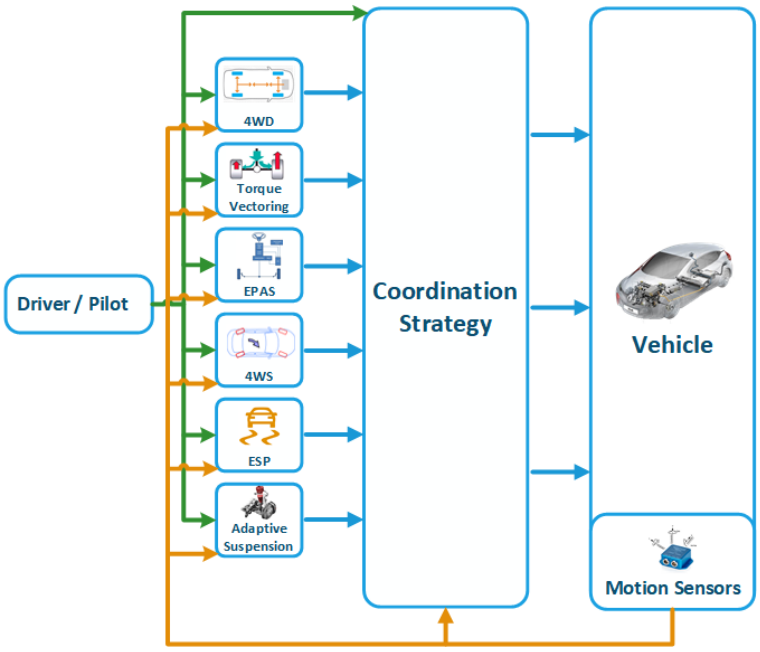

FIGURE 3.1: Structure of the downstream coordination approach.

tralized (Duffie, Chitturi, and Mou, 1988). It follows a parallel structure where each subsystem works separately. Controllers have to work simultaneously. They have their own information system and ECUs, which require additional cost and space (Vivas-Lopez et al., 2015). The only way to add "integration" in the process is by allowing supplementary communications between the controllers as shown in Figure 3.2. The *heterarchical* characteristic of this architecture makes it more suitable for manufacturing systems (Duffie, Chitturi, and Mou, 1988). The fact that no global supervision is provided makes this architecture particularly less suitable for vehicle safety control.

In order to develop a coordination strategy, interactions between the subsystems are preliminary studied. Automakers engineers rely on their "*expert knowledge*" to design the required coordination strategies (Selby, 2003). This is achieved through rule-based controllers arbitration deduced from the preliminary studies of the subsystems' interactions.

3.2 System Modelling

In the downstream approach, each subsystem is designed separately. The coordination comes after studying the influence of each system on the overall vehicle. As each subsystem is isolated and designed for a specific objective, only a reduced model of the vehicle is taken into account. More specifically, spotlight is put on only the physical variable to control.

For lateral tire force based systems for example, one common industrial practice is to reduce the vehicle model into a bicycle model (Ono et al., 1994), (Brennan and Alleyne, 2001), (Yim, 2012). Suppliers are constrained to use approximately the same model in which the design is based. If systems are based on different models, more conflicts are likely to appear. The safest choice would be then the bicycle model as it is the most common one. This model consists of describing both tires of the same axle as one equivalent tire with a doubled stiffness (Figure 3.3).

With:

- F_{y_f} : the lateral force at the front axle,
- F_{y_r} : the lateral force at the rear axle,
- α_f : the front equivalent side-slip,
- α_r : the rear equivalent side-slip,
- δ_f : the front wheel angle,

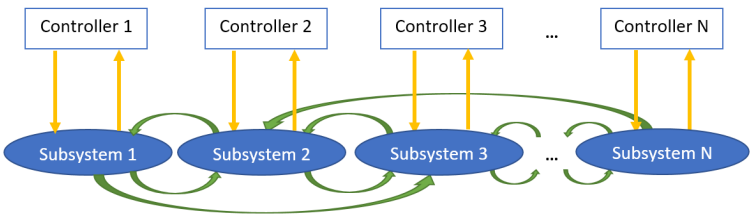

FIGURE 3.2: Decentralized control structure (adapted from (Gordon, Howell, and Brandao, 2003)).

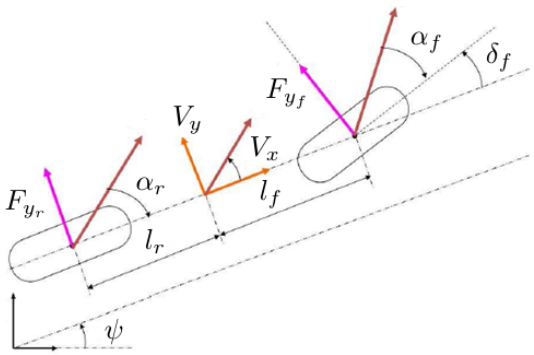

FIGURE 3.3: The bicycle model.

- δ_r : the rear wheel angle,
- l_f : the distance between the front axle and the vehicle's CoG,
- l_r : the distance between the rear axle and the vehicle's CoG,
- V_x : longitudinal velocity of the vehicle,
- V_y : lateral velocity of the vehicle,
- ψ : yaw angle of the vehicle.

The detailed modeling is provided in Chapter 10.

3.3 Control Synthesis

Different subsystems can influence the same physical variable. Controllers are then based on transfer functions from a specific actuator command to directly one of the vehicle control axis. These subsystems should be coordinated. But first of all, a common reference should be imposed in order to specify the overall behavior of the car.

3.3.1 Reference generation

As far as only assistance systems are concerned, the dynamics targets should be calculated from the driver commands. The reference generator takes the steering wheel angle, the gas and brake pedals actuated by the driver as an input. The idealized static bicycle model can be used as a reference model to follow in this case. However, not taking into account the transient response may result in relatively large tracking errors and overshoots at the beginning of steering maneuvers (Zhang and Göhlich, 2018). A time constant can then be added characterizing the yaw rate response of the vehicle. Moreover, to give the driver more flexibility regarding the feeling to generate, this reference can be tuned in order to generate different driving modes. The more common ones are *the normal mode*, *the comfort mode*, and *the sport mode*. Additional feelings can be generated by extrapolating the indexes used to generate the three conventional modes and offer the driver a more personalized experience[1].

[1] This is called the "*Multi-Sense*" in Renault vehicles.

However, for autonomous vehicles, the front steering wheel angle should be an output to be generated by the corresponding controller. Rather than specifying only the yaw rate and velocities' desired profiles, interest is put on the trajectory control at a desired speed for the autonomous vehicles. A different reference generator is needed. Data can come from cameras, Laser Imaging Detection And Ranging (LIDAR) sensors, RAdio Detection And Ranging (RADAR) sensors and so on. These data is then processed and fused to come out with an optimal decision. The trajectory can be afterwards generated. This latter should be smooth enough. Various smooth path functions have been studied, especially for lane changes. In (Bianco and Piazzi, 2000), the path is parameterized by quintic G^2-splines. These splines are devised to guarantee the overall second order geometric continuity of a composite path. Polynomials were used in (Papadimitriou and Tomizuka, 2003) for trajectory planning. The aim was to provide a fast lane changing algorithm for Intelligent Vehicle Highway Systems. Authors of (Funke and Gerdes, 2015) favoured rather simple clothoids for lane change trajectories. The path segments are defined by linearly varying curvature that can interpolate between straights and arcs to generate continuous curvature paths. As we can see, for autonomous vehicles, specific techniques are used for trajectories generation. As this goes beyond the scope of our research, the reference generator in case of autonomous vehicles will be taken from previous researches without developing it in detail.

3.3.2 Standalone subsystems controllers

Each subsystem has its own controller in a downstream configuration. Because each subsystem is usually developed independently, each controller is based on a different transfer function that links the corresponding command directly to the vehicle's states. Once the transfer function from the subsystem to the vehicle is identified, different control synthesis methods could be applied depending on the nature of the transfer function. In (Ono et al., 1996), $\mathcal{H}_\infty$ synthesis is proposed to control an AFS system to compensate instability against the nonlinear uncertainty and prevent the vehicle from spinning. Authors in (Will, Teixeira, and Zak, 1997) used rather a fuzzy logic 4WS control system design method using a fuzzy vehicle model. An important remark should be mentioned. Let us note $K_1(s)$ the controller of the first subsystem, $K_2(s)$ the controller of the second subsystem, and $P(s)$ the plant[2]. When a controller is designed independently, the stability is studied with respect to the plant in an open-loop procedure (Soltani, 2014). $K_1(s)P(s)$ and $K_2(s)P(s)$ would be stable (Figure 3.4). But when put together in a downstream configuration, both controllers are placed in parallel. Therefore, $[K_1(s) + K_2(s)]P(s)$ should be also stable (Figure 3.5). Controllers might have to be redesigned.

3.3.3 Coordination strategy

In the context of downstream coordination, four coordinator types have been distinguished in (Gordon, Howell, and Brandao, 2003): *Pure Subsumption*, *Largest Modulus Activation*, *Artificial Neural Network* and *Fuzzy Logic Control*.

[2]The vehicle model in this case.

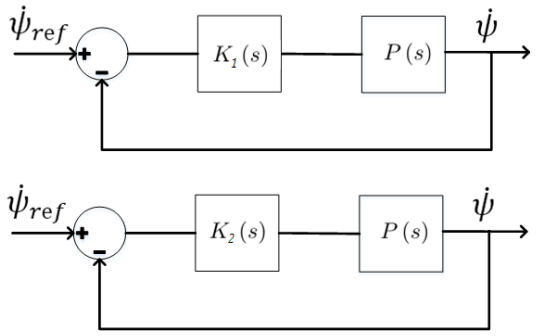

FIGURE 3.4: Simplified control architectures when design is made independently.

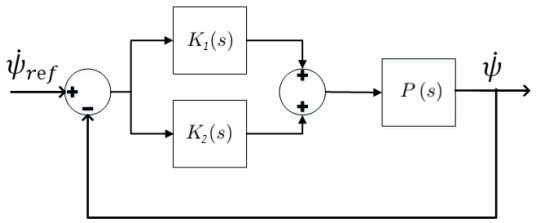

FIGURE 3.5: The control architecture that should be considered in a downstream approach.

Pure Subsumption

Regarding the *pure subsumption* approach, the highest level non-zero command takes precedence over of the other sub-commands. Figure 3.6 illustrates this method.

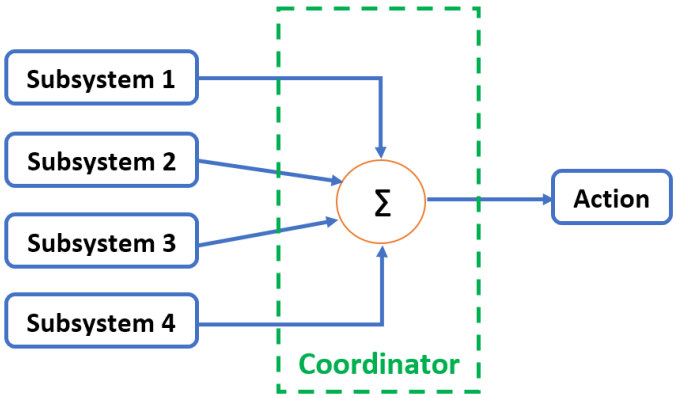

FIGURE 3.6: Pure Subsumption coordination (adapted from (Gordon, Howell, and Brandao, 2003)).

The priority of each system is pre-defined. The secondary systems act as a backup. This method has been applied for example in the work of (Velardocchia, 2013). The vehicle here is equipped by an ADS, ESP, and TV to improve the vehicle's lateral performances. The simple method based on prioritizing one system over another has been used: If the yaw torque demand can be satisfied by the ADS, then the ESP and TV will not be activated. Otherwise, the rest of the yaw torque

demand will be equally shared between the ESP and the TV systems. It is reported that both vehicle performance and safety have been improved within this method. However, one may raise the question of the utility of using several systems for the same objective if only one system will be activated at a time.

Largest Modulus Activation

In the *largest modulus activation*, several high level commands are considered, and the one with the highest modulus takes precedence over the rest (see Figure 3.7).

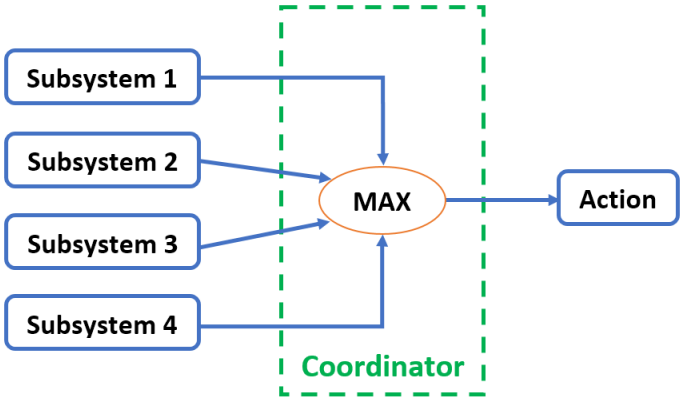

FIGURE 3.7: Largest Modulus Activation coordination (adapted from (Gordon, Howell, and Brandao, 2003)).

The main difference with respect to the *pure subsumption* approach is that here the priority of each subsystem may vary depending on the situation, for example if the effectiveness of subsystems depend on the type of the road. Both pure subsumption and largest modulus activation methods however are characterized by modes switching. These switches generate undesirable transient behaviors that could destabilize the overall system. In this context, the *Artificial Neural Network* and the *Fuzzy Logic Control* were introduced.

Artificial Neural Network

The *Artificial Neural Network* consists of simple averaging or via a non-linear interpolation function weights (see Figure 3.8). These functions can be chosen to ensure smooth transitions between coordination modes, actuator saturation avoidance and more (Nwagboso, Ouyang, and Morgan, 2002). It is also possible to integrate additional sensor or observer information to the neural network to make the coordination adaptive to other factors as high speed or friction shift. The designer should be careful not to over-supply the neural network (Gordon, Howell, and Brandao, 2003). The drawback here is that the problem is not formalized. A learning algorithm should be elaborated to mitigate the conflicts. Regarding integrated systems, as we know their dynamics and their influence on vehicle dynamics, a deterministic approach would be better. A stochastic approach could only hope of approaching the optimal deterministic solution.

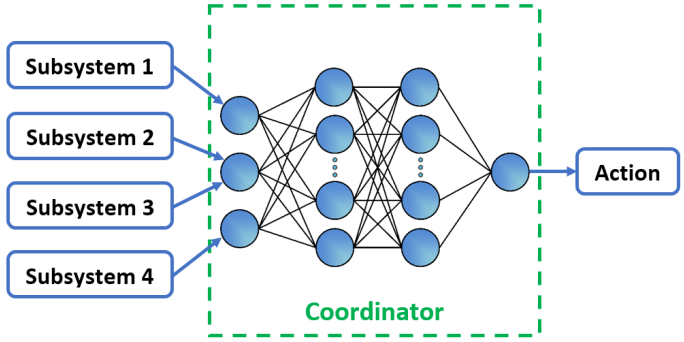

FIGURE 3.8: Artificial Neural Network coordination (adapted from (Gordon, Howell, and Brandao, 2003)).

Fuzzy Logic

The *Fuzzy Logic* uses "easily understood" rule-based coordination functions (see Figure 3.9). Here again, the highest level predominates but smooth transitions are

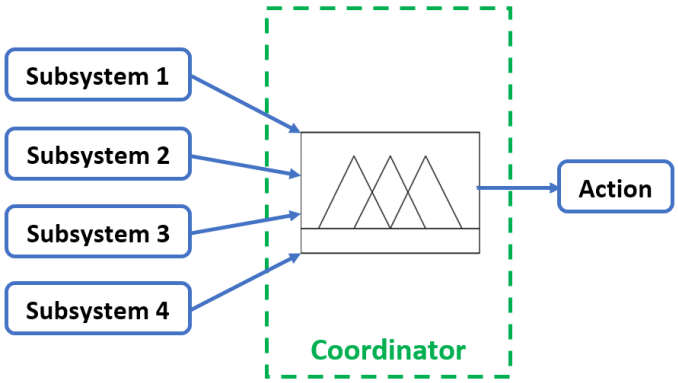

FIGURE 3.9: Fuzzy Logic coordination (adapted from (Gordon, Howell, and Brandao, 2003)).

ensured (Gordon, Howell, and Brandao, 2003). In (Wang et al., 2009) for example, a fuzzy logic scheme and weighting factors are used to coordinate the different systems. The controller agents computes combined control signals for the steering angle and the wheel torque depending on the targeted performances priority. The main advantage is the conflict mitigation, for example, when the braking controller has to track simultaneously the yaw rate reference and the longitudinal acceleration demand. However, here again, the problem is not well formalized. The performance would depend greatly on the rules implemented and therefore the knowledge of the designer.

3.4 Conclusion

The downstream approach have been exposed in this chapter. Four coordinators have been distinguished. Table 3.1 summarizes the pros and cons of each coordination strategy.

TABLE 3.1: Pros and cons of downstream coordinators.

Approach	Pros	Cons
Pure Subsumption	- Simplicity: Pre-studies consist of identifying only the static effectiveness of each subsystem.	- Static prioritization: secondary systems act only as a backup, - Simultaneous operations are avoided, - Abrupt modes switching.
Largest Modulus Activation	- Relatively simple: still depend on pre-studies, - Dynamic prioritization depending on particular situations.	- Simultaneous operations are avoided, - Abrupt modes switching.
Artificial Neural Network	- Smooth transitions between coordination modes, - Can be adaptive to a bigger set of parameters, - Simultaneous operations can be learned.	- Complexity: use of non-linear interpolation function weights, - Stochastic approach: need for a learning algorithm to mitigate the conflicts.
Fuzzy Logic	- Use of "easily understood" rule-based coordination functions, - Smooth transitions, - Simultaneous operations can be handled.	- The problem is not mathematically formalized: The performance depends from the designer's knowledge.

It should be noted that for safety requirements, industrials still avoid the use of stochastic approaches for critical safety systems. In today's situation, only prioritization strategies are implemented. Moreover, because of the use of simplified vehicle models and the negligence of nonlinear couplings as combined slip phenomenon (Pacejka, 2005), systems based on the generation of longitudinal tire forces do not operate when systems based on lateral tire forces are activated. The embedded systems do not operate at the same time only if necessary [3]. One system is then prioritized over the others. By doing so, the overall potential performance can never be reached, and some severe maneuvers cannot be handled, which limits the safety amount of the vehicle even if it has the required potential. To illustrate this limitation, one can use the "*g-g diagram*" that represents the lateral and longitudinal accelerations of the vehicle's center of gravity. (Tanaka, Inoue, and Iwata, 1992)

[3] When one system fails or saturates.

from Toyota presented a schematic overlook about the domain of operation of typical vehicle control systems, and the areas where their simultaneous operation can be beneficial (see Figure 3.10). In Figure 3.10, we replaced the friction circle with a friction ellipse. The reason is that the friction coefficient in the longitudinal direction is generally larger than the friction coefficient in the lateral direction (Pacejka, 2005). The schematic overlook should not be considered literally. Nevertheless, it clearly shows that coordinated embedded systems can enlarge the operation spectrum of the vehicle to expand its potential.

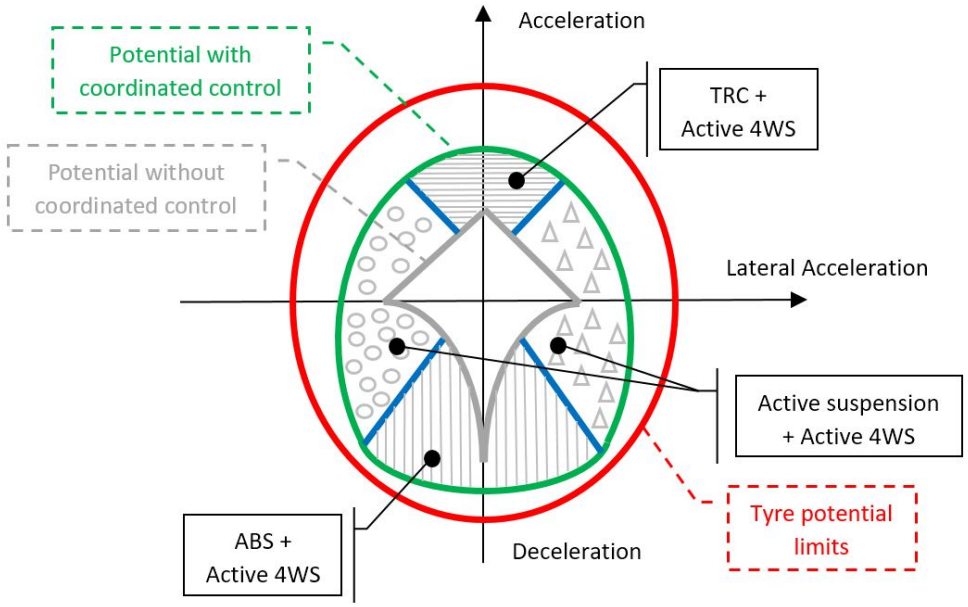

FIGURE 3.10: Benefits of a coordinated control in the gg-diagram (adapted from (Tanaka, Inoue, and Iwata, 1992)).

In addition, in a downstream coordination approach, a preliminary comparison study is required to establish the prioritization strategy. In this approach, it is difficult to prove the optimality of the control structure. Without a proper mathematical formulation, it is even hard to see how key properties of stability, reliability and so on can be validated. It is also likely that rule based coordination strategies cannot handle systems of more than two or three subsystems when interactions get more complex (Selby, 2003). This complexity has already arisen by the emergence and introduction of new technologies to the automotive industry in the 21st century. For example, the signal flow for a hybrid electric vehicle motion control can be found in (Phillips, 2002). Only a functional decomposition has been presented without any details regarding the coordinator. Figure 3.11 shows a glimpse of what an embedded coordinator should handle in real passenger cars, with ISG being the Integrated Starter Generator.

The subsystems should be carefully studied to manage their interactions. An "expert knowledge" is required to prevent interactions hinder the vehicle performance. This level of knowledge should approach the way that advanced drivers understand the interactions between braking and steering for example. The downstream approach is suitable for fast practical implementations. The procedure is rather commercially driven (Selby, 2003). Even though, profits are made only from exploiting the information contained in one vehicle control system, as the yaw rate measurement, into another different system. This allows to reduce the number of sensors,

communications links, switches ... etc, or reduce the computational overheads in case of observers duplication. However, the benefits may also include cost reduction and space saving by reducing the number of ECUs. A high-level more sophisticated controller that specifies the motion of the vehicle and then allocate the commands to the different subsystems would be complex to develop but could be more cost-effective at the same time in case of a large number of integrated chassis systems. In this context, the upstream approach is presented in the following chapter to clarify the additional benefits that could be offered in terms of potential expansion and eventual economical profits.

Our contributions are focused on this alternative upstream approach. Every layer of the control architecture has been studied and designed in such way to be implemented in a real car. A particular care has been given to how to develop control algorithms with higher performances but still making them work in real-time maneuvers using today's ECUs.

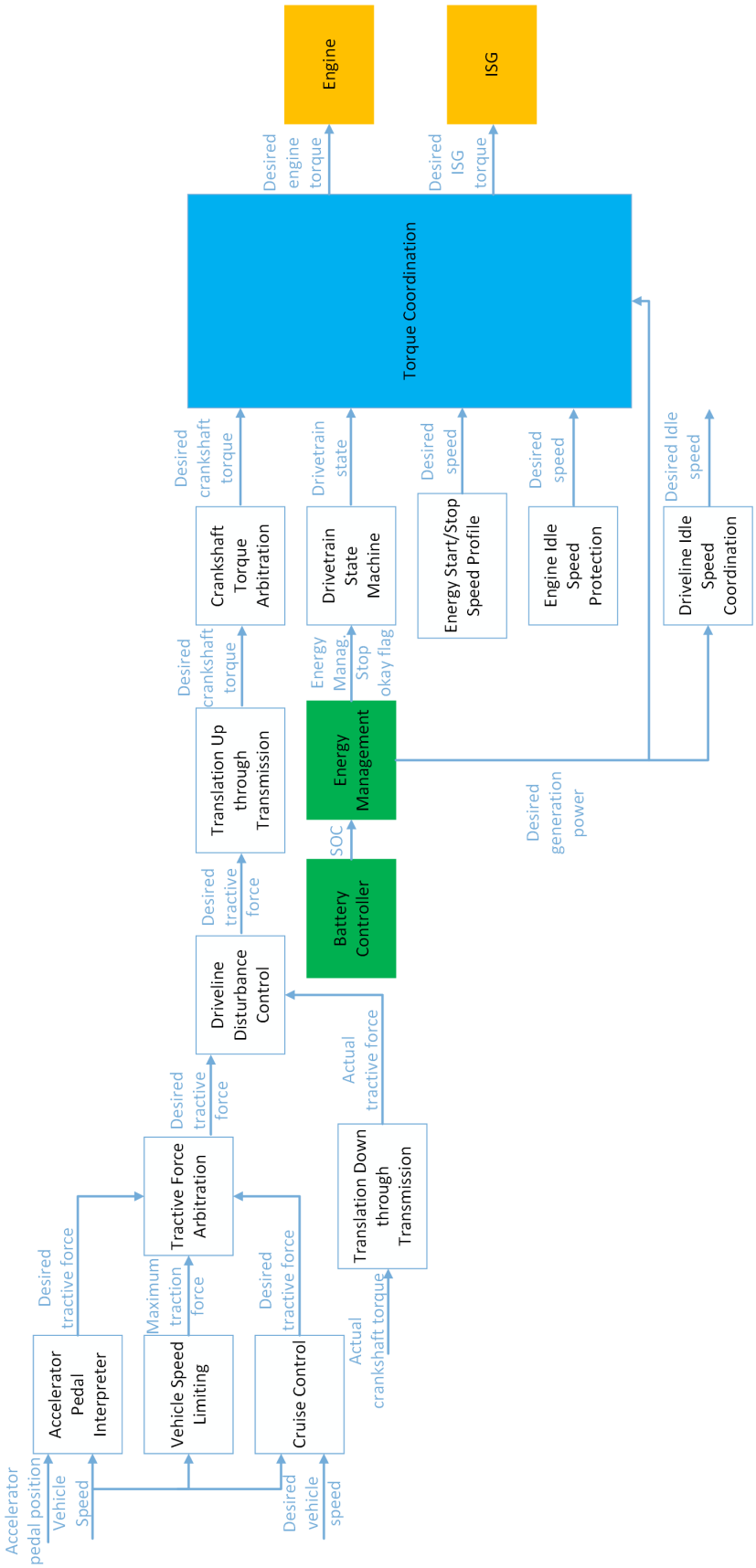

FIGURE 3.11: Signal flow for a hybrid electric vehicle motion control (adapted from (Phillips, 2002)).

In this part, a general state-of-art has been proposed in order to detect the reasons behind adopting a downstream coordination approach. This approach consists in keeping the subsystems with their own standalone controllers, and then adding a coordination layer downstream these subsystems. This layer is designed in such a way to avoid internal conflicts using rule-based algorithms. These algorithms come from pertinent pre-studies focused on different scenarios that might generate jeopardizing conflicts.

The general guidelines of the downstream approach have been also exposed. The control architecture has been detailed along with the simplified system modeling and control synthesis. We can see that the attractiveness of this approach comes from its simplicity and probably its relatively low cost. However, going towards a fully autonomous vehicles with much more embedded systems may be too complex for such a simple approach. This approach may fail to satisfy the criteria defined in the general introduction. Particularly, the coordination strategies depend closely from the scenarios pre-studied. These pre-studies are defined depending on the subsystems implemented. Consequently, whenever an additional system should be implemented, the whole coordination strategy should be redesigned. No "*extensibility*" is ensured, which make this approach less attractive for future vehicles where the hardware design is not frozen yet, and where probably numerous conflicting systems might be added.

The following part is dedicated to the alternative approach of the upstream coordination that we think will remedy to the downstream approach drawbacks and would be more suitable for future over-actuated vehicles. Next we will detail every step of this upstream approach. The architecture is first described, the modeling of vehicle is revisited and a new tire model is proposed. We will recall the guidelines of robust control synthesis and we will dedicate a distinct chapter to focus on control allocation algorithms.

Part II

THE UPSTREAM APPROACH

The move towards autonomous vehicles led car manufacturers, equipment suppliers, and even new actors as Alphabet's Waymo, Uber and so on, to add more and more sensors within the same vehicle. Figure 3.12 shows for example "*the Next Two*" concept of Renault that represents the company's current vision of an autonomous electric vehicle available starting from 2020. "*The Next Two*" prototype-based on a Renault ZOE focuses on two areas: the delegation of driving functions under certain conditions and connectivity. Using sensor technologies, "*the Next Two*" enables the delegation of driving functions from the driver to the car in congested traffic up to 30 km/h on the main roads. It also offers an Automated Valet Parking (AVS) function, which permits the vehicle to park itself autonomously. This includes both finding a parking place and the necessary maneuvering to accomplish the parking.

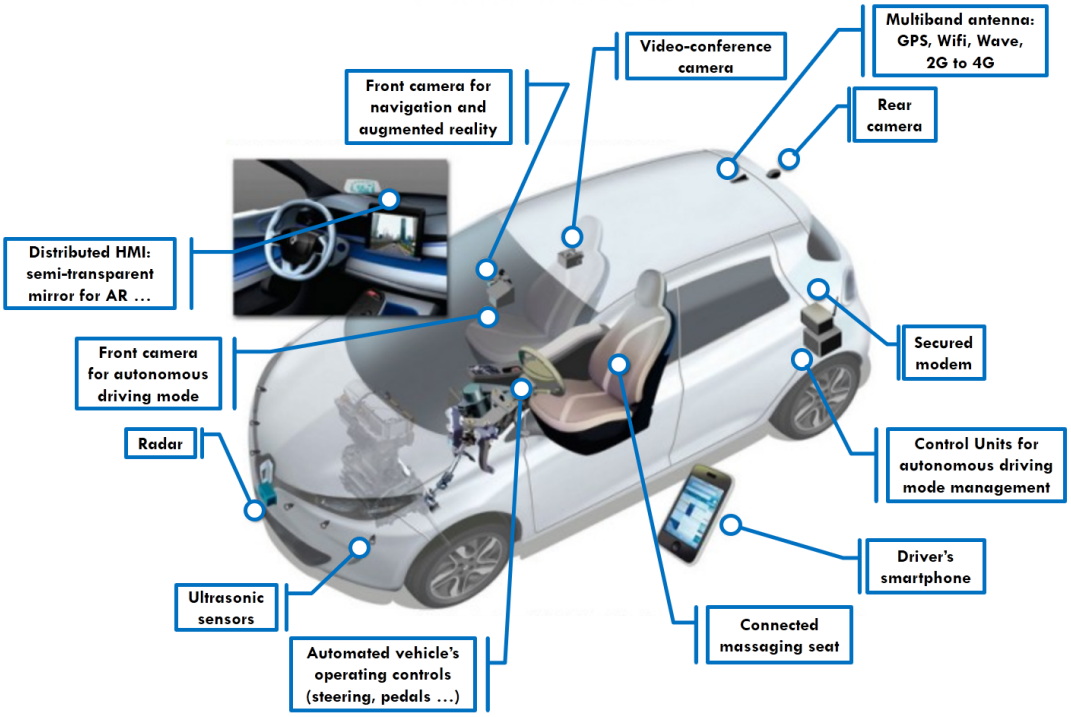

FIGURE 3.12: Autonomous driving systems in "*the Next Two* concept" (adapted from Renault's communication.).

However, this prototype is equipped only by the EPAS system to steer the vehicle, an electric engine to tract the vehicle and the braking-based ESP to stabilize the yaw rate of the vehicle in case of an emergency. This is probably one of the reasons why the vehicle can be actuated in an autonomous mode only for low speed values. In addition, as it is exposed in the research of (Funke et al., 2017), in an obstacle avoidance maneuver for example, large steering wheel angles can be generated. As this maneuver is fast and severe, the steering wheel angular speed limits could be reached, which lead to vibrations of the steering wheel and an undesirable motion behavior. Moreover, as the steering wheel angle is moving rapidly, this might hurt the driver's hands if this latter get scared and decide to take back the control of the vehicle.

One of the solutions that we thought about, is to make the vehicle over-actuated on purpose so we can use the other available chassis systems in a complementary way. This means that we can amplify the use of the ARS system or the TV system in the autonomous mode to mitigate the use of the EPAS system. Another solution is to

use simply the SBW system (Li and Wang, 2007), but this requires a redesign of the vehicle's mechanical architecture which could be more expensive from an industrial point of view. Future vehicles may resemble to what is shown in Figure 3.13.

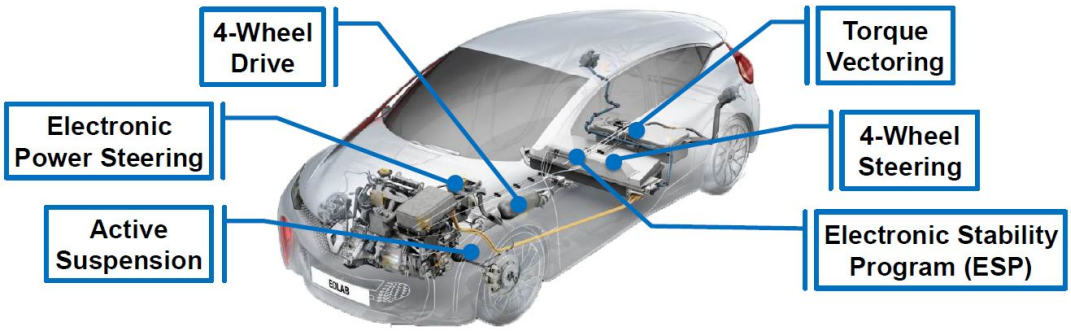

FIGURE 3.13: The possible future intelligent chassis (adapted from Renault's website.).

As mentioned in Chapter 3, the more numerous the embedded systems get, the more complex their interactions become. Rule-based strategies implemented downstream the chassis systems will not be sufficient especially if only prioritizing strategies are used. On one hand, using one system at a time will not solve the problem of mitigating the use of the front steering wheel, and on the other hand, rule-based strategies are based on an "expert knowledge" of vehicle dynamics, which cannot be foreseen for the type of configurations depicted in Figure 3.13. Inter-systems interactions should be formalized and managed upstream the subsystems in an optimal way. When each controller is designed independently to act directly on vehicle dynamics, one usually omits a major constraint level, which is tire potential. Designing each system without considering the possible interactions with other systems, gives a wrong information about the remaining potential of tires. This could lead to high requests of tire forces when these tires are actually saturated by another system (Kissai et al., 2017). In addition, the control architecture should be extensible as long as the hardware architecture of the future intelligent chassis is not frozen yet. This particular feature is not satisfied by the downstream approach as the conflicted scenarios studied are related to the specific embedded systems themselves and not the overall control of the vehicle motion regardless to how many systems are implemented.

This part will focus on the development of the upstream approach that we believe will suits most future vehicles. We detail each step of the control development, from the general architecture to the control synthesis. We expect that by the end of this part, the reader can apply this approach to any chassis systems combination.

4 Control Architecture

In our work, the coordination is carried out upstream the subsystems. The commands are distributed in a way to avoid the conflicts among the subsystems. A multivariable controller is placed between the driver/pilot commands and the chassis systems. The controller design is based on a coupled nonlinear vehicle model that give insights about the possible conflicts before reaching them. Figure 4.1 illustrate this approach.

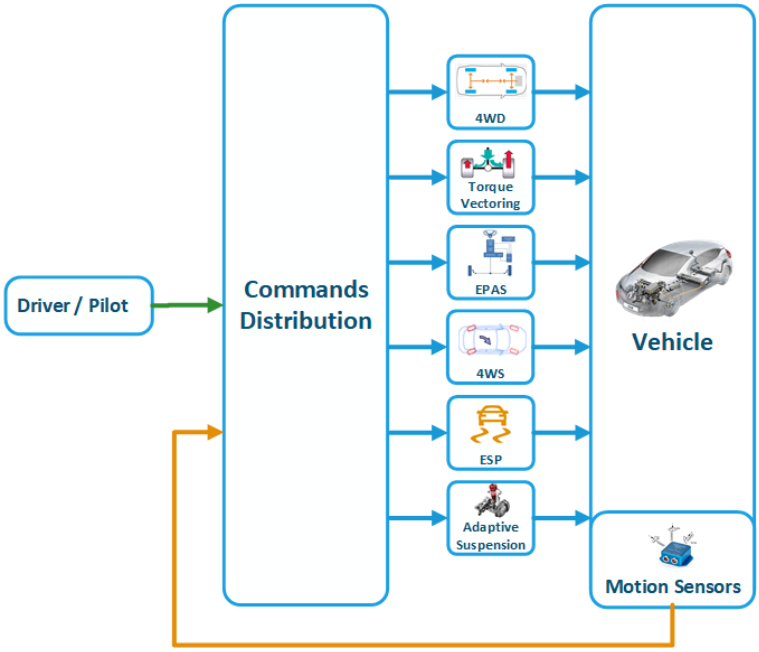

FIGURE 4.1: Structure of the upstream coordination approach (adapted from (Selby, 2003)).

In accordance to this approach, three architectures have been distinguished in (Duffie, Chitturi, and Mou, 1988) and (Gordon, Howell, and Brandao, 2003): *centralized control*, *supervisory control*, and *decentralized control*. By studying each one of them, it seems that the decentralized control corresponds rather to a downstream coordination as presented in the previous part. We will present here only the centralized control and the supervisory control. Nevertheless, a third class could be distinguished, which is more of an extension of the supervisory control, called the *multi-layered architecture*.

4.1 Centralized control

A central global controller is responsible of taking all the control decisions. In general, this controller follows the global multivariable control formalism as it has been

realized in (Nagai, Yamanaka, and Hirano, 1998), (Nagai, Hirano, and Yamanaka, 1998), (Harada and Harada, 1999), (Brennan and Alleyne, 2001). Figure 4.2 illustrates this concept.

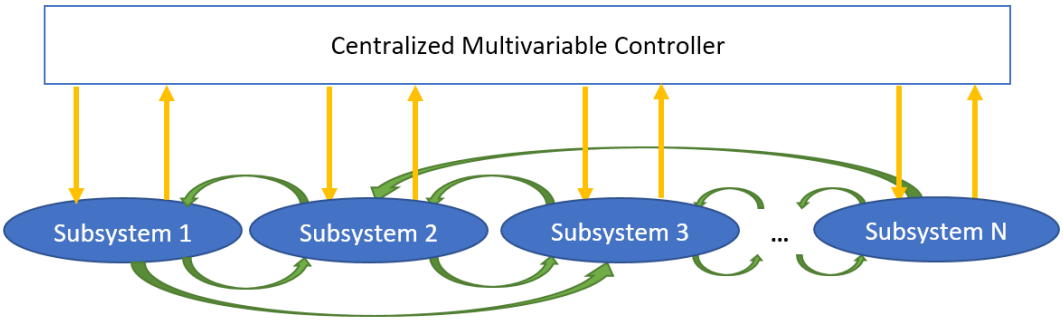

FIGURE 4.2: Centralized control structure (adapted from (Gordon, Howell, and Brandao, 2003)).

As shown in Figure 4.2, the controller is directly connected to the subsystems. As the control is centralized, the stability and performance can be made in tandem at the design stage. However, the architecture's flexibility of is clearly limited. It has been pointed out in (Kelling and Heck, 2002) that any desired fail-safe redundancy of micro-controllers or power converters increases rapidly the cost of the control components. For that matter, a distributed control method has been preferred, which can be assimilated to a supervisory control.

4.2 Supervisory control

Supervisory control represents an intermediate solution between the centralized and decentralized control. In a nutshell, a supervisory layer is added to a decentralized structure to add more information in the process. Figure 4.3 illustrates this approach.

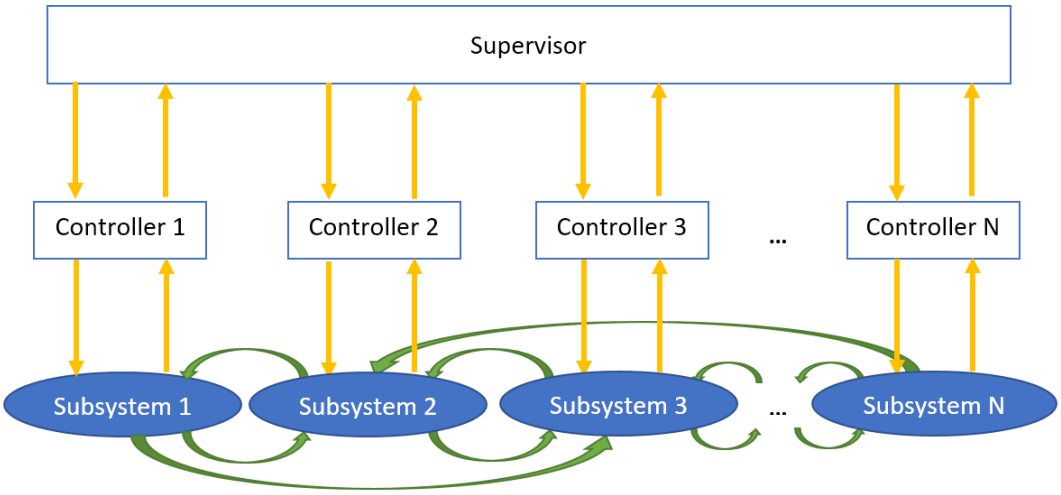

FIGURE 4.3: Supervisory control structure (adapted from (Gordon, Howell, and Brandao, 2003)).

Three advantages can be deduced from this architecture:

- **Fault-tolerance**: it ensures a minimum of operations safety even if the high-level controller fails,
- **Extensibility**: it can be evolved to a multi-layer hierarchical structure to add more functionalities,
- **Modularity**: it allows manufacturers and suppliers develop independently complementary control algorithms.

Using this structure, (Vivas-Lopez et al., 2015) used three main layers with two levels of abstraction:

1. *Decision Layer*: Identifies the current driving situation first and then decide how to coordinate the subsystems actions,
2. *Control Layer*: Transforms the control objectives generated by the Decision Layer to references for each local controller,
3. *Physical Layer*: Contains simply the different actuators and sensors.

It should be noted that the decision layer plays a major role to ensure the overall system safety. It is responsible of two main tasks: classifying the current driving situation and deciding how coordination should be made. For example, in (Vivas-Lopez et al., 2015), a k-means data-based algorithm and a decision logic module based on a set of heuristic rules have been used. However, this architecture does not contain any controller able to specify the behavior of the overall system. The supervisory control configuration still needs additional partitions, hence the *multi-layered architecture*.

4.3 Multi-layered architecture

For more flexibility and more comprehensive control, the functional requirements should rather be separated while ensuring a supervised control. Figure 4.4 illustrates this method.

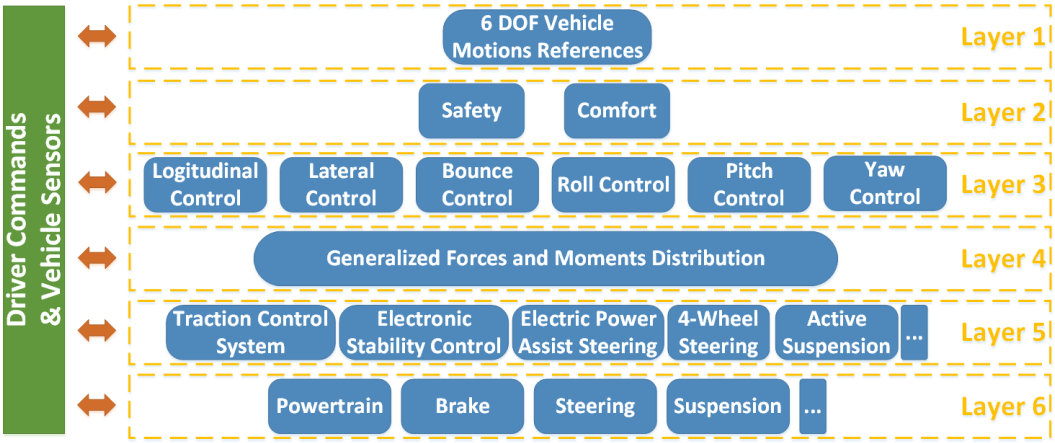

FIGURE 4.4: Multi-layered control architecture (Soltani, 2014).

Each layer has a specific function (Soltani, 2014):

1. Layer 1: Generation of vehicle motion reference. In the general case, this can encompass roll, pitch, yaw, bounce, longitudinal, and lateral velocities. Not only a safe motion is described, but also the level of comfort while ensuring this specific motion is specified. A mathematical definition of qualitative objectives is however difficult to obtain,

2. Layer 2: Decision making on the control mode based on the vehicle state recognition. Mainly, as pointed out in (Soltani, 2014), a choice should be made between providing driver comfort or providing vehicle safety. While safety requirements can be generalized for all vehicles, comfort remains a qualitative objective that depends on the driver preference. In this case, different levels of comfort can be defined and it is up to the driver to choose the vehicle behavior that suits him/her best,

3. Layer 3: Calculation of the generalized forces and moments at the vehicle's CoG through the high-level controllers to follow the reference values. Again, in the general case, the outputs can include the 6 DOF:

$$\begin{bmatrix} F_{x_{tot}} & F_{y_{tot}} & F_{z_{tot}} & M_{x_{tot}} & M_{y_{tot}} & M_{z_{tot}} \end{bmatrix}^t \tag{4.1}$$

   However, due to cost issues, not all vehicles' states can be controlled. In practice, only some of these forces are considered,

4. Layer 4: Distribution of the commands to the available actuators in an optimal or sub-optimal way through CA algorithms. The goal is to achieve the generalized forces required to follow the references. As aerodynamic forces are uncontrollable, only tire forces can be combined to produce the generalized forces. This layer consists then in defining first the relationships between tire forces and forces at the CoG of the vehicle. This is how the "*effectiveness matrix*" is specified. This will be discussed separately in Chapter 9,

5. Layer 5: Control of stand-alone subsystems to follow the commands that comes from the layer 4. Depending on the subsystems, control laws can consist of feedback or only feed-forward control. This relies on the available sensors and the ability to estimate specific variables,

6. Layer 6: Execution of the various operations through smart actuators composed of low-level effectors (e.g. electric motor, hydraulic valve ...etc.) and their own controllers. This part is usually managed by the equipment supplier himself that should satisfy the requirements specified by the car manufacturer.

It seems therefore that this architecture can provide *adaptability*, *extensibility*, and *modularity*. *Fault-tolerance* and *dynamic reconfiguration* can also be ensured by making use of CA algorithms. *Openess* remains a critical issue that should be tackled by negotiations and common sense of car manufacturers, equipment suppliers, and the new actors of the automotive sector.

In the context of this thesis, the fourth layer represents the most important one. In addition, CA algorithms are more suitable in case of a multi-layered architecture (Knobel, Pruckner, and Bünte, 2006), (Shyrokau, Wang, and Lienkamp, 2013), (Soltani, 2014), (Heo et al., 2015). Therefore, a whole Chapter will be dedicated to these algorithms. From a control engineering perspective, the multi-layered architecture can be represented as Figure 4.5 illustrates.

Next, guidelines to design each layer are provided. First of all, as we have adopted a MBD procedure, a precise modeling is required. The modeling of the

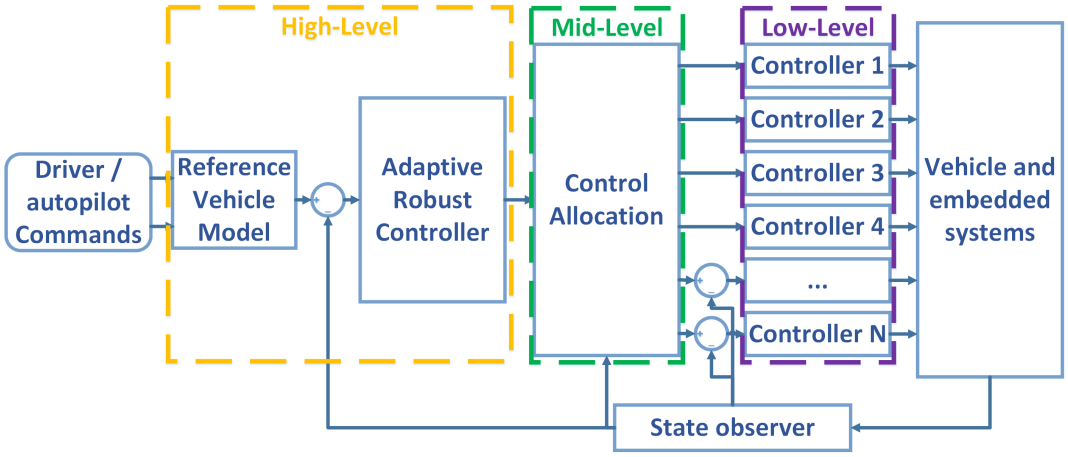

FIGURE 4.5: General block diagram of the integrated vehicle motion control.

vehicle is dissociated from the tire modeling to isolate the nature of couplings apart. The high-level controller will be responsible of managing the vehicle dynamics couplings, and the control allocator will take into account tire couplings for optimal control distribution. Chapter 5 is then focused on vehicle modeling, while Chapter 6 is dedicated to tire modeling. In the optimization procedure of the control allocation, tire forces constraints should be respected. These constraints originate mainly from the friction ellipse concept (Pacejka, 2005). By considering an isotropic friction, we can reduce the problem to a friction "*circle*" estimation. A proposal of the estimation process is provided in Chapter 7. The synthesis of high-level and low-level controllers is described in Chapter 8. We particularly focus on robust control theory. As the upstream approach adds specially a mid-level layer for optimal distribution, Chapter 9 will be focused on control allocation algorithms.

4.4 Contributions

In this chapter, the general structure of the upstream approach have been presented. The description of the control architecture has been made similar to Chapter 3 so the reader can easily compare both approaches. Along the same lines as Chapter 3, we propose the Table 4.1 that summarizes the pros and cons of the architectures presented in this chapter.

Our contributions are the elaboration of a general state-of-art regarding systems coordination and the proposition of two easily distinguishable coordination approaches. This enabled us to directly compare two main approaches and determine what could fit best future vehicles. In this context, two papers have been published to compare both approaches and motivate the automotive control community to adopt the upstream approach for future vehicles:

1. M. Kissai, B. Monsuez and A. Tapus, "Current and Future Architectures for Integrated Vehicle Dynamics Control," *2017 12th National Conference on Software and Hardware Architectures for Robots Control (SHARC17)* Toulouse, 2017. URL: https://sharc2017.sciencesconf.org/data/pages/SHARC2017_paper_7.pdf.

2. M. Kissai, B. Monsuez and A. Tapus, "Review of integrated vehicle dynamics control architectures," *2017 European Conference on Mobile Robots (ECMR)*, Paris, 2017, pp. 1-8. DOI: 10.1109/ECMR.2017.8098687.

TABLE 4.1: Pros and cons of upstream architectures.

Approach	Pros	Cons
Centralized Control	- Ease to ensure the stability/performance of the overall system.	- Neither flexible nor extensible, - Fault-tolerance difficult to conceive, , - No intermediate layers ensuring the internal stability.
Supervisory Control	- Flexible and extensible, - Fault-tolerant, - Modular,	- No high-level control to specify the overall behavior, - No intermediate layers ensure the internal stability.
Multi-Layered Architecture	- Additional flexibility: the control strategy is split to ensure the internal stability, - Modular and extensible, - Fault-tolerant, - High-level control to specify the overall behavior.	- Need for interfaces change, - Openness problem is more concerning.

5 Global Vehicle Modelling

Unlike the downstream approach that relies on simplified vehicle models, here a global four-wheeled vehicle model needs to be developed. We particularly put the spotlight on the vehicle's states internal couplings. These couplings may lead to interactions between subsystems, which may result in conflicts in some cases. For a proper construction of vehicle motion equations, we adopt the ISO 8855-2011 shown in Figure 5.1.

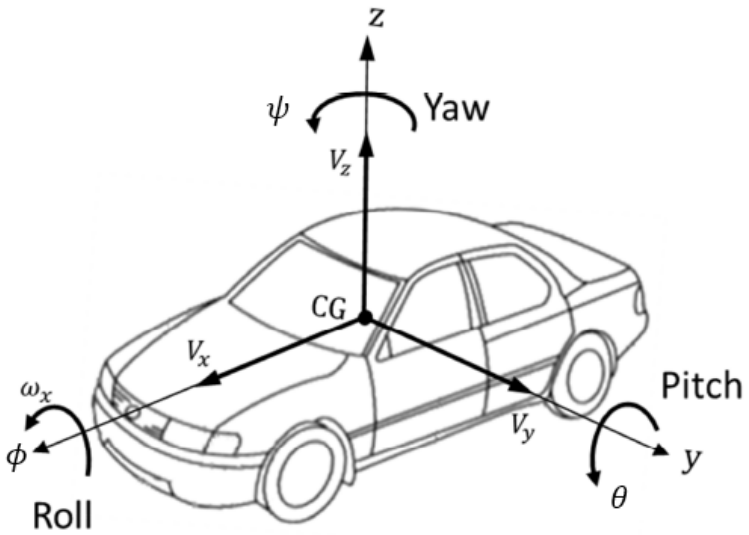

FIGURE 5.1: Vehicle Axis System (ISO 8855-2011).

5.1 Multi-body approach

In order to take into account the dynamic couplings, the vertical load transfer, the influence of suspensions and so on, the vehicle will be broken down into two supposedly undeformable masses: the **sprung mass**[1], and the **unsprung mass**[2], as Figure 5.2 shows.

In addition, to take into account the differences between the influence of the front axle and the rear axle (especially for a 4WS vehicle), the unsprung mass is also decomposed into two supposedly undeformable masses. We then have $\Sigma = S_s + S_{uf} + S_{ur}$, with:

- Σ : the overall vehicle of a mass M and a CoG G,
- S_s : the sprung mass of a mass M_s and a CoG G_s,

[1] Includes the vehicle body, engine, passengers and so on.
[2] Includes the wheels, suspensions, brakes and so on.

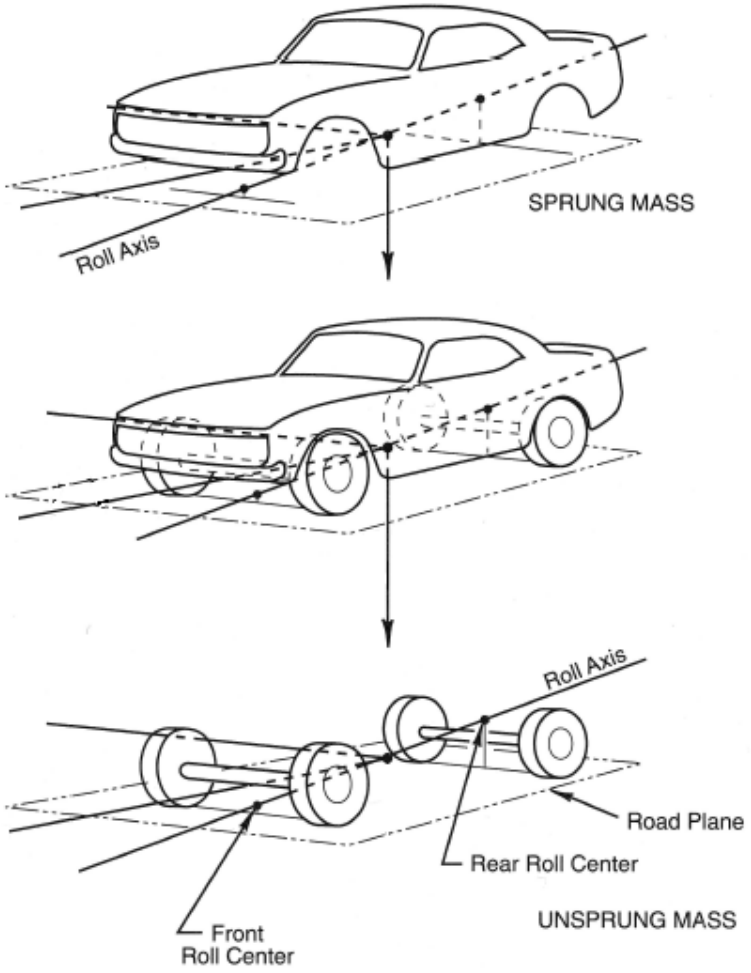

FIGURE 5.2: The sprung and unsprung masses decomposition.

- S_{uf} : the front unsprung mass of a mass M_{uf} and a CoG G_{uf},
- S_{ur} : the rear unsprung mass of a mass M_{ur} and a CoG G_{ur}.

5.2 Vehicle dynamics

The dynamic torsor of the vehicle at the G point is defined as follows:

$$\left\{\mathcal{D}\left(\Sigma/\mathcal{R}_g\right)\right\}_G = \left\{ \begin{array}{c} M\vec{\Gamma}\left(G/\mathcal{R}_g\right) \\ \vec{\delta}\left(G,\Sigma/\mathcal{R}_g\right) = \int_{\forall P\in\Sigma} \overrightarrow{GP} \wedge \vec{\Gamma}\left(P/\mathcal{R}_g\right) dm \end{array} \right\}_G \tag{5.1}$$

With:

- $\mathcal{R}_g$: the inertial frame of reference,
- $\vec{\Gamma}$: the acceleration vector,
- $\vec{\delta}$: the dynamic moment.

The exterior contact efforts torsor is defined as:

$$\left\{\mathcal{A}\left(\overline{\Sigma}\rightarrow\Sigma\right)\right\}_G=\left\{\begin{array}{c}\vec{F}\left(\overline{\Sigma}\rightarrow\Sigma\right)\\ \vec{M}\left(G,\overline{\Sigma}\rightarrow\Sigma\right)\end{array}\right\}_G \tag{5.2}$$

With:

- $\overline{\Sigma}$: the complement of the system Σ,
- $\vec{F}$: the exterior efforts vector,
- $\vec{M}$: the exterior efforts moment vector.

The generalization of the fundamental law of dynamics is then (Pommier and Berthaud, 2010):

$$\left\{\mathcal{D}\left(\Sigma/\mathcal{R}_g\right)\right\}_G=\left\{\mathcal{A}\left(\overline{\Sigma}\rightarrow\Sigma\right)\right\}_G \tag{5.3}$$

This gives two fundamentals laws:

- The dynamic resultant theorem (linear motion):

$$M\vec{\Gamma}\left(G/\mathcal{R}_g\right)=\vec{F}\left(\overline{\Sigma}\rightarrow\Sigma\right) \tag{5.4}$$

- The dynamic moment theorem (angular motion):

$$\vec{\delta}\left(G,\Sigma/\mathcal{R}_g\right)=\vec{M}\left(G,\overline{\Sigma}\rightarrow\Sigma\right) \tag{5.5}$$

Moreover, the decomposition approach adopted allows us to partition the calculations using the torsor's properties:

$$\left\{\mathcal{D}\left(\Sigma/\mathcal{R}_g\right)\right\}_G=\left\{\mathcal{D}\left(S_s/\mathcal{R}_g\right)\right\}_G+\left\{\mathcal{D}\left(S_{uf}/\mathcal{R}_g\right)\right\}_G+\left\{\mathcal{D}\left(S_{ur}/\mathcal{R}_g\right)\right\}_G \tag{5.6}$$

5.2.1 Dynamic torsor calculation

Linear equations of motion

Because the CoG if the sprung mass can move with respect to the unsprung mass, it is simpler to start establishing the equations of motion by considering a fixed point (Noxon, 2012). Here, we start the calculation by considering the roll center that we note O. The velocity of this point is noted:

$$\vec{V}\left(O/\mathcal{R}_g\right)=V_{O_x}\vec{i}+V_{O_y}\vec{j} \tag{5.7}$$

With $\vec{i}$ and $\vec{j}$ are the unit vectors of the chassis frame in the longitudinal and lateral direction respectively.

Because the chassis frame moves with respect to the inertial frame, and because the unsprung mass is not subject to neither the roll nor the pitch motions, we have:

$$\begin{aligned}\vec{\Gamma}\left(O/\mathcal{R}_g\right)&=\left|\begin{array}{c}\dot{V}_{O_x}\\ \dot{V}_{O_y}\\ 0\end{array}\right|+\left|\begin{array}{c}0\\ 0\\ \dot{\psi}\end{array}\right|\wedge\left|\begin{array}{c}V_{O_x}\\ V_{O_y}\\ 0\end{array}\right|\\ &=\left(\dot{V}_{O_x}-\dot{\psi}V_{O_y}\right)\vec{i}+\left(\dot{V}_{O_y}+\dot{\psi}V_{O_x}\right)\vec{j}\end{aligned} \tag{5.8}$$

The same procedure can be applied to the points G_s, G_{uf} and G_{ur}. For the front unsprung mass, we get:

$$\begin{aligned}\vec{V}\left(G_{uf}/\mathcal{R}_g\right) &= \left|\begin{array}{c} V_{O_x} \\ V_{O_y} \\ 0 \end{array}\right| + \left|\begin{array}{c} 0 \\ 0 \\ \dot{\psi} \end{array}\right| \wedge \left|\begin{array}{c} l_f \\ 0 \\ h_f \end{array}\right| \\ &= V_{O_x}\vec{i} + \left(\dot{V}_{O_y} + \dot{\psi} l_f\right)\vec{j}\end{aligned} \tag{5.9}$$

With h_f is the vertical distance between O and G_{uf}. Regarding the acceleration:

$$\begin{aligned}\vec{\Gamma}\left(G_{uf}/\mathcal{R}_g\right) &= \left.\frac{d\vec{V}\left(G_{uf}/\mathcal{R}_g\right)}{dt}\right|_{\mathcal{R}_g} \\ &= \vec{\Gamma}\left(O/\mathcal{R}_g\right) + \left|\begin{array}{c} 0 \\ 0 \\ \ddot{\psi} \end{array}\right| \wedge \left|\begin{array}{c} l_f \\ 0 \\ h_f \end{array}\right| + \left|\begin{array}{c} 0 \\ 0 \\ \dot{\psi} \end{array}\right| \wedge \left(\left|\begin{array}{c} 0 \\ 0 \\ \dot{\psi} \end{array}\right| \wedge \left|\begin{array}{c} l_f \\ 0 \\ h_f \end{array}\right|\right) \\ &= \left(\dot{V}_{O_x} - \dot{\psi} V_{O_y} - l_f\dot{\psi}^2\right)\vec{i} + \left(\dot{V}_{O_y} + \dot{\psi} V_{O_x} + l_f\ddot{\psi}\right)\vec{j}\end{aligned} \tag{5.10}$$

In the same way, we find for the rear unsprung mass:

$$\begin{cases}\vec{V}\left(G_{ur}/\mathcal{R}_g\right) = V_{O_x}\vec{i} + \left(V_{O_y} - \dot{\psi} l_r\right)\vec{j} \\ \vec{\Gamma}\left(G_{ur}/\mathcal{R}_g\right) = \left(\dot{V}_{O_x} - \dot{\psi} V_{O_y} + l_r\dot{\psi}^2\right)\vec{i} + \left(\dot{V}_{O_y} + \dot{\psi} V_{O_x} - l_r\ddot{\psi}\right)\vec{j}\end{cases} \tag{5.11}$$

Regarding the sprung mass, the calculation is slightly more complicated as the vehicle's body turns with respect to the unsprung mass. Roll and pitch angles appear noted respectively ϕ and θ. The relationship between the vehicle's body frame and the chassis frame is:

$$\begin{pmatrix}\vec{i}_s \\ \vec{j}_s \\ \vec{k}_s\end{pmatrix} = \begin{pmatrix}\cos\theta & 0 & -\sin\theta \\ \sin\phi\sin\theta & \cos\phi & \sin\phi\cos\theta \\ \cos\phi\sin\theta & -\sin\phi & \cos\phi\cos\theta\end{pmatrix}\begin{pmatrix}\vec{i} \\ \vec{j} \\ \vec{k}\end{pmatrix} \tag{5.12}$$

We then obtain:

$$\vec{V}\left(G_s/\mathcal{R}_g\right) = \left|\begin{array}{c} V_{O_x} - \dot{\theta}\left(l_s\sin\theta + h_s\cos\phi\cos\theta\right) + \dot{\phi} h_s\sin\phi\sin\theta - \dot{\psi} h_s\sin\phi \\ V_{O_y} + \dot{\phi} h_s\cos\phi + \dot{\psi}\left(l_s\cos\theta - h_s\cos\phi\sin\theta\right) \\ \dot{\theta}\left(l_s\cos\theta - h_s\cos\phi\sin\theta\right) - \dot{\phi} h_s\sin\phi\cos\theta \end{array}\right| \tag{5.13}$$

With l_s and h_s are the horizontal and vertical distances between G_s and O respectively.

However, due to the transformation in equation (5.12), the acceleration equations obtained are very large to express. Nevertheless, we can propose at this point several simplifications. We suppose relatively small values of the roll and pitch angles and angular velocities with respect to yaw dynamics. This gives:

$$\left\{\begin{array}{cccc} \sin\phi \approx \phi & \cos\phi \approx 1 & \sin\theta \approx \theta & \cos\theta \approx 1 \\ \phi\theta \approx 0 & \dot{\phi}\dot{\theta} \approx 0 & \dot{\phi}^2 \approx 0 & \dot{\theta}^2 \approx 0 \end{array}\right\} \tag{5.14}$$

In addition, to be able to apply the dynamic resultant theorem (5.4), we have to bring the calculation to a single point: G. To do so, we make use of the definition of the

center of mass:

$$\overrightarrow{OG} = \frac{\sum_i m_i \overrightarrow{OG_i}}{\sum_i m_i} \tag{5.15}$$

Therefore, with the simplifications in (5.14):

$$\begin{aligned} M\vec{\Gamma}\left(G/\mathcal{R}_g\right) &= M_s\vec{\Gamma}\left(G_s/\mathcal{R}_g\right) + M_{uf}\vec{\Gamma}\left(G_{uf}/\mathcal{R}_g\right) + M_{ur}\vec{\Gamma}\left(G_{ur}/\mathcal{R}_g\right) \\ &= \left| \begin{array}{c} M\left(\dot{V}_{O_x} - \dot{\psi}V_{O_y}\right) - \ddot{\theta}M_s\left(l_s\theta + h_s\right) - \ddot{\psi}M_s h_s\phi + \dot{\psi}^2 M h_g\theta - 2\dot{\phi}\dot{\psi}M_s h_s \\ M\left(\dot{V}_{O_y} + \dot{\psi}V_{O_x}\right) + \ddot{\phi}M_s h_s - \ddot{\psi}M h_g\theta - \dot{\psi}^2 M_s h_s\phi - 2\dot{\theta}\dot{\psi}M_s\left(l_s\theta + h_s\right) \\ \ddot{\theta}M_s\left(l_s - h_s\theta\right) - \ddot{\phi}M_s h_s\phi \end{array} \right. \end{aligned} \tag{5.16}$$

With h_g is the horizontal distance between O and G.

Angular equations of motion

The dynamic moment, defined in any point A, is deduced from the "angular moment" noted σ using the definition (Pommier and Berthaud, 2010):

$$\vec{\delta}\left(A, S/\mathcal{R}_g\right) = \left.\frac{d\vec{\sigma}\left(A, S/\mathcal{R}_g\right)}{dt}\right|_{\mathcal{R}_g} + M\vec{V}\left(A/\mathcal{R}_g\right) \wedge \vec{V}\left(G/\mathcal{R}_g\right) \tag{5.17}$$

By choosing $A = G$, this definition is simplified into:

$$\vec{\delta}\left(G, \Sigma/\mathcal{R}_g\right) = \left.\frac{d\vec{\sigma}\left(G, \Sigma/\mathcal{R}_g\right)}{dt}\right|_{\mathcal{R}_g} \tag{5.18}$$

Again, we calculate the angular moment with respect to the reference point O and for each undeformable mass apart. The definition of the angular moment applied to the front unsprung mass is as follows (Pommier and Berthaud, 2010):

$$\vec{\sigma}\left(O, S_{uf}/\mathcal{R}_g\right) = M_{uf}\overrightarrow{OG_{uf}} \wedge \vec{V}\left(O/\mathcal{R}_g\right) + \overline{I_{uf}}\left(O, S_{uf}\right).\vec{\Omega}_c \tag{5.19}$$

Where I_{uf} is the inertia tonsor of the mass S_{uf}. Its definition applied to any vector $\vec{u}$ at the point O is:

$$\overline{I_{uf}}\left(O, S_{uf}\right).\vec{u} = -\int_{P\in S_{uf}} \left[\overrightarrow{OP} \wedge \left(\overrightarrow{OP} \wedge \vec{u}\right)\right] dm \tag{5.20}$$

The vector $\overrightarrow{\Omega_c}$ is the angular velocity vector, which in this case contains only the yaw rate.

Using the theorem of Huygens-Steiner (Pommier and Berthaud, 2010), we obtain:

$$\overline{I_{uf}}\left(O, S_{uf}\right) = \begin{pmatrix} I_{x_{uf}} + M_{uf}h_{uf}^2 & 0 & -I_{xz_{uf}} + M_{uf}l_f h_{uf} \\ 0 & I_{y_{uf}} + M_{uf}\left(l_f^2 + h_{uf}^2\right) & 0 \\ -I_{xz_{uf}} + M_{uf}l_f h_{uf} & 0 & I_{z_{uf}} + M_{uf}l_f^2 \end{pmatrix} \tag{5.21}$$

With $I_{x_{uf}}$, $I_{y_{uf}}$, and $I_{z_{uf}}$ are the inertia moment in the longitudinal, lateral, and vertical direction with respect to the point G_{uf} respectively. The zeros are due to the fact that S_{uf} is symmetric with respect to the plan $\left(G_{uf}, x, z\right)$. The additional terms are due to the theorem of Huygens-Steiner and the fact that the expressions have been brought

to the point O. We finally get:

$$\vec{\sigma}\left(O, S_{uf}/\mathcal{R}_g\right) = \left| \begin{array}{c} M_{uf}h_{uf}\left(V_{O_y} + l_f\dot{\psi}\right) - I_{xzuf}\dot{\psi} \\ -M_{uf}h_{uf}V_{O_x} \\ M_{uf}l_f\left(V_{O_y} + l_f\dot{\psi}\right) + I_{zuf}\dot{\psi} \end{array} \right. \tag{5.22}$$

Using the same procedure, we can find:

$$\vec{\sigma}\left(O, S_{ur}/\mathcal{R}_g\right) = \left| \begin{array}{c} M_{ur}h_{ur}\left(V_{O_y} - l_r\dot{\psi}\right) - I_{xzur}\dot{\psi} \\ -M_{ur}h_{ur}V_{O_x} \\ -M_{ur}l_r\left(V_{O_y} - l_r\dot{\psi}\right) + I_{zur}\dot{\psi} \end{array} \right. \tag{5.23}$$

For the sprung mass, the equations are more complicated because of the relationship (5.12) and because the angular velocity vector is more sophisticated:

$$\vec{\Omega}\left(S_s/\mathcal{R}_c\right) = \dot{\phi}\,\vec{i}_s + \dot{\theta}\,\vec{j}_s + \dot{\psi}\,\vec{k} \tag{5.24}$$

Where $\mathcal{R}_c$ is the vehicle's body frame. In a lateral acceleration, the pitch axis is inclined. The same remark stands for the roll axis in case of a longitudinal acceleration. The yaw axis remains the same. We then have:

$$\vec{\Omega}\left(S_s/\mathcal{R}_g\right) = \left| \begin{array}{c} \dot{\phi}\cos\theta + \dot{\theta}\sin\phi\sin\theta \\ \dot{\theta}\cos\phi \\ -\dot{\phi}\sin\theta + \dot{\theta}\sin\phi\cos\theta + \dot{\psi} \end{array} \right. \tag{5.25}$$

The expression of the angular moment in this case is too long and its derivative (to obtain the dynamic angular moment) is even more. The same simplifications as in (5.14) can be applied to moderate the results.

In addition, we should again bring the expressions to the point G:

$$\begin{cases} \vec{\sigma}\left(G, S_s/\mathcal{R}_g\right) = \vec{\sigma}\left(O, S_s/\mathcal{R}_g\right) + M_s\vec{V}\left(O/\mathcal{R}_g\right) \wedge \overrightarrow{OG} & (5.26) \\ \vec{\sigma}\left(G, S_{uf}/\mathcal{R}_g\right) = \vec{\sigma}\left(O, S_{uf}/\mathcal{R}_g\right) + M_{uf}\vec{V}\left(O/\mathcal{R}_g\right) \wedge \overrightarrow{OG} & (5.27) \\ \vec{\sigma}\left(G, S_{ur}/\mathcal{R}_g\right) = \vec{\sigma}\left(O, S_{ur}/\mathcal{R}_g\right) + M_{ur}\vec{V}\left(O/\mathcal{R}_g\right) \wedge \overrightarrow{OG} & (5.28) \end{cases}$$

And using again the torsor properties:

$$\vec{\sigma}\left(G, \Sigma/\mathcal{R}_g\right) = \vec{\sigma}\left(G, S_s/\mathcal{R}_g\right) + \vec{\sigma}\left(G, S_{uf}/\mathcal{R}_g\right) + \vec{\sigma}\left(G, S_{ur}/\mathcal{R}_g\right) \tag{5.29}$$

Noting I_{i_k} the inertia moment in the direction i of the mass S_k with respect to its CoG, and I_{ij_k} the inertia moment in the plan ij of the mass S_k with respect to its CoG, we obtain the dynamic moment at the point G:

$$
\begin{cases}
\delta_{G_x} = \ddot{\phi}\left(I_{x_s} + I_{xz_s}\theta + M_s h_s^2\right) + \dot{\phi}\dot{\psi}M_s h_s \phi\left(2h_s\theta - l_s\right) \\
\quad + \ddot{\theta}\phi\left[I_{x_s}\theta - I_{xz_s} + M_s l_s\left(l_s\theta + h_s\right)\right] \\
\quad + \dot{\theta}\dot{\psi}M_s\left[\left(l_s^2 - h_s^2\right) - 4l_s h_s\theta\right] \\
\quad - \ddot{\psi}\left\{I_{xz_s} + I_{xz_{uf}} + I_{xz_{ur}} - M_{uf}h_{uf}l_f + M_{ur}h_{ur}l_r - M_s\left[\left(l_s 2 - h_s^2\right)\theta + l_s h_s\right]\right\}
\end{cases} \tag{5.30}
$$

$$
\delta_{G_y} = \ddot{\theta}\left(I_{y_s} + M_s l_s^2\right) \tag{5.31}
$$

$$
\begin{cases}
\delta_{G_z} = -\ddot{\phi}\left[I_{z_s}\theta + I_{xz_s} - M_s h_s\left(l_s - h_s\theta\right)\right] + \ddot{\theta}\phi\left[I_{z_s} - I_{xz_s}\theta + M_s\left(l_s^2 - l_s h_s\theta\right)\right] \\
\quad + 2\dot{\phi}\dot{\psi}M_s h_s\phi\left(l_s\theta + h_s\right) - \dot{\theta}\dot{\psi}M_s\left[2\theta\left(l_s^2 - h_s^2\right) + 2l_s h_s\right] \\
\quad + \ddot{\psi}\left[I_{z_s} + I_{z_{uf}} + I_{z_{ur}} + M_{uf}l_f^2 + M_{ur}l_r^2 + M_s\left(l_s - h_s\theta\right)^2\right]
\end{cases} \tag{5.32}
$$

5.2.2 Exterior forces torsor calculation

This torsor shows the influence of the exterior forces, for example tire forces, on the chosen isolated system. In order to show the influence of the suspensions, we should isolate only the sprung mass where the suspension forces are at the exterior of the studied system. Let us consider the Figure 5.3.

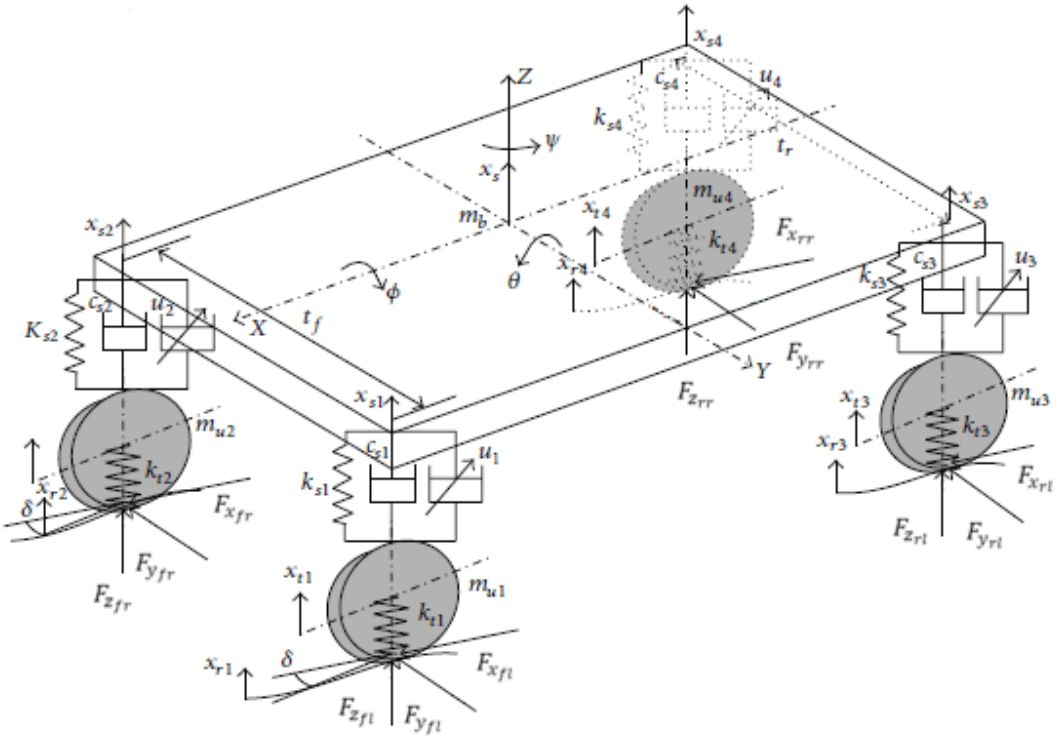

FIGURE 5.3: 14-DOF vehicle dynamic model (adapted from (Zhao, Li, and Qu, 2014)).

Here we can see that if we consider the overall system Σ, the exterior forces are:

- $F_{x_{i,j}}$: $i - j$ longitudinal tire force[3],

[3]Where "i" is front or rear, and "j" is right or left.

- $F_{y_{i,j}}$: $i-j$ lateral tire force,
- $F_{z_{i,j}}$: vertical load on the $i-j$ tire, with $F_{z_{i,j}} = k_{t_i}\left(x_{r_{i,j}} - x_{t_{i,j}}\right)$, $k_{t_{i,j}}$ being the vertical stiffness of tires, $x_{t_{i,j}}$ the vertical travel of tires, and $x_{r_{i,j}}$ is the vertical profile of the road,
- $\vec{P}$: the vehicle's weight.

Notice that we do not take into account the aerodynamic forces for example. These forces are not controllable and would be considered as disturbances. They should be rejected by the robust control strategy. Next, we apply the fundamental law of dynamics (5.3) on the overall system Σ first.

The dynamic resultant theorem

For the linear motion, we apply the equation (5.4) using the formulas obtained in equation (5.16):

$$\begin{cases} M\left(\dot{V}_{O_x} - \dot{\psi}V_{O_y}\right) - \ddot{\theta}M_s\left(l_s\theta + h_s\right) - \ddot{\psi}M_s h_s\phi + \dot{\psi}^2 M h_g\theta - 2\dot{\phi}\dot{\psi}M_s h_s \\ \qquad = \left(F_{x_{f,l}} + F_{x_{f,r}}\right)\cos\delta_f + \left(F_{x_{r,l}} + F_{x_{r,r}}\right)\cos\delta_r \qquad (5.33) \\ \qquad - \left(F_{y_{f,l}} + F_{y_{f,r}}\right)\sin\delta_f - \left(F_{y_{r,l}} + F_{y_{r,r}}\right)\sin\delta_r \\ M\left(\dot{V}_{O_y} + \dot{\psi}V_{O_x}\right) + \ddot{\phi}M_s h_s - \ddot{\psi}M h_g\theta - \dot{\psi}^2 M_s h_s\phi - 2\dot{\theta}\dot{\psi}M_s\left(l_s\theta + h_s\right) \\ \qquad = \left(F_{y_{f,l}} + F_{y_{f,r}}\right)\cos\delta_f + \left(F_{y_{r,l}} + F_{y_{r,r}}\right)\cos\delta_r \qquad (5.34) \\ \qquad + \left(F_{x_{f,l}} + F_{x_{f,r}}\right)\sin\delta_f + \left(F_{x_{r,l}} + F_{x_{r,r}}\right)\sin\delta_r \\ \ddot{\theta}M_s\left(l_s - h_s\theta\right) - \ddot{\phi}M_s h_s\phi = Mg - F_{z_{f,l}} - F_{z_{f,r}} - F_{z_{r,l}} - F_{z_{r,r}} \qquad (5.35) \end{cases}$$

With g is the standard gravity.

The dynamic moment theorem

Let us consider:

- t_f, t_r : the front and rear track of the vehicle respectively,
- h_O : the height of the center of the roll/pitch[4] axis,
- $\sum M_z$: the influence of the self-aligning moments of the tires.

We apply the equation (5.5) using the formulas obtained in equations (5.30)-(5.32) to calculate the angular motion:

[4]Supposed the same in this thesis for further simplifications.

$$\begin{cases} \delta_{G_x} = Mgh_g\phi + \dfrac{t_f}{2}\left(F_{z_{f,l}} - F_{z_{f,r}}\right) + \dfrac{t_r}{2}\left(F_{z_{r,l}} - F_{z_{r,r}}\right) \\ \quad - \left(h_O + h_g\right)\left[\left(F_{y_{f,l}} + F_{y_{f,r}}\right)\cos\delta_f + \left(F_{y_{r,l}} + F_{y_{r,r}}\right)\cos\delta_r\right] \\ \quad - \left(h_O + h_g\right)\left[\left(F_{x_{f,l}} + F_{x_{f,r}}\right)\sin\delta_f + \left(F_{x_{r,l}} + F_{x_{r,r}}\right)\sin\delta_r\right] \end{cases} \tag{5.36}$$

$$\begin{cases} \delta_{G_y} = Mgh_g\theta + l_f\left(F_{z_{f,l}} + F_{z_{f,r}}\right) - l_r\left(F_{z_{r,l}} + F_{z_{r,r}}\right) \\ \quad + \left(h_O + h_g\right)\left[\left(F_{x_{f,l}} + F_{x_{f,r}}\right)\cos\delta_f + \left(F_{x_{r,l}} + F_{x_{r,r}}\right)\cos\delta_r\right] \\ \quad - \left(h_O + h_g\right)\left[\left(F_{y_{f,l}} + F_{y_{f,r}}\right)\sin\delta_f + \left(F_{y_{r,l}} + F_{y_{r,r}}\right)\sin\delta_r\right] \end{cases} \tag{5.37}$$

$$\begin{cases} \delta_{G_z} = l_f\left[\left(F_{y_{f,l}} + F_{y_{f,r}}\right)\cos\delta_f + \left(F_{x_{f,l}} + F_{x_{f,r}}\right)\sin\delta_f\right] \\ \quad - l_r\left[\left(F_{y_{r,l}} + F_{y_{r,r}}\right)\cos\delta_r + \left(F_{x_{r,l}} + F_{x_{r,r}}\right)\sin\delta_r\right] \\ \quad + \dfrac{t_f}{2}\left[\left(F_{x_{f,l}} - F_{x_{f,r}}\right)\cos\delta_f - \left(F_{y_{f,l}} - F_{y_{f,r}}\right)\sin\delta_f\right] \\ \quad + \dfrac{t_r}{2}\left[\left(F_{x_{r,l}} - F_{x_{r,r}}\right)\cos\delta_r - \left(F_{y_{r,l}} - F_{y_{r,r}}\right)\sin\delta_r\right] + \sum M_z \end{cases} \tag{5.38}$$

5.2.3 The sprung mass dynamics

Regarding roll dynamics, pitch dynamics and the pure vertical dynamics, the vehicle's body should be isolated. This enables the introduction of the suspension forces. In case of active suspensions, as it is the case in Figure 5.3, we have (Zhao, Li, and Qu, 2014):

$$\begin{cases} F_{s_{f,l}} = k_{s_{f,l}}\left(x_{t_{f,l}} - x_{s_{f,l}}\right) + c_{s_{f,l}}\left(\dot{z}_{p_{f,l}} - \dot{z}_{s_{f,l}}\right) - \dfrac{k_{\phi_f}}{2t_f}\left(\phi - \dfrac{x_{t_{f,l}} - x_{s_{f,l}}}{2t_f}\right) + u_{f,l} \end{cases} \tag{5.39}$$

$$\begin{cases} F_{s_{f,r}} = k_{s_{f,r}}\left(x_{t_{f,r}} - x_{s_{f,r}}\right) + c_{s_{f,r}}\left(\dot{z}_{p_{f,r}} - \dot{z}_{s_{f,r}}\right) + \dfrac{k_{\phi_f}}{2t_f}\left(\phi - \dfrac{x_{t_{f,r}} - x_{s_{f,r}}}{2t_f}\right) + u_{f,r} \end{cases} \tag{5.40}$$

$$\begin{cases} F_{s_{r,l}} = k_{s_{r,l}}\left(x_{t_{r,l}} - x_{s_{r,l}}\right) + c_{s_{r,l}}\left(\dot{z}_{p_{r,l}} - \dot{z}_{s_{r,l}}\right) + \dfrac{k_{\phi_r}}{2t_r}\left(\phi - \dfrac{x_{t_{r,l}} - x_{s_{r,l}}}{2t_r}\right) + u_{r,l} \end{cases} \tag{5.41}$$

$$\begin{cases} F_{s_{r,r}} = k_{s_{r,r}}\left(x_{t_{r,r}} - x_{s_{r,r}}\right) + c_{s_{r,r}}\left(\dot{z}_{p_{r,r}} - \dot{z}_{s_{r,r}}\right) - \dfrac{k_{\phi_r}}{2t_r}\left(\phi - \dfrac{x_{t_{r,r}} - x_{s_{r,r}}}{2t_r}\right) + u_{r,r} \end{cases} \tag{5.42}$$

Where:

- $x_{s_{i,j}}$: vertical travel of suspensions,
- $k_{s_{i,j}}$: suspension's stiffness,
- $c_{s_{i,j}}$: suspension's damping,
- k_{ϕ_f}, k_{ϕ_r}: the front and rear anti-roll bars stiffness respectively,
- $u_{s_{i,j}}$: control forces of the active suspensions.

Using again the same theorems (5.4) and (5.5) and the same simplifications in (5.14), we can get:

$$
\begin{cases}
\ddot{\phi}\left(I_{x_s}+I_{xz_s}\theta\right)+\ddot{\theta}\phi\left(I_{x_s}\theta-I_{xz_s}\right)-\ddot{\psi}I_{xz_s}=M_s g h_s\phi+\dfrac{t_f}{2}\left(F_{s_{f,l}}-F_{s2}\right) \\
\qquad\qquad +\dfrac{t_r}{2}\left(F_{s_{r,l}}-F_{s4}\right)-\left(h_O+h_s\right)\left[\left(F_{y_{f,l}}+F_{y_{f,r}}\right)\cos\delta_f+\left(F_{y_{r,l}}+F_{y_{r,r}}\right)\cos\delta_r\right] \\
\qquad\qquad -\left(h_O+h_s\right)\left[\left(F_{x_{f,l}}+F_{x_{f,r}}\right)\sin\delta_f+\left(F_{x_{r,l}}+F_{x_{r,r}}\right)\sin\delta_r\right] \qquad (5.43) \\
\ddot{\theta}I_{y_s}=M_s g h_s\theta+l_f\left(F_{s_{f,l}}+F_{s2}\right)-l_r\left(F_{s_{r,l}}+F_{s4}\right) \\
\quad +\left(h_O+h_s\right)\left[\left(F_{x_{f,l}}+F_{x_{f,r}}\right)\cos\delta_f+\left(F_{x_{r,l}}+F_{x_{r,r}}\right)\cos\delta_r\right] \qquad (5.44) \\
\quad -\left(h_O+h_s\right)\left[\left(F_{y_{f,l}}+F_{y_{f,r}}\right)\sin\delta_f+\left(F_{y_{r,l}}+F_{y_{r,r}}\right)\sin\delta_r\right] \\
M_s\left[\ddot{\theta}\left(l_s-h_s\theta\right)-\ddot{\phi}h_s\phi\right]=M_s g-F_{s_{f,l}}-F_{s_{f,r}}-F_{s_{r,l}}-F_{s_{r,r}} \qquad (5.45)
\end{cases}
$$

5.3 Model simplification and validation

The vehicle equations of motion developed until now are quite heavy but can be used for control strategies validation. However, our aim is to develop an overall vehicle model so we can synthesize the control strategy. This model should be simple enough but not too simple. To validate the vehicle model, we use as a reference a high-fidelity vehicle model provided by Simcenter Amesim®[5] in a black-box[6]. Figure 5.4 illustrates the 15 DOF chassis selected. Nevertheless, Amesim provides an interface to modify the masses and inertias at each wheel axle, approximate localization of car-body points, including the vehicle's CoG ... etc. Complex axle kinematics are used to model the specific joint between sprung and unsprung masses.

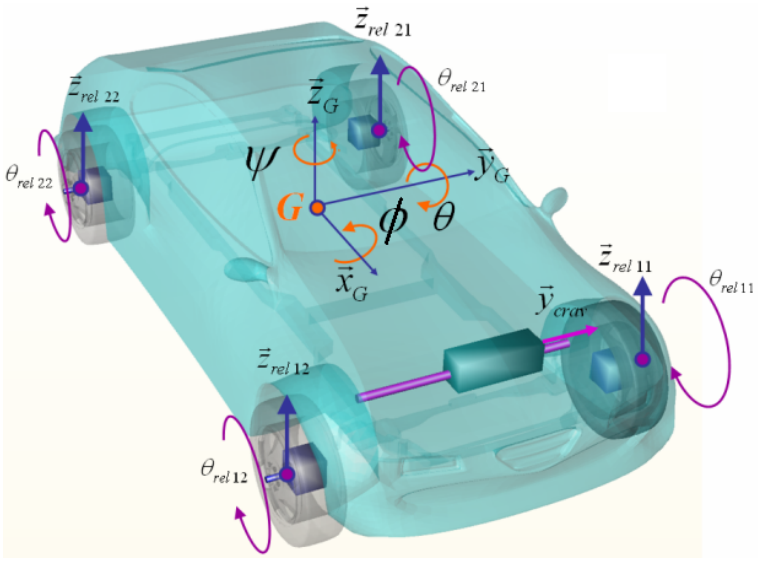

FIGURE 5.4: The 15 DOF chassis of Amesim®.

The procedure is simple. We simulate the high fidelity vehicle model of Amesim® in several scenarios and we compare it with the vehicle model developed in this chapter. We identify the order of magnitude of each term in every equation before

[5] A Siemens PLM Software called previously LMS Imagine.Lab Amesim.
[6] We do not know for sure the equations used for modeling.

summing all the components of the equations presented. Then we just simplify the least influencing terms. For a simulation that covers the excitation of all vehicle dynamics, we selected a 3D road reproduced by Amesim's engineers from a real life race track: the approved International Circuit of Magny-Cours depicted in Figure 5.5.

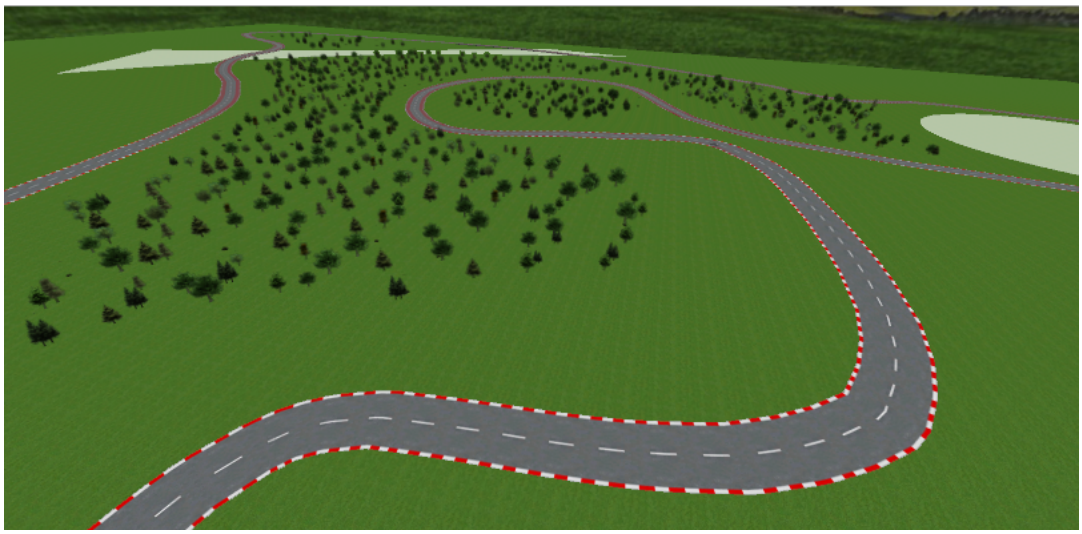

FIGURE 5.5: 3D aspect of the Magny-Cours race track with hills area.

The trajectory tracked at high velocities is illustrated in Figure 5.6.

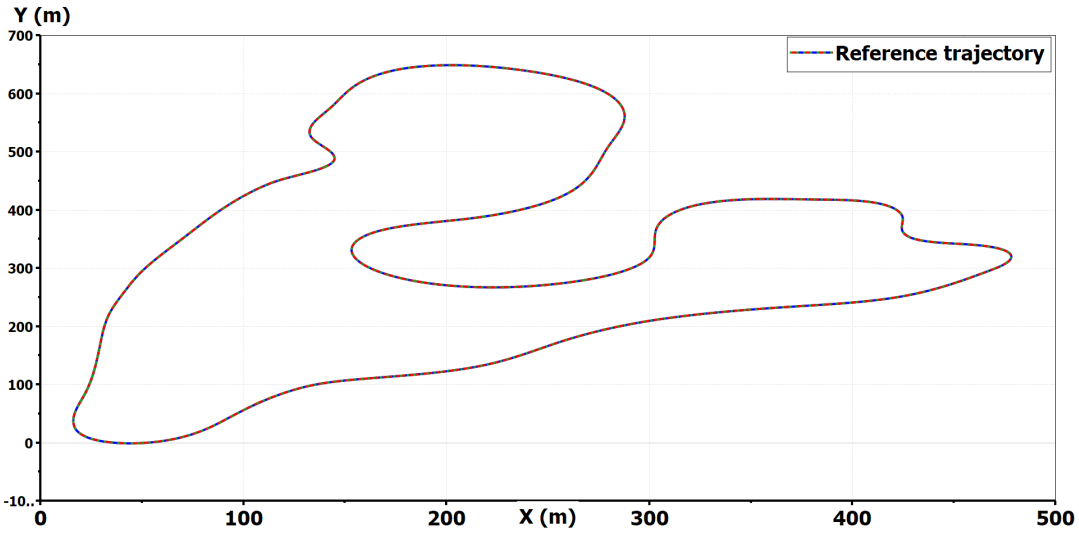

FIGURE 5.6: Magny-Cours trajectory.

After a careful simplification procedure by simulation, we obtained the following state-space representation:

$$
\begin{bmatrix}
1 & 0 & 0 & 0 & 0 & 0 & 0 & 0 \\
0 & 1 & 0 & 0 & 0 & 0 & 0 & 0 \\
0 & 0 & 1 & 0 & 0 & 0 & 0 & 0 \\
0 & 0 & 0 & 1 & 0 & 0 & 0 & 0 \\
0 & 0 & 0 & 0 & 1 & 0 & 0 & 0 \\
0 & 0 & 0 & 0 & 0 & 1 & 0 & 0 \\
\dfrac{\frac{K_p}{g} + M_s h_s}{I_{y_s}} & 0 & 0 & 0 & 0 & 0 & 0 & 1 & 0 \\
\dfrac{M_s h_s}{I_z}\phi & 0 & 0 & 0 & 0 & 0 & 0 & 0 & 1
\end{bmatrix}
\begin{bmatrix} \dot{V}_x \\ \dot{V}_y \\ V_z \\ \dot{V}_z \\ \dot{\phi} \\ \ddot{\phi} \\ \dot{\theta} \\ \ddot{\theta} \\ \ddot{\psi} \end{bmatrix} =
$$

$$
\begin{bmatrix}
0 & 0 & 0 & 0 & 0 & 0 & \frac{M_s}{M}g & 0 & V_y \\
0 & 0 & 0 & 0 & 0 & 0 & 0 & 0 & -V_x \\
0 & 0 & 0 & 1 & 0 & 0 & 0 & 0 & 0 \\
0 & 0 & 0 & 0 & 0 & 0 & 0 & 0 & 0 \\
0 & 0 & 0 & 0 & 0 & 1 & 0 & 0 & 0 \\
0 & 0 & 0 & 0 & -\frac{K_r}{I_{x_s}} & -\frac{C_{s_r}}{I_{x_s}} & 0 & 0 & 0 \\
0 & 0 & 0 & 0 & 0 & 0 & 0 & 1 & 0 \\
0 & 0 & 0 & 0 & 0 & 0 & -\frac{M - M_s}{M}\frac{K_p}{I_{y_s}} & -\frac{C_{s_p}}{I_{y_s}} & 0 \\
0 & 0 & 0 & 0 & 0 & 0 & 0 & 0 & 0
\end{bmatrix}
\begin{bmatrix} V_x \\ V_y \\ z \\ V_z \\ \phi \\ \dot{\phi} \\ \theta \\ \dot{\theta} \\ \dot{\psi} \end{bmatrix}
\tag{5.46}
$$

$$
+
\begin{bmatrix}
\frac{1}{M} & 0 & 0 & 0 & 0 & 0 \\
0 & \frac{1}{M} & 0 & 0 & 0 & 0 \\
0 & 0 & 0 & 0 & 0 & 0 \\
0 & 0 & \frac{1}{M} & 0 & 0 & 0 \\
0 & 0 & 0 & 0 & 0 & 0 \\
0 & 0 & 0 & \frac{1}{I_{x_s}} & 0 & 0 \\
0 & 0 & 0 & 0 & 0 & 0 \\
0 & 0 & 0 & 0 & \frac{1}{I_{y_s}} & 0 \\
0 & 0 & 0 & 0 & 0 & \frac{1}{I_z}
\end{bmatrix}
\begin{bmatrix} F_{x_{tot}} \\ F_{y_{tot}} \\ F_{z_{tot}} \\ M_{x_{tot}} \\ M_{y_{tot}} \\ M_{z_{tot}} \end{bmatrix}
$$

Where:

- z : vertical travel of the sprung mass,
- V_z : vertical velocity of the sprung mass,
- K_r : equivalent overall antiroll bar stiffness,
- C_{s_r} : equivalent overall roll suspension damping,
- K_p : equivalent overall pitch suspension stiffness,
- C_{s_p} : equivalent overall pitch suspension damping,
- I_z : yaw inertia moment of the overall vehicle with respect to its CoG,
- $F_{i_{tot}}$: combination of tire forces projected at the axis "i",
- $M_{i_{tot}}$: combination of moments generated by tire forces with respect to the axis "i".

With:

$$\begin{cases} F_{x_{tot}} = \left(F_{x_{f,l}} + F_{x_{f,r}}\right)\cos\delta_f + \left(F_{x_{r,l}} + F_{x_{r,r}}\right)\cos\delta_r \\ \qquad - \left(F_{y_{f,l}} + F_{y_{f,r}}\right)\sin\delta_f - \left(F_{y_{r,l}} + F_{y_{r,r}}\right)\sin\delta_r & (5.47) \\ F_{y_{tot}} = \left(F_{y_{f,l}} + F_{y_{f,r}}\right)\cos\delta_f + \left(F_{y_{r,l}} + F_{y_{r,r}}\right)\cos\delta_r \\ \qquad + \left(F_{x_{f,l}} + F_{x_{f,r}}\right)\sin\delta_f + \left(F_{x_{r,l}} + F_{x_{r,r}}\right)\sin\delta_r & (5.48) \\ F_{z_{tot}} = F_{z_{f,l}} + F_{z_{f,r}} + F_{z_{r,l}} + F_{z_{r,r}} & (5.49) \\ M_{x_{tot}} = \dfrac{t_f}{2}\left(F_{z_{f,l}} - F_{z_{f,r}}\right) + \dfrac{t_r}{2}\left(F_{z_{r,l}} - F_{z_{r,r}}\right) & (5.50) \\ M_{y_{tot}} = l_f\left(F_{z_{f,l}} + F_{z_{f,r}}\right) - l_r\left(F_{z_{r,l}} + F_{z_{r,r}}\right) & (5.51) \\ M_{z_{tot}} = l_f\left[\left(F_{y_{f,l}} + F_{y_{f,r}}\right)\cos\delta_f + \left(F_{x_{f,l}} + F_{x_{f,r}}\right)\sin\delta_f\right] \\ \qquad - l_r\left[\left(F_{y_{r,l}} + F_{y_{r,r}}\right)\cos\delta_r + \left(F_{x_{r,l}} + F_{x_{r,r}}\right)\sin\delta_r\right] \\ \qquad + \dfrac{t_f}{2}\left[\left(F_{x_{f,l}} - F_{x_{f,r}}\right)\cos\delta_f - \left(F_{y_{f,l}} - F_{y_{f,r}}\right)\sin\delta_f\right] \\ \qquad + \dfrac{t_r}{2}\left[\left(F_{x_{r,l}} - F_{x_{r,r}}\right)\cos\delta_r - \left(F_{y_{r,l}} - F_{y_{r,r}}\right)\sin\delta_r\right] + \sum M_z & (5.52) \end{cases}$$

And:

$$\begin{cases} K_r = K_{\phi_f} + K_{\phi_r} & (5.53) \\ C_{s_r} = 2c_{s_f}\left(\dfrac{t_f}{2}\right)^2 + 2c_{s_r}\left(\dfrac{t_r}{2}\right)^2 & (5.54) \\ K_p = 2k_{s_f}l_f^2 + 2k_{s_r}l_r^2 & (5.55) \\ C_{s_p} = 2c_{s_f}l_f^2 + 2c_{s_r}l_r^2 & (5.56) \end{cases}$$

Where:

- k_{s_f}, k_{s_r} : the front and rear suspension stiffness respectively[7],
- c_{s_f}, c_{s_r} : the front and rear suspension damping respectively.

[7] The front suspensions are alike by design due to the presence of the front steering wheel system. Same remark holds for the rear suspensions.

By inverting the first matrix, we finally get the state-space representation in the standard form:

$$
\begin{cases}
\begin{bmatrix} \dot{V}_x \\ \dot{V}_y \\ \dot{V}_z \\ \dot{V}_z \\ \dot{\phi} \\ \ddot{\phi} \\ \dot{\theta} \\ \ddot{\theta} \\ \ddot{\psi} \end{bmatrix} = \begin{bmatrix} 0 & 0 & 0 & 0 & 0 & 0 & \frac{M_s}{M}g & 0 & V_y \\ 0 & 0 & 0 & 0 & 0 & 0 & 0 & 0 & -V_x \\ 0 & 0 & 0 & 1 & 0 & 0 & 0 & 0 & 0 \\ 0 & 0 & 0 & 0 & 0 & 0 & 0 & 0 & 0 \\ 0 & 0 & 0 & 0 & 0 & 1 & 0 & 0 & 0 \\ 0 & 0 & 0 & 0 & -\frac{K_r}{I_{x_s}} & -\frac{C_{s_r}}{I_{x_s}} & 0 & 0 & 0 \\ 0 & 0 & 0 & 0 & 0 & 0 & 0 & 1 & 0 \\ 0 & 0 & 0 & 0 & 0 & 0 & -\frac{MK_p + M_s^2 h_s g}{MI_{y_s}} & -\frac{C_{s_p}}{I_{y_s}} & 0 \\ 0 & 0 & 0 & 0 & 0 & 0 & -\frac{M_s^2 h_s g}{MI_z}\phi & 0 & 0 \end{bmatrix} \begin{bmatrix} V_x \\ V_y \\ z \\ V_z \\ \phi \\ \dot{\phi} \\ \theta \\ \dot{\theta} \\ \dot{\psi} \end{bmatrix} \\
+ \begin{bmatrix} \frac{1}{M} & 0 & 0 & 0 & 0 & 0 \\ 0 & \frac{1}{M} & 0 & 0 & 0 & 0 \\ 0 & 0 & 0 & 0 & 0 & 0 \\ 0 & 0 & \frac{1}{M} & 0 & 0 & 0 \\ 0 & 0 & 0 & 0 & 0 & 0 \\ 0 & 0 & 0 & \frac{1}{I_{x_s}} & 0 & 0 \\ 0 & 0 & 0 & 0 & 0 & 0 \\ -\frac{M_s h_s}{MI_{y_s}} & 0 & 0 & 0 & \frac{1}{I_{y_s}} & 0 \\ -\frac{M_s h_s}{MI_z}\phi & 0 & 0 & 0 & 0 & \frac{1}{I_z} \end{bmatrix} \begin{bmatrix} F_{x_{tot}} \\ F_{y_{tot}} \\ F_{z_{tot}} \\ M_{x_{tot}} \\ M_{y_{tot}} \\ M_{z_{tot}} \end{bmatrix} \qquad (5.57) \\
\begin{bmatrix} V_x \\ V_y \\ z \\ \phi \\ \theta \\ \dot{\psi} \end{bmatrix} = \begin{bmatrix} 1 & 0 & 0 & 0 & 0 & 0 & 0 & 0 & 0 \\ 0 & 1 & 0 & 0 & 0 & 0 & 0 & 0 & 0 \\ 0 & 0 & 1 & 0 & 0 & 0 & 0 & 0 & 0 \\ 0 & 0 & 0 & 0 & 1 & 0 & 0 & 0 & 0 \\ 0 & 0 & 0 & 0 & 0 & 0 & 1 & 0 & 0 \\ 0 & 0 & 0 & 0 & 0 & 0 & 0 & 0 & 1 \end{bmatrix} \begin{bmatrix} V_x \\ V_y \\ z \\ V_z \\ \phi \\ \dot{\phi} \\ \theta \\ \dot{\theta} \\ \dot{\psi} \end{bmatrix} \qquad (5.58)
\end{cases}
$$

Regarding the validation procedure, we make use of a driver model provided by Simcenter Amesim® and designed using a MPC algorithm to track the Magny-Cours path with an adapted velocity profile. Simulations for this severe maneuver are shown in Figures 5.7-5.12.

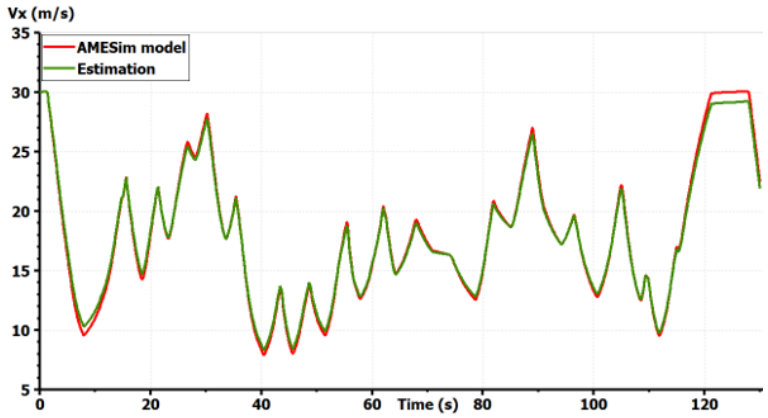

FIGURE 5.7: Validation of the vehicle model: longitudinal speed.

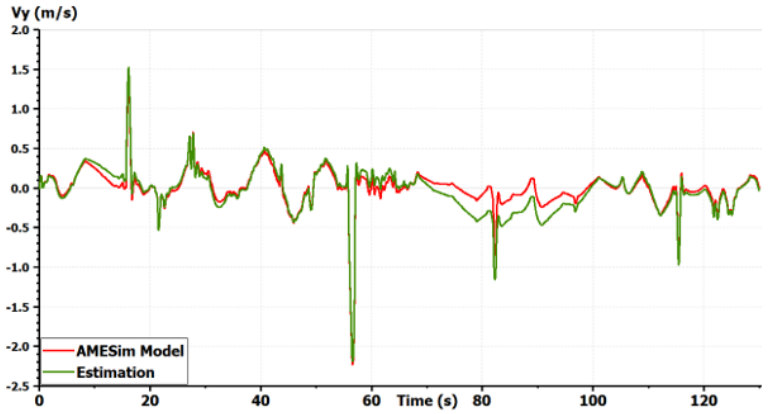

FIGURE 5.8: Validation of the vehicle model: lateral speed.

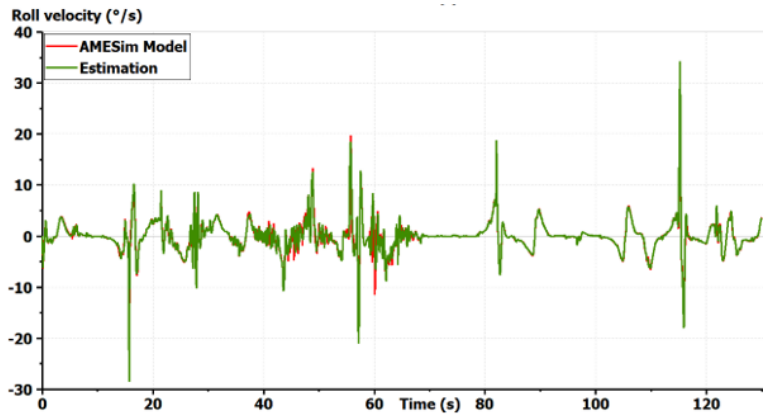

FIGURE 5.10: Validation of the vehicle model: roll velocity.

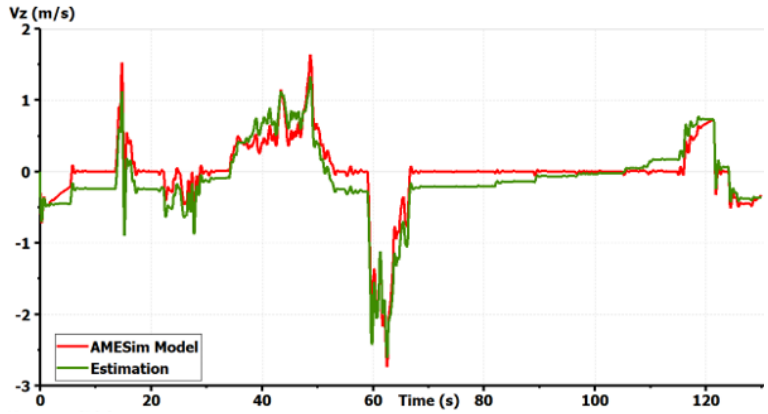

FIGURE 5.9: Validation of the vehicle model: vertical velocity of the sprung mass.

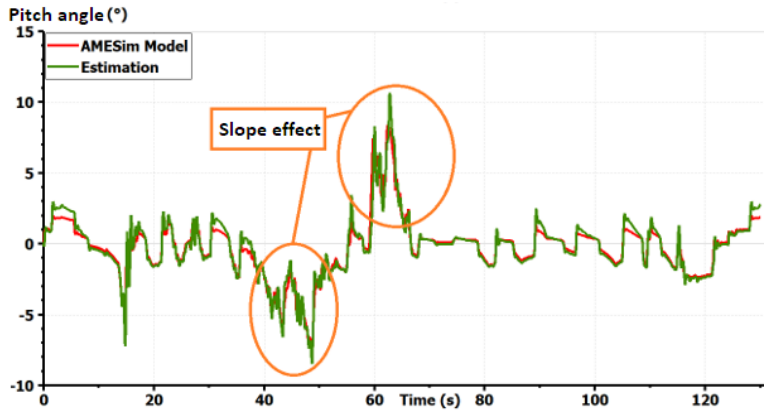

FIGURE 5.11: Validation of the vehicle model: pitch angle taking into account the slopes.

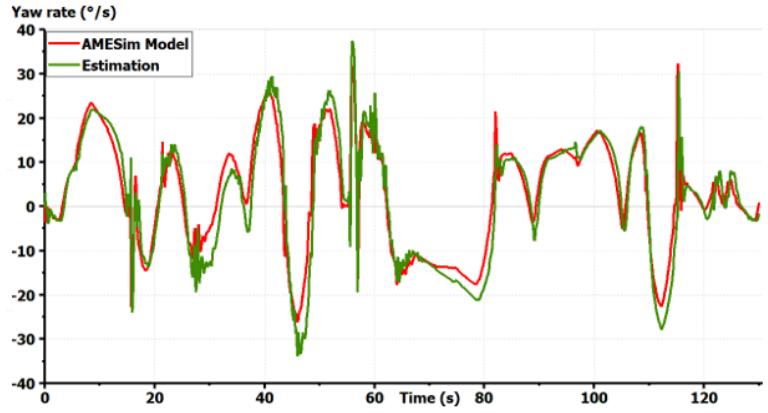

FIGURE 5.12: Validation of the vehicle model: yaw rate.

The model shows good precision for all states in a coupled maneuver. The Root Mean Squared Error (RMSE) of the longitudinal speed is only 0.24, for the pitch angle is 0.01, for the roll speed is 0.012 and so on. The effect of slopes was also taken into account. This model can then be chosen as a starting model for all Global

Chassis Control (GCC) synthesis. It is important to start with a complex full vehicle model and then reduce it while justifying each simplification. Starting with a simplified model, as the bicycle model, could lead to the ignorance of important dynamics and couplings making the control fail. If only the horizontal motion is concerned, vertical dynamics can be simplified in the control synthesis. Only couplings between the remaining states should be studied to justify the shape of the controller. However, the vertical forces applied to the tires should always be taken into account as they modify the potential of each tire to drive, brake or steer the vehicle (Pacejka, 2005).

5.4 Contributions

We reexamined the equations of motion of the vehicle in this chapter. The vehicle has been decomposed in order to use a multi-body approach. By simplifying only the justified terms, we contributed by developing our own vehicle model that can serve to develop high-level controllers for the upstream coordination approach. Both the model and the robust high-level controller synthesis have been published in:

1. M. Kissai, B. Monsuez, A. Tapus, X. Mouton, D. Martinez, "Gain-Scheduled H_∞ for Vehicle High-Level Motion Control", in *Proceedings of the 6th International Conference on Control, Mechatronics and Automation (ICCMA 2018)*. ACM, Tokyo, Japan, pp. 97-104. DOI: https://doi.org/10.1145/3284516.3284544.

2. An extended version of the latter paper has been published in:

   Kissai, M.; Monsuez, B.; Mouton, X.; Martinez, D.; Tapus, A. "Adaptive Robust Vehicle Motion Control for Future Over-Actuated Vehicles". *Machines* 2019, 7, 26. DOI: https://doi.org/10.3390/machines7020026.

6 Tire Modeling Review

If the vehicle is equipped by subsystems based on the lateral forces of the tire like the 4WS, and others, based on the longitudinal forces of the tire like the VDC, the combined slip phenomenon should be taken into account for an optimal management of subsystems' interactions. From a control synthesis point of view, this requires a tire model giving enough insights to handle coupled operations, for example braking while turning. In this context, and as mentioned in Chapter 2, the literature is abundant by either empirical models that relies on experimental measures to make simulation more accurate, or complex physical models developed to improve the tire construction by the finite element method. Empirical and semi-empirical models are well-known for their high-fidelity and accuracy with respect to the reality (Pacejka, 2005), since they are derived from real experiments. However, these models usually depend on identified parameters without much physical significance, which makes them hard to measure or estimate in real-time. This is not suitable for online control problems, especially for adaptive control. Analytic models give a good understanding of tire mechanisms to control the vehicle and foresee its loss of stability. Nonetheless, either these models are not accurate enough for combined slip maneuvers, or they are too complex to be implemented or to use in order to precompute a control law. We believe that a new tire model especially fitted for global chassis control should be designed. To do so, in this chapter, we review the most famous tire models that are used in the literature. We compare these models in order to identify the gap that exists with respect to global chassis control. We will keep our focus on the substantial characteristics that the new tire model should adopt. These characteristics can be summarized as follows:

- The tire model should respect the tire physical fundamentals to give enough insight about tire behavior. It is important for control problems to identify the source of any disturbance in order to isolate it. The tire model should be able to depict any perturbation due to tire dynamics to adapt the control strategy, and not mix it with external disturbances that should be rejected.
- The tire model should describe as precise as possible the combined slip behavior. This is one of the pillars of this thesis as we are interested in combined maneuvers. Couplings between tire forces should be taken into account.
- The tire model should be simple enough for controllability issues. The main objective remains developing control algorithms to improve vehicle motion. The tire model should be easily invertible, and if possible, linear.
- The tire model should depend on a minimum set of parameters that can be measured or estimated so as to favor real-time operations. Also, these parameters should be easily and fastly estimated and updated online.

6.1 Tire physical fundamentals

In vehicle dynamics, the interface between tires and the road matters most. We are therefore interested in only the outer layer made of rubber blocks. The rubber is a *viscoelastic* material (Michelin, 2001): the stress is proportional to the deformation (elastic behavior) and phase-shifted to it (viscous behavior). To understand this, a closer look into the friction concept is needed. First, we define the tire coordinate system. Same as for the vehicle model, the ISO 8855-2011 depicted in Figure 6.1 is adopted:

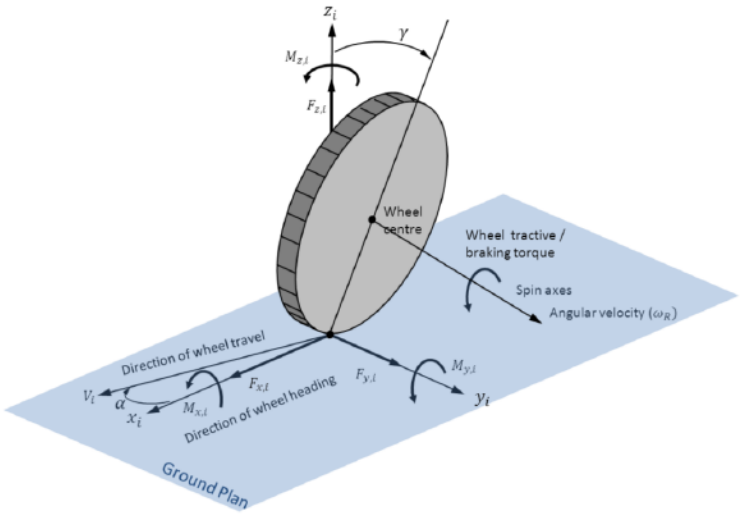

FIGURE 6.1: ISO tire coordinate system.

6.1.1 Friction

Two phenomena characterize the rubber/ground friction: indentation and adhesion (Michelin, 2001). In the indentation, the rubber deforms by sliding on the ground asperities. Because of its viscous behavior, the rubber block does not go back to its initial height immediately on the other side of the asperity[1]. As Figure 6.2 shows, this asymmetry creates a reaction force opposed to the sliding direction.

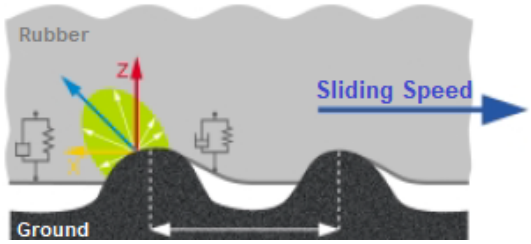

FIGURE 6.2: Indentation phenomenon (Michelin, 2001).

Regarding adhesion, molecular interactions occur at the rubber/ground interface, called *Van der Waals bonds*. Figure 6.3 illustrates the different steps: the bonds are formed, stretched, broken, and then reformed further.

[1] hysteresis phenomenon.

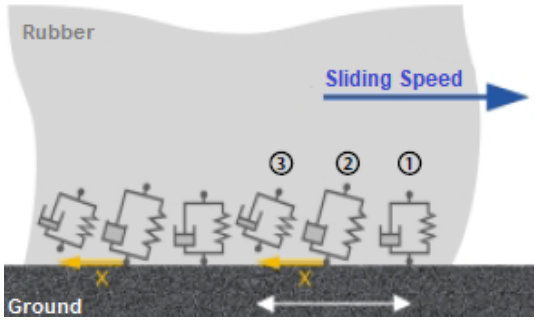

FIGURE 6.3: Adhesion phenomenon (Michelin, 2001).

6.1.2 Longitudinal Force

Two mechanisms occur when the tire adheres to the ground: shearing and sliding (Michelin, 2001). Shearing means that the rubber block deforms without sliding, which generates a resistance force proportional to the deformation. This phase is also called *pseudo-slip* because the superior rigid plate actually slide with respect to the ground (see Figure 6.4). The resistance force continue growing until it reaches its maximum[2]. This limit depends on the vertical load applied by the vehicle F_z, the rubber state, and the ground surface condition. First, let us suppose that the wheel only rolls without steering. This generates a longitudinal force:

$$F_{x_{max}} = \mu_x F_z \tag{6.1}$$

Where μ_x is the longitudinal friction coefficient, a conventional quantity that characterizes the interface rubber/ground condition, and consequently, the adhesion potential. Beyond this limit, the interface rubber/ground can no longer resist and the rubber block starts sliding with respect to the ground (Figure 6.4). The tire suffers then from a loss of potential, which may lead to the instability of the vehicle. It is then very important to predict this maximum value. The slip κ is defined as the ratio

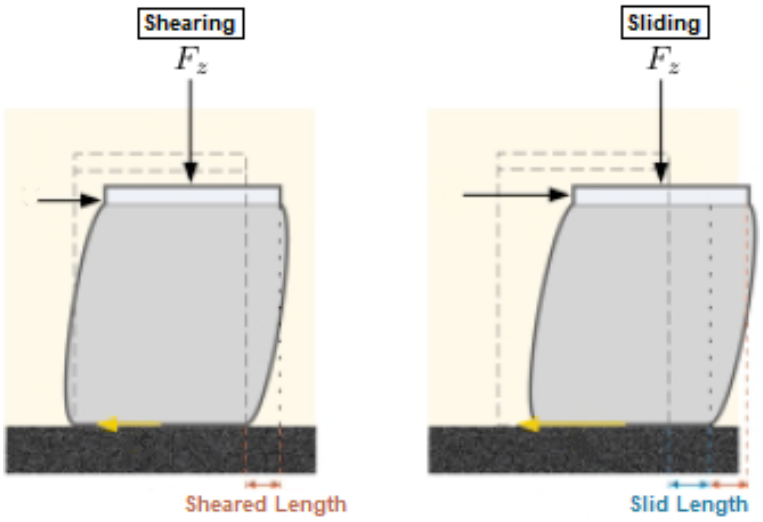

FIGURE 6.4: Friction mechanisms (Michelin, 2001).

[2]Coulomb friction force.

(Maakaroun, 2011)[3]:

$$\kappa = \frac{R\omega - V}{max\,(R\omega, V)} \tag{6.2}$$

Where:

- R : wheel's dynamic radius,
- ω : wheel's angular velocity,
- V : vehicle's speed.

$\kappa > 0$ indicates an acceleration situation while $\kappa < 0$ indicates a braking one. Figure 6.5 shows the longitudinal force as a function of slip. Three regions are distinguished:

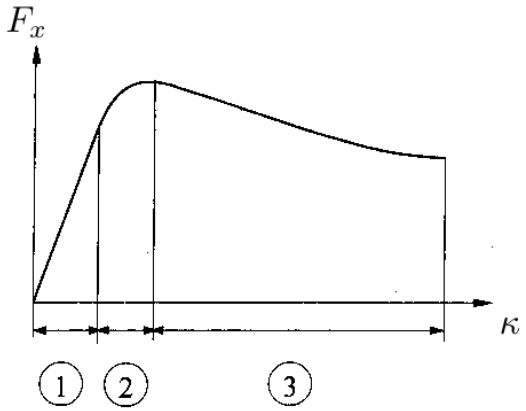

FIGURE 6.5: Longitudinal force variation with slip (Halconruy, 1995).

- Region 1 : the curve is linear and increasing, The stress is mainly due to the rubber deformation (pure shearing).
- Region 2 : the curve is nonlinear, increasing and ends up reaching the maximum $\mu_x F_z$. A portion of the contact area begins to slide.
- Region 3 : the curve is decreasing. There is total sliding of the tire. The tire behavior is unstable.

The tire overall behavior is highly nonlinear.

6.1.3 Lateral Force

When cornering, the vehicle is subjected to a centrifugal force. To maintain the vehicle on its trajectory, the rubber/ground interface should provide centripetal force of equal value to the centrifugal force. The wheels are then directed towards not the trajectory but rather the inside of the turn (Michelin, 2001). This introduces an offset between the wheel's plan of rotation and trajectory of the wheel's center. This offset is called the side-slip. It induces friction between the tire and the road which generates the centripetal transverse force. The side-slip angle is defined as (Michelin,

[3]The max function is used to avoid singularity.

2001):

$$\alpha = -arctan\left(\frac{V_y}{V_x}\right). \tag{6.3}$$

Figure 6.6 illustrates this phenomenon.

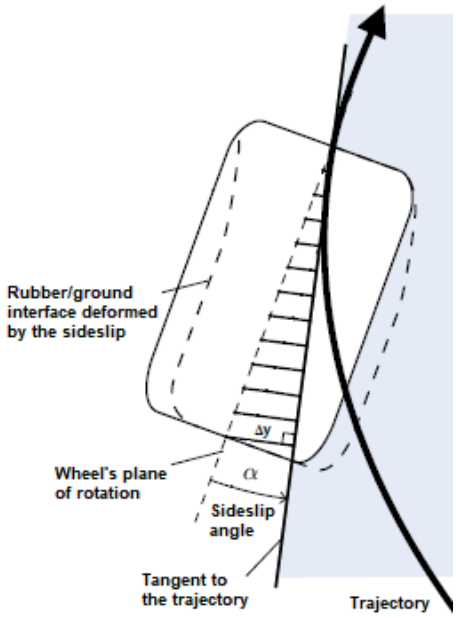

FIGURE 6.6: The side-slip (Michelin, 2001).

The lateral force follows the same mechanisms as the longitudinal one. At the entrance of the contact area, the rubber blocks remain vertical with respect to the ground. As they progress towards the back of the contact area, they deform laterally to follow the trajectory until reaching their maximum. This limit has the same formulation as the previous one:

$$F_{y_{max}} = \mu_y F_z \tag{6.4}$$

Beyond this maximum, the rubber blocks begin to slide. Here, μ_y is the lateral friction coefficient. Because of the tire's geometry, there is no reason for μ_y to be of the same value than μ_x. Consequently $F_{y_{max}} \neq F_{x_{max}}$.

6.1.4 Global Friction Force

The longitudinal force and the lateral force are competing: they must share the adhesion potential provided by the rubber/ground interface (Michelin, 2001). Because $F_{y_{max}} \neq F_{x_{max}}$, the overall adhesion is delimited by a *friction ellipse* (Wong, 2001), (Svendenius, 2003), (Pacejka, 2005). Longitudinal and lateral tire forces maximum cannot therefore be reached simultaneously. This concept is illustrated in Figure 6.7.

A longitudinal force request would penalize a lateral force request if the limits of adhesion are reached. Figure 6.8 shows the impact of the lateral force on the longitudinal force.

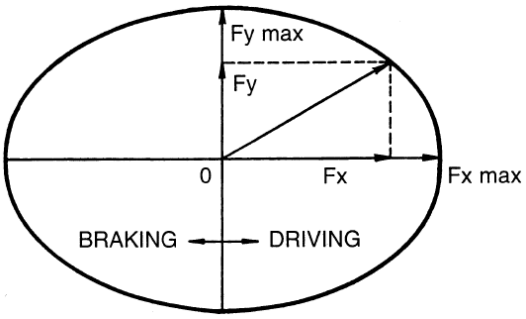

FIGURE 6.7: The friction ellipse concept (Wong, 2001).

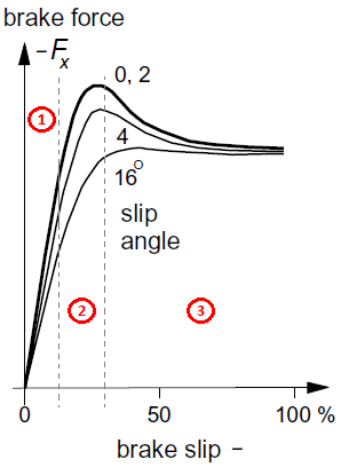

FIGURE 6.8: Combined side force and brake force characteristics (adapted from (Pacejka, 2005)).

6.2 Tire behavioral models

As we have mentioned, two major classes can be distinguished: empirical models and theoretical models. Next, classic models developed pursuing both approaches are exposed. SAE ISO notation (Svendenius and Wittenmark, 2003) is used to enable their comparison.

6.2.1 Empirical Models

These models are developed from experimental data only or by using similarity method. In the first approach, regression procedures are used to develop mathematical formulations whose parameters fit best the measured data. The similarity approach uses rather simple distortion and re-scaling methods to develop simpler empirical models.

Holmes Model

Holmes has proposed a particular empirical structure for the lateral force. A vehicle speed dependent model has been developed to express the behavior of the force for

large slip value (Svendenius, 2003):

$$F_y = a_0 + a_1 V_x + a_2 V_x^2 + a_3 \alpha + a_4 \alpha^2 + a_5 \alpha^3 + a_6 R + a_7 P \tag{6.5}$$

Where:

- R, P : two characteristic constants of the tire,
- $a_{0...7}$: parameters used for curve fitting.

However, the $a_{0...7}$ parameters have no physical meaning. Equation (6.5) characterizes the relation between the lateral force and the side-slip angle, but with minor changes, the same structure can be used to express the longitudinal behavior of the tire (Svendenius, 2003).

The Magic Formula of Pacejka

Due to its high precision, this model is perhaps the most used model in vehicle dynamics analysis (Soltani, 2014). The tire forces are defined as follows (Pacejka, 2005):

$$Y(X) = y(x) + S_v \tag{6.6}$$

With:

$$\begin{cases} x = X + S_h & (6.7) \\ y = D \sin\left[C \arctan\left\{Bx - E\left(Bx - \arctan\left(Bx\right)\right)\right\}\right] & (6.8) \end{cases}$$

Where:

- Y : F_x (longitudinal force), F_y (lateral force) or M_z (aligning torque),
- X : κ (longitudinal slip) or $\tan\alpha$ (where α is the side-slip angle),

And:

- B : stiffness factor,
- C : shape factor,
- D : peak value,
- E : curvature factor,
- S_H : horizontal shift,
- S_V : vertical shift.

The offsets S_H and S_V appear to occur when ply-steer, conicity effects, and possibly the rolling resistance cause the F_x and F_y curves not to pass through the origin (Pacejka, 2005).

Weighting functions are used to take into account the combined slip:

$$G = D \cos\left[C \arctan\left(Bx\right)\right] \tag{6.9}$$

The parameters have the same signification as before. These weighting functions are multiplied by the original functions (6.6)-(6.8) to produce the interactive effects of κ on F_y or α on F_x.

Regarding the lateral force for instance, we have:

$$F_y = G_{y\kappa} F_{y0} + S_{Vy\kappa} \tag{6.10}$$

With:

$$\begin{cases} G_{y\kappa} = \dfrac{\cos\left[C_{y\kappa} \arctan\left\{B_{y\kappa}\left(\kappa + S_{Hy\kappa}\right)\right\}\right]}{\cos\left[C_{y\kappa} \arctan\left\{B_{y\kappa} S_{Hy\kappa}\right\}\right]} & (6.11) \\ S_{Vy\kappa} = D_{Vy\kappa} \sin\left[r_{Vy5} \arctan\left(r_{Vy6}\kappa\right)\right] & (6.12) \end{cases}$$

Where:

$$\begin{cases} B_{y\kappa} = r_{By1} \cos\left[\arctan\left\{r_{By2}\left(\alpha - r_{By3}\right)\right\}\right] & (6.13) \\ C_{y\kappa} = r_{Cy1} & (6.14) \end{cases}$$

F_{y0} is the lateral force in case of pure side-slip calculated using equations (6.6)-(6.8). $S_{Vy\kappa}$ is caused by the ply-steer phenomenon induced by κ. The different r coefficients are constant curve fitting parameters which values can be found in the appendix of (Pacejka, 2005). The same procedure is used for the longitudinal force F_x. To illustrate the combined slip effects, Pacejka uses a 3D diagram as shown in Figure 6.9.

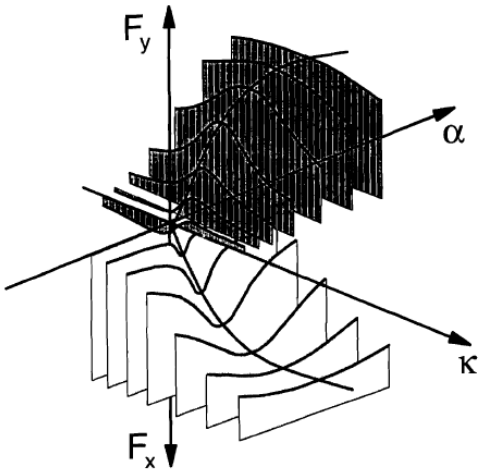

FIGURE 6.9: Forces interactions in a combined slip (Pacejka, 2005).

Brach equations for combined slip

To describe the effects of the combined slip, Nicholas and Comstock have proposed in 1972 the following formulas:

$$\begin{cases} F_x(\kappa, \alpha) = \dfrac{F_x(\kappa) F_y(\alpha) \kappa}{\sqrt{\kappa^2 F_y^2(\alpha) + \tan^2(\alpha) F_x^2(\kappa)}} & (6.15) \\ F_y(\kappa, \alpha) = \dfrac{F_x(\kappa) F_y(\alpha) \tan(\alpha)}{\sqrt{\kappa^2 F_y^2(\alpha) + \tan^2(\alpha) F_x^2(\kappa)}} & (6.16) \end{cases}$$

Where $F_x(\kappa)$ and $F_y(\alpha)$ are calculated using the Magic Formula in the case of pure slip (6.6)-(6.8).

However, we have in this case:

$$\begin{cases} F_x(\kappa, 0) \neq F_x(\kappa) & (6.17) \\ F_y(0, \alpha) \neq F_y(\alpha) & (6.18) \end{cases}$$

To solve this, Brach introduced a modification in (Brach and Brach, 2000):

$$\begin{cases} F_x(\kappa, \alpha) = \dfrac{F_x(\kappa) F_y(\alpha)}{\sqrt{\kappa^2 F_y^2(\alpha) + \tan^2(\alpha) F_x^2(\kappa)}} \dfrac{\sqrt{\kappa^2 C_\alpha^2 + (1-\kappa)^2 \cos^2(\alpha) F_x^2(\kappa)}}{C_\alpha} & (6.19) \\ F_y(\kappa, \alpha) = \dfrac{F_x(\kappa) F_y(\alpha)}{\sqrt{\kappa^2 F_y^2(\alpha) + \tan^2(\alpha) F_x^2(\kappa)}} \dfrac{\sqrt{(1-\kappa)^2 \cos^2(\alpha) F_y^2 + \sin^2(\alpha) C_s^2}}{C_s \cos(\alpha)} & (6.20) \end{cases}$$

Where C_s is the longitudinal stiffness of the tire and C_α is the cornering one.

Kiencke's Model

In (Kiencke and Nielsen, 2000), the authors use two techniques:

- Calculation of the friction coefficient using Burckhardt extended model (Seddiki et al., 2006),
- Calculation of the different contact points' speed. The displacement of the resultants center (detachment point) with respect to the vertical projection of the wheel center is evaluated through the forces acting on the tire.

The friction coefficient expression is given by:

$$\mu = \left(c_1 \left(1 - e^{-c_2 S}\right) - c_3 S\right) e^{-c_4 S V_G} \left(1 - c_5 F_z^2\right) \quad (6.21)$$

Where:

- $S = \sqrt{\kappa^2 + \alpha^2}$: the resultant slip,
- V_G : velocity of the vehicle's CoG,
- c_1, c_2, c_3 : parameters depending on the ground surface condition,
- c_4 : parameter depending on the maximal vehicle speed,
- c_5 : parameter depending on the maximal vertical load.

The tire forces are then determined by:

$$\begin{cases} F_x = \mu \dfrac{F_z}{S} \left(\kappa \cos(\alpha) - c_{\mu t} \alpha \sin(\alpha)\right) & (6.22) \\ F_y = \mu \dfrac{F_z}{S} \left(c_{\mu t} \alpha \cos(\alpha) + \kappa \sin(\alpha)\right) & (6.23) \end{cases}$$

Where $c_{\mu t}$ is a weighting coefficient (varies between 0.9 and 0.95 (Seddiki et al., 2006)).

We have also:

$$\begin{cases} \mu_x = \mu \dfrac{\kappa}{S} & (6.24) \\ \mu_y = \mu \dfrac{\tan(\alpha)}{S} & (6.25) \end{cases}$$

The different parameters c_i used by Burckhardt can be found in (Kiencke and Nielsen, 2000) or (Maakaroun, 2011). This gives different friction curves with respect to the ground surface condition (see Figure 6.10).

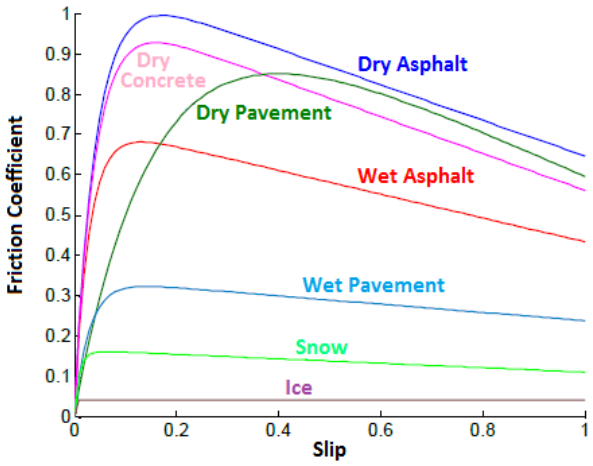

FIGURE 6.10: Friction coefficient for different surface types (Maakaroun, 2011).

6.2.2 Theoretical Models

To get a better understanding of the tire behavior, theoretical models are based on physical models. More complex models, related to its construction and especially designed to improve tire performances, can be found. In this case, complex finite element based models are usually adopted (Pacejka, 2005). These latter exceed the scope of this thesis. Relatively simple models should be intended for control synthesis. We will focus on theoretical models based on physical models.

The Brush model

As its name may reveal, the tire is assimilated to a set of brush bristles (Figure 6.11).

When rolling without sliding, a tread element is assumed to enter the contact zone being vertical (Pacejka, 2005). It remains vertical until it leaves this zone without deforming. In contrast, when $V \neq R\omega$, a horizontal deformation of the element is developed. The base point of this element moves backwards at a speed equal to $R\omega$ with respect to the wheel's axis. The same point moves at a speed called slip[4] velocity with respect to the ground. The lower part of the element remains attached to the ground. The element adheres to the ground as long as the friction limits allow

[4]The slip of the carcass with respect to the ground.

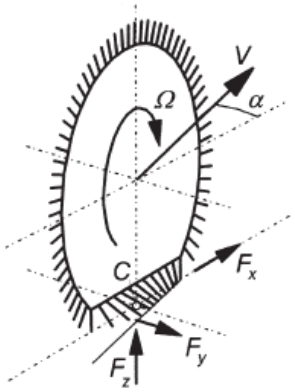

FIGURE 6.11: The Brush model (Pacejka, 2005).

it. The maximum deformation depends on the coefficient of friction μ, the distribution of the vertical load q_z, and the element stiffness c_p. Once this maximum is reached, the element begins to slide. As shown in the Figure 6.11, this phenomenon begins at the rear of the wheel. The sliding part can be distinguished from the adhering part by an intersection point. When slip increases, this point moves towards the front of the wheel until it reaches its edge: total sliding occurs.

Several mathematical formulations were adopted regarding this physical representation (Svendenius, 2003),(Svendenius and Wittenmark, 2003),(Pacejka, 2005). These formulas differ according to the assumptions considered regarding the tire physical characteristics, namely, the friction coefficient and the vertical load distribution. Here, we suppose a parabolic distribution of vertical load:

$$q_z = \frac{3F_z}{4a}\left[1 - \left(\frac{x}{a}\right)^2\right] \tag{6.26}$$

Where:

- a : half the contact length,
- x : the tread element coordinate (see Figure 6.12 or 6.13).

Next, we present the brush model formulas for the most frequent cases:

- For pure longitudinal slip (Figure 6.12), we find (Svendenius, 2003):
  - if $\sigma_x < \frac{3\mu F_z}{C_s}$

$$F_x = C_s\sigma_x\left[1 - \frac{C_s\sigma_x}{3\mu F_z} + \frac{1}{3}\left(\frac{C_s\sigma_x}{3\mu F_z}\right)^2\right] \tag{6.27}$$

  - if $\sigma_x \geq \frac{3\mu F_z}{C_s}$

$$F_x = \mu F_z \tag{6.28}$$

  Where $\sigma_x = \frac{\kappa}{1+\kappa}$ is the "theoretical longitudinal slip". Note that the tire force does not decrease when it reaches its maximum. We can already see that this model is not accurate in the unstable region. Same remark holds for the following expressions.

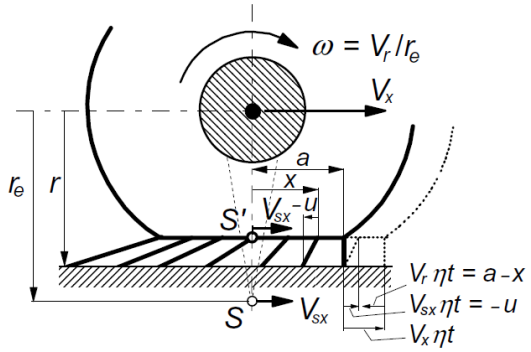

FIGURE 6.12: Side view of Brush model when braking (Pacejka, 2005).

- For pure side-slip (Figure 6.13), we find (Pacejka, 2005),(Svendenius, 2003):

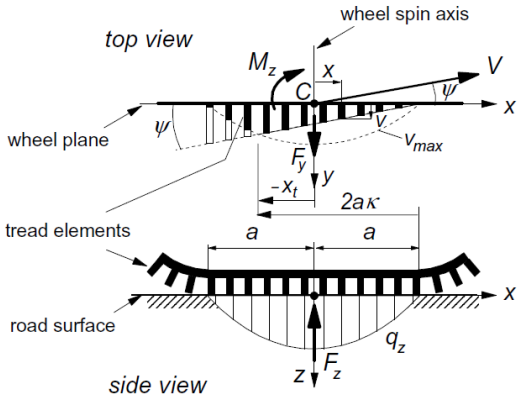

FIGURE 6.13: Top and side view of Brush model at pure side-slip (Pacejka, 2005).

– if $\sigma_y < \dfrac{3\mu F_z}{C_\alpha}$

$$F_y = C_\alpha \sigma_y \left[1 - \frac{C_\alpha \sigma_y}{3\mu F_z} + \frac{1}{3}\left(\frac{C_\alpha \sigma_y}{3\mu F_z}\right)^2\right] \tag{6.29}$$

– if $\sigma_y \geq \dfrac{3\mu F_z}{C_\alpha}$

$$F_y = \mu F_z \tag{6.30}$$

Where $\sigma_y = \dfrac{\tan(\alpha)}{1+\kappa}$ is the "theoretical lateral slip".

- For combined slip (Figure 6.14), the formulas depend on the assumptions considered regarding friction and tire stiffness:

  – In the case of an isotropic friction with equal longitudinal and lateral stiffnesses $C_s = C_\alpha = C$, we find (Pacejka, 2005):

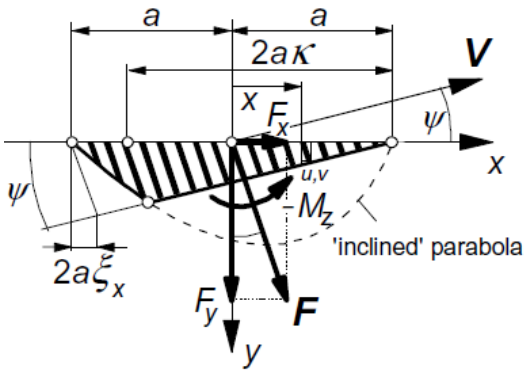

FIGURE 6.14: Brush model deformation at combined slip (Pacejka, 2005).

* If $\|\vec{\sigma}\| < \frac{3\mu F_z}{C}$

$$\|\vec{F}\| = \mu F_z \left[3\theta\|\vec{\sigma}\| - 3\left(\theta\|\vec{\sigma}\|\right)^2 + \left(\theta\|\vec{\sigma}\|\right)^3\right] \tag{6.31}$$

* If $\|\vec{\sigma}\| \geq \frac{3\mu F_z}{C}$

$$\|\vec{F}\| = \mu F_z \tag{6.32}$$

Where:

* $\|\vec{\sigma}\| = \sqrt{\sigma_x^2 + \sigma_y^2}$
* $\vec{F} = \frac{\vec{\sigma}}{\|\vec{\sigma}\|}\|\vec{F}\|$
* $\theta = \frac{C}{3\mu F_z}$

– In the case of an isotropic friction and a rectangular tire/ground contact surface, the longitudinal stiffness is different from the cornering one. Pursuing the same development logic in (Svendenius, 2003), and considering the engine operation instead of braking operation, we find:

* If $\psi\left(\sigma_x, \sigma_y\right) < 1$

$$\begin{cases} F_x\left(\sigma_x, \sigma_y\right) = C_s\sigma_x\left(1 - \psi\left(\sigma_x, \sigma_y\right)\right)^2 \\ \qquad + \frac{\sigma_x}{\sqrt{\sigma_x^2 + \sigma_y^2}}\mu F_z\psi^2\left(\sigma_x, \sigma_y\right)\left(3 - 2\psi\left(\sigma_x, \sigma_y\right)\right) \end{cases} \tag{6.33}$$

$$\begin{cases} F_y\left(\sigma_x, \sigma_y\right) = C_\alpha\sigma_y\left(1 - \psi\left(\sigma_x, \sigma_y\right)\right)^2 \\ \qquad + \frac{\sigma_y}{\sqrt{\sigma_x^2 + \sigma_y^2}}\mu F_z\psi^2\left(\sigma_x, \sigma_y\right)\left(3 - 2\psi\left(\sigma_x, \sigma_y\right)\right) \end{cases} \tag{6.34}$$

* If $\psi\left(\sigma_x, \sigma_y\right) \geq 1$

$$\begin{cases} F_x\left(\sigma_x, \sigma_y\right) = \dfrac{\sigma_x}{\sqrt{\sigma_x^2 + \sigma_y^2}} \mu F_z & (6.35) \\ F_y\left(\sigma_x, \sigma_y\right) = \dfrac{\sigma_y}{\sqrt{\sigma_x^2 + \sigma_y^2}} \mu F_z & (6.36) \end{cases}$$

Where $\psi\left(\sigma_x, \sigma_y\right) = \sqrt{\left(\dfrac{C_s \sigma_x}{3\mu F_z}\right)^2 + \left(\dfrac{C_\alpha \sigma_y}{3\mu F_z}\right)^2}$ represents the adhesion limits when the vertical load distribution is parabolic.

– In the case of an anisotropic friction, interest is given to the friction ellipse. The forces' expressions are a combination of the influence of tread element deformation and the influence of the tread element sliding:

$$\begin{cases} F_x\left(\sigma_x, \sigma_y\right) = F_{dx}\left(\sigma_x, \sigma_y\right) + F_{sx}\left(\sigma_x, \sigma_y\right) & (6.37) \\ F_y\left(\sigma_x, \sigma_y\right) = F_{dy}\left(\sigma_x, \sigma_y\right) + F_{sy}\left(\sigma_x, \sigma_y\right) & (6.38) \end{cases}$$

Where the adhesive forces expressions are (Svendenius, 2003):

* If $\psi\left(\sigma_x, \sigma_y\right) < 1$

$$\begin{cases} F_{dx}\left(\sigma_x, \sigma_y\right) = -C_s \sigma_x \left[1 - \psi\left(\sigma_x, \sigma_y\right)\right]^2 & (6.39) \\ F_{dy}\left(\sigma_x, \sigma_y\right) = -C_\alpha \sigma_y \left[1 - \psi\left(\sigma_x, \sigma_y\right)\right]^2 & (6.40) \end{cases}$$

* If $\psi\left(\sigma_x, \sigma_y\right) \geq 1$

$$F_{dx} = F_{dy} = 0 \quad (6.41)$$

With $\psi\left(\sigma_x, \sigma_y\right) = \sqrt{\left(\dfrac{C_s \sigma_x}{3\mu_{sx} F_z}\right)^2 + \left(\dfrac{C_\alpha \sigma_y}{3\mu_{sy} F_z}\right)^2}$ this time, and μ_{sx} and μ_{sy} denote the longitudinal and lateral static friction coefficients. The sliding forces consists in the distribution of the vertical load acting on the sliding portion between the longitudinal and lateral directions. This vertical load is expressed as (Svendenius, 2003):

$$F_{sz} = F_z \psi^2\left(\sigma_x, \sigma_y\right)\left[3 - 2\psi^2\left(\sigma_x, \sigma_y\right)\right] \quad (6.42)$$

There are three methods to describe how the vertical load is distributed in case of an anisotropic friction: *collinear slide forces*, *maximum dissipation rate*, and *slip-projection method* (Svendenius, 2003).

* Collinear slide forces:

$$\begin{cases} F_{sx}\left(\sigma_x, \sigma_y\right) = -\cos\left(\beta^-\right) \mu_{kx} F_{sz} & (6.43) \\ F_{sy}\left(\sigma_x, \sigma_y\right) = -\sin\left(\beta^-\right) \mu_{ky} F_{sz} & (6.44) \end{cases}$$

Where $\tan\left(\beta^-\right) = \dfrac{\mu_{kx} vsy}{\mu_{ky} vsx}$, with μ_k is the kinetic friction coefficient and v_s is the sliding speed.

* Maximum dissipation rate:

The resulting sliding friction force $\vec{F}_s''$ is the one which maximizes the mechanical work $W = -\vec{v}_s\vec{F}_s''$ under the constraint:

$$\left(\frac{F_{sx}''}{\mu_{kx}F_{sz}}\right)^2 + \left(\frac{F_{sy}''}{\mu_{ky}F_{sz}}\right)^2 \leq 1 \tag{6.45}$$

This gives:

$$\begin{cases} F_{sx}''\left(\sigma_x, \sigma_y\right) = -\cos\left(\beta'\right)\mu_{kx}F_{sz} & (6.46) \\ F_{sy}''\left(\sigma_x, \sigma_y\right) = -\sin\left(\beta'\right)\mu_{ky}F_{sz} & (6.47) \end{cases}$$

Where $\tan\left(\beta'\right) = \dfrac{\mu_{ky}vsy}{\mu_{kx}vsx}$.

* Slip-projection method:

$$\begin{cases} F_{sx}'\left(\sigma_x, \sigma_y\right) = -\cos\left(\beta\right)\mu_{kx}F_{sz} & (6.48) \\ F_{sy}'\left(\sigma_x, \sigma_y\right) = -\sin\left(\beta\right)\mu_{ky}F_{sz} & (6.49) \end{cases}$$

Where $\tan\left(\beta\right) = \dfrac{vsy}{vsx}$.

Figure 6.15 summarizes the three methods.

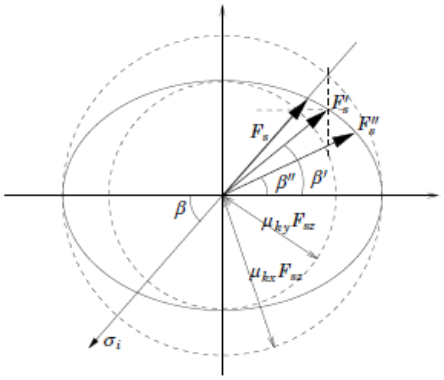

FIGURE 6.15: Illustration of methods to describe kinetic friction in case of anisotropic friction (Svendenius, 2003).

The Brush Model Derivatives

Three hypothesis limit the Brush model's accuracy in the non-linear region: parabolic distribution of vertical load, rigid carcass, and constant friction. Changing these three hypothesis gives different expressions.

- Asymmetric vertical load distribution:

  Only the longitudinal tire force has been studied in this case. In (Svendenius and Wittenmark, 2003), the authors use a parameter d to express an asymmetric vertical load distribution:

$$q_{zd} = \frac{3F_z}{4a}\left(1 - \left(\frac{x}{a}\right)^2\right)\left(1 + d\frac{x}{a}\right) \tag{6.50}$$

Changing d value[5] influences the distribution maximum position. However, the mathematical formula becomes too heavy. In (Svendenius, 2003), authors used a Taylor expansion to simplify the force expression. This gives:

- If $\sigma_x < \frac{3\mu F_z}{C_s}(d+1)$

$$F_{xd} = C_s\sigma_x + \frac{1}{3}\frac{(C_s\sigma_x)^2}{(d-1)\mu F_z} - \frac{1}{27}\frac{(3d+1)(C_s\sigma_x)^3}{(d-1)^3(\mu F_z)^2} + \mathcal{O}\left(\sigma_x^4\right) \quad (6.51)$$

- If $\sigma_x \geq \frac{3\mu F_z}{C_s}(d+1)$

$$F_x = \mu F_z \quad (6.52)$$

- The lateral force is more concerned by *carcass flexibility* (Pacejka, 2005). The total deformation consists in the sum of the bristle and carcass deflections. The carcass deformation is treated as a beam (Pacejka, 2005). However, no smooth expression is given when considering this phenomenon.

- Variable friction:

  Three cases are distinguished in (Svendenius, 2003):

  1. The friction coefficient is constant but has two different values: μ_s (static) if the tread element is in the adhesion portion and μ_k (kinetic) if the tread element is in the sliding portion,
  2. The friction coefficient is linearly dependent of the sliding speed[6],
  3. the friction coefficient is exponentially dependent of the sliding speed.

  - Case of a constant friction:
    The force can be expressed as:
    * If $\sigma_x < \frac{3\mu_s F_z}{C_s}$

$$F_x = C_s\sigma_x + \frac{1}{3}\frac{(\mu_k - 2\mu_s)(C_s\sigma_x)^2}{\mu_s^2 F_z} + \frac{1}{27}\frac{(3\mu_s - 2\mu_k)(C_s\sigma_x)^3}{\mu_s^3 F_z^2} \quad (6.53)$$

    * If $\sigma_x \geq \frac{3\mu_s F_z}{C_s}$

$$F_x = \mu_k F_z \quad (6.54)$$

  - Case of linear dependency:
    Here we simply make the replacement:

$$\mu_k(\sigma_x, v_x) = \mu_0 - n v_x \frac{\sigma_x}{1+\sigma_x} \quad (6.55)$$

    Where $\mu_0 = \mu_s$ and n is a parameter used or curve fitting.
  - Case of exponential dependency:
    According to (Canudas-de-Wit et al., 2001):

$$\mu_k(\sigma_x, v_x) = \mu_k + (\mu_s - \mu_k)\exp\left[\left|\frac{\sigma_x v_x}{(1+\sigma_x)v_{st}}\right|^{\varepsilon}\right] \quad (6.56)$$

[5] $d \in [-0.5, 1]$. See (Svendenius, 2003) or (Svendenius and Wittenmark, 2003) for more details.
[6] $v_{sx} = \frac{\sigma_x}{1+\sigma_x} v_x$

Where v_{st} is the stribeck velocity and ε is a curve fitting parameter. This model require then four parameters. To reduce parameter numbers, the authors of (Svendenius, 2003) consider $\varepsilon = 0.5$ and $v_{st} = 30m/s$, and introduce a parameter h so they have:

$$\mu_k(\sigma_x, v_x) = \mu h + \mu(1-h)\exp\left[\left|\frac{\sigma_x v_x}{30(1+\sigma_x)}\right|^{0.5}\right] \tag{6.57}$$

The physical model of Dugoff

Dugoff developed an analytic model based on the classical analysis of Fiala (Dugoff, Fancher, and Segel, 1969). He assumed a constant friction coefficient and a constant vertical load distribution. These assumptions give:

$$\begin{cases} F_x = C_s \dfrac{\kappa}{1-\kappa}\tau & (6.58) \\ F_y = C_\alpha \dfrac{\tan(\alpha)}{1-\kappa}\tau & (6.59) \end{cases}$$

τ is introduced to take into account the combined slip:

$$\tau = \begin{cases} (2-\sigma)\sigma & \text{if } \sigma < 1 \\ 1 & \text{otherwise} \end{cases} \tag{6.60}$$

Where:

$$\sigma = \frac{(1-\kappa)\mu F_z}{2\sqrt{C_s^2\kappa^2 + C_\alpha^2 \tan^2(\alpha)}} \tag{6.61}$$

Note that in case of a pure longitudinal slip $(\alpha = 0)$, and we have:

$$\lim_{\kappa \to 1} F_x = \mu F_z \tag{6.62}$$

Same remark holds for the pure side-slip. Dugoff suppose therefore that the tire force does not experience a loss of potential when it reaches its maximum. However, he pointed out that considering a sliding speed dependent coefficient of friction improves the tire force curve in the unstable region.

Modified Dugoff Model

To improve Dugoff's model accuracy in the unstable zone, the authors in (Bian et al., 2014) adjusted Dugoff's model to Pacejka's using curve fitting methods. This has led them to develop weighting functions to be multiplied by the original model of Dugoff:

- For the longitudinal force:

$$G_s = (1.15 - 0.75\mu_{max})\kappa^2 - (1.63 - 0.75\mu_{max})\kappa + 1.27 \tag{6.63}$$

- For the lateral force:

$$G_\alpha = (\mu_{max} - 1.6)\tan(\alpha) + 1.155 \tag{6.64}$$

As expected the model's accuracy has improved. However, the weighting functions make the model lose its analytic nature.

LuGre Model

"Lu" stands for Lund (Sweden) and "Gre" for Grenoble (France). This model has been developed in a joint cooperation between the Automatic Control Departments of the two cities' universities. The model is expressed as (Canudas-de-Wit et al., 2003):

$$\begin{cases} \dot{z} = v_s - \dfrac{\sigma_0 \left|v_s\right|}{g\left(v_s\right)} z & (6.65) \\ F_x = \left(\sigma_0 z + \sigma_1 \dot{z} + \sigma_2 v_s\right) F_z & (6.66) \\ g\left(v_s\right) = \mu_k + \left(\mu_s - \mu_k\right) \exp\left(-\sqrt{\left|\dfrac{v_s}{v_s t}\right|}\right) & (6.67) \end{cases}$$

Where:

- z : deflection of the material in the friction surface,
- $g\left(v_s\right)$: friction function[7],
- v_s : sliding velocity,
- v_{st} : stribeck velocity,
- σ_0 : the rubber longitudinal lumped stiffness,
- σ_1 : the rubber longitudinal lumped damping,
- σ_2 : the viscous relative damping.

There exists several representations of this model in the same way of the Brush model. It should be noted that this the only dynamic model presented here. Regarding the other models, the relaxation length should be taken into account, which is detailed further in this chapter. For more information, see (Svendenius, 2003) and (Canudas-de-Wit et al., 2003).

Gim's Model

It is a model that separates the longitudinal slip effects from the side-slip ones (Seddiki et al., 2006). Gim supposes a rectangular contact surface. The model is based on the pressure calculation along the contact surface. The vertical force is calculated through the pressure integration along the contact surface. This gives:

$$\begin{cases} F_x = C_s \kappa l_n^2 + \mu_x F_z \left(1 - l_n^2 + 2 l_n^3\right) & (6.68) \\ F_y = C_\alpha \alpha l_n^2 + \mu_y F_z \left(1 - 3 l_n^2 + 2 l_n^3\right) & (6.69) \end{cases}$$

Where:

$$\begin{cases} C_s = \dfrac{K_x W}{2} & (6.70) \\ C_\alpha = \dfrac{K_y W}{2} & (6.71) \\ l_n = 2 l_r \left(1 - \dfrac{2 W l_r^2}{3 \mu F_z} \sqrt{K_x^2 \kappa^2 + K_y^2 \alpha^2}\right) & (6.72) \end{cases}$$

With:

[7] The friction is assumed to be dependent on the sliding velocity.

- l_r : contact surface length,
- W : contact surface width,
- K_x : longitudinal stiffness per unit area,
- K_y : lateral stiffness per unit area.

6.2.3 Comparison

The Magic Formula is widely used by car manufacturers to simulate and validate dynamic performances due to its precision. Its parameters are changed offline to take into account the different road conditions. Our goal is to develop a model for control synthesis. The different parameters should be changed online. To do this, we should use physical parameters that could be measured or at least estimated. Consequently, we also use the Magic Formula only for validation.

To compare the physical models with Pacejka's, the Magic Formula parameters should be interpreted to meet a physical meaning. In (Pacejka, 2005), Pacejka pointed out that the product BCD is equivalent to the stiffness. Indeed, considering the equation (6.8), the product BCD represents the tangent at the origin in the same way as C_s for the longitudinal force in equation (6.33) or (6.58), and C_α for the lateral force in equation (6.34) or (6.59). For numerical applications, we can use the shape coefficients given in (Wong, 2001) for a vertical load of 4000 N for example. The stiffness coefficients are then given the value of the product BCD.

First, we only consider the physical model of Dugoff and the Brush model in the case of an isotropic friction coefficient and a rectangular distribution of the vertical load. Our goal remains the development of a simple tire model for global chassis control using physical parameters. The other models either depends on empirical parameters or too complex to be used for control synthesis. Figure 6.16 depicts the differences for the longitudinal force in a combined slip with a side-slip angle equal to 3° in the case of the magic formula, Brush model and Dugoff's model. Nevertheless, a global comparison of all models including the new model developed in this thesis will be given in Section 6.5.

Although the brush model uses physical parameters, it does not take into account the loss of potential phenomenon when maximum friction force is reached. In (Svendenius, 2003), this model has been improved by considering a speed dependent friction, and in (Svendenius and Wittenmark, 2003), an asymmetric vertical load is considered to improve the peak value location accuracy. However, the complexity also increases.

Dugoff's model suffers from the same drawback. The force's shape is totally inaccurate in the nonlinear region given that the coefficient of friction and the vertical load distribution are considered constant.

In control synthesis, these criteria are not crucial. As we mentioned, the third region of Figure 6.8 is unstable. There is no point to control the vehicle in this region. This behavior should be predicted and avoided. Thereby, the Brush model and Dugoff's model represent good candidates.

These two models respect three out of the four requirements that we proposed. They both respect the tire physical fundamentals, they represent precisely enough the combined slip in the stable region and they are dependent on physical parameters. However, their mathematical formulas are still too complex to manipulate. They should be linearized.

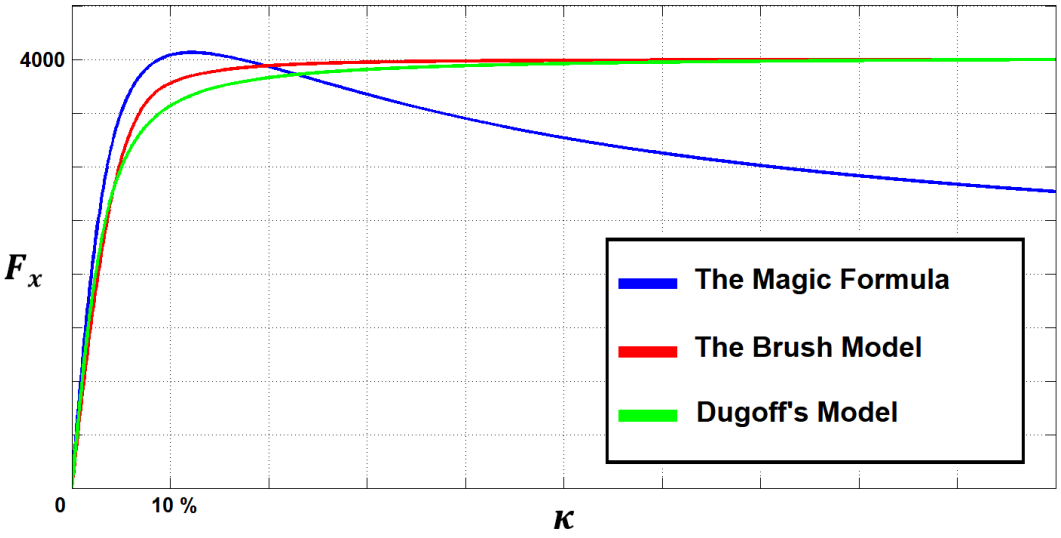

FIGURE 6.16: Comparison of models' longitudinal force shapes in combined slip.

6.3 Tire physical models linearization

In the following, we present the new linear tire model with varying parameters that we have developed. This is the model that will be mostly used in the following chapters. As we have mentioned at the beginning of this chapter, a new simple analytic tire model that takes into account the combined slip behavior is needed for GCC problems. We proceed first by linearizing the combined physical tire models.

Dugoff's model differs from the brush model by the vertical load distribution assumptions. Dugoff supposes a constant vertical load distribution (Dugoff, Fancher, and Segel, 1969). In the brush model, a parabolic distribution is considered (Svendenius, 2003). Figure 6.16 shows however that little improvement is brought by this assumption. But then again, the formulas (6.33) and (6.34) are more complex to manipulate than (6.58) and (6.59). The brush model equations' derivatives are too heavy to be exposed. Hence, only Dugoff's model linearization is presented, but both results will be illustrated.

According to (6.60), Dugoff's model has two expressions depending on whether the tire effort has reached its saturation or not. As our concern is the stable part of the tire behavior, it is the expression related to the case where $\sigma < 1$ that should be linearized.

6.3.1 Longitudinal force linearization

Let κ^* be the stable operating point located in the linear region of the tire force curve (Figure 6.8). After replacing the variable τ in equation (6.58) by its expression in equation (6.60), and σ by its expression in (6.61), we perform a first-order Taylor series approximation of F_x about κ^*:

$$F_x(\kappa) = \left[F_x(\kappa^*) - \left.\frac{dF_x(\kappa^*)}{d\kappa}\right|_{\kappa=\kappa^*} \kappa^*\right] + \left.\frac{dF_x(\kappa^*)}{d\kappa}\right|_{\kappa=\kappa^*} \kappa \tag{6.73}$$

As the linear region is concerned, κ^* is very small:

$$(\kappa^* \ll) \Rightarrow \left(F_x(\kappa^*) \cong \left. \frac{dF_x(\kappa^*)}{d\kappa} \right|_{\kappa=\kappa^*} \kappa^* \right) \tag{6.74}$$

Therefore:

$$(\kappa^* \ll) \Rightarrow \left(F_x(\kappa) \cong \frac{F_x(\kappa^*)}{\kappa^*} \kappa \right) \tag{6.75}$$

Equation (6.75) shows that the term $\frac{F_x(\kappa^*)}{\kappa^*}$ corresponds to a longitudinal stiffness. Let us symbolize it C_s^*. Using Dugoff's model equations (6.58), (6.60), and (6.61), we find:

$$C_s^*(\alpha, \mu, F_z) = \frac{4\sqrt{C_s^2 \kappa^{*2} + C_\alpha^2 \tan^2(\alpha)} - (1-\kappa^*)\mu F_z}{4\left(C_s^2 \kappa^{*2} + C_\alpha^2 \tan^2(\alpha)\right)} \mu F_z C_s \tag{6.76}$$

This longitudinal stiffness depends on varying-parameters α, μ, and F_z. These parameters could be estimated online (Svendenius, J., 2007),(Soltani, 2014),(Singh and Taheri, 2015). It depends also on constant parameters C_s, C_α, and κ^*. An explicit expression of κ^* will be given afterwards. By setting:

$$\rho = \frac{4\sqrt{C_s^2 \kappa^{*2} + C_\alpha^2 \tan^2(\alpha)} - (1-\kappa^*)\mu F_z}{4\left(C_s^2 \kappa^{*2} + C_\alpha^2 \tan^2(\alpha)\right)} \mu F_z \tag{6.77}$$

It appears that C_s^* is the product of C_s and a coupling term ρ. As a result, the linearized longitudinal force can be rewritten as:

$$F_x(\kappa) = C_s^* \kappa \tag{6.78}$$

This formulation respect the proposed requirements:

- Follows the physical nature as it depends on α, μ, and F_z,
- Take into account the combined slip by means of ρ,
- It is Linear and therefore simple from a control synthesis perspective,
- Dependents on online estimable parameters (Svendenius, J., 2007), (Soltani, 2014), (Singh and Taheri, 2015).

6.3.2 Lateral force linearization

The same reasoning is pursued. Here we suppose an α^* to be a stable operating point in the tire linear region. Again, we have $\alpha^* \ll$. We proceed then to the same simplifications as (6.74) and (6.75). Moreover, in the vicinity of α^*:

$$(\alpha \ll) \Rightarrow (\tan(\alpha) \cong \alpha) \tag{6.79}$$

Again, a lateral stiffness C_α^* can be defined using Dugoff's model equations (6.59), (6.60), and (6.61):

$$C_\alpha^*(\kappa, \mu, F_z) = \frac{4\sqrt{C_s^2\kappa^2 + C_\alpha^2\alpha^{*2}} - (1-\kappa)\mu F_z}{4\left(C_s^2\kappa^2 + C_\alpha^2\alpha^{*2}\right)}\mu F_z C_\alpha \tag{6.80}$$

The linearized lateral force is expressed as:

$$F_y(\alpha) = C_\alpha^*\alpha \tag{6.81}$$

The proposed requirements are again fulfilled. The only difference is that C_α^* depends on κ instead of α.

6.3.3 Dynamic saturation

The linearized forces developed are indefinitely increasing. As we have mentioned, the overall adhesion is delimited by a "friction ellipse" (see Figure 6.7). The tire potential is delimited by the product μF_z. In general, the friction can be anisotropic. The maximum longitudinal force could be therefore superior to the maximum lateral force. To simplify the problem, we have considered an isotropic friction. Thus, we are facing a "friction circle concept". Despite this simplification, the same logic is applied. When the tire is only solicited longitudinally, the maximum longitudinal force is equal to μF_z. If the tire is solicited laterally while accelerating or braking, the overall force moves along the friction circle. The maximum overall tire force is still μF_z, but the the maximum longitudinal force is penalized. The different forces saturation should be then dynamic:

$$\begin{cases} F_x \leq \sqrt{(\mu F_z)^2 - F_y^2} & (6.82) \\ F_y \leq \sqrt{(\mu F_z)^2 - F_x^2} & (6.83) \end{cases}$$

6.3.4 Summary

A new linear tire model with varying parameters has been developed in this section. This model is particularly suitable for GCC problems. The LPV tire model takes into account the combined slip and depends only on physical parameters that can be estimated only. To summarize, the model has the following structure:

$$\begin{cases} F_{x_{i,j}} = C_s^*\left(\alpha_{i,j}, \mu_{i,j}, F_{z_{i,j}}\right)\kappa_{i,j} & (6.84) \\ F_{y_{i,j}} = C_\alpha^*\left(\kappa_{i,j}, \mu_{i,j}, F_{z_{i,j}}\right)\alpha_{i,j} & (6.85) \end{cases}$$

Where:

$$\begin{cases} C_s^*(\alpha, \mu, F_z) = \dfrac{4\sqrt{C_s^2\kappa^{*2} + C_\alpha^2\alpha^2} - (1-\kappa^*)\mu F_z}{4\left(C_s^2\kappa^{*2} + C_\alpha^2\alpha^2\right)}\mu F_z C_s & (6.86) \\ C_\alpha^*(\kappa, \mu, F_z) = \dfrac{4\sqrt{C_s^2\kappa^2 + C_\alpha^2\alpha^{*2}} - (1-\kappa)\mu F_z}{4\left(C_s^2\kappa^2 + C_\alpha^2\alpha^{*2}\right)}\mu F_z C_\alpha & (6.87) \end{cases}$$

With κ^* and α^* are stable operating points that were chosen in way to ensure that the new tire model becomes equivalent to the simpler one when no combined slip is

involved:

$$\begin{cases} \kappa^* = \dfrac{\mu F_z}{8C_s^2}\left[\mu F_z + 4C_s + \sqrt{(\mu F_z)^2 + 8\mu F_z C_s}\right] & (6.88) \\ \alpha^* = \dfrac{\mu F_z}{2C_\alpha} & (6.89) \end{cases}$$

In addition, dynamic forces saturations should be considered to respect the friction ellipse phenomenon:

$$\begin{cases} F_{x_{i,j}} \leq \sqrt{\left(\mu F_{z_{i,j}}\right)^2 - F_{y_{i,j}}^2} & (6.90) \\ F_{y_{i,j}} \leq \sqrt{\left(\mu F_{z_{i,j}}\right)^2 - F_{x_{i,j}}^2} & (6.91) \end{cases}$$

6.4 Simulation and analysis of the linearized model

By reassembling the equations (6.76), (6.78), (6.80)-(6.83), we simulate the new linearized tire model and compare it to Pacejka model using the equations (6.6)-(6.9) in Matlab/Simulink® environment. The linearized Brush-based model is also plotted.

6.4.1 Brush-based and Dugoff-based linearized models comparison

Here, we only present the longitudinal force in combined slip with a side-slip angle of 1° (see Figure 6.17). The lateral force follows the same behavior but with different parameters.

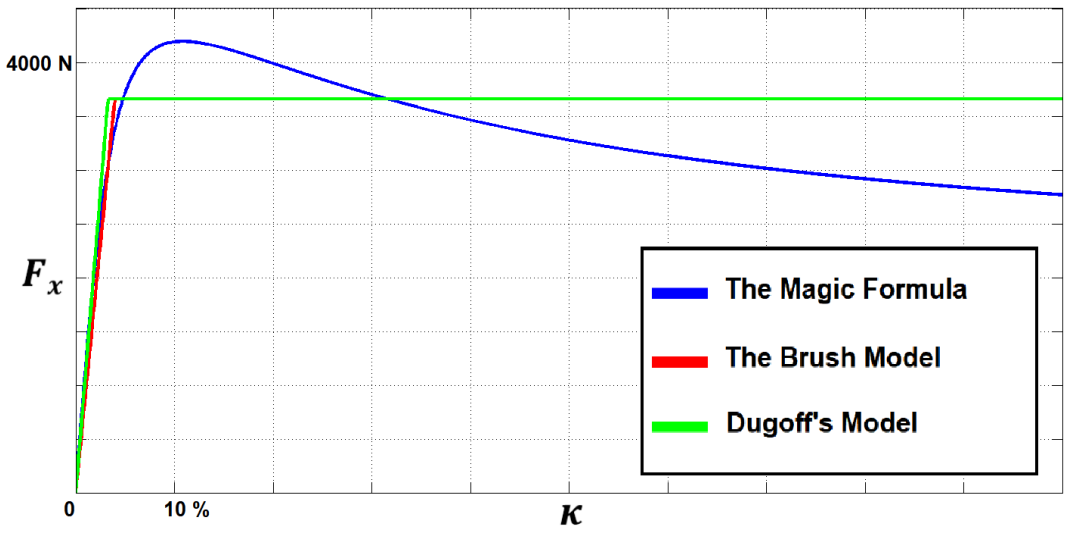

FIGURE 6.17: Comparison of Pacejka model with both linearized models in combined slip.

Although the brush model considers a parabolic vertical load distribution, once linearized, it does not offer much more precision with respect to Dugoff's model. The linearized model based on Dugoff's model provides a better simplicity/precision compromise. This latter will be then retained.

6.4.2 Linearized Dugoff-based model evaluation

Note in Figure 6.17 that the longitudinal force does not reach the maximum of $\mu F_z = 4000N$ because a part of the tire potential is already consumed by the lateral force. The curve's slope of the longitudinal force also varies with the side-slip angle because the longitudinal stiffness varies (see Figure 6.18).

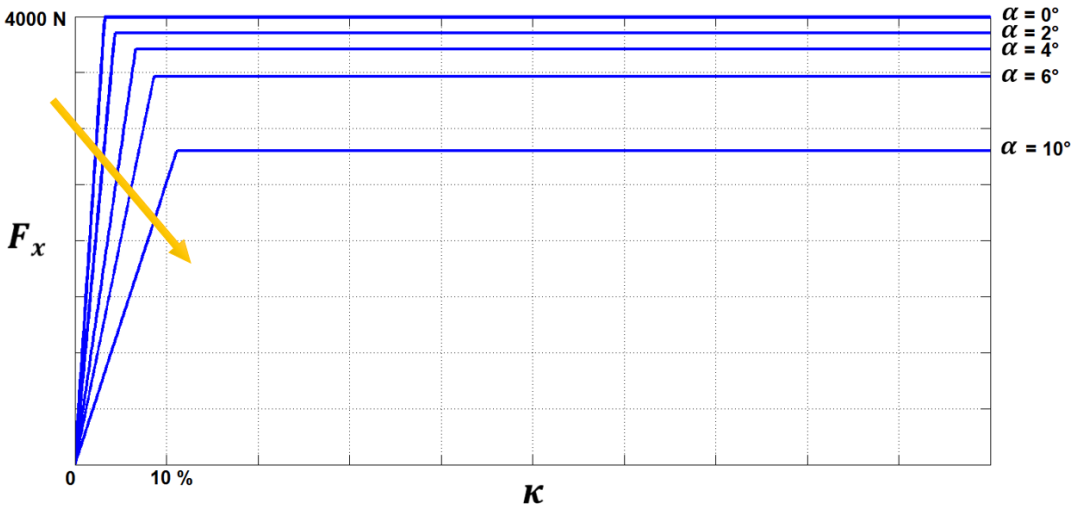

FIGURE 6.18: Variation of the longitudinal force slope with respect to side-slip angle (Linearized Dugoff-based model).

The same remark holds for the lateral force with respect to the longitudinal slip (Figure 6.19).

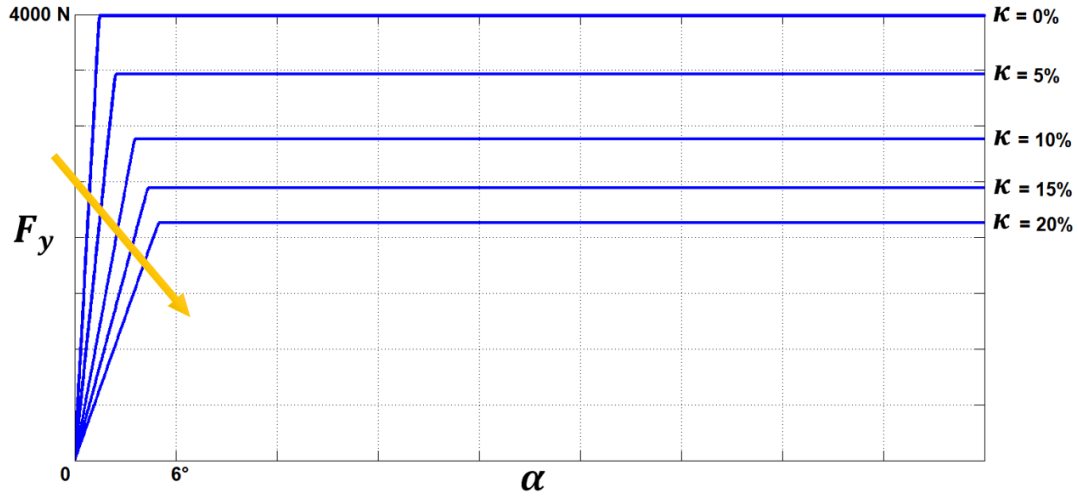

FIGURE 6.19: Variation of the lateral force slope with respect to longitudinal slip (Linearized Dugoff-based model).

That is to say that the linearized Dugoff-based model represent well the combined slip behavior in the stable region of the tire. More realistic simulations can be provided using a high-fidelity software as Simcenter Amesim®. This procedure will be used for the new tire model validation in Section 6.6.

6.5 Tire models comparison

Here again, empirical models' parameters are interpreted in order to meet a physical meaning, using the fact that the multiplication of Pacejka's parameters BCD is equivalent to the stiffness.

6.5.1 Case of Pure Longitudinal Slip

Here we present the simulation of the different models when the tire is only solicited longitudinally. Equations (6.6)-(6.8) are then used for Pacejka's model, (6.21)-(6.22) for Kiencke's, (6.27)-(6.28) for the Brush model, (6.58),(6.60)-(6.61) for Dugoff's, we add (6.63) for the modified version, we use (6.76),(6.78),(6.82) for the linearized version, and (6.65)-(6.67) for LuGre. The other left models lack from reliable data to be adapted to the rest of the models. Instead, we add the brush model with a varying friction coefficient to show its impact. Figure 6.20 gathers the different simulations in the same graph to enable their comparison.

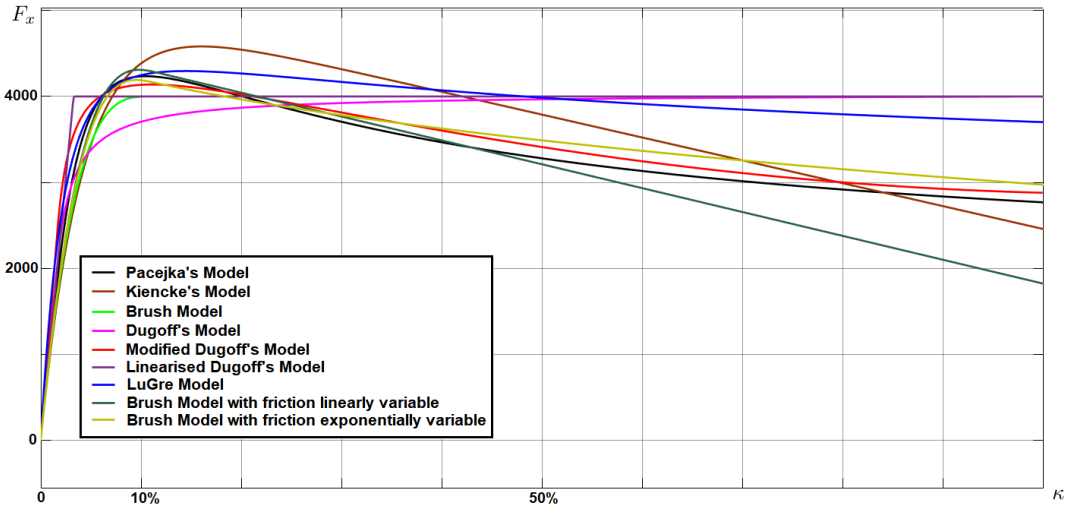

FIGURE 6.20: Comparison of tire models in case of pure longitudinal slip.

For its well-known accuracy, Pacejka's model can be taken as a reference. We can see that all the models describe well the linear behavior. As soon as the non-linear zone is reached, the models diverge. While several models exceed 4000N, the Brush model, Dugoff's model, and its linearized version do not because of the constraints imposed (see equations (6.28),(6.60),(6.82)). Regarding the unstable zone, only Kiencke's model, the LuGre model, the modified Dugoff's model and the Brush models with varying friction coefficient approximate this behavior. The reason, apart from the modified Dugoff's model, is the variable friction coefficient hypothesis. The approximation gets even better when the friction is considered exponentially variable.

6.5.2 Case of Pure Side Slip

We present here the simulation of different models when the tire is only solicited laterally. Equations (6.6)-(6.8) are then used for Pacejka's model with different parameters (see Pacejka, 2005), (6.21),(6.23) for Kiencke's, (6.29)-(6.30) for the Brush

model, (6.59)-(6.61) for Dugoff's, we add (6.64) for the modified version, and we use (6.80),(6.81),(6.83) for the linearized version. Figure 6.21 gathers the different simulations in the same graph to enable their comparison.

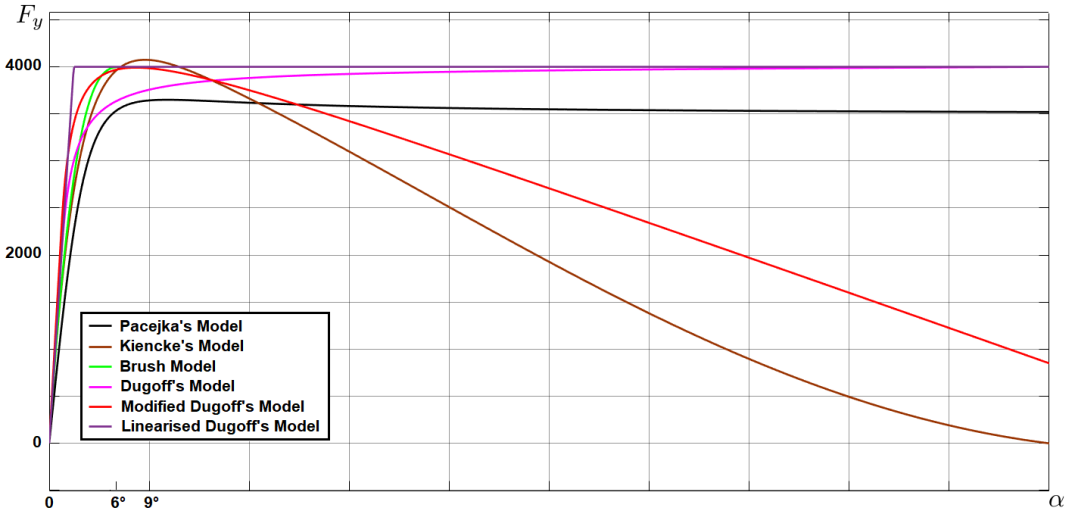

FIGURE 6.21: Comparison of tire models in case of pure side-slip.

The models here are less accurate with respect to Pacejka's model. The main reason is that Pacejka take into account several additional criteria whose most important are carcass flexibility and camber (Pacejka, 2005). Another difference is that Pacejka considers an anisotropic friction. In fact, while the longitudinal force exceeds 4000 N, the lateral force does not even reach it. However, in the linear zone, the models exhibit the same behavior. In the unstable region, the Brush model, Dugoff's model, and its linearized version saturate without decreasing because of the constraints imposed (see equations (6.30),(6.60),(6.83)). In contrast, Kiencke's model and the modified Dugoff's model decrease in the unstable zone, but fail to describe well the true behavior of the tire. For more precision, one could think of the Brush model in case of anisotropic friction with exponentially varying friction coefficient.

6.5.3 Case of Combined Slip

The Longitudinal Force

We introduce a constant side-slip angle of 4° and we vary the longitudinal slip to see the friction ellipse effect. The weighting functions (6.9) are then added to Pacejka's model, equation (6.19) are used for Brach's model using Pacejka's equations of pure slip, (6.21),(6.22) for Kiencke's, and (6.31)-(6.32) for the Brush model. Same equations than pure longitudinal slip are used for Dugoff's model, its modified version, and its linearized version. Figure 6.22 reassemble the different simulations in the same graph to enable their comparison.

As combined slip is concerned, the models' slopes decrease in the linear zone. Here accuracy of the different models is acceptable. As we approach the non-linear zone, errors become more obvious. In the unstable zone, only Brach's model, Kiencke's model, and modified Dugoff's model (all semi-empirical models) illustrate the tire loss of potential phenomenon. Kiencke's model is less accurate whereas Pacejka's curve and Brach's curve overlap. The Bruch model and Dugoff's model

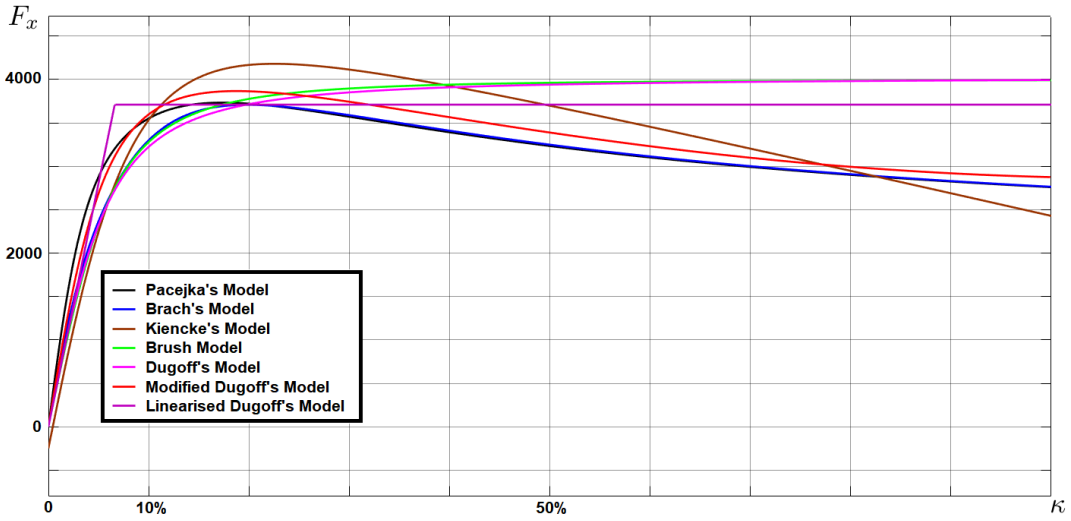

FIGURE 6.22: Comparison of tire models in case of combined slip - The longitudinal force with a side-slip of 4°.

saturate and reach a maximum of 4000 N, which is impossible in practice. The reason is the constant constraints imposed. The linearized Dugoff model solves this problem using dynamic constraints.

The Lateral Force

Here, we introduce a constant longitudinal slip of 10% and we vary the side-slip. Same weighting functions are added to Pacejka's model, equation (6.20) are used for Brach's model using Pacejka's equations of pure slip, and (6.31)-(6.32) for the Brush model. Same equations than pure side-slip are used for Dugoff's model, its modified version, and its linearized version. Figure 6.23 reassemble the different simulations in the same graph to enable their comparison.

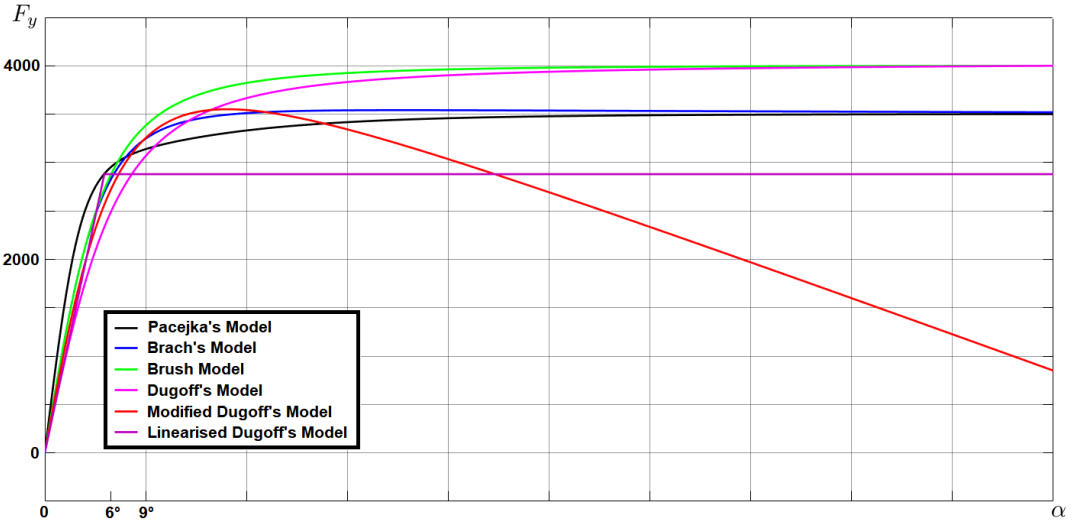

FIGURE 6.23: Comparison of tire models in case of combined slip - The lateral force with longitudinal slip of 10%.

As expected, the lateral force's slope decrease. The difference between models is more obvious in the non-linear zone. Regarding the unstable zone, only Brach's model describe well the tire behavior with respect to Pacejka's model. Again, the constant constraints used in the Brush model and Dugoff's model are wrong. A dynamic constraint should be used as it is the case in the linearized Dugoff's model.

6.5.4 Tire models' assignment

Tire modelling is essential for vehicle performances improvements, and for the tire performance itself. Four main challenges related to this context can be distinguished: *vehicle dynamics simulation*, *vehicle states estimation*, *vehicle motion control*, and *tire construction*.

Vehicle Dynamics Simulation

This gives an overview of the vehicle global performances off-line. It enables automotive engineers to determine the vehicle weaknesses according to real life scenarios. An exploded view of vehicle subsystems helps then to isolate the problem. This is done by studying the influence of a particular subsystem on the overall vehicle. For a reliable study, vehicle motion should be precisely described. Consequently, tire forces should be as close as possible to experimental data. It is well known that simulations enable time and cost-saving. Vehicle dynamics simulation improve even chassis and its subsystems design (Dieter, 2005).

High precision is required to meet experimental data. As simulations are done off-line, tire parameters could be updated manually. Empirical models seem to be a good match for these requirements:

- For high precision, **the Magic Formula of Pacejka** is perhaps the most widely used model. This model was develop to match as close as possible experimental data. Automotive software, e.g. CarSim® or Amesim®, make use of this model for high fidelity simulations. For pure longitudinal operations or pure lateral performances, one could use equations (6.6)-(6.8). For combined slip, weighting functions should be added (6.9).
- For explicit friction studies, one may favor **Kiencke's model** where a detailed expression of the friction coefficient is provided. Equations (6.21)-(6.23) are then used.
- Note that **Brach** was particularly interested by accident reconstruction (Brach and Brach, 2009). Equations (6.19)-(6.20) could be used for that matter.

Vehicle Motion Control

This is the part that interests us the most. Along with the relevant researches in terms of robotic vision and vehicle connectivity, chassis systems control is primary. In automatic control, related dynamics should be modelled, and relations between control inputs and desired performances should be formalized. Transfer functions are then deduced for control synthesis. As control synthesis consists of almost inverting the model, tire model should be simple enough. The automation engineer looks most of the time for a linear representation in at least a specific frequency range. This may induce modeling errors and uncertainties. Robust control is then used to ensure plant control despite the uncertainties (Doyle et al., 1989). Consequently, a simpler

model is sufficient. Note that there are subsystems designed for a single physical quantity control (Brennan and Alleyne, 2001). Combined slip is then neglected. In contrast, it is important to take account of the combined slip as long as combined maneuvers are concerned.

Simplicity is most of the time translated into linearization. Consequently, the **linearized Dugoff Model** represents an adequate solution for control synthesis. Equations (6.76)-(6.83) could then be used to synthesize control commands even in case of combined slip. The simpler linear model that is usually selected (Brennan and Alleyne, 2001) can only be used to synthesize stand-alone subsystems designed for single physical quantity control. The reason is that its parameters C_s and C_α are constant, and therefore, combined slip is not considered.

Vehicle States Estimation

For vehicle control or driver warning, not all the required states are measurable. Few key parameters should then be estimated to ensure vehicle safe operation. A major difference with respect to vehicle dynamics simulation is that these parameters should be estimated on-line. In this context, the automotive engineer needs a fast computing model depending on a minimum number of parameters. Moreover, vehicles are operating on unpredictable environments. Parameters should then be updated. To do this, parameters should have a physical meaning so they can be estimated from other measurable parameters through physical equations. A common example is the problem of friction coefficient estimation (Patra and Datta, 2012), (Singh and Taheri, 2015). In fact, this conventional parameter depends on the road surface condition that the driver cannot act on. This parameter could be estimated if the tire forces are calculated in advance. As these latter are also not measured in commercial vehicles due to sensors' cost, vehicle motion's sensors are used to estimate them (M'sirdi et al., 2005). Theoretical models are then necessary to face this kind of challenges:

- For fast computation, **Dugoff's model** seems to be a good solution. Minimum parameters are required. And because constant vertical load along a single tire is assumed, relatively simpler equations are used (6.58)-(6.61).
- For more precise estimation, one could consider a parabolic vertical load distribution. That is to say choosing the **Brush model**. Several conditions are distinguished in this case:
  - For pure slip, equations (6.27)-(6.30) are used.
  - For combined slip and isotropic friction, equations (6.33)-(6.36) are preferred.
  - For combined slip and anisotropic friction, equations (6.37)-(6.41) are used, and equations (6.46)-(6.47) are preferred.

Tire Construction

Here, interest is given to the tire's structure. Specific tire performances are studied and improved. For example, in wet soils, indentation phenomenon is corrupted (Michelin, 2001). Water must be evacuated to maintain a decent friction potential. Tread elements geometry is then redesigned to enable water evacuation while keeping optimal operation in dry soils (Figure 6.24). A 2-D model is no longer sufficient,

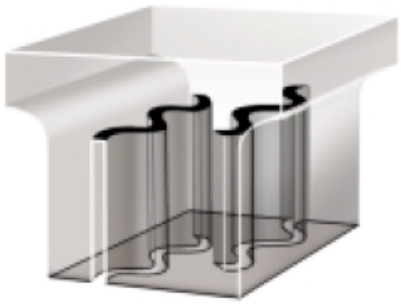

FIGURE 6.24: Wavy sipes used for water evacuation since the 1930's (Michelin, 2001).

3-D models are often favored. Ad-hoc Finite Element Methods (FEM) are then used. These non-behavioral methods exceed the scope of this paper.

6.6 Validation and relevance of the new tire model

As we have mentioned earlier, reduced vehicle models are used in the downstream approach. Typically, the bicycle model is preferred for control synthesis in most of the research papers (Selby, 2003),(Soltani, 2014),(Xiong and Yu, 2011),(Bächle et al., 2014). This hypothesis relies on a linear but non coupled model of the tire. Therefore, it has a simpler representation:

$$\begin{cases} F_x = C_s \kappa & (6.92) \\ F_y = C_\alpha \alpha & (6.93) \end{cases}$$

The tire behavior is well represented in the linear region, but the model does not take into account the combined slip. This model is more suitable for vehicle stand-alone subsystems. For example, in (Xiong and Yu, 2011), this simple model is used to develop vehicle longitudinal control logic for a 4WD Hybrid Electric system. In (Harada and Harada, 1999) and (Shuai et al., 2014), the bicycle model is used for lateral control performance improvement. With the arrival of autonomous vehicles, the virtual pilot must handle multi-objective control problems. Couplings should be therefore considered, especially at the tire level. For GCC, the linearized Dugoff-based model proposed in this paper is necessary. To illustrate this, a vehicle global dynamic analysis is described next using Simcenter Amesim® platform.

6.6.1 Comparison of linear models

To compare both linear models, another requirement should be added. The new linear tire model should be equivalent to the simpler one when there is no combined slip. This requirement enables giving explicit expressions to the different stable operating points κ^* and α^*.

Respecting the previous requirement means:

$$C_s^*(0, \mu, F_z) = C_s \quad (6.94)$$

According to the expression (6.76), we find:

$$\kappa^* = \frac{\mu F_z}{8C_s^2}\left[\mu F_z + 4C_s \pm \sqrt{(\mu F_z)^2 + 8\mu F_z C_s}\right] \tag{6.95}$$

Both results are acceptable because $\mu F_z + 4C_s \gg \sqrt{(\mu F_z)^2 + 8\mu F_z C_s}$. Here, we consider the highest one.

Again, the previous requirement leads to:

$$C_\alpha^*(0, \mu, F_z) = C_\alpha \tag{6.96}$$

According to the expression (6.80), we find:

$$\alpha^* = \frac{\mu F_z}{2C_\alpha} \tag{6.97}$$

The Amesim® demo used describes a complete chassis model and provides global dynamics analysis (Figure 6.25).

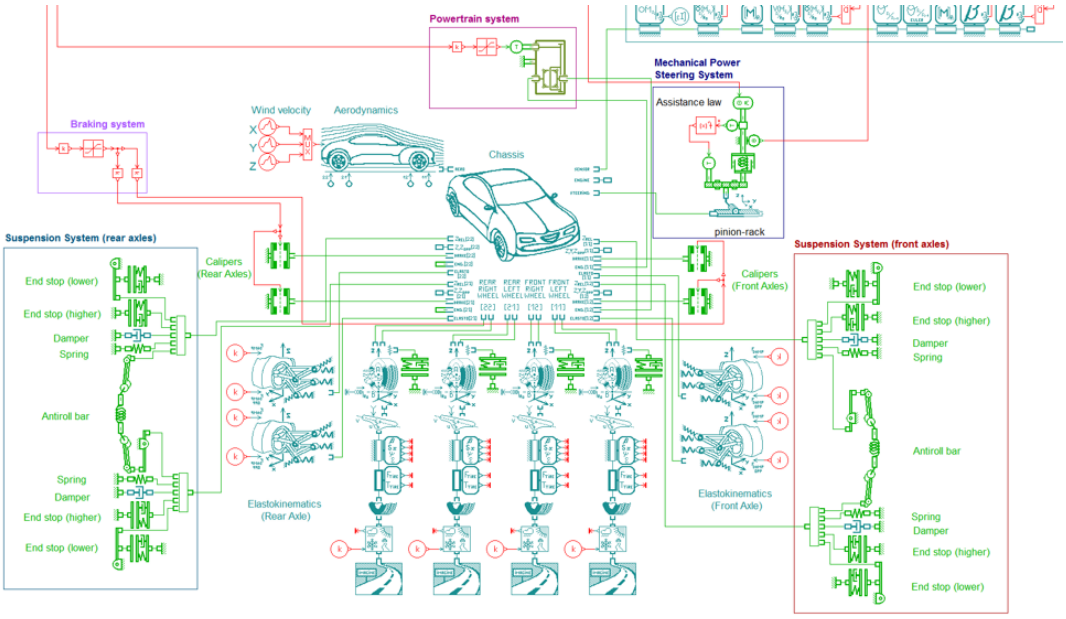

FIGURE 6.25: The chassis model of 15 degrees of freedom in Amesim® environment.

Inputs are steering angle and engine torque. The combined slip could then be observed. The vehicle is a B-segment class car. The model is composed of a chassis model with 15 degrees of freedom with associated subsystems: elastokinematics module, suspension (spring, damper, lower and higher end stop, antiroll bar), aerodynamic module, tire, road, sensors, powertrain unit, braking system and powersteering system. It is a highly nonlinear global model whose purpose is to represent as precise as possible the vehicle behavior. Most importantly, it uses Pacejka's model to calculate tires' efforts. We add supplementary modules that include the new linear Dugoff-based tire model and the classic linear tire model and compare them with The Magic Formula of Pacejka. Figure 6.26 illustrates the longitudinal force and Figure 6.27 illustrates the lateral force.

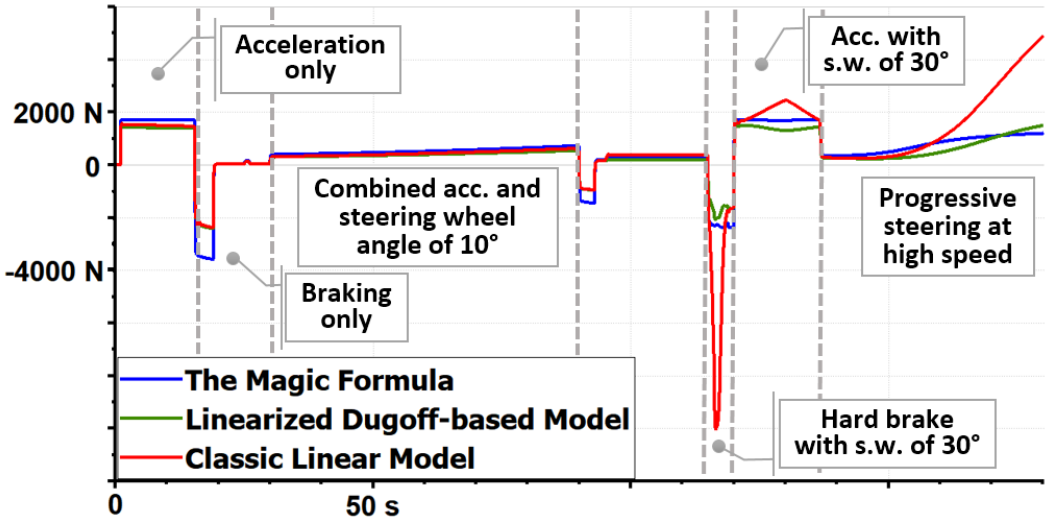

FIGURE 6.26: Amesim® comparison of Pacejka model with linearized models - Front left tire longitudinal force.

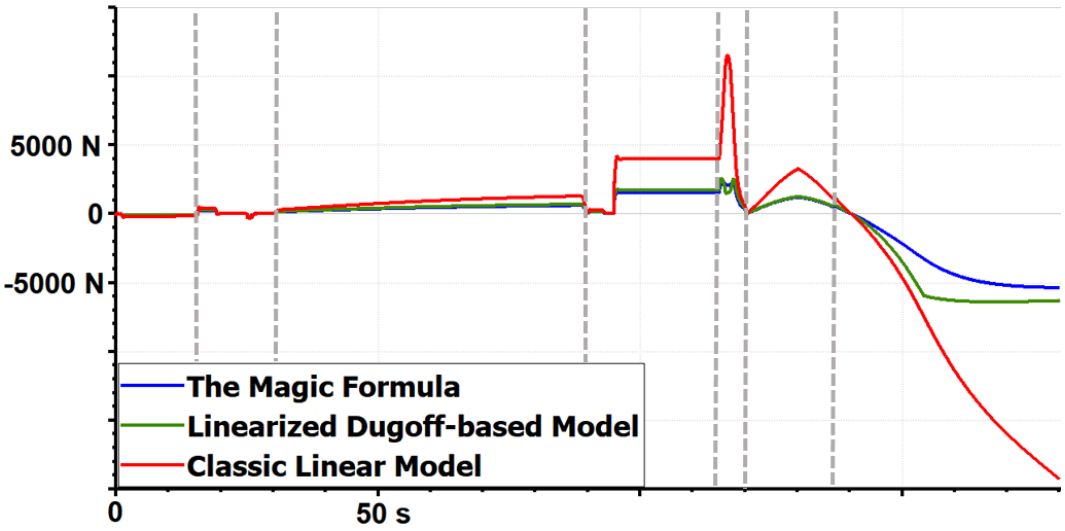

FIGURE 6.27: Amesim® comparison of Pacejka model with linearized models - Front left tire lateral force.

When only longitudinal force is requested (acceleration or braking), both linear models are close enough to Pacejka's model. The lateral force of the classic linear model starts to deviate as soon as the tire is solicited longitudinally and laterally at the same time. Both longitudinal and lateral forces of the classic linear model diverge at severe conditions, for example in a hard brake maneuver while steering or progressive steering at high velocity. In contrast, the new linearized model follows close enough the Magic Formula. When the tire is solicited longitudinally and laterally at the same time, both longitudinal and lateral stiffnesses are updated and dynamic saturations are recalculated. The values of the forces are then lower. This is crucial from a control perspective. Ignoring combined slip may lead to high tire force demand. This could exceed the saturated value and destabilize the vehicle. The new linearized model proposed aims to prevent this scenario.

6.6.2 Further improvements

So far, all mathematical formulas developed are expressed in steady state conditions. In control synthesis, time response is an important criterion. Subsequently, the transient behavior should be considered. Tire force delay is caused by carcass deflections (Svendenius, 2003), (Pacejka, 2005). This is usually represented by a first order lag (Di Martino, 2005), (Klomp and Lidberg, 2006):

$$F_i = \frac{1}{1+\tau_i s} F_i^{ss} \tag{6.98}$$

i is either x or y, τ_i is the time-constant, s is the Laplace operator, and F_i^{ss} is the steady-state force that have been developed in the previous sections.

The carcass deflections change with the vehicle speed (Svendenius, 2003),(Pacejka, 2005),(Di Martino, 2005),(Klomp and Lidberg, 2006). Time-constant in equation (6.98) depends then on the vehicle's speed:

$$\tau_i = \frac{3L_i}{V_x} \tag{6.99}$$

L_i is defined as the relaxation length and V_x is the vehicle longitudinal speed. The relaxation length represent the distance that tire rolls before the lateral force reaches 63% of its final value (Pacejka, 2005). This does not influence much the shape of the tire response as the Figure 6.28 shows.

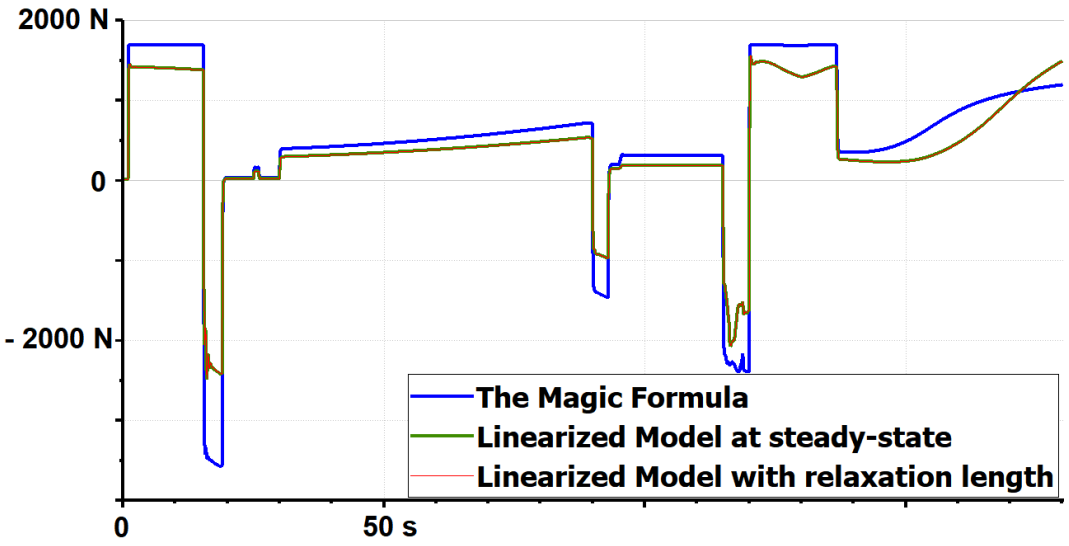

FIGURE 6.28: Amesim® comparison of Pacejka model and linearized models with and without transient behavior - Front left tire longitudinal force.

This is mainly due to the low value of the relaxation length (around 0.02 m). In control synthesis, the transient behavior could be ignored to prevent the generation of high order controllers.

6.6.3 Controllability

The linearized model is developed for control synthesis suitability. A state-space representation can be proposed:

$$\begin{cases} \dot{x}(t) = A(t)\,x(t) + B(t)\,u(t) & (6.100) \\ y(t) = C(t)\,x(t) & (6.101) \end{cases}$$

Where:

- $x(t) = \begin{bmatrix} F_x \\ F_y \end{bmatrix}$: is the state vector,
- $y(t) = \begin{bmatrix} F_x \\ F_y \end{bmatrix}$: is the output vector,
- $u(t) = \begin{bmatrix} \kappa \\ \alpha \end{bmatrix}$: is the input vector,
- $A(t) = \begin{bmatrix} -\frac{1}{\tau_x} & 0 \\ 0 & -\frac{1}{\tau_y} \end{bmatrix}$: is the state matrix,
- $B(t) = \begin{bmatrix} \frac{C_s^*}{\tau_x} & 0 \\ 0 & \frac{C_\alpha^*}{\tau_y} \end{bmatrix}$: is the input matrix,
- $C(t) = \begin{bmatrix} 1 & 0 \\ 0 & 1 \end{bmatrix}$: is the output matrix.

Without forgetting the constraints (6.82) and (6.83).

Note that both state and input matrices contain varying parameters. Although stiffness coefficients depend on input variables, they cannot be split as we need the whole expression to be multiplied by its corresponding input variable. According to the structure of the matrices A, B and C, the system is clearly stable, controllable and observable as long as the varying parameters are positive, which is the case. Finally, this representation is suitable for modular and flexible control architectures. A simple tire module can be added as the Figure 6.29 shows where the tire block contains equations (6.100) and (6.101) and constraints (6.82) and (6.83).

6.6.4 Relevance of the new tire model

We recall that this model was developed to face Global Chassis Control issues. As far as the overall chassis is concerned, coordination is a key aspect. We saw that in the downstream coordination approach, rule-based strategies are generally preferred. Autonomous vehicles require additional subsystems. As the number of subsystems increases, development of such rule-based strategies becomes less obvious. Optimization techniques performed upstream the standalone subsystems present a promising alternative in this situation. For ground vehicles, tires are the sole effectors. The command distribution is mainly constrained by tires' potential and actuators' limits. As far as coupled operations and therefore combined slip is concerned, the potential available for one direction varies due to the other direction. This

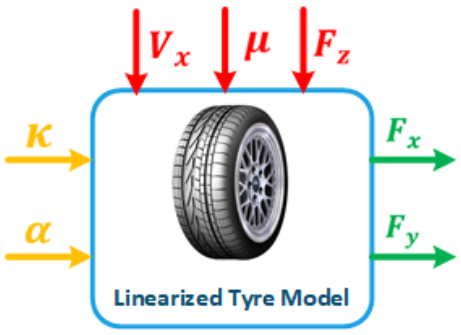

FIGURE 6.29: Linearized tire module with varying-parameters.

new tire model offers the possibility to take into account this phenomenon by varying the tires' stiffness in each direction when the tire is solicited both longitudinally and laterally. In addition, the overall potential may vary if the friction changes or the vertical load varies. For the first cause, this can happen for example if it starts raining and the road becomes wet. For the second cause, the vertical load can vary due to roll dynamics when turning, and pitch dynamics when braking or accelerating, which is more likely to happen. The new tire model depends on both the fiction coefficient and the vertical load. The maximum efforts are then updated if μ and F_z are well estimated. To sum up, three reasons can lead to an overestimation of the tire potential and lead to a wrong control distribution: combined slip, friction change or vertical load variation. The new tire model takes into account these three phenomenon in order to favor the tires with greater potential when allocation the commands, and optimize the vehicle's overall potential.

6.7 Contributions

In this chapter, the most used tire models have been reviewed. The relevant tire models have been assigned to a specific purpose to guide automotive engineers into choosing a tire model depending on their needs. We particularly noticed that there is a lack in tire models specifically designed for control synthesis, especially when it comes to GCC. Due to the importance of the tire model to the upstream control distribution, we developed our own tire model. Our contributions manifest in the guidelines to choose of the classical tire models and the proposal for a new one to fill the gap in tire models designed for control synthesis. Our new tire model and a review on tire models have been published in:

1. M. Kissai, B. Monsuez, A. Tapus and D. Martinez, "A new linear tire model with varying parameters," *2017 2nd IEEE International Conference on Intelligent Transportation Engineering (ICITE)*, Singapore, 2017, pp. 108-115. DOI: 10.1109/ICITE.2017.8056891.

2. M. Kissai, B. Monsuez, D. Martinez and A. Tapus, "Review Update of Tire Behavior Models," *The International Journal of Automotive Technology*, 2019. ***Submitted***.

7 Friction Circle Estimation

As we previously have seen in Chapter 6, in order to distribute optimally the effort into the four tires, the maximum potential of each tire should be known in advance. The maximum tire force varies not only due to forces couplings, but varies also with the tire normal force and the friction coefficient (Figure 7.1). These two variables should be estimated.

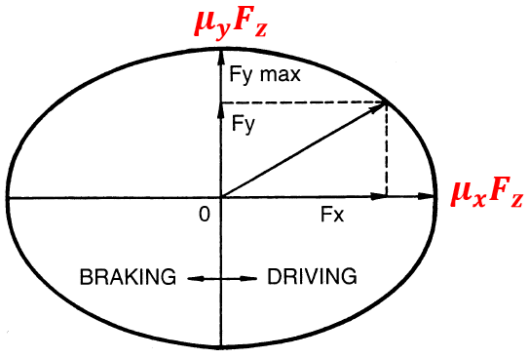

FIGURE 7.1: The friction ellipse concept (adapted from (Wong, 2001)).

As much as tire normal forces have been successfully estimated in previous researches (Soltani, 2014), the friction coefficient estimation still presents several difficulties for automakers' engineers. In this chapter, we will first discuss the tire normal forces estimation, and then we will present a simple yet effective method to approximate the friction coefficient. To simplify, we consider $\mu_x = \mu_y$, hence the title of this chapter: friction *circle* estimation.

7.1 Tire normal forces

Tire normal forces vary with accelerations. Most of researches use directly accelerations measurement to represent vertical loads variations (Soltani, 2014), (Shuai et al., 2014), (Doumiati et al., 2013). However, the vertical load affects first the suspensions, then the tires. Using accelerations signals, which vary sometimes very quickly, give noisy and imprecise vertical loads signals. Here, we use rather the roll and pitch dynamics, which give filtered and more representative signals. Tire normal forces are then expressed as:

$$\begin{cases} F_{z_{fl}} = \frac{1}{2}M_s g\frac{l_r}{L} + k_{s_f}\frac{t}{2}\phi + c_{s_f}\frac{t}{2}\dot{\phi} - k_{s_f}l_f\theta - c_{s_f}l_f\dot{\theta} & (7.1) \\ F_{z_{fr}} = \frac{1}{2}M_s g\frac{l_r}{L} - k_{s_f}\frac{t}{2}\phi - c_{s_f}\frac{t}{2}\dot{\phi} - k_{s_f}l_f\theta - c_{s_f}l_f\dot{\theta} & (7.2) \\ F_{z_{rl}} = \frac{1}{2}M_s g\frac{l_f}{L} + k_{s_r}\frac{t}{2}\phi + c_{s_r}\frac{t}{2}\dot{\phi} + k_{s_r}l_r\theta + c_{s_r}l_r\dot{\theta} & (7.3) \\ F_{z_{rr}} = \frac{1}{2}M_s g\frac{l_f}{L} - k_{s_r}\frac{t}{2}\phi - c_{s_r}\frac{t}{2}\dot{\phi} + k_{s_r}l_r\theta + c_{s_r}l_r\dot{\theta} & (7.4) \end{cases}$$

Where:

- L : vehicle's wheelbase[1],
- t : vehicle's track[2].

Therefore, roll and pitch dynamics should be also estimated. Roll dynamics are mainly caused by the vehicle's lateral acceleration a_y (Ellis, 1969). By supposing that the spring stiffness and the damper ratio of the four suspensions are approximately identical, roll dynamics can be expressed as follows:

$$I_{xx}\ddot{\phi} = Ma_y h_G + M_s g h_G - 4k_s\left(\frac{t}{2}\right)^2\phi - 4c_s\left(\frac{t}{2}\right)^2\dot{\phi} \quad (7.5)$$

The advantage is that only lateral acceleration measurement is needed. A second-order transfer function is then used to determine the roll angle. The same method can be adopted for the pitch dynamics using this time the longitudinal acceleration measurement. It should be noted that the accelerometer do not differentiate between accelerations induced by the vehicle and the gravitational acceleration. Care should be given to signal processing in case of roads with slopes.

In equations (7.1)-(7.4), the first terms represent the vehicle static weight distribution on each wheel. The additional terms are "*the load transfer*" due to longitudinal and lateral accelerations (dynamic loads), which is more of a dynamic distribution of support than a load transfer. Indeed, the mass does not change from one side to another, unless there are some mobile objects in the vehicle. In conclusion, it is clear that the normal loads on the four tires are not the same when the vehicle is subject to longitudinal and/or lateral acceleration. Figure 7.2 shows for example the case of normal forces when a vehicle is braking in a turn. Both lateral and longitudinal accelerations are experienced. Here, the highest normal force is applied to the front right tire, while the normal load on the rear left tire is the lowest. By assuming a similar coefficient of friction for all the four tires, the radius of friction circle on each tire is determined by its normal force. The control distribution should be done in such a way to favor the tire with the biggest potential. Hence the importance of estimating the normal tire forces.

7.2 Friction estimation strategy

The friction coefficient is a representative ratio between the tire force and the vertical load (Majdoub et al., 2012): it cannot be directly measured. Usually, when instrumenting a vehicle prototype, the costly sensors equipped at the tire rubber blocks

[1] $L = l_f + l_r$.

[2] Here the front and rear track are considered equal. A slight difference can appear in practical applications.

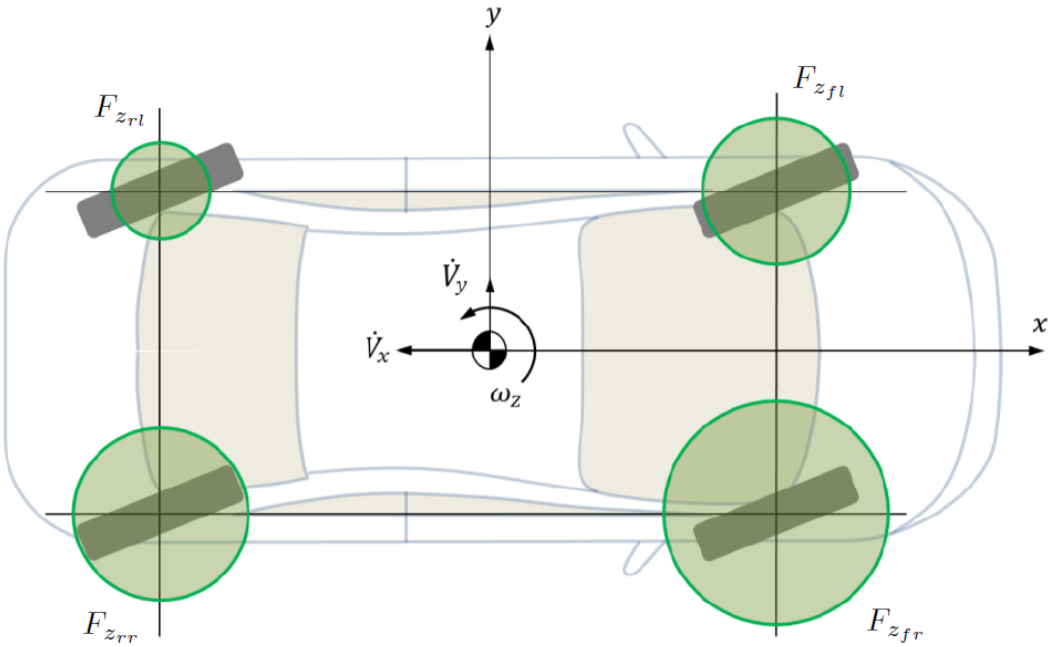

FIGURE 7.2: Normal forces on tires in left hand cornering while braking (adapted from (Soltani, 2014).).

are rather used for tire force measurement and not to directly measure the friction coefficient. For example, in (Erdogan, 2009), a wireless piezoelectric tire sensor has been presented. This sensor is used to measure tire deformations, and then deduce the friction coefficient. A broader state-of-art on friction estimation techniques is provided in Chapter 2. The conclusion was that most research papers focused on estimating the friction coefficient in pure longitudinal maneuvers (Zhao et al., 2017), (Patra and Datta, 2012), (Rath, Veluvolu, and Defoort, 2015), or using only the lateral dynamics (Liu et al., 2017). The longitudinal tire force for example can be penalized due to a friction coefficient change but also due to a lateral force demand. In order to estimate the friction coefficient, the causes should be differentiated. That is why we believe that the initial overall modeling is very important. It should be precise enough to limit the number of errors to be corrected by data-based techniques. In this thesis, we focus on the initial modeling putting on the spotlight the importance of roll and pitch dynamics. Our investigations showed that particularly the vertical dynamics have an important influence on variables estimation, but are neglected in most research papers. The purpose is to approximate the friction coefficient rapidly without any complicated observation method, update the control logic, and avoid the vehicle's loss of control even in severe conditions. Future works will focus on how to use data-based techniques to improve the estimation process in different use-cases.

As it was reported in (Kritayakirana, 2012) and (Funke and Gerdes, 2015), the speed profile of a path should be generated while respecting the friction circle[3]. This can also be represented as:

$$\sqrt{a_x^2 + a_y^2} \leq \mu g \tag{7.6}$$

Where a_x and a_y are the longitudinal and lateral accelerations respectively. "μg" represents then the maximum achievable global acceleration. Therefore, by using

[3]Considering an isotropic friction.

an effect-based estimation method, μ can only be estimated at the limits of handling. In other words, if we are able to reliably estimate the overall acceleration and if the estimated acceleration exceeds the measured one $a_{g_{mes}}$, this means that the real acceleration has reached its maximum "μg". We can simply divide $a_{g_{mes}}$ by g to get the friction coefficient μ. Figure 7.3 gives an overview of the estimation method.

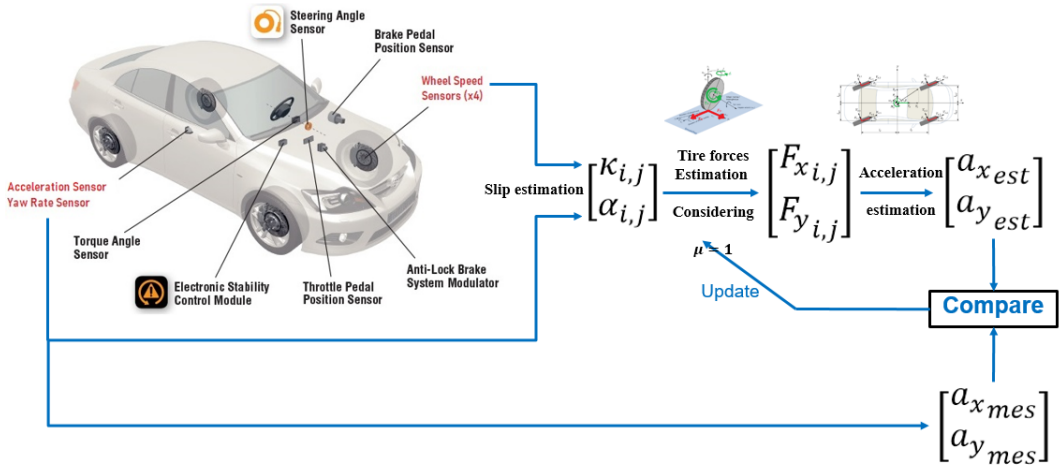

FIGURE 7.3: The friction coefficient estimation method.

The algorithm of this approach is therefore:

Algorithm 1 μ estimation

Let μ_0 be a starting value

$\mu_0 \leftarrow 1$
if $a_{g_{est}} > a_{g_{mes}}$ **then**
  if $a_{g_{est}} - a_{g_{mes}} \geq \eta$ **then**
    $\mu \leftarrow \frac{a_{g_{mes}}}{g}$
  end if
else
  if $a_{g_{est}} - a_{g_{mes}} \leq -\eta$ **then**
    $\mu \leftarrow \mu + \varepsilon$
  end if
end if

Where η is a threshold that takes account of the remaining modeling errors, and ε is a small factor that enables testing the surface potential gradually.

As Figure 7.3 shows, in order to estimate the overall vehicle's acceleration, several vehicle states should be precisely estimated. The idea is then to compare permanently the estimated acceleration to the measured one. If the difference between the two signals starts to grow, this would mean that friction is no longer sufficient to generate the desired acceleration, and we can therefore update as fast as possible the control logic, more specifically the maximum tire forces values, to avoid the loss of control of the vehicle. A simple and fast estimation approach is then needed. Here, we show that by only reviewing every state estimation, interesting results can be obtained. Due to time limits and the scope of the thesis, complex observers are not investigated yet.

Moreover, by updating the control in low friction surfaces, the performance would be limited. The algorithm should be able to improve the vehicle's performances when regaining a high friction surface. In this thesis, we simply increase gradually the value of the friction coefficient without destabilizing the overall system. The idea is to continually test the surface potential, and benefit from its maximum when needed, without jeopardizing the vehicle's stability. It should be noted that a threshold that takes account of the remaining modeling errors has been added. In the following paragraphs, the estimations of states that are necessary to estimate the overall accelerations are exposed.

7.2.1 Tire Slip

The first stop is the tire slip. As detailed in Chapter 6, tire forces originate from this phenomenon. We differentiate between the longitudinal slip and the side-slip.

Longitudinal slip

The longitudinal slip is defined most of the time as follows (Pacejka, 2005):

$$\kappa_{ij} = \frac{R_{ij}\omega_{ij} - V_x}{max\left(R_{ij}\omega_{ij}, V_x\right)} \tag{7.7}$$

The "max" function is used to avoid singularity.

To simplify, V_x is usually considered as the vehicle's velocity at its CoG. But as several authors have reported (Dugoff, Fancher, and Segel, 1969), (Svendenius, 2003), it is the component of the tire velocity along its longitudinal axis that should be considered. While several works did take into account this aspect by adding the influence of the yaw rate (Soltani, 2014), the tire velocity should be actually calculated at the tire/road interface as long as the slip is concerned. The vertical distance between the vehicle's CoG and the road level introduces therefore roll and pitch dynamics. This is mainly caused by the sprung mass motions by means of suspensions, inducing rubber crushing into the road surface. This modifies slip values and therefore tire forces. The longitudinal slip is then calculated here as follows:

$$\kappa_{ij} = \frac{R_{ij}\omega_{ij} - v_{wx_{ij}}}{max\left(R_{ij}\omega_{ij}, v_{wx_{ij}}\right)} \tag{7.8}$$

Where $v_{wx_{ij}}$ is the component of the tire velocity along its longitudinal axis at the tire/road interface. It should be noted that this variable is calculated at the steered non-cambered frame. Camber has little influence in our case and the vehicle is not equipped by any camber sensor. Calculation of $v_{wx_{ij}}$ is done in two steps. First, we express the tire velocity in the non-steered frame using Varignon's theorem, then we determine the velocity value at the steered frame. Let us call "G" the vehicle's CoG, and "P_{fl}" the center of the contact area of the front-left tire with the road surface. We have then:

$$\overrightarrow{V\left(P_{fl}\right)} = \overrightarrow{V\left(G\right)} + \overrightarrow{P_{fl}G} \wedge \overrightarrow{\Omega} \tag{7.9}$$

With $\overrightarrow{\Omega}$ is the rotational vector of the sprung mass.

This gives:

$$\begin{vmatrix} V_x\left(P_{fl}\right) \\ V_y\left(P_{fl}\right) \\ V_z\left(P_{fl}\right) \end{vmatrix} = \begin{vmatrix} V_x - \frac{t}{2}\dot{\psi} - h_G\dot{\theta} \\ V_y + l_f\dot{\psi} + h_G\dot{\phi} \\ V_z - l_f\dot{\theta} + \frac{t}{2}\dot{\phi} \end{vmatrix} \tag{7.10}$$

Where h_G is the height of the CoG with respect to the ground. Consequently, in the steered frame we have:

$$\begin{cases} v_{wx_{fl}} = V_x\left(P_{fl}\right)\cos\left(\delta_f\right) + V_y\left(P_{fl}\right)\sin\left(\delta_f\right) \\ v_{wy_{fl}} = -V_x\left(P_{fl}\right)\sin\left(\delta_f\right) + V_y\left(P_{fl}\right)\cos\left(\delta_f\right) \end{cases} \tag{7.11}$$

Where $v_{wy_{ij}}$ is the lateral component of the tire velocity at the tire/road interface. The same method is adopted for the remaining wheels. Care should be given to the signs. Roll dynamics are estimated using equation (7.5). Pitch dynamics are calculated using the same structure for the longitudinal acceleration.

Regarding the vehicle's longitudinal and lateral speed, the vehicle is actually equipped by only four wheel speed sensors, a steering wheel angle sensor, an accelerometer, and a yaw rate sensor. Both longitudinal and lateral speeds responses should be estimated. We use then the accelerometer and the yaw rate sensor to get these estimations by means of the following equations:

$$\begin{cases} V_x = \int a_{x_{mes}} - V_y\dot{\psi} \end{cases} \tag{7.12}$$

$$\begin{cases} V_y = \int a_{y_{mes}} + V_x\dot{\psi} \end{cases} \tag{7.13}$$

Where $a_{x_{mes}}$ and $a_{y_{mes}}$ represent the longitudinal and lateral measured accelerations respectively. As both equations (7.12) and (7.13) are coupled, V_x is simply estimated one sample time earlier than V_y.

7.2.2 Side-slip

Noted here α_{ij}, the side-slip can be defined as follows (Brach and Brach, 2000):

$$\tan\left(\alpha_{ij}\right) = \frac{v_{wy_{ij}}}{v_{wx_{ij}}} \tag{7.14}$$

Once again, several papers consider only the longitudinal velocity of the vehicle's CoG, and calculate the lateral velocity at the non-steered tire frame (Schofield, 2008). Even the most rigorous calculations that take into account the steered tire frame do not take into account vertical dynamics in the side-slip calculation (Soltani, 2014). Here, the side-slip is calculated using expressions as it was shown in equations: (7.9)-(7.11).

7.2.3 Tire Forces

In this thesis, a new linear tire model with varying parameters has been developed for global chassis control synthesis. The aim was a simple invertible model that can depicts the combined slip precisely enough. In contrast, for state estimation, precision is more important than simplicity as there is no intention to inverse the model.

The most precise one is Pacejka's model, or what is referred to as the *Magic Formula* (Pacejka, 2005). This semi-empirical model depends on numerous parameters with no physical significance. As our goal is to estimate the friction coefficient online, we prefer to choose a physical model that depends on parameters representing explicitly friction variations. Consequently, Dugoff's model has been chosen here (Dugoff, Fancher, and Segel, 1969). This model depicts well the combined slip phenomenon, but only in the stable zone of the tire. In this work, this do not represent any drawback, because the CA strategy takes into account the dynamic saturations of tire forces using equation (6.82) and (6.83). This prevents the vehicle from entering the unstable zone of the tire. Equations (6.58)-(6.61) are then used for tire forces estimation.

7.3 Accelerations Estimation

Once tire forces are estimated at each wheel, accelerations can be estimated as follows:

$$\begin{bmatrix} a_{x_{est}} \\ a_{y_{est}} \end{bmatrix} = \begin{bmatrix} \cos(\delta_f) & \cos(\delta_f) & \cos(\delta_r) & \cos(\delta_r) & -\sin(\delta_f) & -\sin(\delta_f) & -\sin(\delta_r) & -\sin(\delta_r) \\ \sin(\delta_f) & \sin(\delta_f) & \sin(\delta_r) & \sin(\delta_r) & \cos(\delta_f) & \cos(\delta_f) & \cos(\delta_r) & \cos(\delta_r) \end{bmatrix} \begin{bmatrix} F_{x_{fl}} \\ F_{x_{fr}} \\ F_{x_{rl}} \\ F_{x_{rr}} \\ F_{y_{fl}} \\ F_{y_{fr}} \\ F_{y_{rl}} \\ F_{y_{rr}} \end{bmatrix} \tag{7.15}$$

The global horizontal acceleration can be then calculated as follows:

$$a_{g_{est}} = \sqrt{a_{x_{est}}^2 + a_{y_{est}}^2} \tag{7.16}$$

The **Algorithm 1** is then applied to estimate the friction coefficient. This method will be tested further by co-simulation in Chapter 11 where a vehicle equipped by an ARS, a VDC and a RTV is controlled in severe maneuvers.

7.4 Contributions

The major contribution in this chapter is the simple estimation method for friction coefficient by revisiting the vehicle dynamics equations. Vertical loads have been also adapted by using roll and pitch dynamics instead of directly using accelerations signals. This method applied in the case of ARS-VDC-RTV coordination has been published in:

- M. Kissai, B. Monsuez, X. Mouton, D. Martinez and A. Tapus, "Importance of Vertical Dynamics for Accurate Modelling, Friction Estimation and Vehicle Motion Control," *2018 21st International Conference on Intelligent Transportation Systems (ITSC)*, Maui, HI, 2018, pp. 1370-1377.
  DOI: 10.1109/ITSC.2018.8569751.

8 Robust Control Synthesis

Regarding the reference generation, the same strategy adopted in the downstream approach can be adopted here. The target is common and does not depend on the type of approach adopted. It should be noted though that in the upstream approach, motion feelings can be tuned not only by modifying the reference, but also by distributing the control differently (Kissai et al., 2018d). This will be discussed in Chapter 10 and 12 in different manners. For the coordination strategy, the core of this control architecture is the use of CA algorithms. Chapter 9 is dedicated to these type of algorithms. Here, we focus on the controllers' design procedure, especially when robustness is substantial.

8.1 High-level control

We aim at specifying the motion of the vehicle's CoG. The high-level controller's mission is to generate the generalized forces and moments required at the CoG of the vehicle in order to achieve a specific motion behaviour. In the general case, a multivariable high-level controller is needed. This controller should be able to handle the couplings that exist between the vehicle's inner states. These dynamic couplings should be first studied. To use classical methods, as the RGA or Bode diagrams, we first linearize the vehicle model. This is usually done by employing a Taylor series expansion around a nominal system trajectory representing the operating points (Soltani, 2014).

Regarding the RGA method, the goal is to "quantify" interactions between inputs and outputs of a MIMO system (Bristol, 1966). It helps the controller designer to decide a suitable input/output pairing for the MIMO system, and also gives few hints on pairings to avoid. Let $\mathbf{G}$ be a general non-singular square complex transfer matrix. The RGA of $\mathbf{G}$ is defined as:

$$RGA(\mathbf{G}(\mathbf{i\Omega})) = \mathbf{\Lambda}(\mathbf{G}(\mathbf{i\Omega})) = \mathbf{G}(\mathbf{i\Omega}) \circ \left(\mathbf{G}(\mathbf{i\Omega})^{-1}\right)^{t} \tag{8.1}$$

Where "$\circ$" denotes the Hadamard product[1], the superscript "^{t}" denotes the matrix transpose, and Ω the considered frequency at which the couplings are studied. Note that the RGA depends on this latter. Therefore, it should be calculated at the crossover frequency chosen by designer. A study in the frequency domain should be carried out. The rules of RGA are simple: prefer pairings so that Λ_{ij} is close to 1, and avoid pairings with negative Λ_{ij}.

In addition, as uncertainties might exist in the vehicle's parameters (Chebly, Talj, and Charara, 2017), it is important for this controller to be robust. The control should be valid whether there is only the driver in the vehicle or with other passengers, whether tires are brand new or not and so on. Several robust techniques exist, e.g., the SMC that got recently a lot of attention (Shyrokau, Wang, and Lienkamp, 2013), (Feng et al., 2014), (Zhao, Li, and Qu, 2014), (Yim, S., 2015). This technique,

[1] Known as elements-by-elements multiplication.

however, still suffers from several problems as chattering (Zhao, Li, and Qu, 2014). An optimal design would be preferable. In this context, the $\mathcal{H}_\infty$ synthesis is a good candidate to optimize the controller parameters.

8.1.1 $\mathcal{H}_\infty$ design guidelines

In the following, the case of SISO systems will be detailed. Few words on MIMO systems are added at the end of these guidelines. Further details can be found in (Skogestad and Postlethwaite, 2005) and (Scorletti and Fromion, 2009).

The biggest advantage of $\mathcal{H}_\infty$ control[2] is that it allows the designer to express explicitly the system's uncertainties. The major idea is to establish a stabilizing controller for a set of uncertain models where the expected model[3] is contained. The set of uncertain models should not be very large as this may lead to conservatism: a controller able to stabilize a large number of models would have poor performances even for the nominal model.

Definition

The $\mathcal{H}_\infty$ norm of the plant G is defined as follows:

$$\|G\|_\infty = \sup_{\omega \in [0,+\infty[} |G(j\omega)| \tag{8.2}$$

This norm can be applied to different specific signals in order to satisfy different requirements. In general, we select an "*augmented plant*" composed of the studied plant itself and weighting functions used to shape the desired transfer functions. Then by applying the $\mathcal{H}_\infty$ norm to the augmented plant, we can enforce the selected signals to follow a desired shape thanks to the weighting functions. A controller, if it exists, is synthesized in this process, and enables to respect all requirements if possible. The control requirements should be first interpreted into the $\mathcal{H}_\infty$ norm.

Control specifications interpretation

Let us consider the general system in closed loop in Figure 8.1. With:

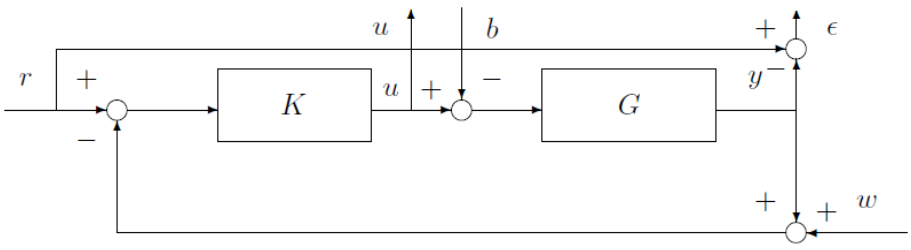

FIGURE 8.1: Illustrative system in a closed loop.

- r : reference command,
- u : control signal,

[2] Which is based on the $\mathcal{H}_\infty$ norm as you may expect.
[3] Called the nominal model.

- b : exogenous disturbances,
- y : plant output signal,
- ϵ : tracking error,
- w : sensor noise,
- G : the system (plant) to be controlled,
- K : the controller to be designed.

The relevant transfer functions are:

- $T_{r\to\epsilon}(s) = S(s) = \dfrac{1}{1+G(s)K(s)}$: is the "*Sensitivity function*[4]". It is used for **the reference signal tracking** specification,
- $T_{r\to y}(s) = T(s) = \dfrac{G(s)K(s)}{1+G(s)K(s)}$: is the "Transmittance function" or complementary sensitivity function[5],
- $T_{b\to\epsilon}(s) = G(s)S(s)$: is used for **disturbance rejection** specification,
- $T_{r\to u}(s) = K(s)S(s)$: is used for **command moderation**,
- $T_{w\to u}(s) = -K(s)S(s)$: is used for **noise mitigation** specification.

With s is the Laplace operator. Let us take the reference signal tracking specification. A good tracking is interpreted by a low value of the error ϵ. We can define therefore a set of low signals $\epsilon(t)$ as:

$$\mathcal{E} = \{\epsilon \text{ with } |\epsilon(j\omega)| \leq \epsilon_{sup} A\} \tag{8.3}$$

Where ϵ_{sup} is a small positive constant, and A characterizes the amplitude of the input signal. In case of the step signal for example[6] we get:

$$\begin{aligned} \forall\omega,\ |\epsilon(j\omega)| \leq \epsilon_{sup} A &\iff \forall\omega,\ \left|T_{r\to\epsilon}(j\omega)\frac{A}{j\omega}\right| \leq \epsilon_{sup} A \\ &\iff \forall\omega,\ |T_{r\to\epsilon}(j\omega)| \leq \epsilon_{sup}|j\omega| \end{aligned} \tag{8.4}$$

In this way, the requirement on the error signal transforms into requirement on the module of $T_{r\to\epsilon}$. We can generalize this by defining weighting functions as:

$$\begin{cases} \mathcal{R} = \{r \text{ with } |r(j\omega)| \leq |W_r(j\omega)|\} \\ \mathcal{E} = \{\epsilon \text{ with } |\epsilon(j\omega)| \leq \dfrac{1}{|W_\epsilon(j\omega)|}\} \end{cases} \tag{8.5}$$

[4] Lower values of this function suggest further attenuation of the external disturbance (Åström, 2000).

[5] $S(s) + T(s) = 1$

[6] $r(s) = \dfrac{A}{s}$.

The specification is then assured if:

$$\begin{aligned} \forall r(j\omega) \in \mathcal{R}, \forall \omega,\ |\epsilon(j\omega)| &\leq \frac{1}{|W_\epsilon(j\omega)|} \\ &\iff \forall r(j\omega) \in \mathcal{R}, \forall \omega,\ |T_{r\to\epsilon}(j\omega)\, r(j\omega)| \leq \frac{1}{|W_\epsilon(j\omega)|} \\ &\iff \forall \omega,\ |T_{r\to\epsilon}(j\omega)\, W_r(j\omega)| \leq \frac{1}{|W_\epsilon(j\omega)|} \\ &\iff \forall \omega,\ |W_\epsilon(j\omega)\, T_{r\to\epsilon}(j\omega)\, W_r(j\omega)| \leq 1 \end{aligned} \tag{8.6}$$

If $W_r(s)$ and $W_\epsilon(s)$ are stable, the last condition can be rewritten as (Scorletti and Fromion, 2009):

$$\|W_\epsilon T_{r\to\epsilon} W_r\|_\infty \leq 1 \tag{8.7}$$

The reference tracking specification is therefore interpreted into the minimization of $\mathcal{H}_\infty$ norm of $W_\epsilon T_{r\to\epsilon} W_r$. Moreover, if $T_{r\to\epsilon}$ is stable, we can write (Scorletti and Fromion, 2009):

$$(8.7) \iff \forall \omega,\ |T_{r\to\epsilon}(j\omega)| \leq \frac{1}{|W_r(j\omega)\, W_\epsilon(j\omega)|} \tag{8.8}$$

In this case, the $\mathcal{H}_\infty$ norm can be interpreted as a constraint on the shape of the sensitivity function $T_{r\to\epsilon}$. The controller is designed in a way to make the module of $T_{r\to\epsilon}$ inferior to the module of $\frac{1}{W_r W_\epsilon}$. Next, we define $W_1(s) = W_r(s)\, W_\epsilon(s)$. As we have seen, we can opt for $W_1(s) = \frac{1}{\epsilon_{sup} s}$. However, this function is unstable. The common practice is to slightly disturb this function to make it stable:

$$W_1(s) = \frac{1}{\epsilon_{sup}(s + \bar{\epsilon})} \tag{8.9}$$

With $\bar{\epsilon}$ is very low and positive. A typical shape of $T_{r\to\epsilon}$ is illustrated in Figure 8.2.

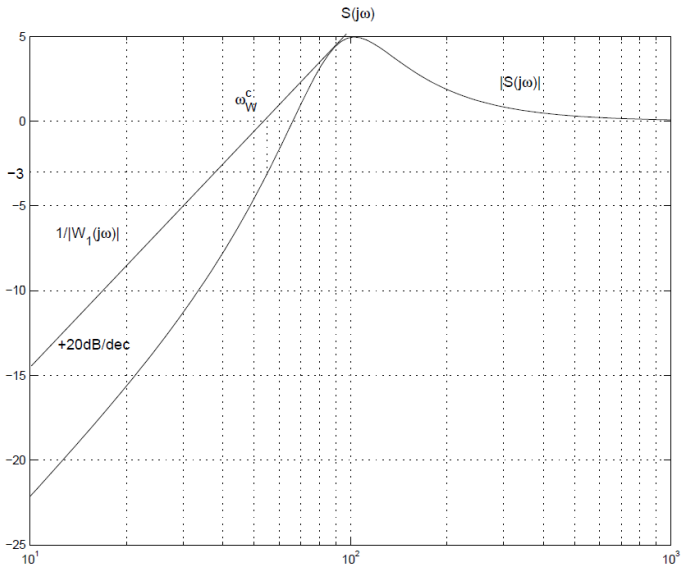

FIGURE 8.2: Typical shape of $T_{r\to\epsilon}$ with its weighting function W_1 (Scorletti and Fromion, 2009).

The crossover frequency ω_W^c where $\left|W_1\left(j\omega_W^c\right)\right| = 1$ is very important for the controller design because $\omega_W^c \approx \frac{1}{\epsilon_{sup}}$. Therefore, the bigger is ω_W^c the lower is the error $|\epsilon\left(j\omega\right)|$. The same procedure is adopted for the other specifications. To sum up, we give the functions to be minimized for each specification:

- **The reference signal tracking** specification : $\|W_1 T_{r\to\epsilon}\|_\infty \leq 1$,
- **The disturbance rejection** specification : $\|W_2 T_{b\to\epsilon}\|_\infty \leq 1$,
- **The noise mitigation** specification : $\|W_3 T_{w\to u}\|_\infty \leq 1$,
- **The command moderation** specification : $\|W_4 T_{r\to u}\|_\infty \leq 1$.

Explicit uncertainty

One big advantage of the $\mathcal{H}_\infty$ control synthesis is that it allows to explicitly take into account the plant uncertainties. Let us consider a set of transfer function where the nominal model G_{nom} is the "center". The uncertainty can be parametric, where one or more parameters of the nominal model do not correspond to the values of the real plant G_{real}. The uncertainty can be also dynamic where the real order of the plant differs from the order of the plant model. In this case, the uncertainty usually varies with the frequency, because as a common practice in modeling one may neglect the high-frequency poles (Scorletti and Fromion, 2009). Subsequently, the nominal model is usually more precise at low frequencies and becomes more uncertain at high frequencies. To generalize, we introduce a stable transfer $\Delta\left(j\omega\right)$ as:

$$G_{real}\left(j\omega\right) = G_{nom}\left(j\omega\right) + \Delta\left(j\omega\right) \tag{8.10}$$

We can quantify this uncertainty by choosing a real and positive parameter β in a way that $\forall\omega,\ |\Delta\left(j\omega\right)| \leq \beta$. This condition can be rewritten as $\|\Delta\|_\infty \leq \beta$. The real closed loop system is illustrated in Figure 8.3.

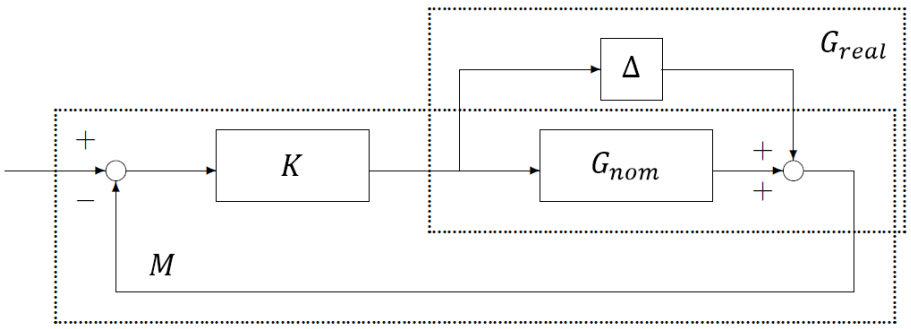

FIGURE 8.3: An illustrative real closed loop system (adapted from (Scorletti and Fromion, 2009).).

Theorem 1 (Small-gain theorem) *The set of systems* (M, Δ) *represented in Figure 8.3 is stable for every transfer function* Δ *satisfying the condition* $\|\Delta\|_\infty \leq \beta$ *(respectively ,*$\|\Delta\|_\infty < \beta$*), if and only if* $\|M\|_\infty < \frac{1}{\beta}$ *(respectively* $\|M\|_\infty \leq \frac{1}{\beta}$*).*

Note that here we presented an "*additive uncertainty*". Other types of uncertainties can be adopted. For further details and for the demonstration of the theorem, please refer to (Scorletti and Fromion, 2009).

In addition, a modeling of the plant synthesized analytically or experimentally by identification represents only the dynamics in the low frequencies that can be experimentally achieved (Scorletti and Fromion, 2009). Therefore, $\Delta(j\omega)$ grows with respect to frequency. To take into account this characteristic, a stable weighting function $W_{unc}(j\omega)$ can be characterized as follows:

$$\forall\omega,\ |\Delta(j\omega)| \leq |W_{unc}(j\omega)| \tag{8.11}$$

This enables defining the set of uncertainties as the set of $\Delta(j\omega) = W_{unc}(j\omega)\,\tilde{\Delta}(j\omega)$ with $\tilde{\Delta}(j\omega) \leq 1\ \forall\omega$, which means $\left\|\tilde{\Delta}\right\|_\infty \leq 1$.

For MIMO systems, two weighting functions are needed. The definition becomes $\Delta = W^l_{unc}\tilde{\Delta}W^r_{unc}$ with $\left\|\tilde{\Delta}\right\|_\infty \leq 1$. This leads to the second theorem:

Theorem 2 (Small-gain theorem with weighting functions) *Considering two invertible matrices with stable transfer functions W^l_{unc} and W^r_{unc}, The set of closed-loop systems (M, Δ) represented in Figure 8.3 is stable for every stable transfer function Δ where $\Delta = W^l_{unc}\tilde{\Delta}W^r_{unc}$ with $\left\|\tilde{\Delta}\right\|_\infty \leq 1$ if and only if $\left\|W^r_{unc}MW^l_{unc}\right\|_\infty < 1$.*

Again, please refer to (Scorletti and Fromion, 2009) for the demonstration of the theorem.

Control synthesis

The generation of the controller is based on the minimization of the $\mathcal{H}_\infty$ norm of the transfer functions augmented by the weighting functions detailed above. The control objectives should be first determined. Let us consider for example only two criteria to be fulfilled as Figure 8.4 shows.

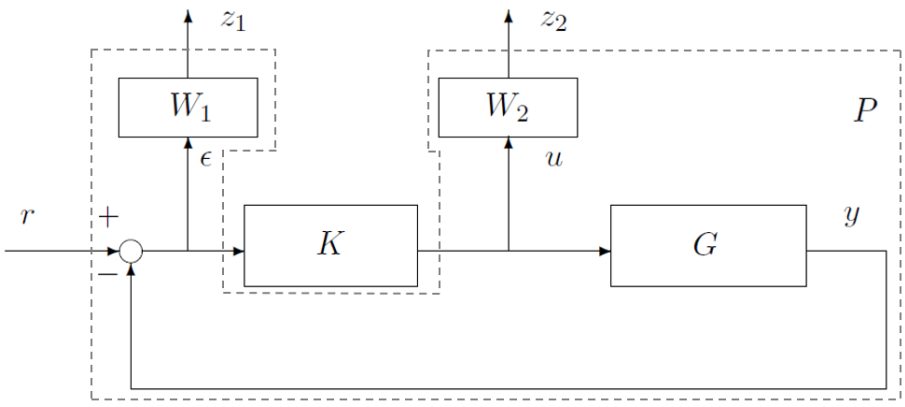

FIGURE 8.4: Example of a double criteria $\mathcal{H}_\infty$ problem.

The augmented plant P can be rewritten as:

$$\begin{cases} \dot{\vec{x}}(t) = A\vec{x}(t) & +B_w\vec{w}(t) & +B_u\vec{u}(t) \\ \vec{z}(t) = C_z\vec{x}(t) & +D_{zw}\vec{w}(t) & +D_{zu}\vec{u}(t) \\ \vec{y}(t) = C_y\vec{x}(t) & +D_{yw}\vec{w}(t) & +D_{yu}\vec{u}(t) \end{cases} \tag{8.12}$$

Where:

- $\vec{x}(t)$: the state vector,

- $\vec{z}(t) \in \mathbb{R}^{p_z}$: the controllable output vector,
- $\vec{w}(t) \in \mathbb{R}^{m_w}$: the criteria input vector,
- $\vec{y}(t) \in \mathbb{R}^{p_y}$: the measurable output vector,
- $\vec{u}(t) \in \mathbb{R}^{m_u}$: the control vector.

Figure 8.4 is then transformed into Figure 8.5. Let us note n the order of the aug-

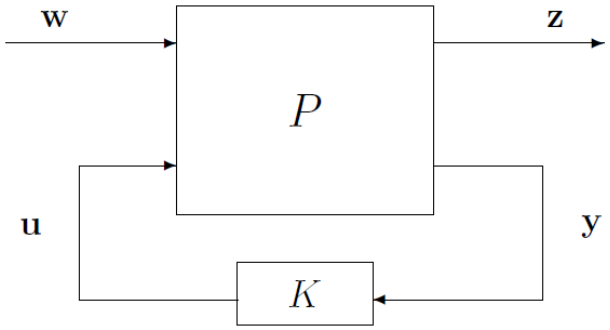

FIGURE 8.5: $\mathcal{H}_\infty$ standard problem.

mented state-space representation P. In the Laplace domain, the augmented plant is expressed as follows:

$$P(s) = \begin{bmatrix} P_{zw}(s) & P_{zu}(s) \\ P_{yw}(s) & P_{yu}(s) \end{bmatrix} = \begin{bmatrix} D_{zw}(s) & D_{zu}(s) \\ D_{yw}(s) & D_{yu}(s) \end{bmatrix} + \begin{bmatrix} C_z(s) \\ C_y(s) \end{bmatrix} (sI - A)^{-1} \begin{bmatrix} B_w(s) & B_u(s) \end{bmatrix} \tag{8.13}$$

We then have:

$$\begin{bmatrix} z(s) \\ y(s) \end{bmatrix} = P(s) \begin{bmatrix} w(s) \\ u(s) \end{bmatrix} \tag{8.14}$$

With $\vec{u}(s) = K(s)\,\vec{y}(s)$. Therefore:

$$\vec{z}(s) = \left(P_{zw}(s) + P_{zu}(s) K(s) \left(I - P_{yu}(s) K(s) \right)^{-1} P_{yw}(s) \right) \vec{w}(s) \tag{8.15}$$

The last product in equation 8.1.1 is mostly known as "*Redheffer Product*" and noted by the symbol "$\star$". The standard $\mathcal{H}_\infty$ problem is then defined as: "*Considering a positive real parameter $\gamma > 0$, find a controller K that satisfies $P \star K$ is asymptotically stable (the real parts of the all the poles of the closed loop system are negative), and $\|P \star K\|_\infty < \gamma$,* ***if it exists***."

Two well-known design procedures can be adopted: solving a series of Riccati equations, or solving a convex optimization problem under Linear Matrix Inequality (LMI) constraints. While the first solution is simpler and more reliable but requires the verification of a certain amount of hypothesis, the second one do not rely on these hypothesis, can take account of additional constraints, but uses a more complex algorithm. The design of the controller is usually done using numerical software as Matlab®. In this latter, both methods can be used[7]. Details of the algorithms used for the controller synthesis can be found in (Scorletti and Fromion, 2009).

[7] Use the "*hinfsyn*" Matlab function for $\mathcal{H}_\infty$ synthesis. The default method uses Riccati equations. Use 'LMI' as a 'METHOD' in the options field to favour optimization under LMIs constraints.

Case of MIMO systems

Here the transfer function is a matrix. Weighting functions should be also matrices. They allow indeed to favor one control axis over another in case of system decoupling. The gain does not depend on only the frequency, but also on the direction of the input signal. For MIMO systems, we cannot define only one value for the gain (Scorletti and Fromion, 2009). In this case, we use the singular value decomposition: Let us consider a complex matrix $A \in \mathbb{C}^{m\times n}$ with $m \geq n$. The singular value decomposition is defined as the product of three matrices $A = U\Sigma V^*$, where $U \in \mathbb{C}^{m\times m}$, $UU^* = I_m$, $V \in \mathbb{C}^{n\times n}$, $VV^* = I_n$, and:

$$\Sigma = \begin{bmatrix} \sigma_1 & 0 & \dots & 0 \\ 0 & \sigma_2 & \dots & 0 \\ \dots & & & \\ 0 & 0 & \dots & \sigma_n \\ 0 & 0 & \dots & 0 \\ \dots & & & \\ 0 & 0 & \dots & 0 \end{bmatrix} \tag{8.16}$$

With $\sigma_1 \geq \sigma_2 \geq \dots \geq \sigma_n \geq 0$ are the singular values of A. And we have:

$$\begin{cases} \sigma_n(A) = \min\limits_{\|v\|\neq 0} \dfrac{\|Av\|}{\|v\|} \\ \sigma_1(A) = \max\limits_{\|v\|\neq 0} \dfrac{\|Av\|}{\|v\|} \end{cases} \tag{8.17}$$

Where $\|.\|$ is the Euclidean norm. For a MIMO system where the transfer matrix is $H(s)$, the $\mathcal{H}_\infty$ norm is defined as:

$$\|H\|_\infty = \sup_\omega \sigma_1(H(j\omega)) \tag{8.18}$$

The notation $\overline{\sigma}$ is usually preferred to σ_1 in the literature. The same guidelines can be applied after. For more details, please refer to (Skogestad and Postlethwaite, 2005) or (Scorletti and Fromion, 2009).

Practical drawbacks and improvements

As no perfect technique exists, $\mathcal{H}_\infty$ control has its own drawbacks that could be overcome. The first drawback is the high order of the resulting controller in case of high-order plants. The order of the controller resulting is equal to the number of states in the plant plus the number of states in the requirements weights plus twice the number of states in the feedthrough matrix (Skogestad and Postlethwaite, 2005). In the conventional method (Scorletti and Fromion, 2009), we first express an augmented plan taking into account tracking errors, control inputs, reference signals, external forces and noises. MIMO performance objectives are then formulated and weighting functions are defined according to these objectives and added to the augmented system in order to enforce the controller to respect all the objectives. Dynamic and/or parametric uncertainties are also added to the augmented plant in order to generate a valid controller to a set of systems and not only the nominal system. This of course enhance the controller robustness, but could lead to the conservatism of the controller performances. A too big augmented plant could lead to a

controller with too high order terms, and too many objectives to fulfill could lead to performance conservatism.

A common practice consists in reducing the controller in the frequency domain while keeping an acceptable level of robustness (Pita-Gil, 2011). Here, a second methodology is also investigated. As most industrial companies prefer Proportional-Integral-Derivative (PID) controllers for implementation issues, we simply add the controller's structure as a requirement in the $\mathcal{H}_\infty$ synthesis. To choose the suitable structure to be adopted, a pre-study of the plant is required. This can enables to specify if we should adopt coupled or decoupled controllers, PID or only PI or phase-lag structure at each axis, and so on. Both methods can be tested using Matlab®. The conventional method is ensured by the Matlab® function "*hinfsyn*" and the fixed-structure method by the function "*hinfstruct*". In this latter, to mitigate the risk of local minima, one could run several optimizations started from randomized initial values of the tunable parameters of the controller. For more details, see (Apkarian and Noll, 2006). Regarding performance weighting functions, closed loop shaping is used for defining control design requirements (Doumiati et al., 2013).

Another weakness in the classic design is the dependency on the operating points used to linearize the plant model. For different operating points, different controller parameters values are generated, which influence the controller performance. A proper way to proceed would be rather to consider all feasible and stable operating points and make the controller parameters change with respect to these operating points. This is called scheduling. This technique consists in considering the nonlinearities in a system as varying parameters. Then different linear controllers are designed for different values of the varying parameters. The controller parameters are after automatically adjusted as a function of the varying parameters, called scheduling variables. The $\mathcal{H}_\infty$ synthesis can be iterated for the selected different values of the varying parameters. The tighter the gap between scheduling variables' values is, the more smooth the scheduling gets. A gain-scheduled $\mathcal{H}_\infty$ controller can be finally synthesized. Note that we could have synthesized, from the beginning, a controller using $\mathcal{H}_\infty$ design applied to q-LPV systems. However, as cited in (Biannic, 2013), Gain scheduling with respect to direct LPV synthesis techniques presents several practical advantages: better behavior in practice, less conservatism, low computation cost and therefore faster regulations in the design process. As our final objective is to control a real passenger car, we privilege designing separate $\mathcal{H}_\infty$ controllers for the different operating points, and then ensure gain scheduling by simple linear interpolation (Biannic, Roos, and Knauf, 2006).

8.1.2 μ Synthesis

According to Theorem 2, a single specification has been assigned to the perturbation block Δ to ensure robust stability. This leaves this block "*unstructured*". The uncertainty accounted might be therefore unnecessarily high, which may lead to an overly conservative controller design (Wal, 1995).

This led Doyle to propose in (Doyle, 1982) the concept of "*structured singular value*" commonly referred to "μ". The structured singular value $\mu_\Delta(T)$ of a complex matrix T with respect to the perturbation structure in Δ in defined as (Wal, 1995):

$$\mu_\Delta(T) := \frac{1}{\min\{\overline{\sigma}(\Delta) : \Delta \in \mathcal{D}, det(I - T\Delta) = 0\}} \tag{8.19}$$

With $\overline{\sigma}$ is the largest singular value, and $\mathcal{D}$ is the class of constant complex matrices having null off-diagonal coefficients. Consequently, the structured singular value $\mu_{\Delta}(T)$ is the inverse of the largest singular value of the smallest perturbation $\Delta \in \mathcal{D}$ that makes $(I - T\Delta)$ singular. Thus, the larger is $\mu_{\Delta}(T)$, the smaller is the perturbation Δ which is needed to make $(I - T\Delta)$ singular. Now the "μ-value" of T is defined as the maximum value over all frequencies:

$$\|T\|_{\Delta} := \sup_{\omega \in \mathbb{R}} \mu_{\Delta}(T(j\omega)) \tag{8.20}$$

Robust performance of the closed-loop system under all structured perturbations $\Delta \in \mathcal{D}$ satisfying $\|\Delta\|_{\infty} \leq 1$ is achieved if and only if (Wal, 1995):

1. the closed-loop system M is nominally stable,
2. $\|M\|_{\Delta} < 1$.

Consequently, the μ-synthesis consists in designing a controller K that stabilizes the nominal closed-loop system and makes $\|M\|_{\Delta} < 1$, or minimizes $\|M\|_{\Delta}$ with respect to all stabilizing controllers K. The designer can again incorporate additional requirements by means of weighting functions.

Unfortunately, there is no analytic method to calculate a μ-optimal controller due to computational difficulties (Wal, 1995),(Vasičkanmová et al., 2015). Nevertheless, an approximate solution, known as "*DK-iteration*", is generally used using Matlab® (Balas et al., 1998). This approach relies on the property:

$$\mu_{\Delta}(T) \leq \overline{\sigma}\left(DT\overline{D}^{-1}\right) \tag{8.21}$$

With D is a scaling matrix chosen so it commutes with Δ: $D\Delta = \Delta D$. The iterative process goes as follows (Skogestad and Postlethwaite, 2005):

1. Synthesize an $\mathcal{H}_{\infty}$ controller for the scaled problem with a fixed D:

$$\min_{K}\left(\left\|DTD^{-1}\right\|_{\infty}\right) \tag{8.22}$$

2. Find $D(j\omega)$ to minimize at each frequency $\overline{\sigma}\left(D(j\omega)TD^{-1}(j\omega)\right)$
3. Fit the magnitude of each element of $D(j\omega)$ to a stable and minimum-phase transfer function. Go to step 1.

The iteration process should be stopped if $\left\|DND^{-1}\right\|_{\infty} \leq 1$ or if the norm no longer decreases. Therefore, the "*DK-iteration*" consists of a series of $\mathcal{H}_{\infty}$ design and μ-analysis sequence. However, convergence is not always guaranteed (Wal, 1995). In addition, the procedure is not convex which may results in only sub-optimal solutions. To top it all off, the controller's order is equal to the order of the generalized plant plus twice the order of $D(s)$ (Balas et al., 1998). Due to implementation limits, it is advisable to use a low order scaling. The only common approach that exists for now in the literature is to reduce afterwards the controller synthesized in the operating frequency range.

8.2 Low-level control

After tire force distribution, the low-level controllers make sure that the allocated forces are applied by generating the right command to the different actuators. In

other words, tire forces commands should be transformed into actuator commands before being fed to the different actuators. Two major criteria have to be considered in controller design for this case. First, the low-level layer is located in the most inner loop. It should be much faster in order not to influence the high-level control. In addition, the same crossover frequency should be chosen for the available actuators. Reallocation should be caused by tire or actuator saturation and not by one of the controllers delay with respect to the others. Secondly, no overshoot should be allowed. CA is made by taking into account the tire saturation. At hazardous situations, it could allocate the maximum allowable tire force. This force must not be exceeded; otherwise, the vehicle could lose its stability. In general, this layer depends on the subsystem to be controlled and the dynamics of its actuators, and consequently cannot be generalized at this section.

Another problem comes from the fact that most of suppliers' subsystems contain inner control laws in black-boxes. The most inner dynamics are generally uncertain. Robustness is also very important at this level. First, we will use only simplified actuator models, as provided in some high-fidelity modeling softwares, that do not need additional sophisticated low-level controllers. In chapters 10, 11 and 12, we will focus on the high-level controller with control allocation algorithms, with only a simple adaptation at the low-level layer. The reason behind this is the fact that we started this thesis without having any idea on the prototype that we will work on. A general and extensible architecture had to be developed. However, we will see in Chapter 13 that shows the first experimental results, that the overall control of the vehicle motion depends on the dynamics of the actuators integrated. These dynamics may add additional constraints on the control synthesis. If suppliers are not willing to open their implemented control algorithms, car manufacturers should start by identifying experimentally the real dynamics of the different subsystems provided, before getting into the design of the overall vehicle motion control's strategy.

9 Control Allocation

In Chapter 8, we saw the control synthesis guidelines that should be adopted in order to robustify the control strategy. In this thesis, the plants considered are over-actuated: more than one actuator can influence the same physical variable. Not only the control should be robust, but the distribution among the conflicting actuators should be optimal. Three different chassis systems combinations will be presented in Chapters 10, 11 and 12. In all of them, the vehicle is considered over-actuated. In order to solve the problem, decision variables and constraints are required in the form of an optimization problem. The decision variable is then derived from a specific cost function that describes trade-offs between actuator properties such as saturation limits, desired equilibrium positions, actuation effort, tracking performance and so on (Berg, 2016). In most passenger cars, the control distribution is performed by applying rule-based algorithms (Shaout and Mcgirr, 2013). Although it was shown that strategies could be robust and relatively simple, they do not make optimal use of the combined capabilities of the actuators. With further increase in complexity due to integration of additional actuators, interaction schemes will become intractable. Therefore, a more sophisticated and optimization-based strategy is required to solve the subsystems coordination problem.

The CA problem has arisen first in the aerospace industry. Most advanced aircrafts are in fact designed to be over-actuated on purpose. The reason behind this is to provide the necessary redundancy in case of an actuator or a set of actuators failures. Here, the problem is somehow different. The distribution does not concern the same redundant subsystems, but completely different subsystems. However, some of the lessons learned in the aerospace sector can be applied to the automotive sector given that the mathematical problem is very similar.

CA problems are defined as follows (Oppenheimer, Doman, and Bolender, 2006): *Find the control vector, $\vec{\delta} \in \mathbb{R}^n$ such that*

$$\mathbf{B}\vec{\delta} = \vec{d}_{des} \tag{9.1}$$

subject to

$$\begin{cases} \vec{\delta}_{min} \leq \vec{\delta} \leq \vec{\delta}_{max} & (9.2) \\ \dot{\vec{\delta}} \leq \dot{\vec{\delta}}_{max} & (9.3) \end{cases}$$

where $\mathbf{B} \in \mathbb{R}^{m \times n}$ is a control effectiveness matrix, $\vec{\delta}_{min}$ and $\vec{\delta}_{max}$ are the lower and upper position limits respectively, $\dot{\vec{\delta}}$ is the control rate, $\dot{\vec{\delta}}_{max}$ is the maximum control rate, $\vec{d}_{des}$ are the desired accelerations, n is the number of control effectors, and m is the number of axes to control ($n > m$).

As $n > m$, several solutions can be found. The CA algorithm should be able to pick the best solution by defining optimization objectives or cost functions. For discrete implementation, the rate constraint can be considered as a time-varying magnitude constraint at each sampling interval. This gives the following combined

constraints (Oppenheimer, Doman, and Bolender, 2006):

$$\underline{\vec{\delta}} \leq \vec{\delta} \leq \overline{\vec{\delta}} \tag{9.4}$$

Where:

$$\begin{cases} \overline{\vec{\delta}} = \min\left(\vec{\delta}_{max}, \vec{\delta} + \Delta t \dot{\vec{\delta}}_{max}\right) & (9.5) \\ \underline{\vec{\delta}} = \max\left(\vec{\delta}_{min}, \vec{\delta} - \Delta t \dot{\vec{\delta}}_{max}\right) & (9.6) \end{cases}$$

In this way, $\overline{\vec{\delta}} \in \mathbb{R}^n$ and $\underline{\vec{\delta}} \in \mathbb{R}^n$ are respectively the most restrictive upper and lower control input limits. Δt represents the sampling interval.

Regarding ground vehicles: $\vec{\delta}$ contains controllable tire forces, $\vec{d}_{des}$ the desired generalized forces, $\mathbf{B}$ represents the geometric relations between the vehicle and its tires, and $\vec{\delta}_{min}$ and $\vec{\delta}_{max}$ reflect tire limits with respect to the friction ellipse concept (Wong, 2001). Two different types of CA algorithms should be distinguished: *static CA* and *dynamic CA*.

9.1 Static CA

In this area, we can find strategies like actuator's ganging, which has been used extensively in the aerospace sector (Oppenheimer, Doman, and Bolender, 2006), (Bodson, 2002), or daisy-chaining which has been applied in the automotive field using the Hardware-In-the-Loop (HIL) validation process (Soltani, 2014).

9.1.1 Ganging

Ganging is achieved by an *a priori* method. Indeed, this method is used when it is obvious how to combine the redundant effectors. It is done by choosing a matrix $\mathbf{G}$ such that $\vec{\delta} = \mathbf{G}\vec{\delta}_{pseudo}$, where $\vec{\delta}$ is the actual control vector, while $\vec{\delta}_{pseudo}$ is a pseudo control that may contains non physical components. An example is given in (Oppenheimer, Doman, and Bolender, 2006) of a vehicle equipped by a left and right ailerons δ_{aL} and δ_{aR} for roll control. A ganging law to produce a single roll control device δ_a could be for example:

$$\delta_a = \frac{\delta_{aL} + \delta_{aR}}{2} \tag{9.7}$$

The problem with this method is that the coordination strategy is not always obvious. Otherwise, a downstream coordination approach is sufficient in this case.

9.1.2 Daisy chaining

Daisy chaining is also referred by sequential control. It consists in using one actuator first to the full, then activating the second one when the first is saturated and so on. Therefore, here one actuator is prioritized over the others. Even though the coordination is managed upstream the subsystems, the design process resembles more to a downstream approach. The terms "*Upstream Approach*" and "*Downstream Approach*" should not be associated to only the position of the coordination layer in the control architecture, but also to the process of development of coordination strategies in the control synthesis. The difference with respect to the downstream approach is the condition to move to the second subsystem. Here, actuator saturation or tire

saturation is the switching condition. In addition, when a control saturates, an error between the desired forces and those generated by control effectors arises. Only this error is transmitted to the second set of subsystems. A schematic representation has been provided in (Oppenheimer, Doman, and Bolender, 2006) (see Figure 9.1).

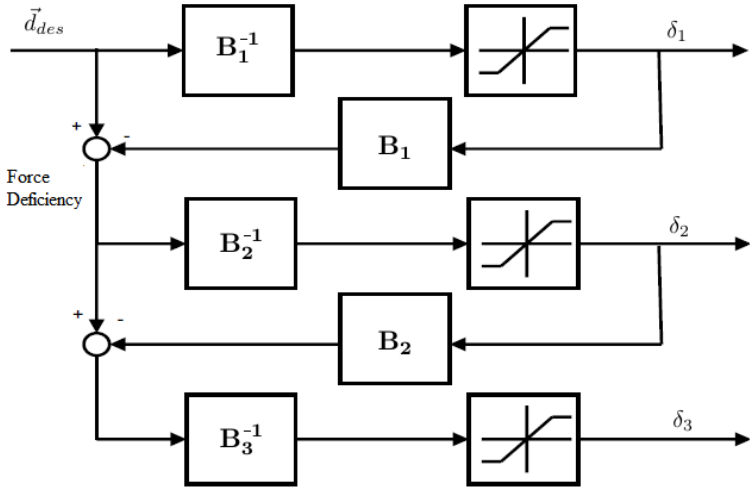

FIGURE 9.1: Schematic representation of daisy-chain method (adapted from (Oppenheimer, Doman, and Bolender, 2006)).

Both methods have proven to be effective in solving the problem. However, they do not rely on optimization methods that limit their potential, especially in order to handle multi-objectives problems.

9.2 Dynamic CA

Here, the optimal actuator configuration is selected dynamically. All algorithms are optimization-based, which leads to find the best control vector by soliciting different subsystems in order the meet the control request while satisfying multiple objectives. (Bodson, 2002) gives a good overview of the different optimization methods that are used in advanced aircrafts to solve CA problems. He also provides comparisons on computational burden relying on few examples. Particularly, predictive C_α algorithms are very demanding in terms of computational effort. In this thesis, only non-predictive CA algorithms are discussed. Nevertheless, predictive CA could be more relevant if subsystems show pure delays and/or do not have the same time response. In this context, (Vermillion, Sun, and Butts, 2007) and (Sill and Ayalew, 2012) show improved performance compared to the usage of simpler CA methods. This will be investigated in our future works. Regarding non-predictive C_α algorithms, different optimization methods have been proposed in the literature, for example in (Berg, 2016), that relies on whether the optimization is done offline or online.

9.2.1 Precomputed laws

In this case, the optimization is solved offline (F. Borrelli and Hrovat, 2006). This results on an analytic law when the problem is simple enough. In this context, we can find *Weighted Pseudo-Inverse (WPI)* method (Soltani, 2014). It is an optimization

technique based on a pseudo inversion of the non-square matrix $\mathbf{B}$ by neglecting the actuator limits. The problem is formulated as follows (Oppenheimer, Doman, and Bolender, 2006):

$$\min_{\vec{\delta}} J = \min_{\vec{\delta}} \frac{1}{2} \left(\vec{\delta} + \vec{c}\right)^T \mathbf{W} \left(\vec{\delta} + \vec{c}\right) \tag{9.8}$$

subject to (9.1), where $\mathbf{W} \in \mathbb{R}^{n \times n}$ is a weighting matrix and $\vec{c} \in \mathbb{R}^n$ is an offset vector used to represent an off-nominal condition. The resolution method using the Hamiltonian can be found in (Oppenheimer, Doman, and Bolender, 2006). The solution is expressed as follows:

$$\begin{aligned} \vec{\delta} &= -\vec{c} + \mathbf{W}^{-1}\mathbf{B}^T \left(\mathbf{B}\mathbf{W}^{-1}\mathbf{B}^T\right)^{-1} \left[\vec{d}_{des} + \mathbf{B}\vec{c}\right] \\ &= -\vec{c} + \mathbf{B}^\sharp \left[\vec{d}_{des} + \mathbf{B}\vec{c}\right] \end{aligned} \tag{9.9}$$

where $\mathbf{B}^\sharp$ is the pseudo inverse of $\mathbf{B}$. The weighting matrix can be adjusted to favor one effector over another. This is done by increasing the weight of the less attractive actuator. In fact, to satisfy (9.8), the command corresponding to the increasing weight is reduced faster and thus could be even delayed. Therefore, to take into account the tire potential, we can introduce the inverse of the tire force saturation in the weighting matrix diagonal (Soltani, 2014). When approaching saturation, the weight denominator approaches to 0 and therefore, the weight approaches to ∞. Moreover, we suppose that tires' stiffness is the same for all tires. No off-nominal condition is considered. Therefore, $\vec{c} = 0$, which gives finally:

$$\vec{\delta} = \mathbf{B}^\sharp \vec{d}_{des} \tag{9.10}$$

If the problem is more complex, the whole set of optimal points can be mapped and used as look-up tables. However, the more complex the problem gets, the larger these look-up tables can become until reaching impractical sizes. In (Soltani, 2014), the Daisy-Chain method has been combined with the WPI method to handle coordination of the ESP with the EPAS system. The advantage of this technique is the fact that it is based on an algebraic calculation that makes it faster with respect to online optimization based methods. However, the Daisy-Chain method imposes a predefined prioritization of one system over another, which contradicts the upstream approach philosophy. And regarding the WPI, it is suitable as long as only one objective is pursued, for example allocation precision respecting tire maximum efforts or actuators constraints. For multi-objectives problems, no algebraic expression exists. On-line optimization algorithms should be then preferred.

9.2.2 Repeated optimization

Here, the optimization is performed at every control cycle as it is proposed in (Bodson, 2002), (Sill and Ayalew, 2012). This method is therefore computationally demanding as the optimization needs to be carried out at every time-step. Two main criteria should be taken into account. First, the algorithm should provide enough potential to solve the CA (and reallocation in case of a failure in one of the subsystems) and converge to the optimum in a finite number of iterations. Secondly, the algorithm should be fast enough to ensure real-time operations.

Various techniques have been tested in the literature. Active Set Algorithms (ASA) have shown good results in this context. Here, the optimal control vector

is expressed as (Harkegard, 2002):

$$\vec{\delta}_{opt} = arg \min_{\vec{\delta}_{min} \leq \vec{\delta} \leq \vec{\delta}_{max}} \left\| \mathbf{A}\vec{\delta} - \vec{b} \right\| \tag{9.11}$$

$\|.\|$ is a norm that depends on the algorithm adopted to perform the minimization. Basically, if l_1 norm is used, the solver is said to be based on Linear Programming (LP), while using l_2 norm leads to Quadratic Programming (QP) (Bodson, 2002). These two norms are respectively defined as follows:

$$\begin{cases} \left\| \vec{\delta} \right\|_1 = \sum_i^n |\delta_i| & (9.12) \\ \left\| \vec{\delta} \right\|_2 = \left(\sum_i^n \delta_i^2 \right)^{1/2} & (9.13) \end{cases}$$

Where δ_i are the components of $\vec{\delta}$, and $|.|$ is their absolute value.

Two different methods based on ASA have been derived. The first one is called the Sequential Least Squares (SLS). This method uses two stage ASA to separate the global problem into two optimization problems (Harkegard, 2002). This leads to the following formulation:

$$\begin{cases} \vec{\delta}_{opt} = arg \min_{\vec{\delta} \in \Omega} \left\| \mathbf{W_u} \left(\vec{\delta} - \vec{\delta}_p \right) \right\| & (9.14) \\ \Omega = arg \min_{\vec{\delta}_{min} \leq \vec{\delta} \leq \vec{\delta}_{max}} \left\| \mathbf{W_v} \left(\mathbf{B}\vec{\delta} - \vec{v} \right) \right\| & (9.15) \end{cases}$$

Where:

- $\vec{\delta}_p$: preferred control vector,
- $\mathbf{W_u}$: non-singular weighting matrix affecting control distribution among the actuators,
- $\mathbf{W_v}$: non-singular weighting matrix affecting the prioritization among the virtual control components when $\mathbf{B}\vec{\delta} = \vec{v}$ cannot be attained due to the actuator constraints.

The second method called the Weighted Least Squares (WLS) solves in contrast the global problem in one stage ASA by means of different weights to determine the importance of each objective (Harkegard, 2002). Generally, the allocation objective is prioritized using a high-value weight of the order $\gamma \simeq 10^6$ (Harkegard, 2002). This gives the following expression:

$$\vec{\delta}_{opt} = arg \min_{\vec{\delta}_{min} \leq \vec{\delta} \leq \vec{\delta}_{max}} \left\| \mathbf{W_u} \left(\vec{\delta} - \vec{\delta}_p \right) \right\|^2 + \gamma \left\| \mathbf{W_v} \left(\mathbf{B}\vec{\delta} - \vec{v} \right) \right\|^2 \tag{9.16}$$

The problem can be further extended to multi-objectives problems:

$$\vec{\delta}_{opt} = arg \min_{\vec{\delta}_{min} \leq \vec{\delta} \leq \vec{\delta}_{max}} \sum_l \gamma_i \left\| \mathbf{W_i} \left(\mathbf{B_i}\vec{\delta} - \vec{v}_i \right) \right\|^2 \tag{9.17}$$

- $\vec{\delta}_{opt}$: optimal control vector,
- l : number of objectives,

- γ_i : weight of the i^{th} objective,
- $\mathbf{W_i}$: non-singular weighting matrices,
- $\vec{v}_i$: desired vector of the i^{th} objective,
- $\mathbf{B_i}$: effectiveness matrix relating the control vector to the desired i^{th} objective.

Other techniques non based on ASA exist as the Interior Point (IP) solver (Petersen and Bodson, 2006) and Cascading Generalized Inverses (CGI) (Bordignon, 1996). One of the most interesting ones is the FPI (Burken et al., 2001) because of its rapidity with respect to other optimization techniques. These techniques are compared in Chapter 10 in the context of a real industrial application through a co-simulation procedure. The reader can refer to (Bodson, 2002), (Harkegard, 2002), (Johansen and Fossen, 2013) for further details on solver algorithms and their comparison.

These techniques have been tested to handle various multi-objectives problems. In (Shyrokau and Wang, 2012), the FPI has been used to handle the CA problem and tested in an HIL procedure. The FPI is suitable for real-time applications (Wang and Longoria, 2009). Energy consumption and energy losses have been selected as performance criteria. However, these criteria were not formulated as additional cost functions. To reduce the computational effort, the authors tuned the objectives' weights to meet the different performance requirements. The drawback is then the off-line pre-design of restriction weights, which approaches the industrial common practice, i.e. the downstream approach. In addition, the choice of energy consumption criteria is more relevant for electrical vehicles (Shyrokau et al., 2013). Authors of (Chen and Wang, 2011) have also focused on energy-efficient CA in the context of electric vehicles by adding an secondary cost function. Stability has been added to energy optimization in (Jing et al., 2017). A two-step optimal CA has been developed: a pre-allocation for energy efficiency optimization assuming that the vehicle is stable, then a reallocation in case of wheels skidding or locking using MPC. Generally, the literature has been more interested in power consumption and tire energy dissipation (Shyrokau et al., 2015). The driving pleasure and comfort have always been ensured by the driver himself. Each driver corrects the vehicle behavior gradually until it fits its comfort and confidence requirements. But what about autonomous vehicles? For vehicle motion control, we are more concerned about the motion feelings that the chassis could bring to passengers. To the best of our knowledge, chassis systems coordination taking into account the feelings generated has been ignored in the literature. In an autonomous driving context, coordination should be made in such a way so as to avoid generation of unexpected car behavior. This particular issue will be discussed in Chapter 12.

Even though the upstream approach have been used for single objective coordination control (Falcone et al., 2007), (Abe and Mokhiamar, 2007), (Boada et al., 2006), the complexity and possible cost of this architecture may not justify the achieved gains. Most of interesting studies carried out using this approach concern rather multiple objectives coordination control. In this context, various integration methods have been adopted. For example, to deal with lateral and vertical integration, the active suspensions have been combined with braking based control in (Gaspar, Szabo, and Bokor, 2009). A LPV design with fault-tolerant control has been used. The commands distribution is made by using three weighting functions for lateral acceleration, heave acceleration, and suspension deflection. The results showed attractive improvements in rough surface conditions.

This gets more relevant when subsystems become more numerous. CA techniques get more and more preponderant. For example the authors of (Heo et al., 2015) used an Integrated Chassis Control (ICC) strategy to improve cornering performance in high speed by combining the ESP, the 4WD and the Active Roll Control (ARC) systems. The control architecture is composed of thee parts: a supervisory controller that determines the target vehicle motions, the upper-level controller that calculates the target forces and moment and the lower-level controller that optimally distributes the actuator inputs. The same architecture has been adopted in (Shyrokau, Wang, and Lienkamp, 2013). The subsystems coordination algorithm uses restriction weights that changes according to the performances targeted. The investigations were carried out by a HIL test rig, which demonstrated potential enhancement for different performances.

Our contributions to these researches manifest in the redefinition of the vehicle dynamics equations involved. Most of the papers published in the context of optimal coordination of chassis systems still start with simplified vehicle models, simplified tire models, simplified slip definitions and so on. This accumulation of errors makes it hard to identify the source of real world problems. Robust control theory can be used to overcome parameters' uncertainties, dynamic uncertainties or external disturbances as long as the nominal model is not too far from the real model. But when the vehicle's behavior changes due to nonlinear phenomenon, because of the friction change for example, the control algorithm should be re-adapted. The control designer should be able to differentiate the causes of perturbations to be able to use the right tool to overcome them. Hence our vehicle modeling revisiting, development of a new tire model, and redefinition of slips and so on.

However, as pointed out by (Ivanov and Savitski, 2015), all the results are made by simulation only or at most by HIL. There is a clear lack of experimental results and benchmark requirements that allow comparison between the different methods. Nevertheless, all the researches on CA algorithms to improve the vehicle's performances (Knobel, Pruckner, and Bünte, 2006), (Shyrokau and Wang, 2012), (Shyrokau, Wang, and Lienkamp, 2013), (Shyrokau, B. and Wang, D., 2013), (Reinold and Traechtler, 2013), (Heidrich et al., 2013), (Shyrokau et al., 2015), (Heo et al., 2015), (Berg, 2016) drive us to believe that this architecture is worth investigating and should be implemented in a real vehicle with different embedded systems. In the upcoming chapters, we start by using simple simulations, then high-fidelity ones. To get the best of each approach we test our algorithms by co-simulation, to finish in Chapter 13 by real experiments using the latest Renault Talisman.

Part III

APPLICATIONS

After developing both architectures, it is interesting to see how each one of them fit in actual real applications and potential future ones. It should be noted that a prototype has been provided at the end of the thesis equipped by both the ARS and the VDC systems. In the last chapter, we focus on a first feedback from experimentations. But first, both approaches are designed and compared within this context to show the differences in terms of complexity and potential.

In Chapters 11 and 12, we focus only on the upstream approach to investigate its capabilities to face more complex situations that future vehicles might face. More than two systems are implemented where the development of the downstream approach is less obvious. In addition, additional objectives are tackled to show that the upstream approach is not able of just solving complex problems without changing the overall architecture, but also transforms the over-actuation problem into additional opportunities to satisfy secondary objectives.

10 Case of ARS-VDC Coordination

10.1 Chassis Systems Presentation

Most assistance systems concerns yaw rate control through helping drivers to steer while ensuring vehicle stabilization. Several methods exist in this context. The most common solution is AFS (Falcone et al., 2007) or ARS (Brennan and Alleyne, 2001). braking-based systems can also be used. When braking one single wheel or two wheels of the same side, a yaw moment can be generated. This is actually the principle of the ESP. However, most of integrated braking-based control systems are activated only in hazardous situations, e.g., the ABS. In fact, the use of braking without requesting it is generally not appreciated by drivers[1]. Car manufacturers use braking-based algorithms only if necessary. The driver himself ensures active longitudinal control. Using braking-based chassis systems, the expected longitudinal performances could be compromised. Additional effort may be required by the driver to keep the desired speed. For autonomous vehicles, both longitudinal and lateral performances should be met via the virtual pilot. Combined behavior is then an interesting case to look at within this framework. Therefore, as a first step, we select a vehicle equipped with two conquering subsystems, but while one depends on lateral tire forces, the other is based on longitudinal tire forces. Several today's passenger cars are equipped with both systems. In our case, we select the Renault Talisman (Moss and Darren, 2015). This vehicle is equipped by an ARS and the braking-based VDC.

10.1.1 Active Rear Steering

In Renault's vehicles, the system actuator is located at the rear axle as illustrated in Figure 10.1[2]. Rear wheels can be steered and reach $\pm 3.5^{\circ}$ at most. When rear wheels steer in the opposite direction with respect to the front wheels, the turning radius decreases, the yaw rate is amplified, and the driver's steering wheel activity is reduced. This is particularly beneficial at low speed for tedious maneuvers as parking. In contrast, when rear wheels steer in the same direction with respect to the front wheels, the yaw rate decreases, which limits the inertial movements of the vehicle's body and stabilizes the vehicle. This is mostly pertinent at high speed hazardous maneuvers such as obstacle avoidance, or just for changing the lane in highways.

[1] According to Renault customers' feedback.

[2] Sketch provided by Renault - Chassis Systems Department.

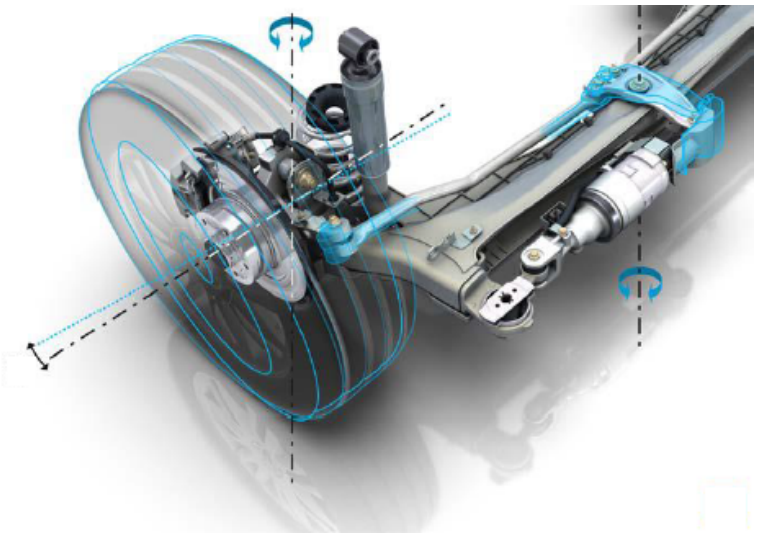

FIGURE 10.1: Active Rear Steering Actuator (Renault's vehicles).

10.1.2 Braking-based Vehicle Dynamics Control

Four continuous pressure modulators are used to provide each individual wheel with its requested brake pressure (Soltani, 2014). One of the ECUs is used to control the four modulators (Liebemann et al., 2004). Figure 10.2 depicts the system components.

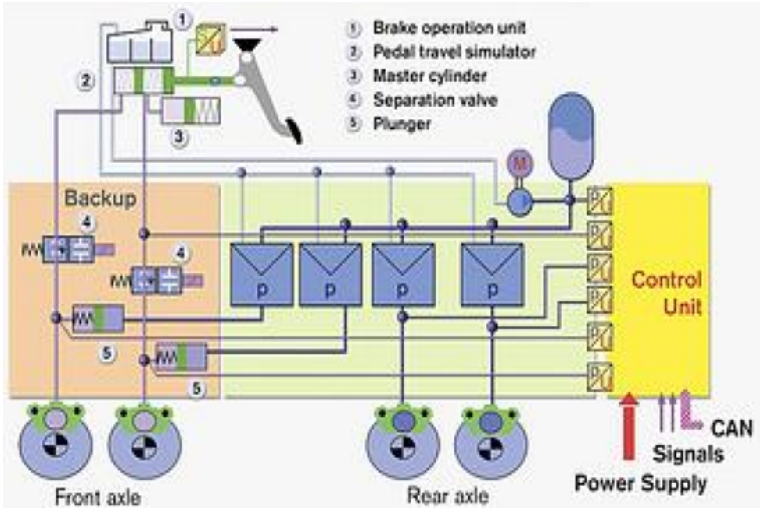

FIGURE 10.2: Differential braking system (Soltani, 2014)

The brake actuator constraint is manifested in the pressure command limitation that should stay in the range of $[0, 200]$ bar.

10.2 Downstream Approach

Most of the chassis systems are provided by car equipment suppliers. Car manufacturers often vary the suppliers for competition strategy matters. Consequently, these

subsystems are based on different vehicle models, have different control strategies, and act independently. Once integrated in the same vehicle, performances of each subsystem may be compromised by the other ones. Interactions become more unpredictable when subsystems are more numerous. We recall, as specified in Chapter 3, that car manufacturers use coordination strategies to mitigate conflicts by prioritizing one system over another (Velardocchia, 2013). Priority is determined in advance by predicting the possible conflicts. Automotive engineers have to foresee a large amount of conflicting scenarios, and use their "expert knowledge" related to vehicle dynamics to avoid hazardous situations.

10.2.1 Control Architecture

As chassis systems are provided by different suppliers, they are often designed without taking into account the influence of the eventual other subsystems integrated in the same vehicle. Suppliers provides then often their subsystems with inputs related directly the vehicle's physical variables. Their outputs are commands fed directly to the related actuator. The chassis system's internal control algorithm is usually provided in a black box. In this framework, the automotive engineer can only act at the very both ends of the integrated subsystem, and usually downstream the subsystems. Figure 10.3 illustrates this approach in the context of our example.

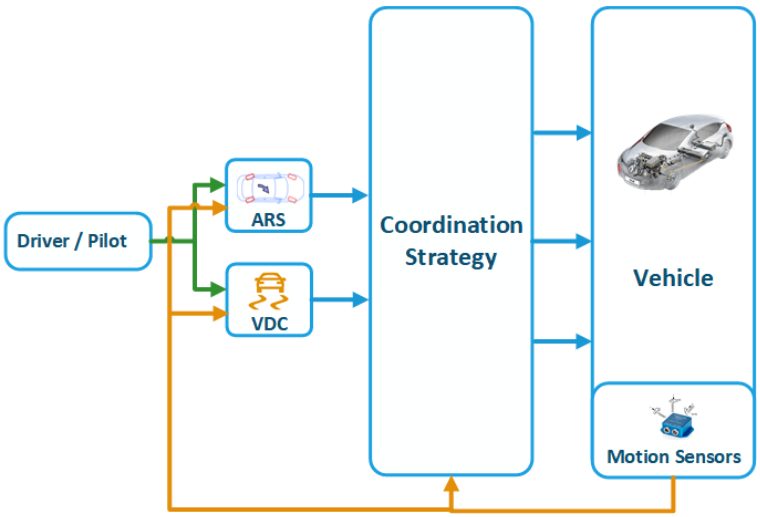

FIGURE 10.3: Structure of the downstream coordination approach (Kissai et al., 2018b)

10.2.2 System Modelling

Here, the main physical variable targeted is the yaw rate. As explained in Chapter 3, one common approach is to bring the two wheels of the same axle into one equivalent wheel (Ono et al., 1994), (Brennan and Alleyne, 2001), (Yim, 2012). The vehicle model is then reduced to a bicycle model (Figure 3.3). As one of our goals is also to first represent today's situation, this model is chosen and detailed in the context of the downstream approach.

In this case, only lateral forces are taken into account. The longitudinal velocity is assumed to be constant. This assumption is indeed acceptable since longitudinal velocity dynamics are much slower to those of the yaw rate. Combined slip is then

neglected. The linear tire model used in this case is expressed as follows (Selby, 2003), (Xiong and Yu, 2011), (Soltani, 2014), (Bächle et al., 2014):

$$\begin{cases} F_{y_f} = 2C_{\alpha_f}\alpha_f & (10.1) \\ F_{y_r} = 2C_{\alpha_r}\alpha_r & (10.2) \end{cases}$$

Where:

$$\begin{cases} \alpha_f = \delta_f - \dfrac{V_y + \dot{\psi} l_f}{V_x} & (10.3) \\ \alpha_r = \delta_r - \dfrac{V_y - \dot{\psi} l_r}{V_x} & (10.4) \end{cases}$$

Note that we multiply by two in equations 10.1 and 10.2, because two tires are involved at each axle. Most of papers use an equivalent cornering stiffness equaling the double of the stiffness of each tire. However, as we want also to control each tire apart, and to avoid any confusion, we decide to clarify it at each equation. By using Newton's second law of motion, we find:

$$\begin{cases} M\left(\dot{\psi} V_x + s V_y\right) = F_{y_f} + F_{y_r} & (10.5) \\ I_z s\dot{\psi} = F_{y_f} l_f - F_{y_r} l_r + M_{vdc} & (10.6) \end{cases}$$

With:

- M_{vdc} : yaw moment generated by the VDC system for example, but it could be any longitudinal force based system able to create a yaw moment as the TV system,
- s : Laplace operator.

The state-space representation of the bicycle model is then:

$$\begin{cases} \dot{x}(t) = \mathbf{A}x(t) + \mathbf{B}u(t) & (10.7) \\ y(t) = \mathbf{C}x(t) + \mathbf{D}u(t) & (10.8) \end{cases}$$

Where:

- $x(t) = \begin{bmatrix} V_y \\ \dot{\psi} \end{bmatrix}$: is the state vector,
- $u(t) = \begin{bmatrix} \delta_f \\ \delta_f \\ M_{vdc} \end{bmatrix}$: is the input vector,
- $A(t) = \begin{bmatrix} -\dfrac{2C_{\alpha_f} + 2C_{\alpha_r}}{MV_x} & \dfrac{-2l_f C_{\alpha_f} + 2l_r C_{\alpha_r}}{MV_x} - V_x \\ \dfrac{-2l_f C_{\alpha_f} + 2l_r C_{\alpha_r}}{I_z V_x} & -\dfrac{2l_f^2 C_{\alpha_f} + 2l_r^2 C_{\alpha_r}}{I_z V_x} \end{bmatrix}$: is the state matrix,
- $B(t) = \begin{bmatrix} \dfrac{2C_{\alpha_f}}{M} & \dfrac{2C_{\alpha_r}}{M} & 0 \\ \dfrac{2l_f C_{\alpha_f}}{I_z} & -\dfrac{2l_r C_{\alpha_r}}{I_z} & \dfrac{1}{I_z} \end{bmatrix}$: is the input matrix.

Today, online accurate measurement of the lateral velocity or the vehicle's side-slip are not available. Therefore, only $\dot{\psi}$ is used for feedback control. Consequently:

- $y(t) = \dot{\psi}$: is the output vector,
- $C(t) = \begin{bmatrix} 0 & 1 \end{bmatrix}$: is the output matrix,
- $D(t) = \begin{bmatrix} 0 & 0 & 0 \end{bmatrix}$: is the feed-through matrix.

To deduce the transfer function of each chassis subsystems, the state-space representation transformation to a transfer function matrix $\mathbf{T}$ property can be used (Antsaklis and Michel, 2007):

$$\mathbf{T}(s) = \frac{y(s)}{u(s)} = \mathbf{C}(s\mathbf{I} - \mathbf{A})^{-1}\mathbf{B} + \mathbf{D} \tag{10.9}$$

ARS transfer function

Using the property (10.9) on the state-space representation (10.7),(10.8), we can find:

$$T_{\delta_r \to \dot{\psi}}(s) = K_{ars}(V_x) \frac{\left(1 - \frac{s}{Z_{ars}(V_x)}\right)}{\frac{s^2}{\omega_n^2(V_x)} + 2\frac{\zeta(V_x)}{\omega_n(V_x)}s + 1} \tag{10.10}$$

Where:

- $K_{ars}(V_x) = -\dfrac{V_x}{L + \left(\dfrac{l_r}{2C_{\alpha_f}} - \dfrac{l_f}{2C_{\alpha_r}}\right)\dfrac{MV_x^2}{L}}$ is the ARS steady-state gain,
- $Z_{ars}(V_x) = -\dfrac{2C_{\alpha_f}L}{MV_x l_r}$ is the ARS zero,
- $\omega_n(V_x)$ is the natural frequency of the vehicle,
- $\zeta(V_x)$ is the damping ratio of the vehicle.

With:

$$\begin{cases} \omega_n(V_x) = \sqrt{\dfrac{4C_{\alpha_f}C_{\alpha_r}L^2}{MI_zV_x^2} + \dfrac{2C_{\alpha_r}l_r - 2C_{\alpha_f}l_f}{I_z}} & (10.11) \\ \zeta(V_x) = \dfrac{M\left(2C_{\alpha_f}l_f^2 + 2C_{\alpha_r}l_r^2\right) + I_z\left(2C_{\alpha_f} + 2C_{\alpha_r}\right)}{MI_zV_x}\dfrac{1}{2\omega_n} & (10.12) \end{cases}$$

VDC transfer function

Using the same procedure, we can find:

$$T_{M_{vdc} \to \dot{\psi}}(s) = K_{vdc}(V_x) \frac{\left(1 - \frac{s}{Z_{vdc}(V_x)}\right)}{\frac{s^2}{\omega_n^2(V_x)} + 2\frac{\zeta(V_x)}{\omega_n(V_x)}s + 1} \tag{10.13}$$

Where:

- $K_{vdc}(V_x) = \dfrac{V_x\left(2C_{\alpha_f}+2C_{\alpha_r}\right)}{4C_{\alpha_f}C_{\alpha_r}L^2+MV_x^2\left(2C_{\alpha_r}l_r-2C_{\alpha_f}l_f\right)}$ is the VDC steady-state gain,
- $Z_{vdc}(V_x) = -\dfrac{2C_{\alpha_f}+2C_{\alpha_r}}{MV_x}$ is the VDC zero.

10.2.3 Control Synthesis

In this case, three commands can influence the yaw rate: the front steering δ_f, the rear steering δ_r, and the differential braking M_{vdc}. Only rear steering (ARS) and differential braking (VDC) are considered in control synthesis. The front steering is directly transmitted to the wheels and used to determine the driver desire, and therefore the yaw rate reference. The control architecture scheme is represented in Figure 10.4.

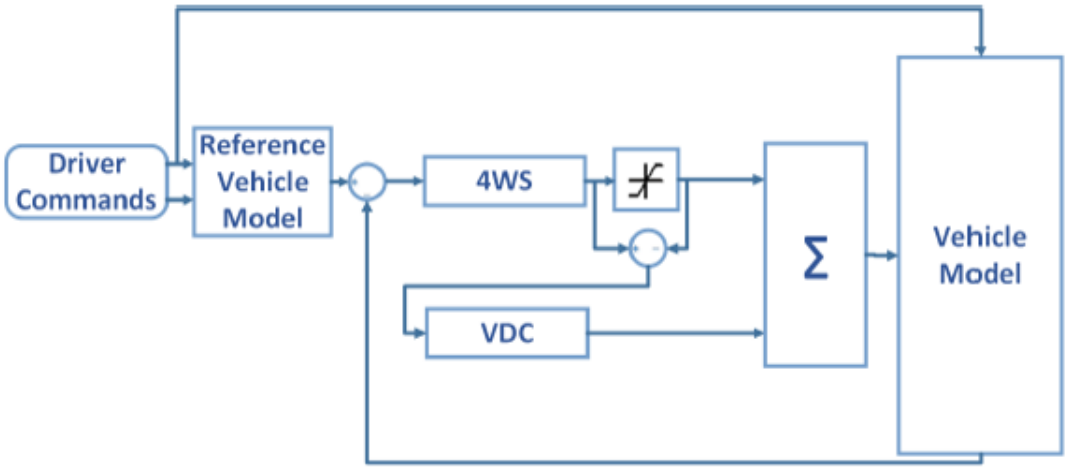

FIGURE 10.4: Downstream control architecture scheme in case of ARS-VDC coordination.

The prioritization depicted in Figure 10.4 is justified below in the paragraph 10.2.3.

Yaw rate reference

A common acceptable assumption is that the driver desires a linear vehicle's yaw rate response (Berg, 2016). In this case, the use of the bicycle model as a reference behavior is justified. As mentioned before, accurate measurement of the lateral velocity or the vehicle's side-slip is not available. Therefore, only $\dot{\psi}_{ref}$ is used for feedback control as a yaw rate target. As a first step, for additional simplicity and fast computations, only the steady state response of the bicycle model is investigated as the yaw rate target. To derive this target from the driver commands, the transfer function from the front steering δ_f to $\dot{\psi}$ is considered. Again, using the property (10.9), we can find:

$$\dot{\psi}_{ref} = T_{\delta_f \to \dot{\psi}}(0) = \frac{V_x}{L+\left(\dfrac{l_r}{2C_{\alpha_f}}-\dfrac{l_f}{2C_{\alpha_r}}\right)\dfrac{MV_x^2}{L}}\delta_f \tag{10.14}$$

A gain can be added to amplify or reduce this reference, and a low-pass filter can be added to tune the desired vehicle behavior. This reference should be limited though. The maximum achievable steady-state yaw rate response can be approximated by (Chang and Gordon, 2007):

$$\dot{\psi}_{max} \approx \mu \frac{g}{V} \tag{10.15}$$

Coordination strategy

In order to coordinate both systems in a downstream approach, these systems should have outputs of the same units. However, the ARS generates a steering angle, while the VDC generates a yaw moment. Either the yaw moment has to be converted to an equivalent angle or the rear angle has to be converted to a yaw moment. In our case, the ARS system provided by Renault can generate a maximum angle of $\pm 3.5^{\circ}$. In contrast, the maximum moment that can be generated by the VDC depends on several parameters, namely, the friction coefficient, the tire stiffness and so on. We choose then to convert the VDC yaw moment to an equivalent angle. In steady-state, the transfer function from the VDC yaw moment to the yaw rate is written as follows:

$$T_{M_{vdc} \rightarrow \dot{\psi}}(0) = K_{vdc}(V_x) = \frac{V_x \left(2C_{\alpha_f} + 2C_{\alpha_r}\right)}{4C_{\alpha_f} C_{\alpha_r} L^2 + MV_x^2 \left(2C_{\alpha_r} l_r - 2C_{\alpha_f} l_f\right)} \tag{10.16}$$

By using again Newton's second law of motion in the longitudinal direction, we find:

$$Ma_{x_{vdc}} = \sum_j F_{x_{i,j}} \tag{10.17}$$

where $\sum_j F_{x_{i,j}}$ is the sum of longitudinal forces at the same side, and $a_{x_{vdc}}$ is the deceleration caused by the activation of the VDC. Moreover:

$$M_{vdc} = \frac{t}{2} \sum_j F_{x_{i,j}} \tag{10.18}$$

Combining the equations (10.16)-(10.18), we find:

$$\begin{aligned} \dot{\psi}(0) &= \frac{V_x \left(2C_{\alpha_f} + 2C_{\alpha_r}\right)}{4C_{\alpha_f} C_{\alpha_r} L^2 + MV_x^2 \left(2C_{\alpha_r} l_r - 2C_{\alpha_f} l_f\right)} \frac{t}{2} Ma_{x_{vdc}} \\ &= \frac{V_x}{L + \frac{MV_x^2}{4C_{\alpha_f} C_{\alpha_r} L} \left(2C_{\alpha_r} l_r - 2C_{\alpha_f} l_f\right)} \frac{\left(2C_{\alpha_f} + 2C_{\alpha_r}\right) Mta_{x_{vdc}}}{8C_{\alpha_f} C_{\alpha_r} L} \\ &= \frac{V_x}{L + \frac{MV_x^2}{L} \left(\frac{l_r}{2C_{\alpha_f}} - \frac{l_f}{2C_{\alpha_r}}\right)} \frac{\left(2C_{\alpha_f} + 2C_{\alpha_r}\right) Mta_{x_{vdc}}}{8C_{\alpha_f} C_{\alpha_r} L} \end{aligned} \tag{10.19}$$

As you may notice, the first fraction corresponds to the static gain of the ARS system[3]. Therefore, the remaining expression correspond to an equivalent steering angle generated by the VDC system:

$$\delta_{vdc} = \left(\frac{1}{2C_{\alpha_f}} + \frac{1}{2C_{\alpha_r}} \right) \frac{Mta_{x_{vdc}}}{2L} \tag{10.20}$$

This angle depends on the longitudinal deceleration generated by the VDC system. It is therefore judicious to prioritize the use of the VDC only if the longitudinal deceleration value would make it possible to exceed an equivalent angle of $\pm 3.5°$. Using typical vehicle's parameters values, we obtain the graph in Figure 10.5.

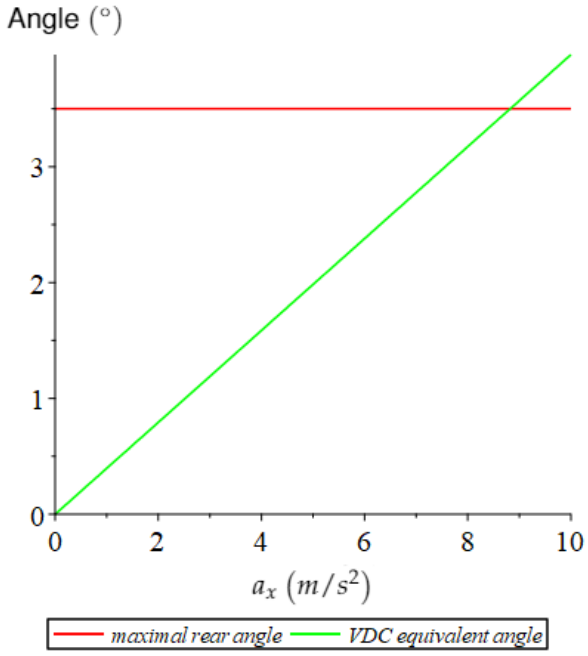

FIGURE 10.5: Comparison of ARS and VDC angle commands.

Consequently, a deceleration of almost $8.82 m/s^2$ is needed in order to exceed the maximal angle provided by the ARS. The VDC should not be prioritized unless the deceleration exceeds $8.82 m/s^2$. This situation is extremely rare. In practice, the ARS system is almost always prioritized. When the ARS system is activated, the VDC is not, unless the ARS is saturated or faulty.

Controllability analysis

The bicycle model can be also used for controllability analysis (Soltani, 2014). Nonetheless, as far as different systems are involved, the actuators' commands should be normalized. We generalized then the problem by considering a yaw moment M_z issued from the combination of actuators. In this case, we have:

[3]This gain is negative for rear steering and positive for front steering, but the same amplitude remains valid for a steering angle in general.

$$\begin{bmatrix} \dot{\beta} \\ \dot{\psi} \\ \dot{M}_z \\ \ddot{M}_z \end{bmatrix} = \begin{bmatrix} -\frac{2C_{\alpha_f}+2C_{\alpha_r}}{MV_x} & \frac{-2l_fC_{\alpha_f}+2l_rC_{\alpha_r}}{MV_x^2}-1 & 0 & 0 \\ \frac{-2l_fC_{\alpha_f}+2l_rC_{\alpha_r}}{I_z} & -\frac{2l_f^2C_{\alpha_f}+2l_r^2C_{\alpha_r}}{I_zV_x} & \frac{1}{I_z} & 0 \\ 0 & 0 & 0 & \rho_1 \\ 0 & 0 & 0 & 0 \end{bmatrix} \begin{bmatrix} \beta \\ \psi \\ M_z \\ \dot{M}_z \end{bmatrix} + \begin{bmatrix} \frac{2C_{\alpha_f}}{MV_x} \\ \frac{2l_fC_{\alpha_f}}{I_z} \\ 0 \\ 0 \end{bmatrix} \delta_f + \begin{bmatrix} 0 \\ 0 \\ 0 \\ \rho_2 \end{bmatrix} \ddot{v} \tag{10.21}$$

With $\tan(\beta) = \frac{V_y}{V_x}$ is the side-slip angle of the vehicle, and $\rho_1, \rho_2 \in \mathbb{R}$ are the gains of the inputs with $\rho_2\ddot{v}$ is the yaw moment acceleration considered as an input (Berg, 2016). The controllability of the overall system is ensured if the Kalman matrix $\mathbf{C}$ is full rank:

$$\begin{aligned} \mathbf{C} &= \begin{bmatrix} \mathbf{B} & \mathbf{AB} & \mathbf{A^2B} & \mathbf{A^3B} \end{bmatrix} \\ &= \begin{bmatrix} 0 & 0 & 0 & \left(\frac{-2l_fC_{\alpha_f}+2l_rC_{\alpha_r}}{MV_x^2}-1\right)\frac{1}{I_z}\rho_1\rho_2 \\ 0 & 0 & \frac{1}{I_z}\rho_1\rho_2 & -\frac{2l_f^2C_{\alpha_f}+2l_r^2C_{\alpha_r}}{I_zV_x}\frac{1}{I_z}\rho_1\rho_2 \\ 0 & \rho_1\rho_2 & 0 & 0 \\ \rho_2 & 0 & 0 & 0 \end{bmatrix} \end{aligned} \tag{10.22}$$

According to equation (10.22), the system is controllable except for the following cases:

- **The cornering stiffness of the four tires are null**. This represents an extreme situation that could only happen in a severe sideways slide for example. Nevertheless, it is advisable to keep the vehicle away from such extreme situations via a well designed high-level controller.
- $\boldsymbol{\rho_1 = 0}$ **or** $\boldsymbol{\rho_2 = 0}$. This happens when the controller saturates. Accordingly, actuators' saturation and friction limits should be taken into account in the design stage.
- $\boldsymbol{2l_rC_{\alpha_r} - 2l_fC_{\alpha_f} = MV_x^2}$. This is a very rare situation where the speed is very low. This case is usually ignored in practical applications (Berg, 2016).

Subsystems' Controllers synthesis

As the subsystems are located downstream the coordination layer (see Figure 10.3), their controllers are based on transfer functions from subsystems' angle commands to directly the vehicle's yaw rate as developed earlier.

- For the ARS system, equation (10.10) shows that its transfer function depends on the longitudinal speed V_x. A varying gain controller is then first developed. The role of the controller varying gain is to simplify the varying steady-state

gain $K_{ars}(V_x)$. A PI controller is then designed for the remaining transfer function in the most difficult situation: when the natural frequency of the vehicle is at its lowest value. The controller expression is then:

$$K_{ars}(s, V_x) = -K_{PI_{ars}} \left(1 + \frac{1}{\tau_{ars} s}\right) \frac{L + \left(\frac{l_r}{2C_{\alpha_f}} - \frac{l_f}{2C_{\alpha_r}}\right) \frac{MV_x^2}{L}}{V_x} \tag{10.23}$$

The natural frequency decreases as the longitudinal speed increases as Figure 10.6 shows.

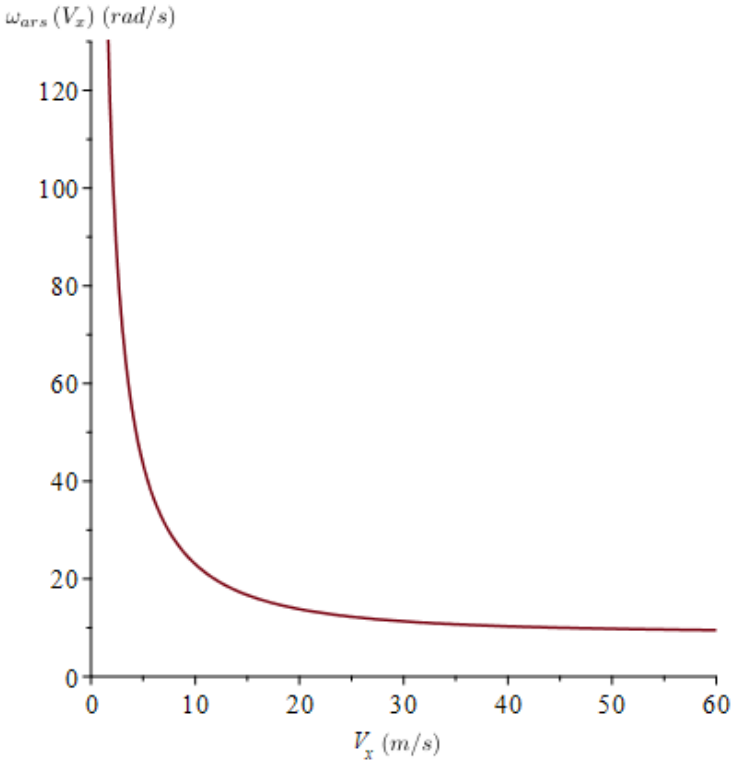

FIGURE 10.6: Variation of the vehicle natural frequency with respect to the longitudinal speed.

The PI controller is then designed for a maximum longitudinal speed value of $220km/h$.

- The same procedure is adopted for the VDC controller considering the equivalent steering angle as an output. The controller expression is then:

$$K_{vdc}(s, V_x) = K_{PI_{vdc}} \left(1 + \frac{1}{\tau_{vdc} s}\right) \frac{L + \left(\frac{l_r}{2C_{\alpha_f}} - \frac{l_f}{2C_{\alpha_r}}\right) \frac{MV_x^2}{L}}{V_x} \tag{10.24}$$

The same method is adopted for PI controller parameters design. Once the equivalent angle command is generated, it is converted back to a yaw moment.

Using equations (10.17),(10.18) and (10.20), we find:

$$M_{vdc} = \frac{2LC_{\alpha_f}C_{\alpha_r}}{C_{\alpha_f} + C_{\alpha_r}}\delta_{vdc} \tag{10.25}$$

It should be noted that the driver could request a braking force to control the longitudinal motion of the vehicle. This gives an additional information about the sum of braking forces ΣF_x. The distribution to the front and rear axles is done by considering the static distribution of the mass, which means using $\frac{l_r}{L}$. This gives two systems of two equations and two unknowns:

$$\begin{cases} F_{x_{f,r}} + F_{x_{f,l}} = \frac{l_r}{L}\Sigma F_x & (10.26) \\ F_{x_{f,r}} - F_{x_{f,l}} = \frac{l_r}{L}\Delta F_x & (10.27) \end{cases}$$

And:

$$\begin{cases} F_{x_{r,r}} + F_{x_{r,l}} = \left(1 - \frac{l_r}{L}\right)\Sigma F_x & (10.28) \\ F_{x_{r,r}} - F_{x_{r,l}} = \left(1 - \frac{l_r}{L}\right)\Delta F_x & (10.29) \end{cases}$$

With $\Delta F_x = \frac{M_{vdc}}{\frac{t}{2}}$. The brake forces can be then easily calculated using equations (10.26)-(10.29).

10.3 Upstream Approach

Coordinating the chassis systems downstream their controllers implies that the nature of conflicts is predictable. Coordination algorithms in the downstream approach are based on a preliminary study of systems interactions. However, one cannot foresee all possible scenarios. Because interactions are not mathematically identified, we cannot prove that the solutions provided using this approach are the best ones. Moreover, when each controller is designed independently to act directly on vehicle dynamics, we usually omit a major constraint level, which is tire potential. Designing each system without considering the possible interactions with other systems, gives a wrong information about the remaining potential of tires. This could lead to high requests of tire forces when these tires are actually saturated by another system. In the upstream approach, the combined dynamics should be formalized in order to distribute optimally the commands. Particularly, the tire model should be able to take into account the combined slip phenomenon. Hence, the relevance of the new linear tire model with varying parameters (Kissai et al., 2017) developed in Chapter 7. This model makes it possible to elaborate a better commands distribution by taking into account a more realistic tire potential. CA favors then tires with the bigger potential to act on the desired vehicle dynamics.

10.3.1 Control Architecture

The layer to be added in order to synergize chassis systems is located now upstream these subsystems. Figure 10.7 illustrates this concept.

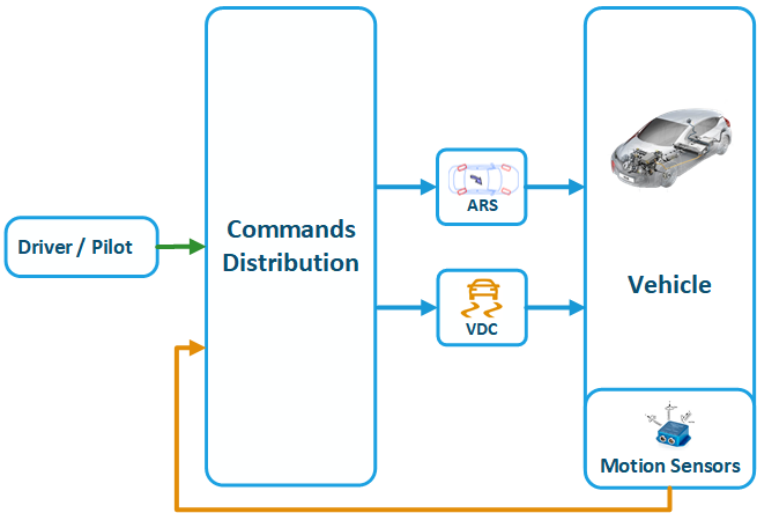

FIGURE 10.7: Structure of the upstream distribution approach (Kissai et al., 2018b).

By putting this layer upstream the subsystems controllers, interactions' treatment is prioritized. Conflicts are prevented rather than mitigated. However, as Figure 10.7 shows, subsystems' inputs have to be modified. This means that chassis systems should no longer be provided in a black box. "*Openness*" presents then a concern in developing this new approach. Nevertheless, the remaining criteria that Integrated Vehicle Dynamics Control (IVDC) architectures should satisfy (Kissai, Monsuez, and Tapus, 2017), namely, *Adaptability*, *Fault-tolerance*, *Dynamic reconfiguration*, *Extensibility* and *Modularity* can be ensured within this approach as we will demonstrate.

10.3.2 System Modelling

The idea is to calculate first the generalized forces that should be applied at the vehicle's CoG. Secondly, these generalized forces should be optimally distributed to the four tires depending on their potentials. Two subsystems are available to control the yaw rate. The overall system is then over-actuated. CA techniques were developed especially for this category of problems (Soltani, 2014). We recall the CA problem (Johansen and Fossen, 2013): *find the control vector,* $\vec{\delta} \in \mathbb{R}^n$ *such that*

$$\mathbf{B}\vec{\delta} = \vec{d}_{des} \tag{10.30}$$

subject to

$$\begin{cases} \vec{\delta}_{min} \leq \vec{\delta} \leq \vec{\delta}_{max} & (10.31) \\ \dot{\vec{\delta}} \leq \dot{\vec{\delta}}_{max} & (10.32) \end{cases}$$

Regarding ground vehicles: $\vec{\delta}$ represents controllable tire forces, $\vec{d}_{des}$ the desired generalized forces, $\mathbf{B}$ the geometric relations between the vehicle and its tires, and $\vec{\delta}_{min}$ and $\vec{\delta}_{max}$ reflect tire limits with respect to the friction ellipse concept (Pacejka, 2005), (Wong, 2001). The modeling consists in simply defining each component of the problem.

Tire forces

The ARS system generates lateral tire forces, while the VDC system generates longitudinal tire forces. The overall adhesion is delimited by the "friction circle" defined in Chapter 6. The tire potential is delimited by the product μF_z. When the tire is only solicited longitudinally, the maximum longitudinal force can reach μF_z. However, if the tire is solicited laterally while accelerating or braking, the overall force moves along the friction circle. The maximum overall tire force is still μF_z, but the maximum longitudinal force is penalized. The different dynamic forces saturations are:

$$\begin{cases} F_{x_{i,j}} \leq \sqrt{\left(\mu F_{z_{i,j}}\right)^2 - F_{y_{i,j}}^2} & (10.33) \\ F_{y_{i,j}} \leq \sqrt{\left(\mu F_{z_{i,j}}\right)^2 - F_{x_{i,j}}^2} & (10.34) \end{cases}$$

The actual difficulty is the fact that tire behavior is highly non-linear. In fact, when reaching its maximum, tire force drops suddenly and the vehicle loses its stability. Control strategy should prevent this from happening. Combined slip should be then taken into account since the beginning so as to prevent the real saturation. Equations (10.1) and (10.2) are no longer valid for tire modelling. As far as control synthesis is concerned, it is preferred to keep a linear tire model. This is why we developed a linear tire model with varying parameters in Chapter 6. We recall here this model (Kissai et al., 2017):

$$\begin{cases} F_{x_{i,j}} = C_s^* \left(\alpha_{i,j}, \mu_{i,j}, F_{z_{i,j}}\right) \kappa_{i,j} & (10.35) \\ F_{y_{i,j}} = C_\alpha^* \left(\kappa_{i,j}, \mu_{i,j}, F_{z_{i,j}}\right) \alpha_{i,j} & (10.36) \end{cases}$$

Where:

$$\begin{cases} C_s^* \left(\alpha, \mu, F_z\right) = \dfrac{4\sqrt{C_s^2\kappa^{*2} + C_\alpha^2\alpha^2} - \left(1 - \kappa^*\right)\mu F_z}{4\left(C_s^2\kappa^{*2} + C_\alpha^2\alpha^2\right)}\mu F_z C_s & (10.37) \\ C_\alpha^* \left(\kappa, \mu, F_z\right) = \dfrac{4\sqrt{C_s^2\kappa^2 + C_\alpha^2\alpha^{*2}} - \left(1 - \kappa\right)\mu F_z}{4\left(C_s^2\kappa^2 + C_\alpha^2\alpha^{*2}\right)}\mu F_z C_\alpha & (10.38) \end{cases}$$

With κ^* and α^* are stable operating points that were chosen in way to ensure that the new tire model becomes equivalent to the simpler one when no combined slip is involved:

$$\begin{cases} \kappa^* = \dfrac{\mu F_z}{8C_s^2}\left[\mu F_z + 4C_s + \sqrt{\left(\mu F_z\right)^2 + 8\mu F_z C_s}\right] & (10.39) \\ \alpha^* = \dfrac{\mu F_z}{2C_\alpha} & (10.40) \end{cases}$$

The ARS system generates the same steering angle in both tires by means of a single actuator as Figure 10.1 shows. Only the overall lateral force at the rear axle is taken into account. Unlike the ARS, the VDC has the ability to generate different longitudinal forces at each tire. The control vector is then:

$$\vec{\delta} = \begin{bmatrix} F_{x_{f,l}} \\ F_{x_{f,r}} \\ F_{x_{r,l}} \\ F_{x_{r,r}} \\ F_{y_r} \end{bmatrix} \quad (10.41)$$

Therefore, assuming that the vertical load and friction coefficient can be different at the level of each tire, control vector limits can be expressed as follows:

$$\vec{\delta}_{min} = \begin{bmatrix} -\sqrt{\left(\mu_{f,l}F_{z_{f,l}}\right)^2 - F_{y_{f,l}}^2} \\ -\sqrt{\left(\mu_{f,r}F_{z_{f,r}}\right)^2 - F_{y_{f,r}}^2} \\ -\sqrt{\left(\mu_{r,l}F_{z_{r,l}}\right)^2 - F_{y_{r,l}}^2} \\ -\sqrt{\left(\mu_{r,r}F_{z_{r,r}}\right)^2 - F_{y_{r,r}}^2} \\ -\sqrt{\left(\mu_{r}F_{z_{r}}\right)^2 - F_{x_r}^2} \end{bmatrix} \quad \text{and} \quad \vec{\delta}_{max} = \begin{bmatrix} \sqrt{\left(\mu_{f,l}F_{z_{f,l}}\right)^2 - F_{y_{f,l}}^2} \\ \sqrt{\left(\mu_{f,r}F_{z_{f,r}}\right)^2 - F_{y_{f,r}}^2} \\ \sqrt{\left(\mu_{r,l}F_{z_{r,l}}\right)^2 - F_{y_{r,l}}^2} \\ \sqrt{\left(\mu_{r,r}F_{z_{r,r}}\right)^2 - F_{y_{r,r}^2}^2} \\ \sqrt{\left(\mu_{r}F_{z_{r}}\right)^2 - F_{x_r}^2} \end{bmatrix} \tag{10.42}$$

Note that the case of different friction coefficients at each tire may seem more complex than the estimation of the overall friction coefficient problem. However, the difference between friction coefficient between right and left tires for example, which is known as the μ-split use-case, creates a yaw rate error that can be overcome by simply a feedback loop control. The real problem is when the maximum friction coefficient among all tires is below normal conditions. This changes the behavior of the car and should be taken into account at the CA layer. μ estimation presented in Chapter 7 can be seen as the mean value of all μ_{ij} that can solve this issue.

Generalized forces

We recall that in this case the main objective is yaw rate control. As long as the brake is concerned, the longitudinal velocity could be penalized. CA algorithms can be also used to mitigate the influence on the longitudinal speed. Two generalized equations are then considered from the global vehicle model developed in Chapter 5:

$$\begin{cases} V_x(s) = \dfrac{F_{x_{tot}}}{Ms} & (10.43) \\ \dot{\psi}(s) = \dfrac{M_{z_{tot}}}{I_z s} & (10.44) \end{cases}$$

In this case, we have:

$$\vec{d}_{des} = \begin{bmatrix} F_{x_{tot}} \\ M_{z_{tot}} \end{bmatrix} \tag{10.45}$$

Because of the differential nature of equations (10.43) and (10.44), a high-level controller is first required to compute $\vec{d}_{des}$.

Effectiveness matrix

In this case, suspensions are not controlled. To compute control commands to the four wheels, only a planar four-wheeled vehicle model is needed. Figure 10.8 illustrates this model.

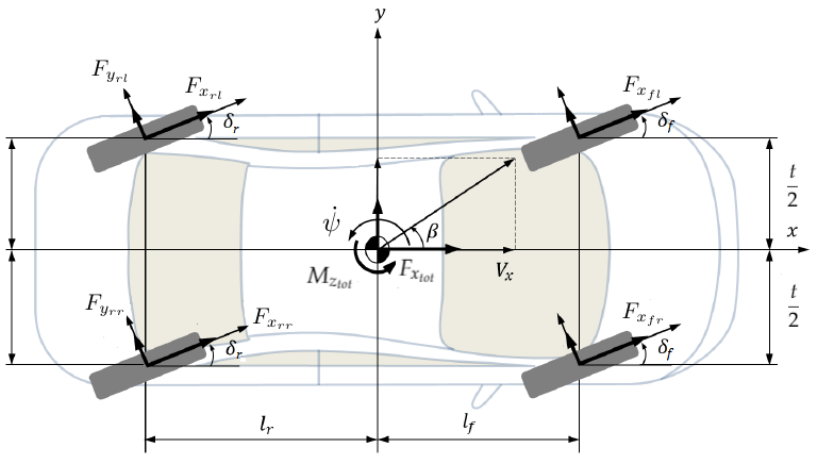

FIGURE 10.8: The four-wheeled planar vehicle model (adapted from (Soltani, 2014)).

From equations developed in Chapter 5, and considering only controllable tire forces with $\delta_r \ll$, we find:

$$F_{x_{tot}} = \left(F_{x_{f,l}} + F_{x_{f,r}}\right)\cos\left(\delta_f\right) + F_{x_{r,l}} + F_{x_{r,r}} \tag{10.46}$$

$$\begin{aligned} M_{z_{tot}} = &\left(F_{x_{f,l}} + F_{x_{f,r}}\right) l_f \sin\left(\delta_f\right) + \left(F_{x_{f,r}} - F_{x_{f,l}}\right)\frac{t}{2}\cos\left(\delta_f\right) \\ &+ \left(F_{x_{r,r}} - F_{x_{r,l}}\right)\frac{t}{2} - F_{y_r} l_r \end{aligned} \tag{10.47}$$

From equations (10.30),(10.41),(10.45), (10.46),(10.47), we get the following effectiveness matrix expression:

$$\mathbf{B} = \begin{bmatrix} \cos\left(\delta_f\right) & \cos\left(\delta_f\right) & 1 & 1 & 0 \\ b_{2,1} & b_{2,2} & -\frac{t}{2} & \frac{t}{2} & -l_r \end{bmatrix} \tag{10.48}$$

where:

- $b_{2,1} = l_f \sin\left(\delta_f\right) - \frac{t}{2}\cos\left(\delta_f\right)$,
- $b_{2,2} = l_f \sin\left(\delta_f\right) + \frac{t}{2}\cos\left(\delta_f\right)$.

10.3.3 Control Synthesis

As you may notice, the CA consists in adding a new abstraction level as a mid-level layer in the control architecture. Rather than calculating actuator commands directly from desired targets by considering an ideal tire behavior as in the downstream approach, we add effector constraints in the middle of the control chain to distribute optimally tire forces by considering a more realistic potential of each one. A high-level controller computes the desired generalized forces from desired velocities, a CA strategy distributes the commands to the available effectors by taking into account their constraints, and low-level controllers convert tire forces into control commands to the different actuators. Figure 10.9 summarizes the control procedure adopted.

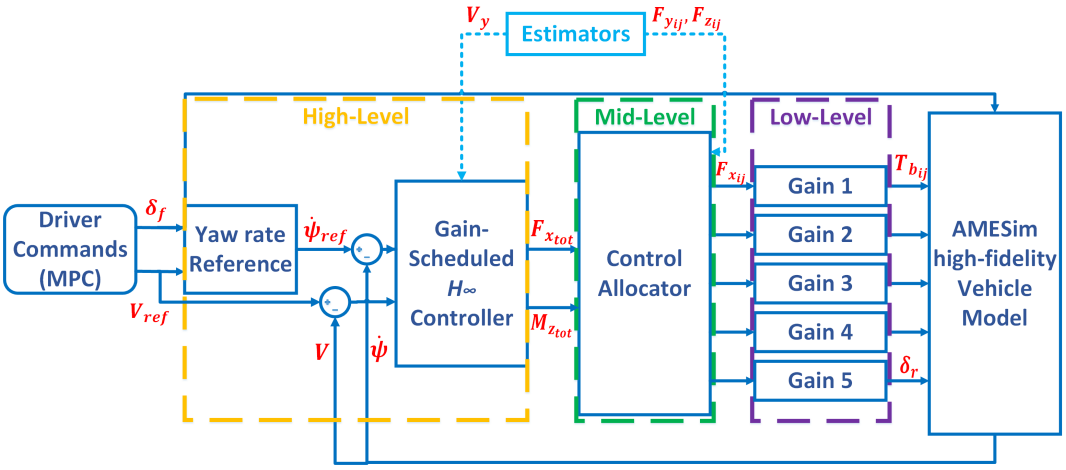

FIGURE 10.9: Upstream control scheme in case of ARS-VDC coordination.

High-level controller

In order to distribute the forces to each effector, the generalized force $F_{x_{tot}}$ and moment $M_{z_{tot}}$ should be first generated. Here, we consider equations (10.43) and (10.44). Actually, it is worth mentioning that equation (10.43) was quite simplified. Considering the vehicle as a moving frame, the longitudinal acceleration should be expressed as:

$$a_x = sV_x - V_y\dot{\psi} \tag{10.49}$$

Couplings between the longitudinal velocity and the yaw rate are related to the lateral velocity value. V_y can be considered as a varying parameter. The vehicle model is then linearized with respect to a range of V_y values. Moreover, according to equations (10.43) and (10.44), corresponding transfer function can be approximated by an integrator. In addition, as several parametric uncertainties exist at the vehicle level[4] and the tire level[5], a robust controller should be designed. For all these reasons, a PI-structured Gain-Scheduled H_∞ controller has been chosen to ensure the high-level control where V_y is the scheduling parameter. The guidelines presented in Chapter 8 are applied using Matlab® to generate robust controllers for each selected value of the scheduling parameter.

CA strategy

We first adopt the solution given by (Soltani, 2014). The author uses *daisy-chain*, which is a static CA method, to prioritize the ESP over the EPAS, then a *WPI* as a precomputed law for brake distribution. However, the reasons that led the author to prioritize the ESP are not clear. In order to give a reliable comparison between both architectures, the ARS is also prioritized here with respect to the VDC by means of the simple *daisy-chain* method. The *WPI* method is then used for brake forces distribution. Secondly, we investigate the potential of online repeated optimization methods using different optimization algorithms.

- **Precomputed solution**

[4] Mass, moment of inertia, and so on.
[5] Basically the friction coefficient

– Daisy-chain

As defined in Chapter 9, the daisy-chaining consists in forcing a static hierarchy for control effectors. The difference with respect to the downstream approach is the condition to move to the second subsystem. Here, actuator saturation or tire saturation is the switching condition. In addition, when a control saturates, an error between the desired forces and those generated by control effectors arises. Only this error is transmitted to the second set of subsystems. The schematic representation of this technique is illustrated in Figure 9.1.

Therefore, the VDC only activates when the rear lateral force saturates or the rear steering angle reaches $\pm 3.5^{\circ}$. The CA problem is then separated into two sub-problems. The first set contains only the ARS system. As only rear steering can be generated. Only the yaw moment is considered. Longitudinal forces are ignored. We have then:

$$F_{y_r} = -\frac{1}{l_r} M_z, \tag{10.50}$$

while taking into account the constraints (10.42).

When ARS is saturated, the deficiency is transmitted to the VDC system. The second sub-problem is then defined as:

$$\begin{bmatrix} F_{x_{tot}} \\ M_z + l_r F_{y_r} \end{bmatrix} = \mathbf{B_2} \begin{bmatrix} F_{x_{i,j}} \\ F_{x_{f,r}} \\ F_{x_{r,l}} \\ F_{x_{r,r}} \end{bmatrix} \tag{10.51}$$

where $\mathbf{B_2} = \begin{bmatrix} \cos(\delta_f) & \cos(\delta_f) & 1 & 1 \\ b_{2,1} & b_{2,2} & -\frac{t}{2} & \frac{t}{2} \end{bmatrix}$. $\mathbf{B_2}$ has to be inverted. However, it is not a square matrix. A pseudo-inverse can still be provided. Moreover, to favor one control command over another depending on tire potential, weighting matrices could be used (Soltani, 2014). Therefore, a "*WPI*" is used for brake forces allocation.

– WPI

It is an offline optimization technique based on a pseudo inversion of the non-square matrix $\mathbf{B}$ to generate a precomputed law as defined in Chapter 9. The problem is formulated as follows:

$$\min_{\vec{\delta}} J = \min_{\vec{\delta}} \frac{1}{2} \left(\vec{\delta} + \vec{c}\right)^T \mathbf{W} \left(\vec{\delta} + \vec{c}\right) \tag{10.52}$$

subject to (10.30), where $\mathbf{W} \in \mathbb{R}^{n \times n}$ is a weighting matrix and $\vec{c} \in \mathbb{R}^n$ is an offset vector used to represent an off-nominal condition. The resolution method using the Hamiltonian can be found in (Oppenheimer, Doman, and Bolender, 2006). The solution is expressed as follows:

$$\begin{aligned} \vec{\delta} &= -\vec{c} + \mathbf{W}^{-1}\mathbf{B}^T \left(\mathbf{B}\mathbf{W}^{-1}\mathbf{B}^T\right)^{-1} \left[\vec{d}_{des} + \mathbf{B}\vec{c}\right] \\ &= -\vec{c} + \mathbf{B}^{\sharp} \left[\vec{d}_{des} + \mathbf{B}\vec{c}\right] \end{aligned} \tag{10.53}$$

where $\mathbf{B}^{\sharp}$ is the pseudo inverse of $\mathbf{B}$. The weighting matrix can be adjusted

to favor one effector over another. This is done by increasing the weight of the less attractive actuator. In fact, to satisfy (10.52), the command corresponding to the increasing weight is reduced faster and thus could be even delayed. Therefore, to take into account the tire potential, we introduce the inverse of the tire force saturation in the diagonal of the weighting matrix. When approaching saturation, the weight denominator approaches 0 and therefore, the weight approaches ∞. The weighting matrix chosen is expressed as:

$$\mathbf{W} = \begin{bmatrix} w_{f,l} & 0 & 0 & 0 \\ 0 & w_{f,r} & 0 & 0 \\ 0 & 0 & w_{r,l} & 0 \\ 0 & 0 & 0 & w_{r,r} \end{bmatrix} \tag{10.54}$$

where $w_{i,j} = \dfrac{1}{\sqrt{\left(\mu_{i,j} F_{z_{i,j}}\right)^2 - F_{y_{i,j}}^2}}$.

Moreover, longitudinal stiffness is supposed to be the same for all tires. No off-nominal condition is considered. Therefore, $\vec{c} = 0$, which gives finally:

$$\vec{\delta} = \mathbf{B}^{\sharp} \vec{d}_{des} \tag{10.55}$$

The advantage of this technique is the fact that it is based on an algebraic calculation which makes it faster with respect to online optimization based methods. However, the Daisy-Chain method imposes a predefined prioritization of one system over another, which contradicts the upstream approach philosophy. The WPI is more suitable as long as only one objective is pursued. For multi-objectives problems, no algebraic expression exists. This limits the use of this method.

- **Online repeated optimization solution**

  The major advantage of online repeated optimization is the ability to solve multi-objective problems. We will mainly use this to ensure fault-tolerance and try to fulfill qualitative secondary objectives. First, we keep the control vector in (10.41) as it is, and also the initial effectiveness matrix $\mathbf{B}$. This enables for example programming directly fault-tolerance features. We assume that we are able to detect and isolate the fault[6]. Moreover, we recall that our objective is to control the vehicle's yaw rate. We modify then only the second line of the effectiveness matrix to take into account systems' failures. Let us note φ_i the flag of the i^{th} actuator expressing its status where:

$$\varphi_i = \begin{cases} 1 & \text{if the actuator is working fine,} \\ 0 & \text{otherwise.} \end{cases} \tag{10.56}$$

  The effectiveness matrix becomes then:

$$\mathbf{B} = \begin{bmatrix} \cos(\delta_f) & \cos(\delta_f) & 1 & 1 & 0 \\ b_{2,1}\varphi_1 & b_{2,2}\varphi_2 & -\dfrac{E}{2}\varphi_3 & \dfrac{E}{2}\varphi_4 & -l_r\varphi_5 \end{bmatrix} \tag{10.57}$$

[6] Renault's smart actuators for both systems contain fault detection modules.

It should be noted that various types of faults exist. Only one type is here exposed to focus on the control reallocation technique. These types are discussed in Chapter 15 where φ may differ from 0 or 1.

Regarding the choice of the optimization algorithm, two main criteria should be taken into account. First, the algorithm should provide enough potential to solve the CA problem and reallocation, and converge to the optimum in a finite number of iterations. Secondly, the algorithm should be fast enough to ensure real-time operations. ASA have shown good results in this context. Here, the optimal control vector is expressed as (Harkegard, 2002):

$$\vec{\delta}_{opt} = arg \min_{\vec{\delta}_{min} \leq \vec{\delta} \leq \vec{\delta}_{max}} \left\| \mathbf{A}\vec{\delta} - \vec{b} \right\| \tag{10.58}$$

Two different methods based on ASA have been derived. SLS uses two stage ASA to separate the global problem into two optimization problems (Harkegard, 2002). This leads to the following formulation:

$$\begin{cases} \vec{\delta}_{opt} = arg \min_{\vec{\delta} \in \Omega} \left\| \mathbf{W_u} \left(\vec{\delta} - \vec{\delta}_p \right) \right\| & (10.59) \\ \Omega = arg \min_{\vec{\delta}_{min} \leq \vec{\delta} \leq \vec{\delta}_{max}} \left\| \mathbf{W_v} \left(\mathbf{B}\vec{\delta} - \vec{v} \right) \right\| & (10.60) \end{cases}$$

Where $\vec{\delta}_p$ is the preferred control vector, usually $\vec{0}$.

In contrast, the WLS solves the global problem in one stage ASA by means of different weights to determine the importance of each objective (Harkegard, 2002). This gives the following expression:

$$\vec{\delta}_{opt} = arg \min_{\vec{\delta}_{min} \leq \vec{\delta} \leq \vec{\delta}_{max}} \left\| \mathbf{W_u} \left(\vec{\delta} - \vec{\delta}_p \right) \right\|^2 + \gamma \left\| \mathbf{W_v} \left(\mathbf{B}\vec{\delta} - \vec{v} \right) \right\|^2 \tag{10.61}$$

Other techniques non based on ASA exist as the IP solver (Petersen and Bodson, 2006), CGI (Bordignon, 1996), and FPI (Burken et al., 2001). These techniques are compared through co-simulation in paragraph 10.4.3.

Regarding the secondary objectives choice, the literature has been more interested in power consumption and tire energy dissipation (Shyrokau et al., 2015). The driving pleasure and comfort have always been ensured by the driver himself. Each driver corrects the vehicle behavior gradually until it fits its comfort and confidence requirements. He remains the controller of the outer loop. This is one of the challenges that autonomous vehicles will have to overcome. To the best of our knowledge, chassis systems coordination taking into account the feelings generated has been ignored in the literature. In an autonomous driving context, coordination should be made in such a way so as to avoid generation of unexpected car behavior. In this chapter, we will raise the question of the ability of CA algorithms to tune the motion behavior of the car. The objective is to prove that with the same reference, we can induce different responses when changing the weight of comfort requirements. The driver can then look for its most suitable car behavior, and the car will do the rest.

The algorithm can try to fulfill several objectives separately in a sequential way (Harkegard, 2002). The objectives order in the algorithm determines the priority of each objective. However, we want this priority to be tunable. That is

why we prefer to merge the optimization criteria into one stage, and by means of different weights, make the objectives prioritization tunable online. And this is what exactly enables the WLS formulation:

$$\vec{\delta}_{opt} = arg \min_{\vec{\delta}_{min} \leq \vec{\delta} \leq \vec{\delta}_{max}} \sum_{l} \gamma_i \left\| \mathbf{W_i} \left(\mathbf{B_i} \vec{\delta} - \vec{v}_i \right) \right\|^2 \tag{10.62}$$

- $\vec{\delta}_{opt}$: optimal control vector,
- l : number of objectives,
- γ_i : weight of the i^{th} objective,
- $\mathbf{W_i}$: non-singular weighting matrices,
- $\vec{v}_i$: desired vector of the i^{th} objective,
- $\mathbf{B_i}$: effectiveness matrix relating the control vector to the desired i^{th} objective.

Stability and robustness of the global control is ensured by the high-level control, the outer loop of the integrated control strategy. If the combination of tire forces achieve the generalized forces required to stabilize the vehicle, then the stability is ensured. One can speculate that the prior objective of the WLS algorithm should be then the CA precision. This prioritization is ensured by setting the CA precision corresponding weight to the highest value. However, when following this procedure, no effect could be obtained in terms of accelerations to change the vehicle's behavior as the algorithm prioritizes forces tracking generated by the high-level control. Here, a penalization of precision is permitted in order to fulfill a secondary objective without jeopardizing the vehicle's stability. The corresponding weighting matrix enables us to favor one control axis instead of another. We remind that our first objective is to control the yaw rate by means of two chassis systems, but we also want to minimize the effect on the longitudinal speed. The weighting matrix, that we note $\mathbf{W_{ca}}$, is then chosen to be diagonal with higher value of the weight corresponding to the generalized yaw moment.

The originality of this part lies rather in the motion feelings objective. Motion sickness and discomfort are tightly related to the vehicle's accelerations (Raimondi and Melluso, 2008). The major problem is how to fit the desired accelerations to each driver perception. The goal of this thesis is just to show the ability of the CA algorithm proposed to change the vehicle's behavior. No standardizations are intended to be given for now as more experimental tests are needed. We chose then in this work to let the user set its preferences manually. In other words, as drivers have the option to select their preferred driving modes in recent cars, those modes are linked here to the second objective criteria. Let us first determine the relations between the control vector and accelerations. The effectiveness matrix is therefore expressed as:

$$\mathbf{B_{mf}} = \begin{bmatrix} \frac{\cos(\delta_f)}{M} & \frac{\cos(\delta_f)}{M} & \frac{1}{M} & \frac{1}{M} & 0 \\ \frac{\sin(\delta_f)}{M} & \frac{\sin(\delta_f)}{M} & 0 & 0 & \frac{1}{M} \end{bmatrix} \tag{10.63}$$

The weighting matrix here, noted $\mathbf{W_{mf}}$, would favor the longitudinal acceleration to the lateral one or the opposite. As we are more interested in the overall

acceleration, without favoring a particular direction with respect to the other, this matrix is set to the identity matrix.

Desired tunable accelerations are contained in the desired vector noted $\vec{v}_{mf}$. This vector should not contain predefined values as this could lead to accelerations demand while the driver does not ask for them. This vector should rather be expressed according to the control vector. The objective is then:

$$\left\| \mathbf{W_{mf}} \left(\mathbf{B_{mf}} \vec{\delta} - \left[\mathbf{B_{mf}} \vec{\delta} + \vec{\varepsilon} \right] \right) \right\| \tag{10.64}$$

where $\vec{\varepsilon}$ is the tunable weight that varies with the driver's preferences. One could think of the risk of divergence of the commands as the subtraction in equation (10.64) is never null for $\vec{\varepsilon} \neq \vec{0}$. However, the first objective prevent the control vector from increasing too much to keep minimal the CA error. A null $\vec{\varepsilon}$ corresponds then to a neutral behavior, a non-null $\vec{\varepsilon}$ with the same sign of the current acceleration would give a higher acceleration than expected and corresponds then to a more sportive mode, and a non-null $\vec{\varepsilon}$ with an opposite sign would give a lower acceleration than expected and corresponds then to a more comfortable mode. The optimal control vector is then:

$$\begin{aligned} \vec{\delta}_{opt} = arg \min_{\vec{\delta}_{min} \leq \vec{\delta} \leq \vec{\delta}_{max}} & \gamma_{ca} \left\| \mathbf{W_{ca}} \left(\mathbf{B_{eff}} \vec{\delta} - \vec{v}_{des} \right) \right\|^2 \\ & + \gamma_{mf} \left\| \mathbf{W_{mf}} \left(\mathbf{B_{mf}} \vec{\delta} - \left[\mathbf{B_{mf}} \vec{\delta} + \vec{\varepsilon} \right] \right) \right\|^2 \end{aligned} \tag{10.65}$$

To solve this problem, we simply have to rewrite the cost function following the ASA formulation:

$$\vec{\delta}_{opt} = arg \min_{\vec{\delta}_{min} \leq \vec{\delta} \leq \vec{\delta}_{max}} \left\| \mathbf{A} \vec{\delta} - \vec{b} \right\| \tag{10.66}$$

The algorithm follows the simple following steps:

1. Initialize the control vector from the previous sampling instant,
2. Rewrite the cost function in (10.65) as:

$$\left\| \begin{pmatrix} \sqrt{\gamma_{ca}} \mathbf{W_{ca}} \mathbf{B_{eff}} \\ \sqrt{\gamma_{mf}} \mathbf{W_{mf}} \mathbf{B_{mf}} \end{pmatrix} \vec{\delta} - \begin{pmatrix} \sqrt{\gamma_{ca}} \mathbf{W_{ca}} \vec{v}_{des} \\ \sqrt{\gamma_{mf}} \mathbf{W_{mf}} \left[\mathbf{B_{mf}} \vec{\delta} + \vec{\varepsilon} \right] \end{pmatrix} \right\|^2 \tag{10.67}$$

3. Solve equation (10.66) using ASA.

The algorithm tries to satisfy both objectives at the same time when possible. If it is not possible, then the cost function is at least minimized by favoring the objective with the highest weight. For real-time maneuvers, number of iterations are limited to a finite value. As the algorithm converges to the optimum, at least a sub-optimal solution could be generated rather than an optimal one.

Low-level controllers

Low-level controllers are responsible of generating the right command to the different actuators that ensure the execution of allocated tire forces. Two major criteria have to be considered in the design of the controller. First, the low-level layer is located in the inner loop. It should be therefore the fastest. The crossover frequency of the low-level control is chosen to be 10 times higher than the high-level's. Moreover, the

same crossover frequency is chosen for rear steering angle command and braking torques commands. Reallocation should be caused by tire or actuator saturations and not by one of the controllers delay with respect to the others. Secondly, no overshoot should be allowed. CA is made by taking into account the tire saturation. At hazardous situations, it could allocate the maximum allowable tire force. This force must not be exceeded, otherwise the vehicle could loose its stability.

In addition, the outputs from the CA algorithm are tire forces. These forces should be reconverted to brake torques and steering angle to make it recognizable by the corresponding actuators. To ensure tire forces following, one could think about adding additional controllers in a feedback loop downstream the CA layer. However, tire forces sensors are extremely expensive, and commercial vehicles are not usually equipped by these sensors (Yang, Kim, and Lee, 2010). Feedback-control cannot be ensured. This leaves us with either a feed-forward control or a direct transformation [7]. To avoid additional phase-lag, we prefer a direct transformation. The following equations are then used:

$$\begin{cases} T_{b_{ij}} = -RF_{x_{i,j}} & (10.68) \\ \delta_r = \dfrac{F_{y_r}}{C_\alpha^*} - \left(\dfrac{I_z}{Ml_r} - l_r\right)\dfrac{\dot{\psi}}{V_x} & (10.69) \end{cases}$$

The minus sign in equation (10.68) is due to the fact that the brake pressure should be positive, while the brake forces are negative. Equation (10.69) comes from a combination of (10.2),(10.5),(10.6),(10.36). What makes it interesting is the fact that the new tire model is not only used in CA, but also in the rear steering angle computation. The value of this angle will be then adapted to respect the rear tires conditions.

Regarding the brakes, a saturation is added regarding the pressure that can be delivered for braking. This pressure is within the range of $[0, 200]$bar. Moreover, the relationship between braking pressure and braking torque is:

$$T_b = \frac{K_{cal}}{1 + s\tau_{cal}} P \tag{10.70}$$

where:

- P : the braking pressure,
- K_{cal} : caliper's gain,
- τ_{cal} : calliper's time constant.

In steady-state, equation (10.70) becomes $T_b = K_{cal}P$, with $K_{cal} = 10$. Therefore, T_b range is $\left[0, 2.10^8\right]$N.m. Note that the actuators' dynamics are considered ideal at this stage. This will be discussed in more details in Chapter 13.

10.4 Comparison of coordination approaches

We first carry simulations using only Matlab/Simulink® with the simplified vehicle models used at each approach. Then, simulations using a more sophisticated vehicle model developed in Amesim® with the same control logic are exposed. However, Amesim does not provide the possibility of implementing online optimization

[7] Which can be considered as a gain.

algorithms. To benefit from the advantages of both softwares, a co-simulation procedure is carried in case of online repeated optimization solutions. Regarding the upstream approach, when using only Matlab/Simulink® or Amesim® apart, only the precomputed solution (offline optimization) is used. The online optimization is rather used when co-simulating between both software.

10.4.1 Matlab/Simulink® Simulations

Both approaches are programmed in Simulink platform to enable their comparison. We recall that the ARS system is prioritized in both approaches with respect to the VDC system. Nevertheless, the upstream approach enable adding an additional abstraction level. This gives the possibility to take into account the tire forces saturation. A more accurate tire model is then injected with respect to the downstream approach. Several maneuvers are considered for comparison and validation.

Rapid lane changing

We first carry a rapid lane changing at a longitudinal speed of $100km/h$. The front wheel steering profile is depicted in Figure 10.10.

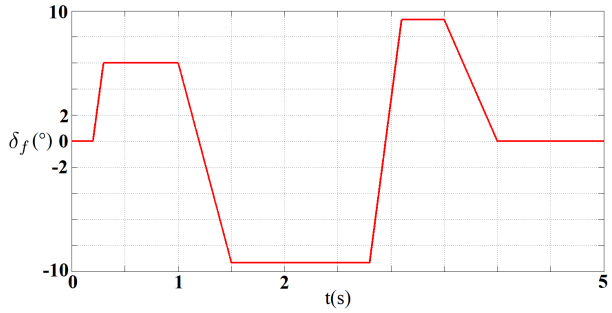

FIGURE 10.10: Front wheel steering profile for a rapid lane changing.

The yaw rate response for both approaches is illustrated in Figure 10.11.

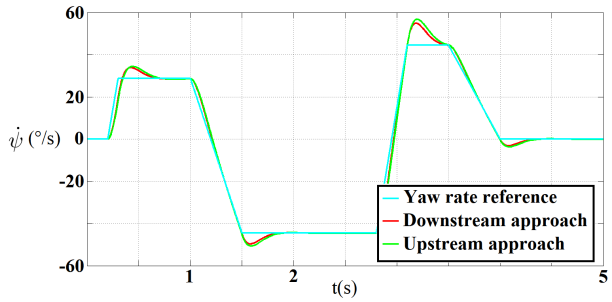

FIGURE 10.11: Yaw rate response for a rapid lane changing.

Both approaches can track the yaw rate reference thanks to the ARS system. Here, the VDC does not activate. However, the rear steer angle generated differs from one approach to another as Figure 10.12 shows.

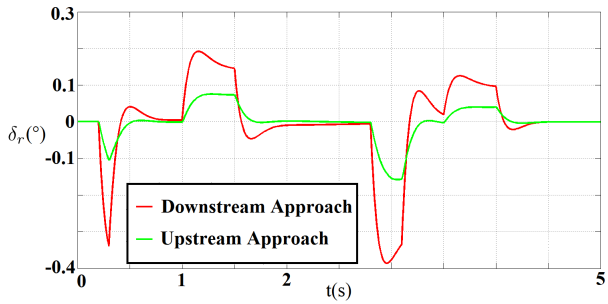

FIGURE 10.12: Rear steering angle in a rapid lane changing.

This is mainly due to the new tire model. In fact, the new tire model takes into account the combined slip and tire saturation. This can be seen in Figure 10.13, where the front lateral force in both approaches has been estimated using the equations (10.1) for downstream approach and (10.36) for upstream one, respectively.

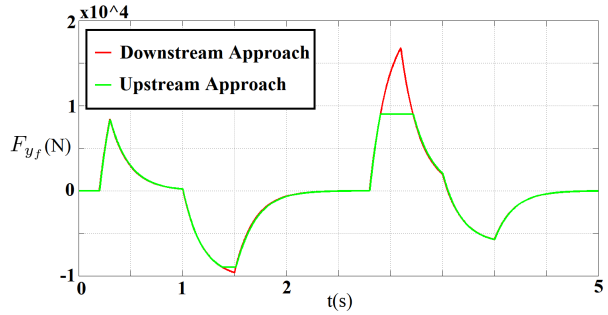

FIGURE 10.13: Front lateral force in a rapid lane changing.

According to equation (10.6), as the front lateral force is smaller, the rear force required to stabilize the vehicle is also smaller. To create this latter, a smaller rear steering angle is then required according to equations (10.4) and (10.36). Therefore, taking into account the tire potential enables realistic actuator requests.

ARS failure in slalom maneuver

A slalom maneuver is carried out with a longitudinal speed of $100km/h$. At time $t = 4s$, we block the ARS system. Figure 10.14 illustrates this failure.

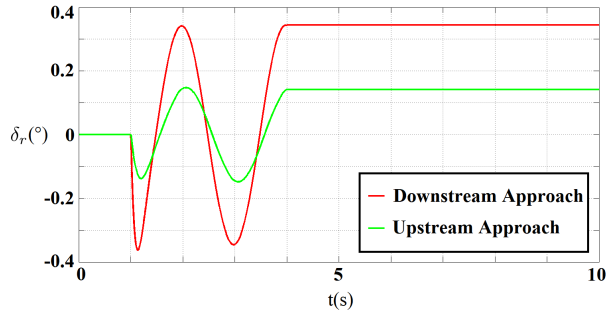

FIGURE 10.14: Rear steering angle when failure.

Again, as no overshoot is allowed, the upstream approach generates a rear angle smaller than the downstream approach. Regarding yaw rate, Figure 10.15 illustrates the fault-tolerance ability of each approach.

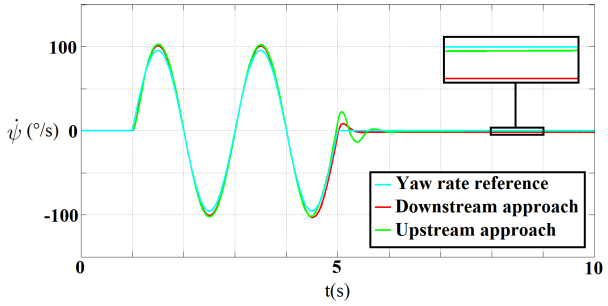

FIGURE 10.15: Yaw rate when rear steering failure.

The upstream approach exhibits a higher overshoot after the failure. This is mainly due to the activation of brake forces as Figure 10.16 shows. As neither the longitudinal acceleration exceeds $8.82 m/s^2$ nor the rear angle actuator saturates, the VDC system does not activate in the downstream approach. No important overshoot is experienced in that case, but a steady-state yaw rate error remains. To keep the vehicle in a straight line, the driver has to continually steer the front wheels.

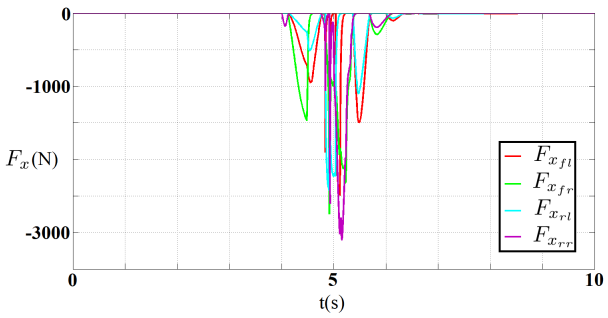

FIGURE 10.16: Brake forces for the upstream approach in case of ARS failure

Regarding brake forces, when left brake forces are activated, the right ones do not and vice-versa in order to create a maximum yaw moment. However, for tires in the same side, there exists a slight difference between activated brake forces. This is caused by the difference in vertical loads at each tire which gives different potentials (Figure 10.17). Thanks to the new tire model, tires with bigger potential are prioritized which gives a better control distribution.

Random braking while steering

To study more closely the interaction between steering and braking, data from a real maneuver conducted by Renault has been collected. A trajectory with several curves is followed. Front steering wheel angle measures and longitudinal speed estimation data have been used as inputs for both approaches. A high-level controller for longitudinal speed control have been added in the downstream approach also to generate the longitudinal force. Negative values of this force corresponds to driver

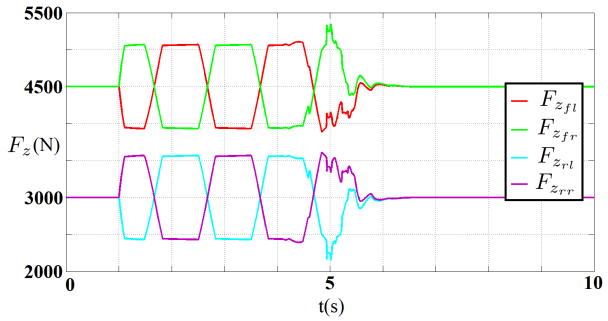

FIGURE 10.17: Vertical loads taken account of in upstream approach.

brake request. In the downstream approach, when VDC is not activated, this force is simply divided by four and distributed equally to the four wheels. The yaw rate response in this case is illustrated in Figure 10.18.

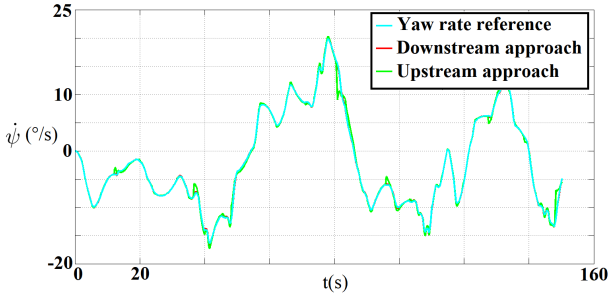

FIGURE 10.18: Yaw rate response in random braking.

Both approaches are able to track the yaw rate reference. However, there is an important difference regarding the rear steering angle generated as Figure 10.19 shows.

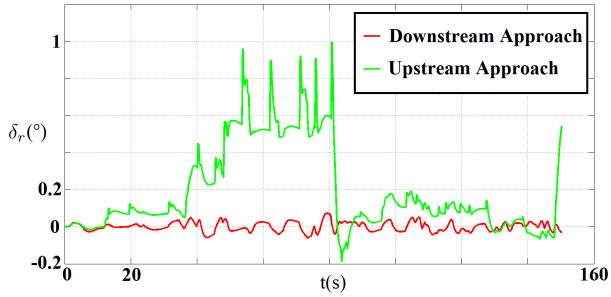

FIGURE 10.19: Rear steering angle while random braking.

Again, the fact that the tire is solicited both longitudinally and laterally makes the cornering (and longitudinal) stiffness drops. This is illustrated in Figure 10.20.

As neither actuator saturation nor tire saturation is experienced in this maneuver, the lateral force requested is almost the same in both approaches. To achieve the requested lateral force in the upstream approach when the cornering stiffness drops, more side-slip is required according to equation (10.36). By taking into account equation (10.4), the rear steering angle should increase for the side-slip to go higher.

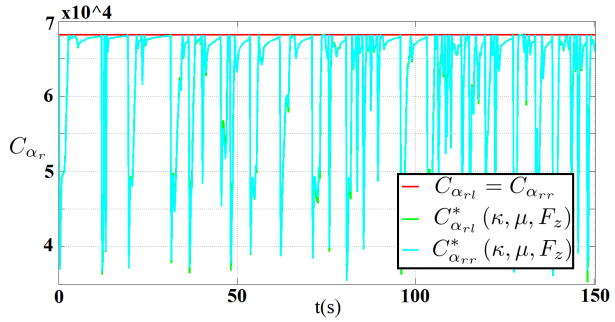

FIGURE 10.20: Cornering stiffness affected by random braking.

The result is illustrated in Figure 10.19. The upstream approach gives then more realistic commands. In fact, the downstream approach "overestimates" the cornering stiffness available when braking and computes smaller real steering angle.

As a conclusion, we can say that the results presented here are biased by the vehicle model chosen for validation. As only a bicycle model is used for the downstream approach, the results are too optimistic. The same vehicle model should be used for validation. The same procedure should be adopted by car manufacturers in their communications with their suppliers. A supplier can present nice results if a simpler vehicle model is used. A common platform should be adopted. Next, a high-fidelity vehicle model developed in Amesim® is used for both approaches.

10.4.2 Amesim® Simulations

Simulations could be very tricky, especially when the model and the environment are developed by the control designer himself. A simplified vehicle model, on which the control design has been based, will give surely good results. For this reason we chose to test our control algorithms in a more sophisticated and realistic models. Amesim® gives this opportunity by means of a larger library of vehicle dynamic components. The vehicle model consists of a 3D sprung mass with advanced options[8], a steering column model, an engine model, a braking system based on independent rotary Coulomb friction to enable the VDC control logic, suspensions, the non-linear coupled Dugoff's tire model, spindle kinematics, and rotational degree of freedom relative to the spindle of both front and rear wheels to enable implementing the ARS control logic. This results on a 16 Degrees-Of-Freedom (DOF) model, with 43 states for the downstream approach and 42 states for the upstream one[9] (Figure 10.21). A road model is also given to enable modifying road conditions, adding slopes, speed bumps and so on. Different realistic scenarios can be then tested. It should be noted that the same crossover frequency has been imposed in both approaches to enable a fair comparison.

Simulations were chosen to shed the light on the safety that each architecture offers. Two scenarios are highlighted where both ARS and VDC can be activated at the same time: μ-split maneuver and ARS failure.

[8] Enables anisotropic friction, roll height modification, aerodynamic disturbances and so on.

[9] As in the downstream approach two controllers are required to control the yaw rate, while in the upstream approach, only one controller is required. The same controller is used for the longitudinal speed in both architectures.

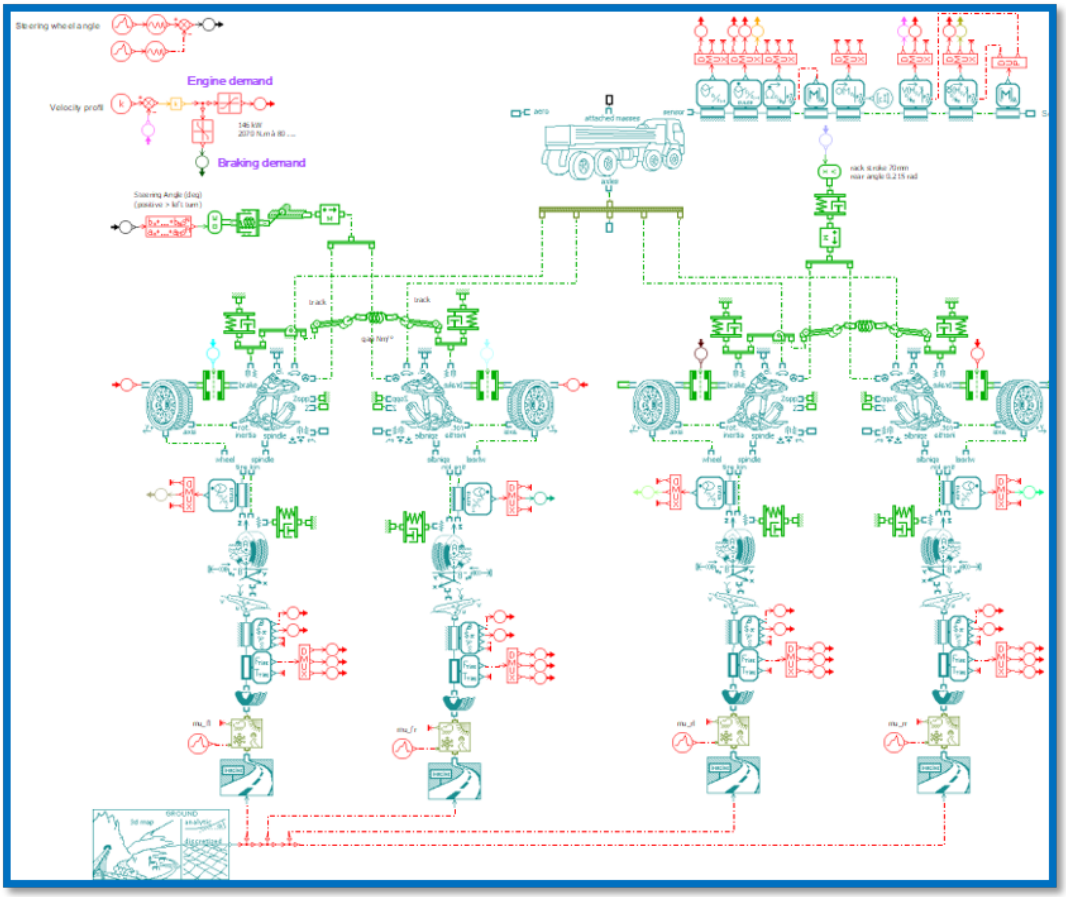

FIGURE 10.21: Amesim high-fidelity vehicle model.

μ-split maneuver

Here we test the robustness of the control to face environmental changes. To do so, we make the friction coefficient drops from 1 to 0.1 during 3 seconds at $t = 8s$. The vehicle is supposed to be in a cornering, and only the exterior tires are affected by this change in road conditions that can lead to an additional undesired yaw rate. The yaw rate responses of both approaches are compared in Figure 10.22.

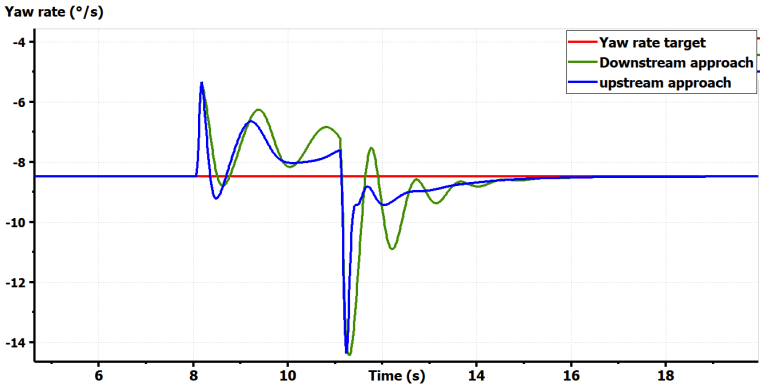

FIGURE 10.22: Yaw rate control comparison - μ-split maneuver.

We can see that the upstream approach provides a more stable regulation with respects to the downstream approach. This latter shows an oscillatory behavior which is unacceptable. Running through commands signals showed that the VDC system has been activated only in the upstream approach as the Figure 10.23 illustrates, even though the ARS system is not saturated in both approaches. The reason

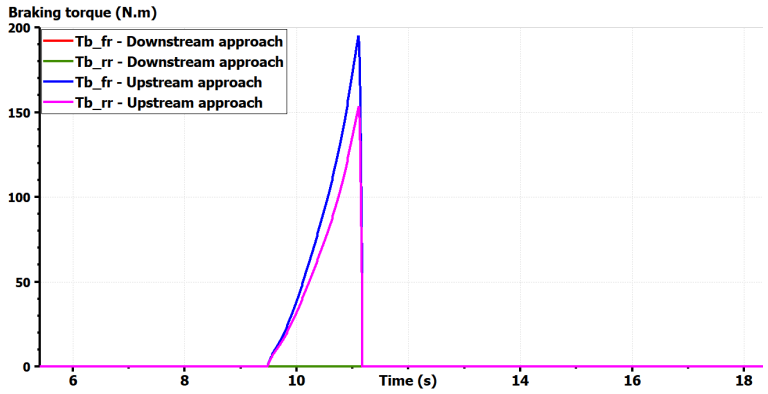

FIGURE 10.23: Brake torques comparison - μ-split maneuver.

is that the CA made in the upstream approach takes account not only of the actuators saturation, but also effectors saturation. In this case, it is the requested lateral rear tire force that exceeds the tire potential (Figure 10.24). Taking into account this phe-

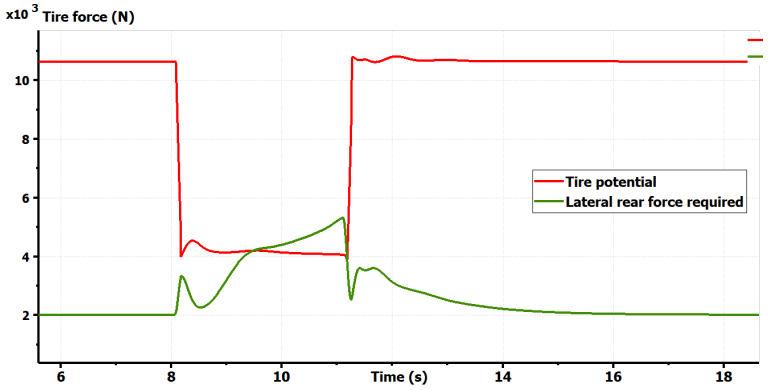

FIGURE 10.24: Lateral rear tire force saturation - μ-split maneuver.

nomenon before distributing the commands, upstream to the subsystems, enables the yaw rate to be stabilized rapidly. Omitting this physical constraints destabilizes the vehicle.

ARS failure

In general, when a system is critical, we ensure some redundancy to avoid any tragic scenario. Regarding the ARS system, it is not considered as a critical system but rather an assistance system. Moreover, due to its relatively high cost, it is not redundant. In this case, one could think about making the VDC complementary to the ARS if this latter fails. To simulate this scenario, we choose a repeating slalom maneuvers, where the ARS fails and blocks at a certain position at time $t = 4s$. The yaw rate responses of both approaches are illustrated in Figure 10.25.

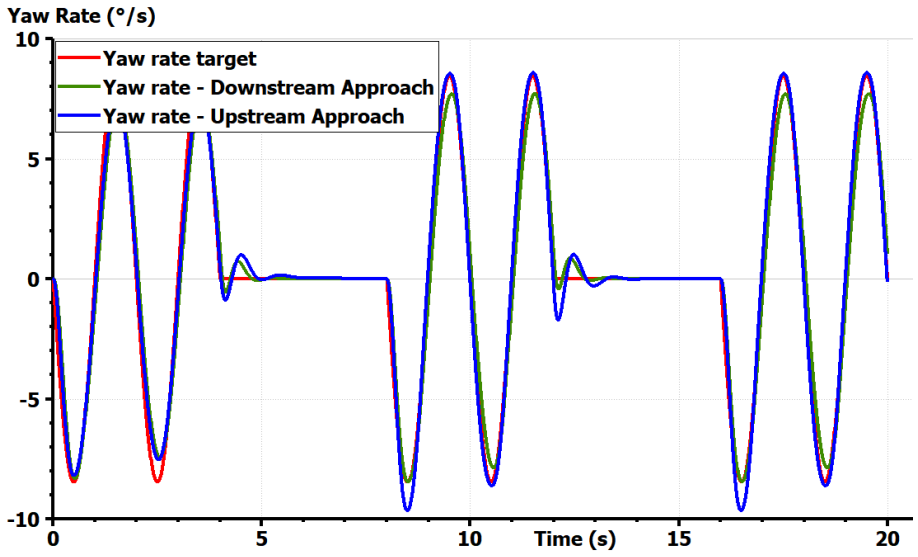

FIGURE 10.25: Yaw rate control comparison - ARS failure.

Here, unlike the upstream approach, the yaw rate response in a downstream approach start loosing its precision at the second set of the slalom maneuver. The brake torques allocation differs from one approach to another (Figure 10.26 and 10.27).

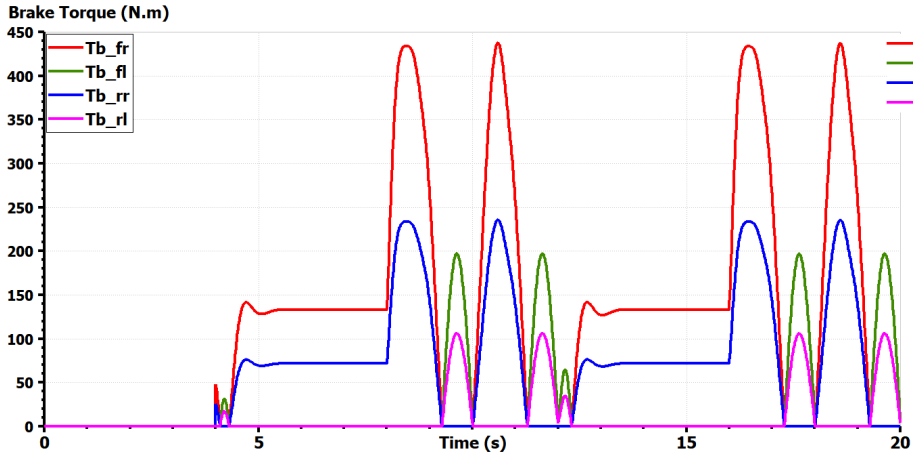

FIGURE 10.26: Brake torques in the downstream approach - ARS failure.

The difference of brake torques between the right and left wheels is less important in the upstream approach. In fact, even if a yaw rate should be generated by the VDC to counter the one generated by the ARS failure, in the slalom maneuver, the vertical load distribution varies. Exterior wheels with respect to the motion will always have a bigger potential. This criterion is taken into account in the CA by means of the weighting matrix. This weighting matrix reduce the weight when the vertical load increases, which favors the corresponding brake torque command. This demonstrates better brake torque allocation when the calculation is made upstream the subsystem.

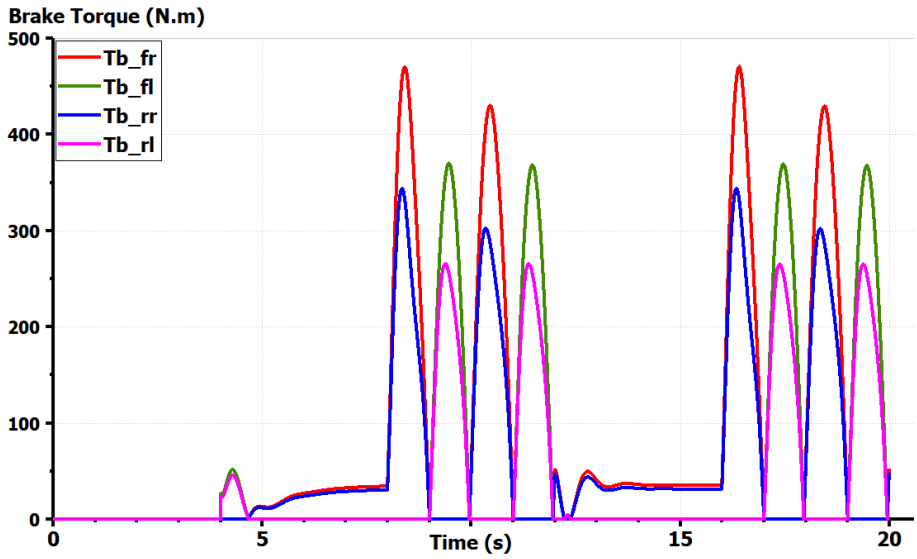

FIGURE 10.27: Brake torques in the upstream approach - ARS failure.

10.4.3 Co-simulation results

To give reliable results regarding online optimization-based C_α, control algorithms have been written in Matlab®, while a high-fidelity vehicle model equipped with an ARS and VDC systems has been developed in Amesim®. Simulink® is used as a bridge to co-simulate Matlab's high performance algorithms and Amesim's high fidelity vehicle model as Figure 10.28 shows. We will focus mainly on the ISO 3888-1:1999(E) standard, also known as the "VDA test". According to ISO 3888-1:1999(E), the desired speed during all the maneuver should be maintained to 80 km/h.

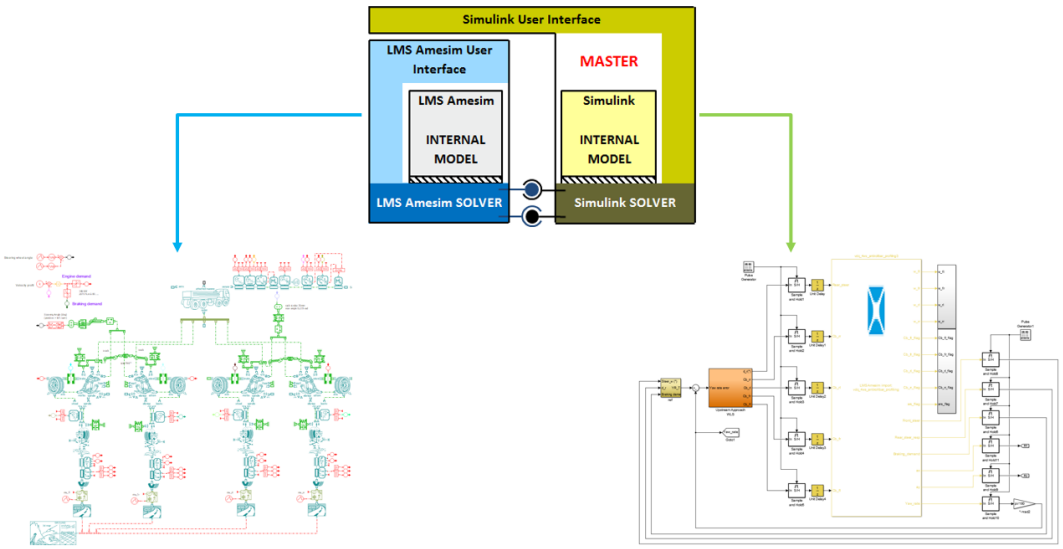

FIGURE 10.28: Co-simulation procedure.

In order to test the effectiveness of the repeated optimization method proposed in terms of safety, three tests are carried out. First, we compare of the classical CA

method without modifying the effectiveness matrix with the method proposed with the effectiveness matrix modification when there is no failure. Secondly, we compare the two methods when the ARS system fails in the middle of the lane-change maneuver. Finally, we compare the classical CA solvers when the failure occurs.

Comparison of methods when no failure - ISO 3888-1:1999(E)

ISO 3888-1:1999(E) is a normalized test aimed to verify vehicle stability through a severe double lane-change maneuver. Figure 10.29 illustrates this severe double lane-change maneuver which consists in rapidly driving a vehicle from its initial lane to another parallel lane, and returning to the initial lane, without exceeding lane boundaries. Track dimensions are mentioned in Table 10.1.

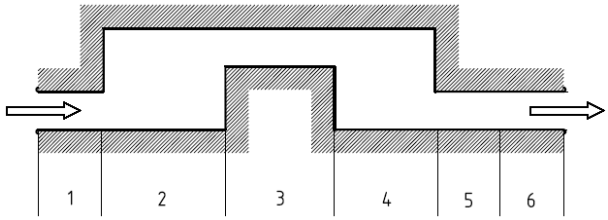

FIGURE 10.29: Double lane-change track.

TABLE 10.1: Double lane-change dimensions of sections

Section	Length	Lane offset	Width
1	15	-	1,1 $\times$ vehcile width $+$ 0.25
2	30	-	-
3	25	3.5	1,2 $\times$ vehcile width $+$ 0.25
4	25	-	-
5	15	-	1,3 $\times$ vehcile width $+$ 0.25
6	15	-	1,3 $\times$ vehcile width $+$ 0.25

In order to focus on the fault-tolerance method used only, the WLS algorithm is used for both methods at first. A discussion about algorithms is provided at the end of this subsection. Here, the VDA test is carried out normally without any failure to validate first the controller involved. Figure 10.30 shows the yaw rate response following both methods.

As expected, both methods exhibit the same performance as the value of the flags φ_i remains equal to 1 during all the maneuver. The effectiveness matrix for both methods is the same. This simulation serves actually to evaluate how each system is solicited. Figure 10.31 shows the ARS actuation and Figure 10.32 shows the VDC one.

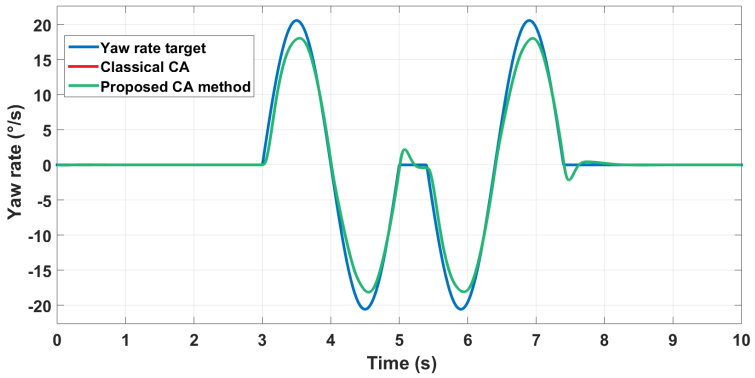

FIGURE 10.30: Comparison of the proposed method and the classical one when no failure.

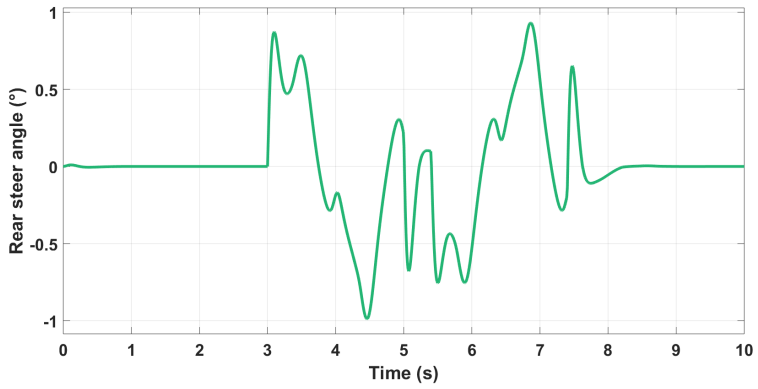

FIGURE 10.31: Rear steer angle when no failure.

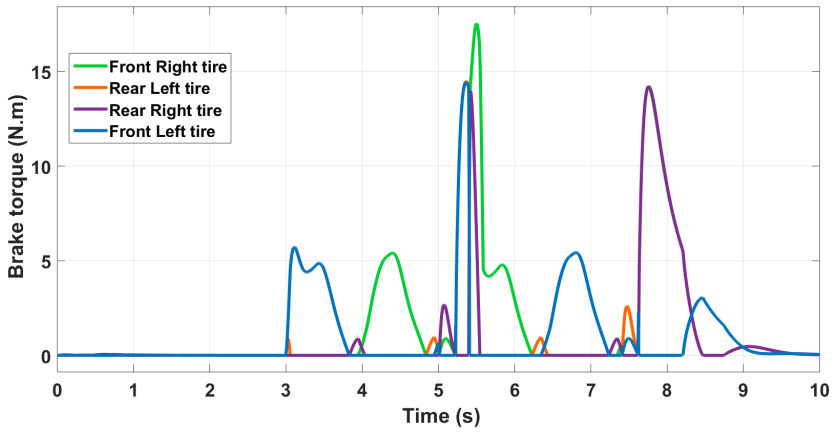

FIGURE 10.32: VDC activation when no failure.

The difference between right brakes and left ones can be ignored because of their low values. The ARS system is then automatically prioritized. This could have been predicted as the yaw moment generated by the ARS system is related to the distance between the rear axle and the vehicle's CoG: l_r, which is bigger than the half value of the vehicle's track t to what the VDC system is related. The ARS system

is more effective than the VDC system. Moreover, the CA algorithm exhibit only few iterations to achieve the optimum as Figure 10.33 shows.

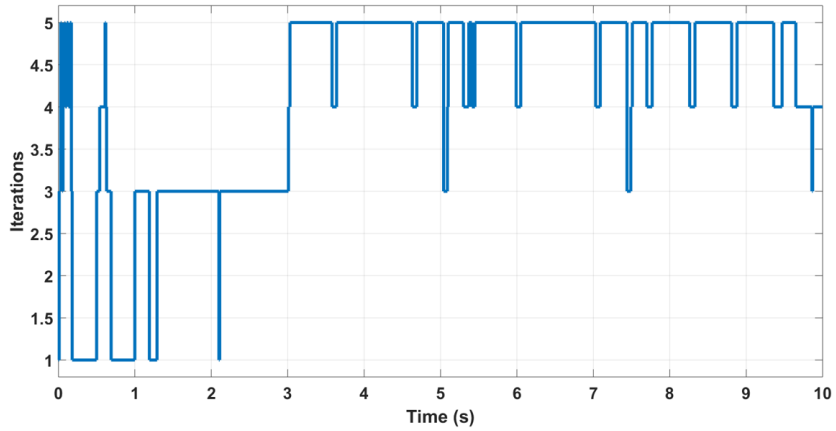

FIGURE 10.33: Number of iterations of the CA algorithm at each sampling time when no failure.

Comparison of methods when failure

As the ARS system is naturally prioritized in this maneuver, making the VDC fail will not give any pertinent result. Therefore, we choose to simulate the ARS failure at time $t = 5s$ as Figure 10.34 shows.

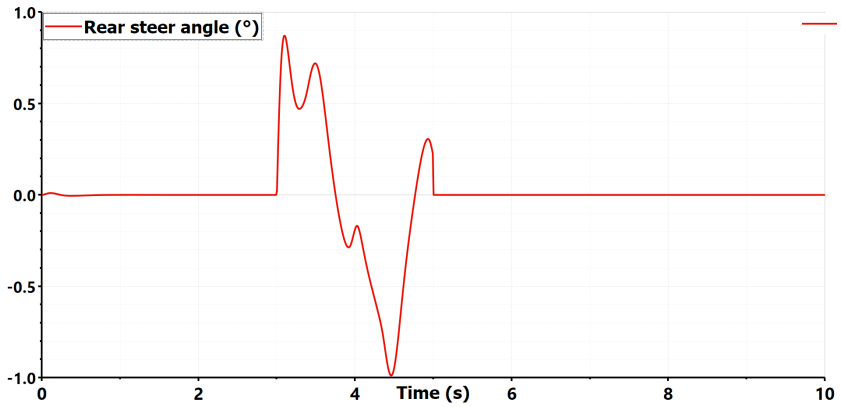

FIGURE 10.34: Rear steer angle when ARS fails.

Both methods are again compared using the WLS algorithm. The yaw rate response is illustrated in Figure 10.35. The proposed method gives nearly the exact same result as the previous case when no failure has occurred, making the failure unnoticeable to the driver. In contrast, the classical CA method loses its precision after the failure. This is due to the fact that in the proposed method the effectiveness matrix is updated to best represent the new situation, while this is ignored in classical methods. Consequently, in the proposed method, the VDC system is more solicited to complete the maneuver that the ARS system should have ensured. This makes both systems complementary as Figure 10.36 shows. In the classical method, the VDC is poorly utilized only because a large yaw rate error is sensed. Here, a slightly

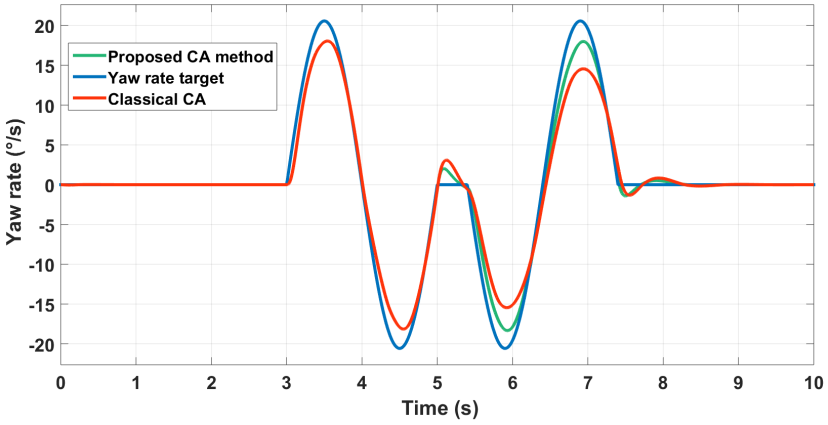

FIGURE 10.35: Comparison of the proposed method and the classical one when ARS fails.

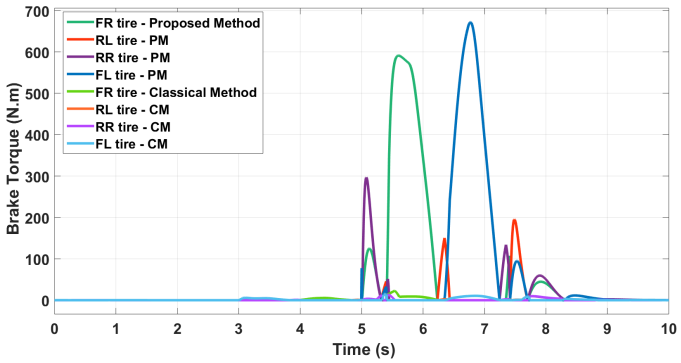

FIGURE 10.36: Comparison of the VDC activation in the proposed method and the classical one when the ARS fails.

higher number of iterations is perceived at the moment of the failure but remains low enough (Figure 10.37).

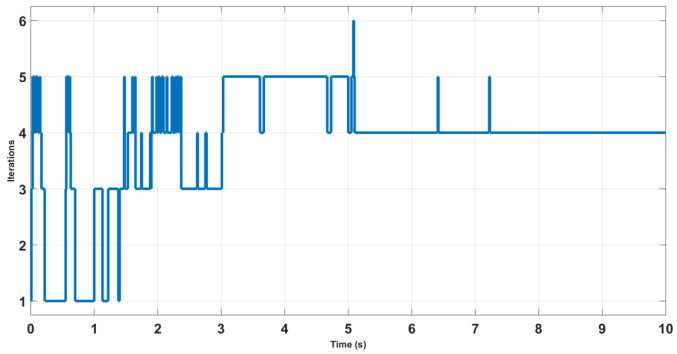

FIGURE 10.37: Number of iterations of the CA algorithm when there is a failure.

To summarize, Figure 10.38 shows the fault-tolerance ability of the control logic step by step in this particular maneuver.

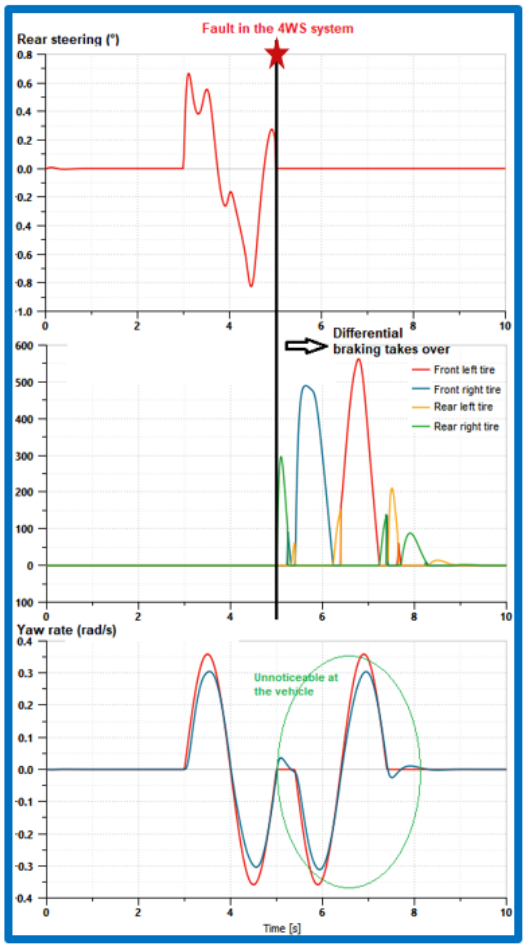

FIGURE 10.38: Fault-tolerance feature of the control logic.

Comparison of CA solvers

Other algorithms are compared in order to justify the utilization of each one. The SLS algorithm, The WLS algorithm, the IP algorithm, the FPI iteration, and the CGI are compared using a CORE i7 7^{th} generation machine in the failure case. Results in terms of the yaw rate response are shown in Figure 10.39.

SLS, WLS, IP, and FPI algorithms exhibit almost the same response. The CGI seems to be more precise. However, when zooming in Figure 10.39, we can notice that the CGI signal is vibrating. This is due to a non-continuous activation of the brake as Figure 10.40 shows. Redistributing Pseudo-Inverses could lead to tire wear more rapidly with respect to other algorithms. Imposing some rate limits may even give different results. In fact, the CGI requires only a finite number of iterations but does not guarantee that the optimal solution is found (Bordignon, 1996).

Regarding other algorithms, simulation time may be used to select the best algorithm for real-time maneuvers. Tic/toc commands have been used for comparison purposes only. The SLS algorithm simulation completed in 175s, WLS in 90s, IP in 243s, FPI in 75s, and CGI in 110s. The WLS and FPI algorithms seems to be the fastest thanks to their non-sequential formulation. The plus of the WLS algorithm is that it gives the option of easily taking into account the multi-objectives problems. This makes the WLS algorithm more attractive especially for problems related to qualitative objectives.

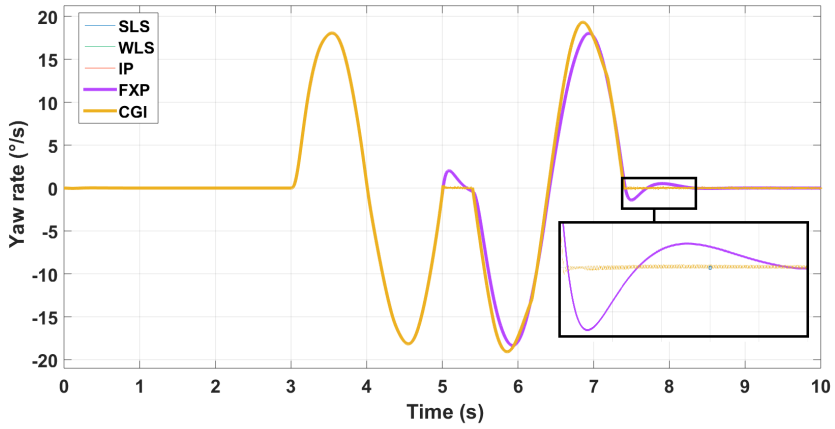

FIGURE 10.39: Comparison of CA algorithms one when ARS fails.

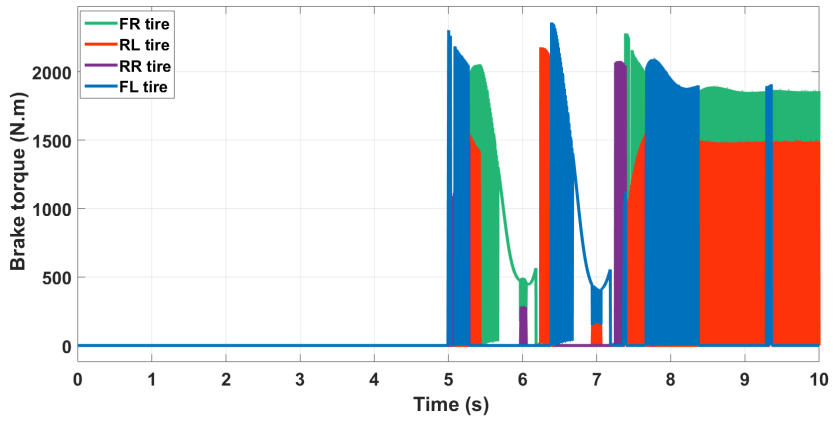

FIGURE 10.40: VDC activation using CGI algorithm when ARS fails.

Multi-behavioral CA

Here we test the ability of our approach to solve multiple objectives by introducing the secondary objective of accelerations tuning. A real experiment on a French road has been conducted by the Group Renault to test only vehicle dynamics. We use the steering wheel angle, the acceleration pedal, and the brake pedal inputs registered to generate longitudinal speed and yaw rate targets and then evaluate the influence that would have the proposed control logic on the vehicle motion. Driving modes are changed manually in Simulink® by means of a rotary switch.

Figure 10.41 and 10.42 show the variation of the longitudinal acceleration and the lateral one respectively when changing the driving modes. We can see that the CA algorithm allows different behaviors, and therefore different motion feelings using the same inputs.

This comes without significance variation of the yaw rate to stay in the stability envelope as Figure 10.43 shows. This is mainly due to the prioritization of the yaw rate control with respect to the longitudinal speed control. This is why a large variation in the longitudinal velocity is noticed in Figure 10.44. This was expected as our objective is to keep a good precision of the yaw rate and to minimize only the influence on the longitudinal speed. In other words, it is about finding a compromise

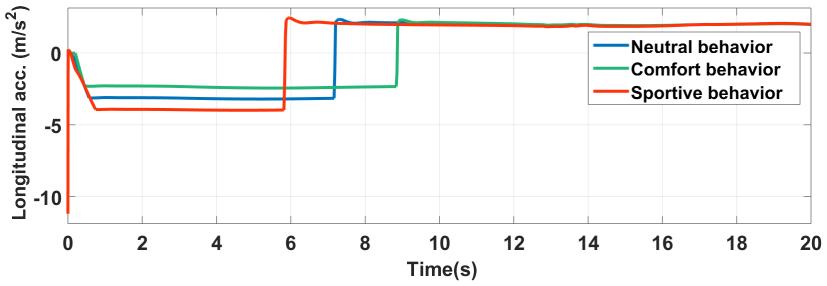

FIGURE 10.41: Longitudinal acceleration depending on driving behavior.

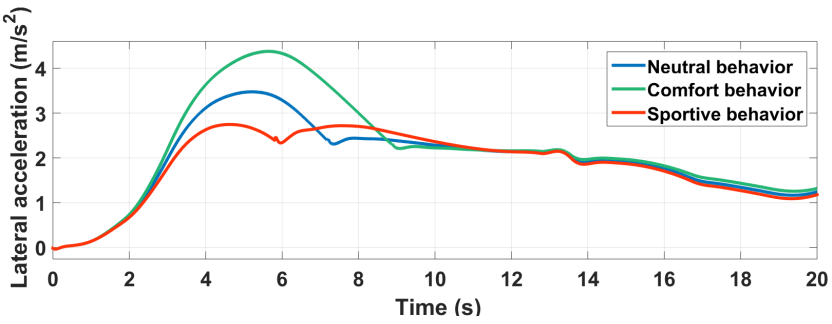

FIGURE 10.42: Lateral acceleration depending on driving behavior.

between a new objective, which is giving different motion feelings and precision by sacrificing the longitudinal speed accuracy.

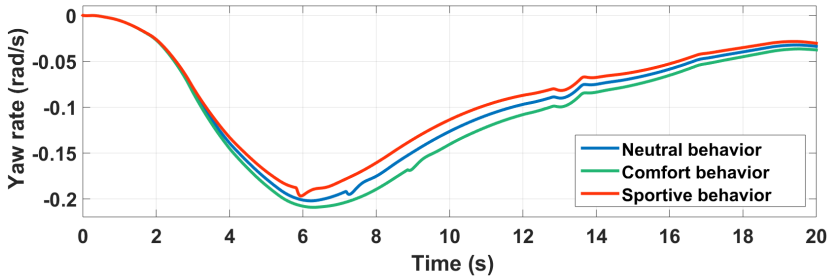

FIGURE 10.43: Vehicle's yaw rate depending on driving behavior.

This influence how chassis systems are solicited. Figure 10.45 shows the braking torque variation of the front-left tire for example from a driving mode to another. As expected, to give a more comfortable feeling, the use of brakes is minimized, while it is maximized in a more sportive behavior. The same remark holds for the rear steering angle as Figure 10.46 illustrates. In a sportive behavior, the rear axle is more agile. It is slowed to give a more comfortable feeling.

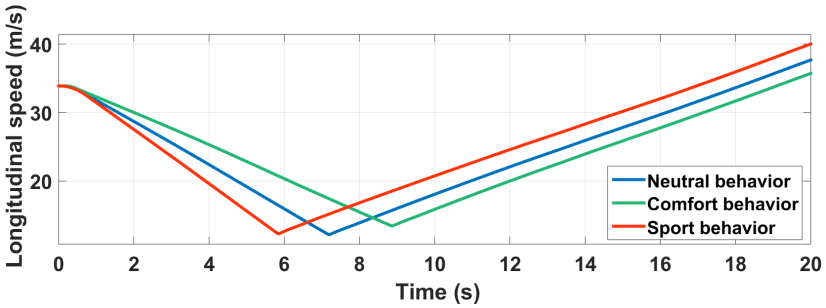

FIGURE 10.44: Longitudinal speed depending on driving behavior.

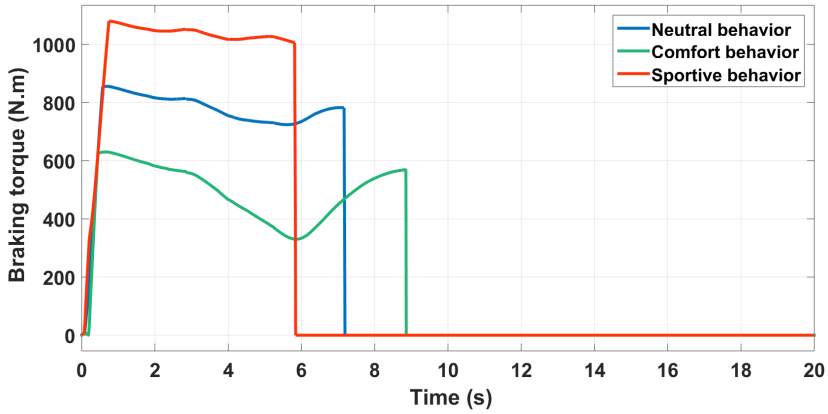

FIGURE 10.45: Front-left tire braking torque depending on driving behavior.

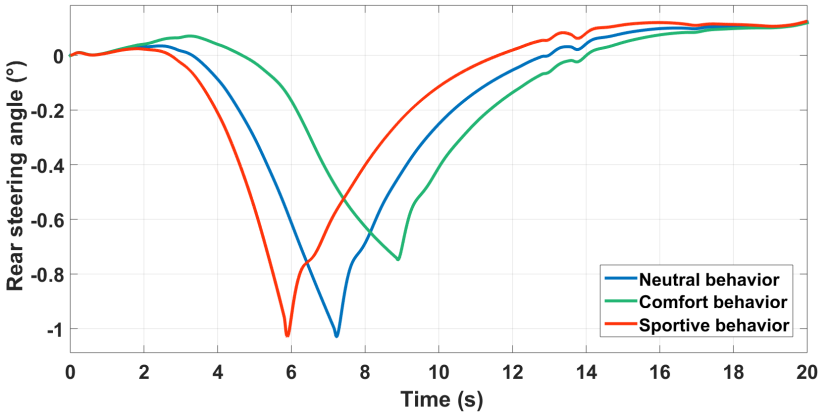

FIGURE 10.46: Rear steering angle depending on driving behavior.

It should be noted also that this variation respects the physical behavior of tires. Thanks to the linear tire model integrated with varying parameters, variation of the rear lateral tire stiffness variation due to brake activation has been estimated to adapt generation of the rear angle to the real potential of the tire (see Figure 10.47).

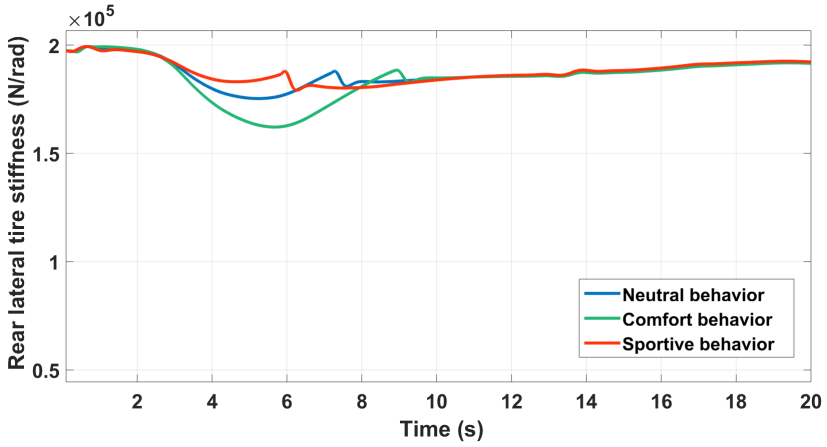

FIGURE 10.47: Rear lateral tire stiffness depending on driving behavior.

The rear steering angle sign could be even changed to steer in the same direction than the front angle, which would give a sort of a lateral transitional motion of the car as experienced drivers do when drifting. Weights of each objective could also be variable depending on the driving mode (including autonomous or not). Further investigations are expected in the future.

10.5 Conclusion

Two chassis systems coordination approaches have been compared in this chapter. The downstream approach uses rule-based algorithms to favor one system over another, which makes it relatively simple. The upstream approach uses optimization-based algorithms to find the best solution for a single or multi-objectives control problem. CA methods are designed especially to handle over-actuated systems. These methods are more complex with respect to rule-based algorithms. A vehicle equipped with an ARS system and a braking-based VDC system has been chosen to study chassis systems interactions as both influence yaw rate dynamics differently. Both architectures exhibit good yaw rate reference track. However, the upstream approach generates more realistic commands as a middle layer is added to take into account the tire dynamic couplings and saturation.

To achieve this, the new linear tire model with varying parameters has been used. This model relates tire forces to their corresponding slips by means of a varying stiffness through a linear equation. Stiffness varies with respect to vertical load, friction coefficient, and takes into account the combined slip. This reflects the true behavior of tires and therefore enables to take action before vehicle destabilization. Upstream approach enables then conflicts prevention rather than mitigation. This proves the potential of the upstream approach to handle more complex problems in a safer manner, which is mandatory for autonomous vehicles. Experimental results of this configuration are given in Chapter 13.

However, car manufacturers may still prefer the downstream approach due to its simplicity in this configuration. In Chapters 11 and 12 we focus on future potential scenarios with higher over-actuation. The goal is to show that with the same control architecture of the upstream approach, these scenarios can be handled proving that

this architecture is extensible to future vehicles where the downstream approach may fail.

10.6 Contributions

Our contributions can be summarized as follow:

1. Application of both downstream and upstream approaches to the ARS-VDC coordination case,
2. Comparison of both approaches in order to identify the advantages that the upstream approach can already provide in today's vehicles,
3. Development of a co-simulation procedure of Matlab/Simulink® Amesim® in order to benefit from the numerical computation potential and flexibility of the first software and the high-fidelity vehicle models of the second one,
4. Comparison of CA algorithms in order to identify the most suitable one for real-time applications,
5. Development of a fault-tolerance strategy to make the integrated subsystems complementary and improve the vehicle's safety in an upstream approach,
6. Tuning of CA algorithms in order to provide different motion feelings.

A journal paper and a conference paper have been published to provide a comprehensive comparison of both approaches in this coordination case:

- M. Kissai, B. Monsuez, A. Tapus, and D. Martinez, "Control Allocation of Active Rear Steering and Vehicle Dynamics Control Using a New Tire Model," *International Journal of Mechanical Engineering and Robotics Research*, Vol. 7, No. 6, pp. 608-616, November 2018. DOI: 10.18178/ijmerr.7.6.608-616,
- M. Kissai, B. Monsuez, D. Martinez, X. Mouton and A. Tapus, "A Comprehensive Comparison of Chassis Systems Coordination Approaches," *2018 18th International Conference on Control, Automation and Systems (ICCAS)*, Daegwallyeong, 2018, pp. 351-356. URL: https://ieeexplore.ieee.org/document/8571569.

Fault-tolerance features and their importance for critical safety systems have been published in:

- M. Kissai, X. Mouton, B. Monsuez, D. Martinez and A. Tapus, "Complementary Chassis Systems for Ground Vehicles Safety," *2018 IEEE Conference on Control Technology and Applications (CCTA)*, Copenhagen, 2018, pp. 179-186. DOI: 10.1109/CCTA.2018.8511622.

The tuning of CA algorithms in order to generate different motion feelings and its relevance for autonomous vehicles have been published in:

- M. Kissai, X. Mouton, B. Monsuez, D. Martinez and A. Tapus, "Multi-Behavioural Control Allocation for Over-Actuated Vehicles," *the 14th International Symposium on Advanced Vehicle Control, AVEC'18*, Beijing, 2018.

11 Case of ARS-VDC-RTV Coordination

In the previous chapter, both the downstream and upstream approaches have been developed and compared. The upstream approach presents more potential to deal with more complicated scenarios. To consolidate this claim, this chapter focuses on the ability of the upstream approach to coordinate more than two chassis systems. We chose to add a RTV system as this configuration represents one of the future prototypes of the Group Renault.

In this chapter, the vehicle is equipped by an ARS, a braking-based VDC, and two rear in-wheel electric motors for RTV. The same modeling procedure adopted in the preceding upstream approach is applied again here. We will focus in this chapter on the potential of CA algorithms.

11.1 Vehicle Motion Control

The multi-layered architecture described in Figure 11.1 is again chosen to handle each complication apart. The motion of the vehicle's CoG can be ensured by a high-level robust controller. The generalized efforts required to move the vehicle can be distributed in an optimal manner via optimization-based CA strategies to the four tires. These tire forces can be then transformed in actuators commands and activate the system concerned avoiding any internal conflicts.

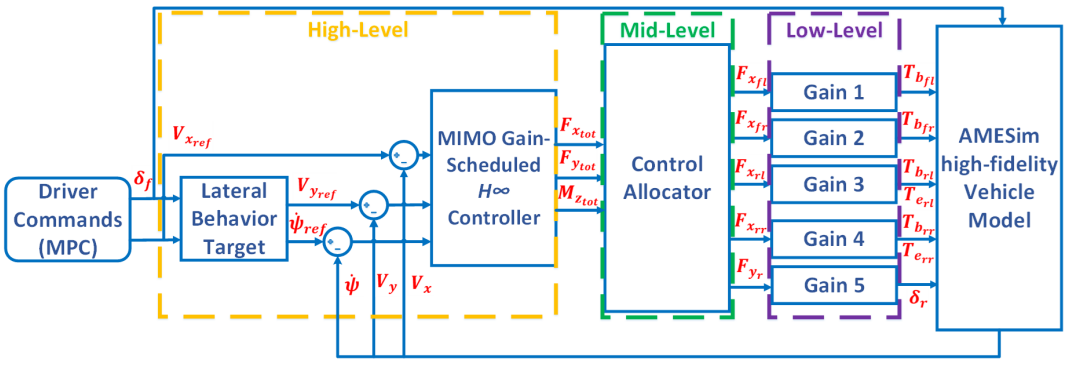

FIGURE 11.1: Vehicle motion multi-layered control architecture.

11.1.1 High-Level Control

The objective here is to calculate the required forces at the vehicle's CoG in order to track the desired velocities. The dynamics at this point are characterized by inertial parameters as the mass and moment of inertia. These parameters are subject to several uncertainties (Chebly, Talj, and Charara, 2017) which require a certain

degree of robustness. Moreover, vehicle motion states are coupled (Soltani, 2014). A MIMO controller is needed to take into accounts the different couplings. As the vehicle is equipped by an ARS, VDC, and RTV, and no access is permitted to active suspensions, only the plane vehicle model is considered at the high-level layer. The importance of vertical dynamics are rather emphasized in the vehicle states estimation. The vehicle high-level model derived from the global vehicle model developed in Chapter 5 is therefore:

$$\begin{cases} \begin{bmatrix} \dot{V}_x \\ \dot{V}_y \\ \ddot{\psi} \end{bmatrix} = \begin{bmatrix} 0 & 0 & V_y \\ 0 & 0 & -V_x \\ 0 & 0 & 0 \end{bmatrix} \begin{bmatrix} V_x \\ V_y \\ \dot{\psi} \end{bmatrix} + \begin{bmatrix} \frac{1}{M} & 0 & 0 \\ 0 & \frac{1}{M} & 0 \\ 0 & 0 & \frac{1}{I_z} \end{bmatrix} \begin{bmatrix} F_{x_{tot}} \\ F_{y_{tot}} \\ M_{z_{tot}} \end{bmatrix} & (11.1) \\ \begin{bmatrix} V_x \\ V_y \\ \dot{\psi} \end{bmatrix} = \begin{bmatrix} 1 & 0 & 0 \\ 0 & 1 & 0 \\ 0 & 0 & 1 \end{bmatrix} \begin{bmatrix} V_x \\ V_y \\ \dot{\psi} \end{bmatrix} & (11.2) \end{cases}$$

As it can be seen, the model is quasi-linear with varying parameters. Effects of the off-diagonal terms should be studied before determining the high-level controller nature. To study the dynamic couplings using classical methods, we first linearize the vehicle model. This is usually done by employing a Taylor series expansion around a nominal system trajectory representing the operating points (Soltani, 2014). Using the Jacobean matrix, the model becomes then:

$$\begin{bmatrix} \dot{V}_x \\ \dot{V}_y \\ \ddot{\psi} \end{bmatrix} = \begin{bmatrix} 0 & \dot{\psi}_e & V_{y_e} \\ -\dot{\psi}_e & 0 & -V_{x_e} \\ 0 & 0 & 0 \end{bmatrix} \begin{bmatrix} V_x \\ V_y \\ \dot{\psi} \end{bmatrix} + \begin{bmatrix} \frac{1}{M} & 0 & 0 \\ 0 & \frac{1}{M} & 0 \\ 0 & 0 & \frac{1}{I_{zz}} \end{bmatrix} \begin{bmatrix} F_{x_{tot}} \\ F_{y_{tot}} \\ M_{z_{tot}} \end{bmatrix} \quad (11.3)$$

Where V_{x_e}, V_{y_e}, and $\dot{\psi}_e$ are the longitudinal velocity, lateral velocity, and yaw rate at the selected stable operating point respectively. Two pre-studies are carried out before moving to the robust control design: the RGA, and Bode diagrams.

The RGA

Here, we aim to quantify interactions between inputs and outputs of a MIMO system. The most commonly used technique is the *RGA* developed by Bristol (Bristol, 1966). It helps the controller designer to decide a suitable input/output pairing for the MIMO system, and also gives few hints on pairings to avoid. Using the definition if the RGA in Chapter 8, we can see that this latter depends on the considered frequency. Therefore, it should be calculated at the crossover frequency chosen by the designer. Discussion about the frequency is provided after the Bode diagrams study. Rules are simple: prefer pairings so that Λ_{ij} is close to 1, and avoid pairings with negative Λ_{ij}. In our case, we use vehicle parameters of a Renault Talisman[1] to first generate a global transfer matrix, and then calculate its RGA. Let $\mathbf{G}$ represent the studied model.

[1] Parameters provided by the Group Renault itself.

For a crossover frequency of 1Hz (or 2πrad/s), we obtain the following matrix:

$$\boldsymbol{\Lambda}\left(\boldsymbol{G}\left(\boldsymbol{i2\pi}\right)\right) = \begin{bmatrix} 1 & 0 & 0 \\ 0 & 1 & 0 \\ 0 & 0 & 1 \end{bmatrix} \tag{11.4}$$

Which means that the system can be decoupled for a crossover frequency of 1Hz by favoring diagonal pairings. However, for low frequencies, for example 10^{-2}rad/s, we find:

$$\boldsymbol{\Lambda}\left(\boldsymbol{G}\left(\boldsymbol{i2\pi}\right)\right) = \begin{bmatrix} 0.05 & 0.95 & 0 \\ 0.95 & 0.05 & 0 \\ 0 & 0 & 1 \end{bmatrix} \tag{11.5}$$

Which means that off-diagonal terms should be prioritized for both longitudinal and lateral velocities. Another study in the frequency domain should be then carried out.

Bode Diagrams

To study the importance of frequency for dynamic couplings, we plot bode diagrams corresponding to the linearized model (11.3). Figures 11.2,11.3,11.4 show Bode diagrams for the longitudinal velocity, the lateral velocity, and the yaw rate respectively.

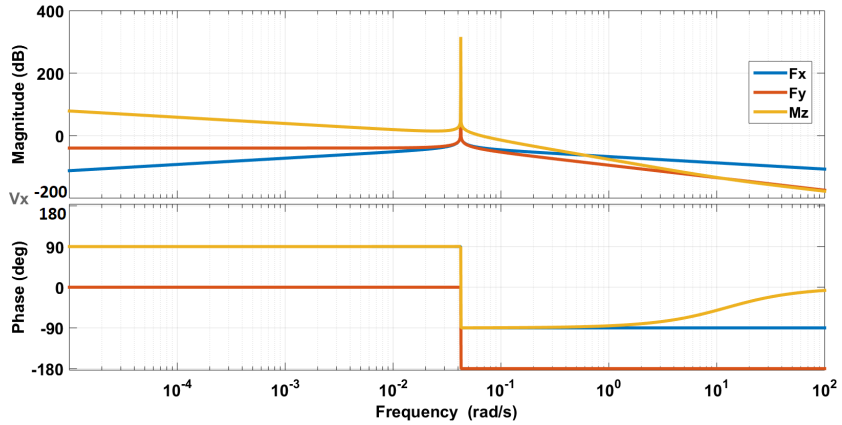

FIGURE 11.2: Bode diagrams for the longitudinal velocity.

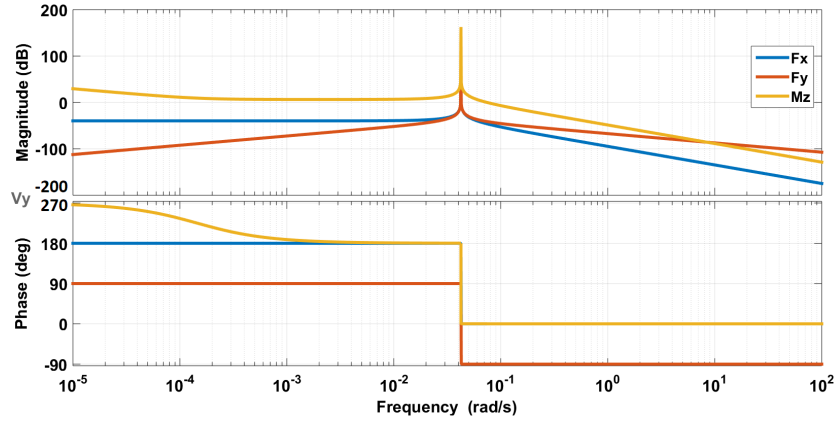

FIGURE 11.3: Bode diagrams for the lateral velocity.

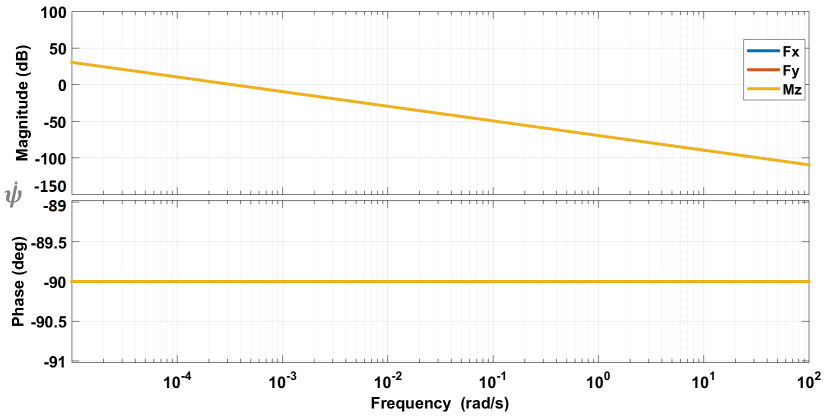

FIGURE 11.4: Bode diagrams for the yaw rate.

Bode diagrams confirm the RGA study. For frequencies higher than 10rad/s, the influence of $F_{x_{tot}}$ on V_x and $F_{y_{tot}}$ on V_y are preponderant with respect to other inputs. The inverse is observed for low frequencies. The yaw rate can be decoupled for both low and high frequencies. This imposes additional requirement for the high-level controller. In addition of performance and stability, a decoupled controller is preferred for easy tuning. In that case, the crossover frequency should be higher than 10rad/s.

Controller Design

As we discussed earlier, several robust techniques exist, e.g. the SMC that got recently a lot of attention (Yim, S., 2015),(Feng et al., 2014),(Zhao, Li, and Qu, 2014). This technique however still suffers from several problems as chattering. An optimal design would be preferable. In this context, $\mathcal{H}_\infty$ based design presents several advantages. This technique allows the designer to express explicitly system uncertainties. $\mathcal{H}_\infty$ drawbacks could be overcome, on one hand, by a different design procedure as it would be shown, and on the other hand, by adding a gain scheduling characteristic.

- **Fixed-structure $\mathcal{H}_\infty$ synthesis**

  The main drawback in an $\mathcal{H}_\infty$ control design is the high order of the resulting controller. The order of the controller resulting is equal to the number of states in the plant plus the number of states in the requirements weights plus twice the number of states in the feedthrough matrix (Skogestad and Postlethwaite, 2005). Here a different methodology is adopted. In the conventional method (Scorletti and Fromion, 2009), we first express an augmented plan taking into account tracking errors, control inputs, reference signals, external forces and noises. MIMO performance objectives are then formulated, and weighting functions are defined according to these objectives and added to the augmented system in order to enforce the controller to respect all the objectives. Dynamic or parametric uncertainties can also be added to the augmented plant in order to generate a valid controller to a set of systems and not only the nominal system. This of course enhance the controller robustness, but could however lead to the conservatism of the controller performances. A too big augmented plant could lead to a too high-order controller, and too many objectives to fulfill could lead to performance conservatism.

Therefore here, first we by-pass the augmented plant step and we keep only the system (11.3), and second, we do not express explicitly the uncertainties. Parameters like tire stiffness are highly nonlinear, and it is hard to define a range of variation of such parameters without penalizing the controller performance. This will rather be managed by gain scheduling for vehicle parameters, and adaptive CA for tire parameters using the new LPV tire model.

Nevertheless, we add a new requirement to the control design problem, which is the fixed-structure of the controller. An additional effort from the control designer is required. The plant should be studied before choosing between coupled or decoupled control, PID or PI or phase-lag structure, and so on. This is the goal of the pre-study presented before. According to Figure 11.2,11.3,11.4, a diagonal controller can be chosen as long as the imposed crossover frequency is higher than 10rad/s. Moreover, we choose the PI structure for each variable due their integral characteristic at higher frequencies. Six tunable parameters are then chosen in the control design problem. The optimal design algorithm is operated using Matlab®. Both methods can be tested. The conventional method is ensured by the Matlab function "*hinfsyn*" and the fixed-structure method by the function "*hinfstruct*". In this latter, to mitigate the risk of local minima, one could run several optimizations started from randomized initial values of tunable parameters. For more details, see (Apkarian and Noll, 2006).

Regarding performance weighting functions, closed loop shaping is used for defining control design requirements as in (Doumiati et al., 2013). Two objectives are selected: tracking performance, and commands moderation. For tracking performance, we choose a steady-state offset less than 1%, a closed-loop bandwidth higher than 10Hz, and an amplification of high-frequency noise less than a factor 2, which give the weighting function:

$$W_{perf} = \frac{1}{2}\frac{\frac{s}{2\pi 10} + 2}{\frac{s}{2\pi 10} + 0.01} \tag{11.6}$$

Regarding commands moderation, we use a static gain representing the inverse of the maximum effort, which gives:

$$W_{act} = \frac{1}{1.2Mg} \tag{11.7}$$

Here we suppose that the maximum friction coefficient is equal to 1.2. The optimization algorithm gives the minimum $\mathcal{H}_\infty$ norm $\gamma = 1.14$ which proves that the different constraints are respected and the high-level controller is stable.

- **Gain-scheduled $\mathcal{H}_\infty$**

  One weakness in the preceding design is the dependency on the operating points used to linearize the plant model. For different operating points, different controller parameters values are generated, which influence the controller performance. A proper way to proceed would be to consider different stable operating points and make the controller parameters change with respect to these operating points. This is called scheduling. This consists in considering the nonlinearities in a system as varying parameters. Different linear

controllers are designed for each value of the varying parameters. The controller parameters are after automatically adjusted as a function of the varying parameters. In our case, the model (11.3) is again used. The difference is that V_{x_e}, V_{y_e}, and $\dot{\psi}_e$ are now considered as varying parameters. As these parameters are also state variables, the system is now quasi-linear with varying parameters, which is more challenging (Rugh and Shamma, 2000).

The same performances cited in the previous paragraph are pursued for each set of scheduling parameters. The same $\mathcal{H}_\infty$ solver also is used for controller robustness. Three-dimensional lookup tables are then generated for each controller parameter. A gain-scheduled $\mathcal{H}_\infty$ controller is then used as in (Doumiati et al., 2013) for example. The main difference in the control procedure is the chosen scheduling variables. In (Doumiati et al., 2013), a stability index is used to coordinate the subsystems. Here, scheduling is used for dynamic couplings management. Coordination is ensured by optimization-based CA techniques.

11.1.2 Middle-Level Control

The three chassis systems, namely the ARS, VDC, and RTV, can influence the yaw rate. The VDC can decelerate the vehicle as it is brake-based, while the RTV can accelerate the vehicle and so on. This middle layer aims to coordinate chassis systems in order to avoid conflicts and ensure the generation of the total forces calculated at the high-level layer. To do so, the total forces should be optimally distributed into the four tires to be able to activate the right system with the right amount of effort. As tires are solicited both longitudinally and laterally, the friction ellipse should be taken into account (Pacejka, 2005). This ellipse representing tires' potential is closely related to the friction coefficient and the vertical load as it was shown in Chapter 7, which makes these variables important to estimate. The C_α problem is to find the tire forces subject to the friction ellipse where:

$$\begin{bmatrix} F_{x_{tot}} \\ F_{y_{tot}} \\ M_{z_{tot}} \end{bmatrix} = \begin{bmatrix} \cos(\delta_f) & \cos(\delta_f) & \cos(\delta_r) & \cos(\delta_r) & -\sin(\delta_r) \\ \sin(\delta_f) & \sin(\delta_f) & \sin(\delta_r) & \sin(\delta_r) & \cos(\delta_r) \\ b_{3,1} & b_{3,2} & b_{3,3} & b_{3,4} & b_{3,5} \end{bmatrix} \begin{bmatrix} F_{x_{f,l}} \\ F_{x_{f,r}} \\ F_{x_{r,l}} \\ F_{x_{r,r}} \\ F_{y_r} \end{bmatrix} \tag{11.8}$$

Where:

- $b_{3,1} = l_f \sin(\delta_f) - \frac{t}{2}\cos(\delta_f)$,
- $b_{3,2} = l_f \sin(\delta_f) + \frac{t}{2}\cos(\delta_f)$,
- $b_{3,3} = -l_r \sin(\delta_r) - \frac{t}{2}\cos(\delta_r)$,
- $b_{3,4} = -l_r \sin(\delta_r) + \frac{t}{2}\cos(\delta_r)$,
- $b_{3,5} = -l_r \cos(\delta_r)$.

Here, $F_{x_{r,l}}$ and $F_{x_{r,r}}$ can be either positive or negative. If a negative value is needed, then the brakes are activated through the VDC, otherwise, the RTV is activated. Regarding the online solver, the WLS based on one stage ASA is used.

11.1.3 Low-Level Control

Once the forces are optimally distributed, tire forces should be transformed into actuators commands before being fed to any embedded system. Here, engine torques, brake torques, and the rear steering angle should be calculated. This layer represent the most inner loop. Hence, it should be the fastest one. In this work, rather than using additional dynamic controllers that can complicate the overall design, a static tire model has been preferred which is used as an interface between tire forces and actuators commands. The tire model should take into account the combined slip phenomenon, be precise enough in the controllable zone, and invertible. For these reasons, the Linear tire model with Parameter Varying (LPV) developed has been chosen again. The reader is kindly asked to refer to Chapter 6 for the vehicle model and Chapter 7 for the friction circle estimation.

11.2 Co-Simulation Results

11.2.1 Control Robustness

First, focus is put on the importance of crossover frequency. Then the improvement brought by gain scheduling is emphasized. Finally, we show the interest of controlling the lateral velocity. Again, the ISO 3888-1:1999(E) is used to validate the control algorithms.

Linear Time Invariant $\mathcal{H}_\infty$ controller

Here we compare a controller designed at 10Hz and another one designed at 10^{-1}Hz. The longitudinal speed is shown in Figure 11.5.

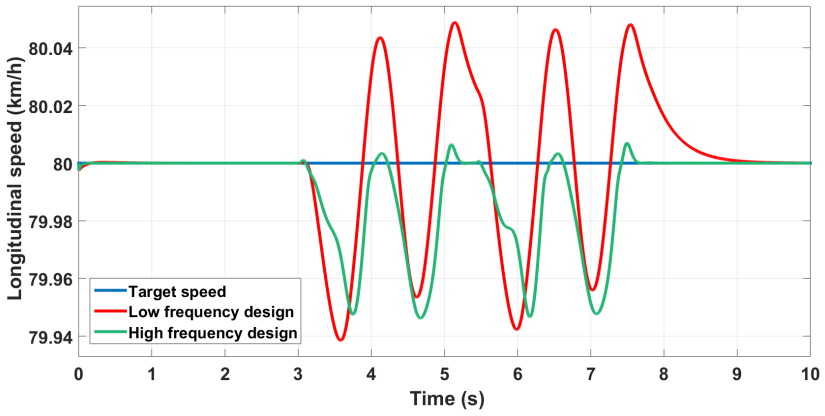

FIGURE 11.5: Longitudinal velocity control with different crossover frequencies.

The controller designed at a higher frequency is better as expected. A loss of precision and stability is noticed for the low-frequency designed controller especially in the yaw rate control (Figure 11.6).

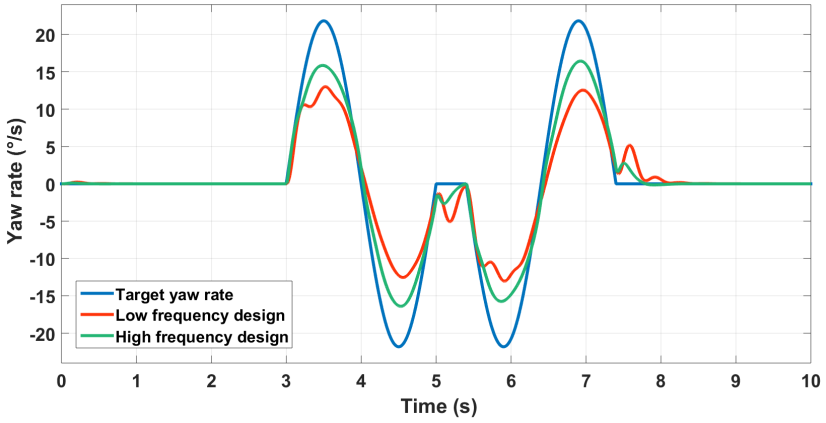

FIGURE 11.6: Yaw rate control with different crossover frequencies.

To test the robustness of the high-level control, we change the vehicle parameters regarding the mass and inertia by 20%, and wheelbase by 7%, and also tire parameters regarding the cornering stiffness by 40% in Amesim®, while we keep the same parameters of the high-frequency designed controller in Simulink®. We obtain the Figure 11.7. We can see that as long as only vehicle parameters are concerned,

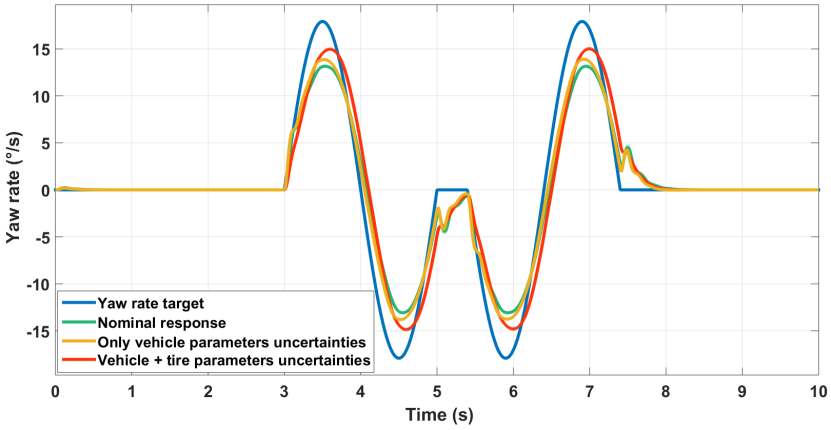

FIGURE 11.7: Different controllers for the yaw rate.

the vehicle exhibits almost the same performance regarding yaw rate tracking. When we considerably change the tire cornering stiffness, the uncertainties effects become noticeable. The vehicle behavior remains although acceptable. This was expected as the high-level controller determines the motion of the vehicle's center of gravity. Tire influence is managed rather by the CA and the low-level control. Robustness at these downstream layers should be improved.

We redo the maneuver with the same steering wheel input but with the reduced longitudinal speed of 20km/h. Results are plotted in Figure 11.8. The controller designed using operating points at a longitudinal speed of 20km/h exhibits better performance than a controller designed using operating points at a longitudinal speed of 40 km/h for example. This shows that the controller performances are closely related to the operating points used for linearization. We can conclude that no fixed operating points can be used for all cases, and no fixed architecture using the $\mathcal{H}_\infty$ only is satisfying.

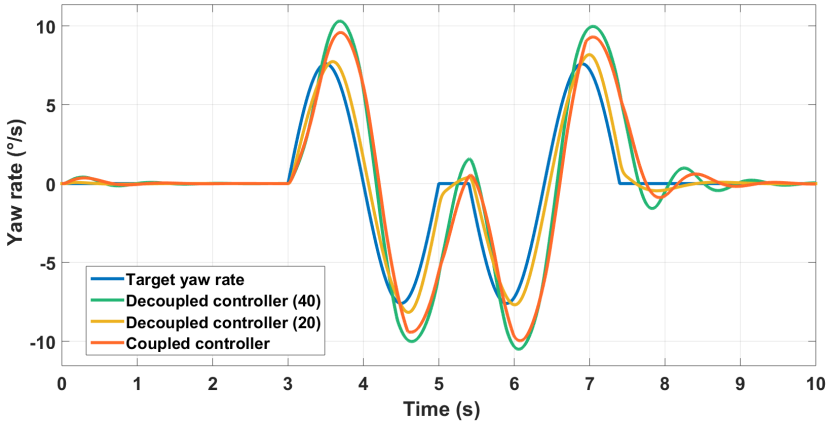

FIGURE 11.8: Different controllers for the yaw rate.

Gain-scheduled $\mathcal{H}_\infty$ controller

Here state-feedback used for closed-loop control and also as scheduling variable for controller parameters. The previous maneuver is repeated for various longitudinal speed values. Satisfying performances regarding the yaw rate control are ensured in different cases where in Figure 11.9 we show only the performance for two different speed values for more clarity.

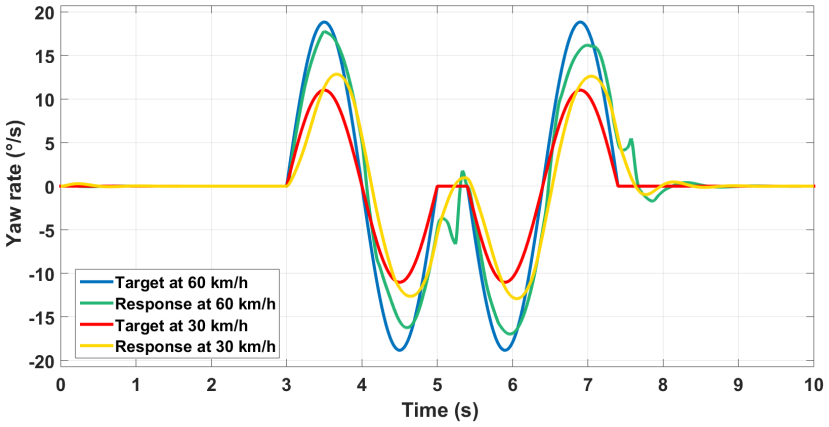

FIGURE 11.9: Various speed control using GS $\mathcal{H}_\infty$.

However, we can remark the odd behavior of the vehicle at the most difficult dynamics changes, especially when we change rapidly the direction. The behavior also changes from a speed value to another. This may be due to the fact that we only used lookup tables with a basic interpolation algorithm for the different parameters of the controller in the gain-scheduling framework. Another way to tackle the problem is to rather parameterize the controller gains as a polynomial function, and then tune the polynomial coefficients at the different operating points. The order of the polynomial can be increased to add more flexibility. The controller gains may be less accurate at the operating points compared to the lookup tables, but the switch from a behavior to another is softer.

Relevance of lateral velocity control

The Gain-Scheduled controller is used here. Two behaviors are compared. We first use the nominal bicycle model for a conventional behavior, and then minimize the yaw rate while keeping the same target for the lateral speed. The goal is to have a lateral transitional behavior that could be beneficial for obstacle avoidance and stability. The lateral velocity control is illustrated in Figure 11.10 and the yaw rate in Figure 11.11.

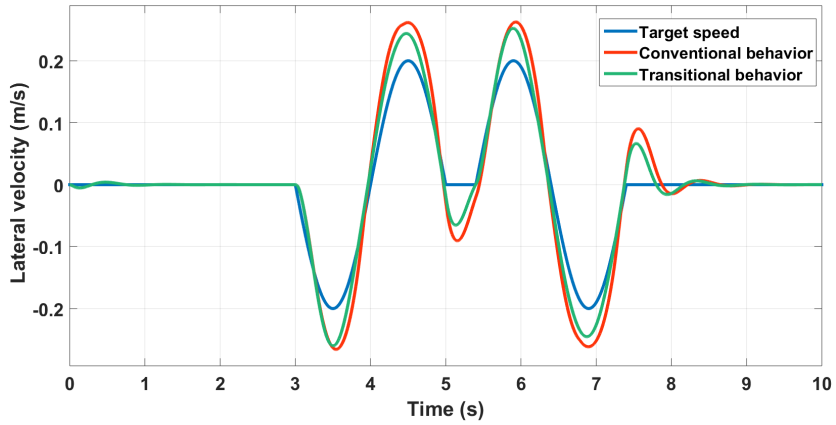

FIGURE 11.10: Lateral speed control using GS $\mathcal{H}_\infty$.

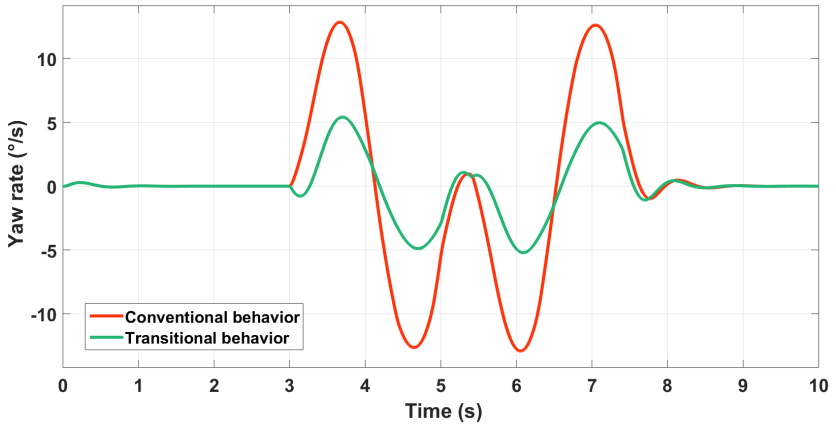

FIGURE 11.11: Yaw rate control using GS $\mathcal{H}_\infty$.

The controller is able to generate both behaviors by changing the reference. Figure 11.12 clarifies the difference between both behaviors.

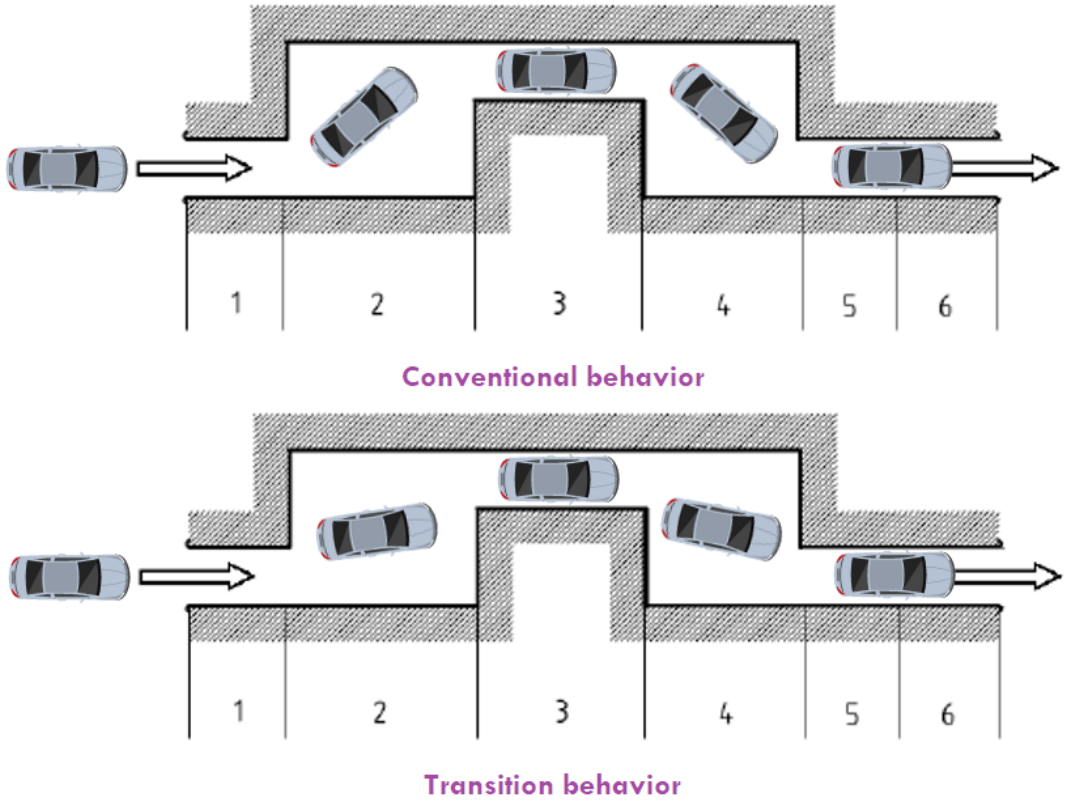

FIGURE 11.12: Illustration of the difference between motion behaviors.

It should be noted that for a vehicle equipped by rear steering control, stability envelopes should be redefined. In fact, in the literature, stability is more related to the vehicle side-slip angle and its time derivative which is called the $\beta - \dot{\beta}$ phase plane (Selby, 2003). Here, $\beta = \frac{V_y}{V_x}$ is the vehicle's side-slip angle. A high value of this ratio in conventional vehicles means a loss of control of the vehicle. However, for a 4-wheel steering vehicle, this can represent only a lateral transitional behavior.

11.2.2 Friction estimation and vehicle motion control

In the following, the friction coefficient estimation algorithm presented in Chapter 7 is used. Here, the interesting use-cases to evaluate manifest when vertical dynamics vary and when the friction changes. The double lane change maneuver (ISO 3888-1:1999(E) standard) is again selected to excite vertical dynamics in a severe maneuver. Moreover, to test the controller adaptability thanks to the estimation process, we force the friction to change in the middle of the maneuver. We reproduce the double lane-change maneuver, but we add a little twist: we change the friction coefficient from 1 to 0.4 at the second lane (at the time t=3.5s), and then we bring it back to 1 at the final lane. This is illustrated in Figure 11.13.

We compare performance of the control logic without friction change, with friction change and without vertical dynamics estimation, and then with taking into account vertical dynamics for better estimations. We get the results for the controlled variables when vertical dynamics are ignored, namely, the longitudinal speed (Figure 11.14), the lateral speed (Figure 11.15), and the yaw rate (Figure 11.16).

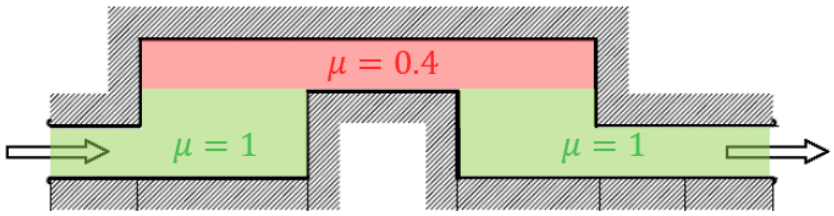

FIGURE 11.13: ISO 3888-1:1999(E) standard with friction variation.

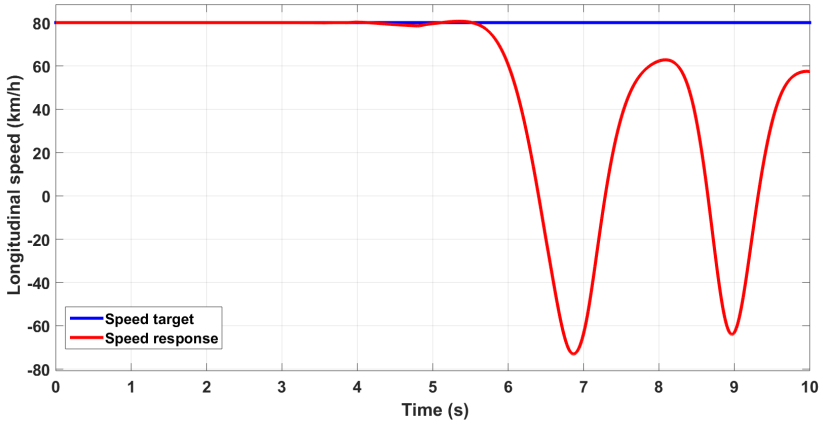

FIGURE 11.14: Longitudinal speed control when vertical dynamics are ignored.

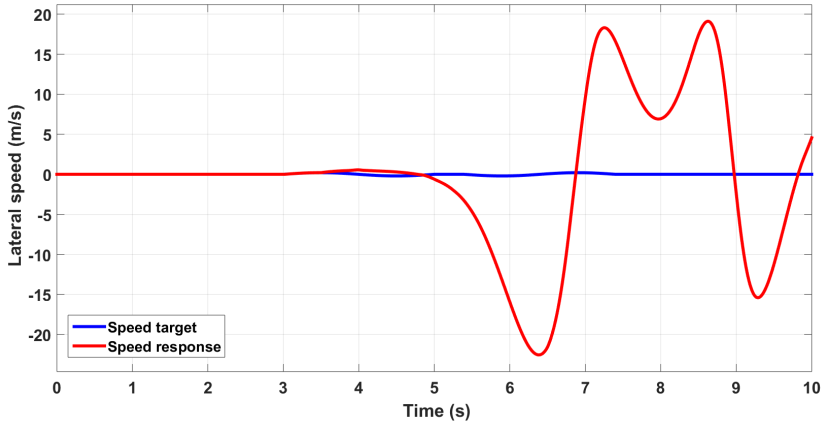

FIGURE 11.15: Lateral speed control when vertical dynamics are ignored.

We notice the complete loss of control of the vehicle as soon as we enter the low friction surface. We choose to represent results when taking into account vertical dynamics in a separate figure to show the effectiveness of the control logic by zooming into the signals (Figure 11.17-11.19).

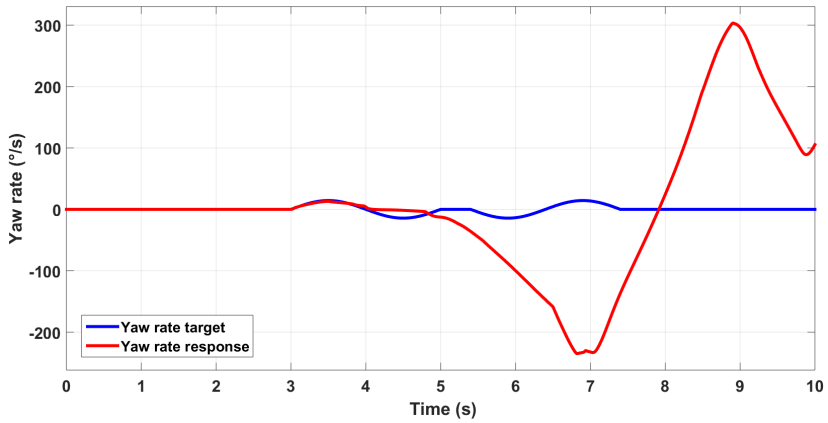

FIGURE 11.16: Yaw rate control when vertical dynamics are ignored.

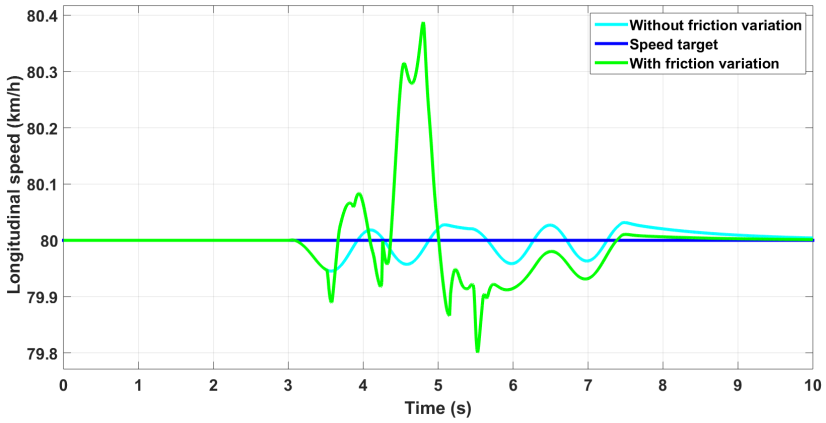

FIGURE 11.17: Longitudinal speed control when vertical dynamics are considered.

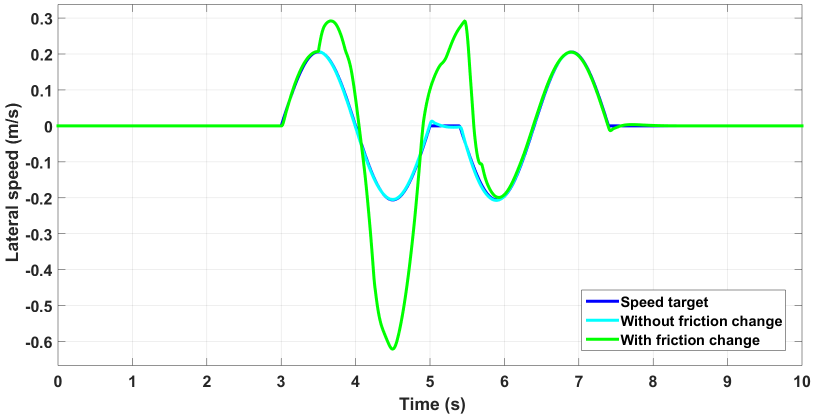

FIGURE 11.18: Lateral speed control when vertical dynamics are considered.

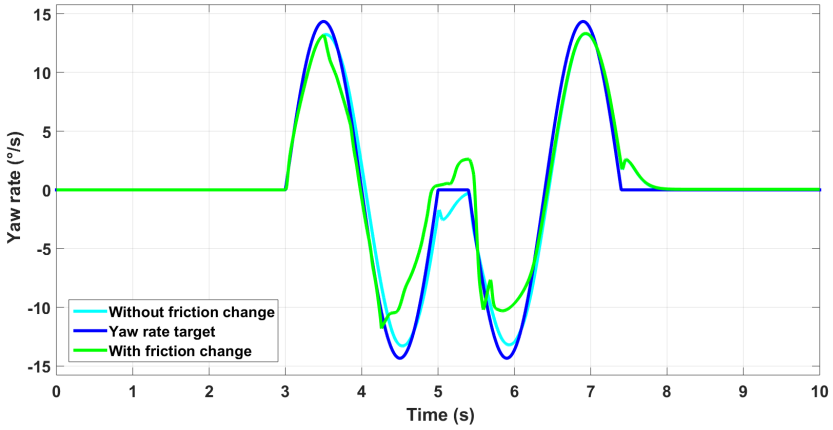

FIGURE 11.19: Yaw rate control when vertical dynamics are considered.

We can see then the ability of the control strategy to keep the vehicle controllable. The reason is simply that with a better estimation of the vehicle dynamics by taking into account the vertical ones, we can get a better approximation of the road friction (Figure 11.20). This enables updating the friction ellipse that represent the limits for the CA strategy. The different chassis systems can then produce commands within the limits of adhesion, and keep the vehicle stable.

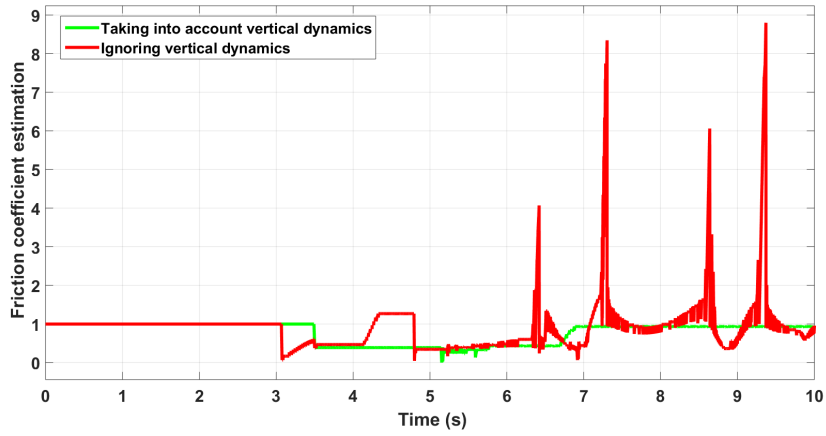

FIGURE 11.20: Importance of vertical dynamics for friction estimation.

It should be noted that vertical dynamics do not interfere in the calculation of the vertical loads only, but also in the slip calculations. These latter change even the shape of tire forces while the vertical loads influence their amplitude. Therefore, taking into account vertical dynamics in the vertical loads only is not sufficient.

11.3 Conclusion

We focused in this chapter on the ability of the upstream approach to handle higher over-actuation. Spotlight has been put on the design of the high-level controller also. In contrast with most researches that favor either complex robust controllers based

on simplified vehicle models or simplified controllers based on a decoupled complex vehicle, here a structural $\mathcal{H}_\infty$ synthesis has been carried out in a MIMO framework based on a four-wheeled vehicle model. CA techniques ensure optimal coordination between chassis systems.

Co-simulation results show better control performances for coupled motion variables. Not only the yaw rate is controlled while minimizing the influence on the longitudinal speed, but also the lateral velocity is separately controlled, providing additional motion behaviors. For good measure, robustness in a wider operation range is ensured thanks to the Gain-Scheduled $\mathcal{H}_\infty$ control. In addition, the scenario of complete change of friction has been handled thanks to a simplified estimation process. However, robustness has been ensured only for the control strategy and not the observation one. If the mass changes, a difference between the estimated acceleration and the measured one could be noticed. This may adapt the friction circle of the CA algorithm and reduce the vehicle's performance. Robustness of the estimation through more effective observation strategies should be investigated.

11.4 Contributions

The contributions of this chapter are summarized below:

1. The upstream approach has been applied to a more complex scenario where three integrated systems are involved: ARS-VDC-RTV. The goal is to show the potential and extensibility of this approach,

2. The global vehicle model has been simplified and decoupled in order to synthesize a high-level MIMO controller,

3. A new vehicle motion behavior is proposed by adding the control of the lateral velocity. Doing so to a vehicle equipped by the ARS system enable a transitional behavior of the car by reducing the vehicle's yaw rate and improve the vehicle's stability. This three contributions along with the global vehicle model have been published as mentioned in Chapter 5 in:

   M. Kissai, B. Monsuez, A. Tapus, X. Mouton, and D. Martinez, "Gain-Scheduled H_∞ for Vehicle High-Level Motion Control", in *Proceedings of the 6th International Conference on Control, Mechatronics and Automation (ICCMA 2018)*. ACM, Tokyo, Japan, pp. 97-104. DOI: https://doi.org/10.1145/3284516.3284544.

4. An extended version of the latter paper has been published in:

   Kissai, M.; Monsuez, B.; Mouton, X.; Martinez, D.; Tapus, A. "Adaptive Robust Vehicle Motion Control for Future Over-Actuated Vehicles". *Machines* 2019, 7, 26. DOI: https://doi.org/10.3390/machines7020026.

5. The friction estimation strategy has been applied and validated by co-simulation in a severe maneuver. This has been published in:

   M. Kissai, B. Monsuez, X. Mouton, D. Martinez and A. Tapus, "Importance of Vertical Dynamics for Accurate Modelling, Friction Estimation and Vehicle Motion Control," *2018 21st International Conference on Intelligent Transportation Systems (ITSC)*, Maui, HI, 2018, pp. 1370-1377.
   DOI: 10.1109/ITSC.2018.8569751.

12 Case of Autonomous Vehicles with EPAS-VDC-4WD-TV

We saw in previous chapters that optimization-based CA techniques offer additional attractive features. More advantages as reduction of energy consumption can be fulfilled (Chen and Wang, 2011), (Shyrokau and Wang, 2012), (Jing et al., 2017). This is particularly beneficial for electric vehicles. Having multiple ADAS or chassis systems can then offer supplementary possibilities. The vehicle motion behavior can be then modified in a way to fulfill multiple objectives.

For autonomous vehicles however, qualitative objectives could be required. When a driver has its hands off the steering wheel, if an unexpected motion is generated, he could be tempted to regain control of the vehicle. In case of a vehicle equipped with an EPAS system, this may present few risks for drivers' hands due to the important amount of steering wheel torque (Soltani, 2014). One way to prevent this, is to tune the vehicle motion in a way to generate expected motions like a human being would do. To the best of our knowledge, there exist only one method to tune the vehicle behavior, that is to act on motion references to be followed by the vehicle so the controllers impose different commands to actuators. Here, we also investigate the modification of the CA strategy so the commands are distributed differently. The first purpose of this chapter is to compare these two methods to highlight the advantages and drawbacks of each one. The goal is to give few insights about the ability of modern control techniques to provide additional degrees of freedom regarding motion feelings control. Investigations aiming to adapt these techniques to drivers' profiles are still needed with the help of experiments. The second objective is to show the relevance of adding supplementary integrated systems as one may say that only two integrated systems are sufficient. We particularly focus on the performance of the vehicle in severe situations on race tracks to validate the safety and performance of this over-actuated vehicle.

Here, a MPC provided by Simcenter Amesim® is used for trajectory tracking. Focus has been put more on vehicle motion control tuning. A Gain-Scheduled $\mathcal{H}_\infty$ controller has been selected as the high-level controller for its robustness and dynamic couplings management. Optimization-based CA methods are then used to distribute the commands into the different actuators taking into account tire potential. The vehicle considered in this paper is equipped with an EPAS system, an VDC, and a 4WD-TV. What we mean by 4WD-TV is that we can provide different engine torques to the four tires by means of four independent motor-wheels. The EPAS is mainly controlled by an MPC. The goal is to study interactions between systems and what a better coordination can bring to the vehicle motion control.

12.1 System Modeling

As no active suspensions are considered, again the four-wheeled planar vehicle model can be adopted. By simplifying the global vehicle model developed in Chapter

5, we can find the following state-representation:

$$\begin{cases} \begin{bmatrix} \dot{V}_x \\ \ddot{\psi} \end{bmatrix} = \begin{bmatrix} 0 & V_y \\ 0 & 0 \end{bmatrix} \begin{bmatrix} V_x \\ \dot{\psi} \end{bmatrix} + \begin{bmatrix} \frac{1}{M} & 0 \\ 0 & \frac{1}{I_z} \end{bmatrix} \begin{bmatrix} F_{x_{tot}} \\ M_{z_{tot}} \end{bmatrix} & (12.1) \\ \begin{bmatrix} V_x \\ \dot{\psi} \end{bmatrix} = \begin{bmatrix} 1 & 0 \\ 0 & 1 \end{bmatrix} \begin{bmatrix} V_x \\ \dot{\psi} \end{bmatrix} & (12.2) \end{cases}$$

With this time:

$$\begin{cases} F_{x_{tot}} = \left(F_{x_{fl}} + F_{x_{fr}}\right) \cos\left(\delta_f\right) + F_{x_{rl}} + F_{x_{rr}} & (12.3) \\ M_{z_{tot}} = \left(F_{x_{f,l}} + F_{x_{f,r}}\right) l_f \sin\left(\delta_f\right) + \left(F_{x_{f,r}} - F_{x_{f,l}}\right) \frac{t_r}{2} \cos\left(\delta_f\right) \\ \qquad\qquad + \left(F_{x_{r,r}} - F_{x_{r,l}}\right) \frac{t_r}{2} & (12.4) \end{cases}$$

Note that due to the lack of the ARS system, there is no intention to control the lateral velocity. V_y will be considered as a varying parameter. We again consider only controllable forces to distribute by the CA algorithm. The lateral force induced by the front steering is rather controlled by the MPC. Introducing this force also in the vehicle motion control induces request conflicts[1]. In addition, the new linear tire model with varying parameters is used again for tire forces and dynamic couplings.

12.2 Vehicle Motion Control

The vehicle considered is over-actuated. This presents additional opportunities as the vehicle's potential is extended, but presents at the same time several complexities regarding the control synthesis procedure. Typically, the torque vectoring increases the over-actuation. Again, by separating the vehicle's CoG motion control from the control distribution problem, we can both simplify the control synthesis and make the overall architecture extensible to additional chassis systems and ADAS. This is of a major import for future vehicles as their control architecture is not standardized yet, and should be therefore flexible enough. The control architecture adopted in this paper is illustrated in Figure 12.1.

The control architecture is divided into a high-level control to generate the required sum of forces and moments necessary to move the vehicle, a middle-level control is used to distribute optimally the commands into the four wheels, and a low-level control is used to transform the forces into torques to be generated by the different actuators.

In Figure 12.1, the front steering angle δ_f and the speed of reference V_{ref} is generated by means of a MPC provided by Amesim®. Details about the MPC controller fall beyond the scope of this thesis. We will focus more on the inner control process. The MPC controller can be considered as an autopilot or a driver following a trajectory for a more general discussion. Once δ_f and V_{ref} are generated, a yaw rate reference can be generated. Here again, we use the statical bicycle model to

[1] This case has been verified by simulation.

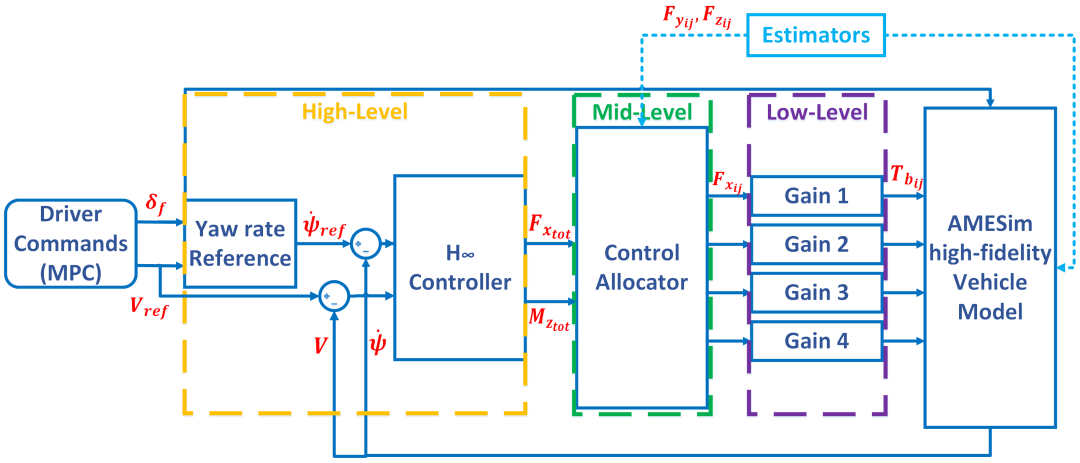

FIGURE 12.1: The global control architecture.

generate the yaw rate target:

$$\dot{\psi}_{ref} = \frac{V_x}{L + \frac{MV_x^2}{LC_{\alpha_f}C_{\alpha_r}}\left(C_{\alpha_r}l_r - C_{\alpha_f}l_f\right)}\delta_f \tag{12.5}$$

Note that in case of autonomous vehicles, the front steering angle should be generated by the controller and not the driver. Therefore, it should be located normally downstream the C_α layer. However, researches on trajectory control and dynamics control are today separated. One of our missions is to provide roadmap from today's vehicles to future vehicles. The method used here is a first step toward integrating advanced vehicle dynamics of over-actuated vehicles and the MPC used for trajectory control of autonomous vehicles.

12.2.1 High-Level Control

The objective of this layer is to generate the generalized forces and moments to be applied at the vehicle's CoG. Equations (12.1) and (12.2) are considered. The model can be then considered as linear with the varying parameter V_y. To take into account this variation, a gain scheduled controller is chosen with V_y as the scheduling variable. In fact, today's vehicles are equipped with an inertial measurement unit and a yaw rate sensor. Therefore, V_y can be estimated as shown in equation 7.13.

Moreover, as stated before, vehicle motion control faces also robustness issues related to parameter uncertainties. The control should stay valid whether there is only the driver in the vehicle or with other passengers, whether tires are brand new or not and so on. A robust controller is then needed. The $\mathcal{H}_\infty$ synthesis has been selected to be able to optimize the controller parameters. As this synthesis usually generate high order controllers (Skogestad and Postlethwaite, 2005), a common practice consists in reducing the controller in the frequency domain while keeping an acceptable level of robustness (Pita-Gil, 2011). Here again, the alternative methodology is adopted. As most industrials prefer PID controllers for implementation issues, we add the controller structure as a requirement in the $\mathcal{H}_\infty$ synthesis.

Equation (12.1) shows the existence of the varying parameter V_y. This introduces a non-linearity that could be overcome by a nonlinear controller as the SMC

or Gain-Scheduling. The SMC suffer from the chattering problem which makes it unsuitable for mechanical actuators (Zhao, Li, and Qu, 2014), and the Gain-Scheduling pass muster only for scheduling parameters that vary slowly (Johansen and Fossen, 2013). As we aim to control the vehicle also in a race mode, we have noticed fast variations of V_y by simulations which might destabilize the vehicle dynamics. Subsequently, here we only take into account the linearized nominal model at the operating point $V_{y_e} = 0$ to synthesize a simple $\mathcal{H}_\infty$ controller. To choose the suitable structure to be adopted, a pre-study of the plant is required. As we considered only $V_{y_e} = 0$, a decoupled controller can be chosen. Moreover, due to the integral characteristic of each control axis, a PI controller can be chosen at each axis. Four tunable parameters are then chosen in the optimization $\mathcal{H}_\infty$ problem.

Regarding performance weighting functions, closed loop shaping is used for defining control design requirements. Two objectives are selected: tracking performance, and commands moderation. For tracking performance, we choose a steady-state offset less than 1%, a closed-loop bandwidth higher than 1Hz, and an amplification of high-frequency noise less than a factor 3, which give the weighting function:

$$W_{perf} = \frac{1}{3}\frac{\frac{s}{2\pi}+3}{\frac{s}{2\pi}+0.01} \tag{12.6}$$

Regarding commands moderation, we use a static gain representing the inverse of the maximum effort, which gives:

$$W_{act} = \frac{1}{Mg} \tag{12.7}$$

Here we suppose that the maximum friction coefficient is equal to 1. The optimization algorithm gives the minimum $\mathcal{H}_\infty$ norm $\gamma = 1.16$ which proves that the different constraints are respected and the high-level controller is stable.

12.2.2 Middle-Level Control

The goal of middle-level control is to optimally distribute the generalized forces generated by the high-level control to ensure the execution of these forces. As long as an over-actuated system is concerned, multiple objectives can be fulfilled. This is very important for this study as several problems are aimed to be addressed regarding autonomous vehicles. Online optimization-based CA techniques are then selected to handle the forces distribution problem.

Several solvers can be used to solve a multi-objective problem. SLS uses a two stage ASA to handle two optimization problems (Harkegard, 2002). The WLS solves the bounded least squares problem using one stage ASA after few matrix transformations by means of different weights (Harkegard, 2002). We choose here the WLS for its flexibility to express multiple objectives, and for its relative rapidity due to its one stage formulation. The optimal solution is then:

$$\vec{\delta}_{opt} = arg \min_{\vec{\delta}_{min} \leq \vec{\delta} \leq \vec{\delta}_{max}} \sum_{l} \gamma_i \left\| \mathbf{W_i} \left(\mathbf{B_i}\vec{\delta} - \vec{v}_i \right) \right\|^2 \tag{12.8}$$

- $\vec{\delta}_{opt}$: optimal control vector,
- l : number of objectives,

- γ_i : weight of the i^{th} objective,
- $\mathbf{W_i}$: non-singular weighting matrices defining preferences of each axis,
- $\vec{v}_i$: desired vector of the i^{th} objective,
- $\mathbf{B_i}$: effectiveness matrix relating the control vector to the desired i^{th} objective.

Regarding the VDC-4WD-TV coordination:

$$\vec{\delta} = \begin{bmatrix} F_{x_{f,l}} \\ F_{x_{f,r}} \\ F_{x_{r,l}} \\ F_{x_{r,r}} \end{bmatrix} \tag{12.9}$$

$\vec{\delta}_{min}$ and $\vec{\delta}_{max}$ reflect tire limits with respect to the friction ellipse concept.

For the friction coefficient, the problem is more complex in case of autonomous vehicles. In fact, tires are the only effectors for ground vehicles. Their behavior changes with friction. Control logic would not be as effective as in the normal situation. The changes in friction should then be predicted to reconfigure the control algorithm and act differently on tire, and on the reference in order to follow feasible targets. The difficulty is that, using effect-based estimation methods, this coefficient can only be estimated when exceeding it (Villagra et al., 2011), as shown in Chapters 7 and 11. It could be then too late to control the vehicle afterwards. Data-based techniques could provide better solutions (Liu et al., 2017). Experimental tests showed promising results. These techniques should be further investigated. In this chapter, we suppose that the friction coefficient is known in advance. $\mathcal{H}_\infty$ synthesis has been chosen in order the generate a high-level robust controller and reduce the negative effects of this hypothesis.

The desired acceleration $\vec{v}_{des}$ in this case is:

$$\vec{v}_{des} = \begin{bmatrix} F_{x_{tot}} \\ M_{z_{tot}} \end{bmatrix} \tag{12.10}$$

The effectiveness matrix related to CA precision $\mathbf{B_{eff}}$ is:

$$\mathbf{B_{eff}} = \begin{bmatrix} \cos(\delta_f) & \cos(\delta_f) & 1 & 1 \\ b_{2,1} & b_{2,2} & -\frac{t_r}{2} & \frac{t_r}{2} \end{bmatrix} \tag{12.11}$$

where:

- $b_{2,1} = l_f \sin(\delta_f) - \frac{t_r}{2}\cos(\delta_f)$,
- $b_{2,2} = l_f \sin(\delta_f) + \frac{t_r}{2}\cos(\delta_f)$.

12.2.3 Low-Level Control

The low-level control corresponds to the most intern loop. Adopting a closed loop here leads to very high crossover frequencies. Moreover, the CA algorithm generates tire forces. Therefore, for a closed-loop low-level control, either we should be able to measure online tire forces, which is not the case in commercial vehicles, or we can use the inverse of the linear tire model with varying parameters as an interface between the two layers, and control the wheels' speed. For simplicity, and in

order to avoid adding any lag to the overall control logic, the following algorithm is adopted:

Algorithm 2 Torques calculation

Let $T_{d_{i,j_0}}$ $T_{b_{i,j_0}}$ be starting values
1: $T_{d_{i,j_0}} \leftarrow 0$
2: $T_{b_{i,j_0}} \leftarrow 0$
3: **if** $F_{x_{i,j}} > 0$ **then**
4: $\quad T_{d_{i,j}} \leftarrow R_{i,j} F_{x_{i,j}}$
5: $\quad T_{b_{i,j}} \leftarrow 0$
6: **else**
7: $\quad T_{d_{i,j}} \leftarrow 0$
8: $\quad T_{b_{i,j}} \leftarrow -R_{i,j} F_{x_{i,j}}$
9: **end if**

With $T_{d_{i,j}}$ is the driving torque at the $i-j$ wheel.

12.3 Tunable Motion Behavior

Several challenges need to be overcome regarding autonomous vehicles. Most researches focus on trajectory planning and tracking problems. This needs to be designed by taking into account the human in the loop. The vehicle behavior should mimic human driving. However, drivers have different profiles and different driving styles. Motions generating excitement feelings among certain people could generate in contrast fear feelings among others. The goal of this work is to prove the ability of modern control techniques to provide different motion behaviors, and therefore different motion feelings to passengers.

Two different approaches to tune the vehicle motion behavior are exposed here. The first approach consists of modifying the motion targets to follow. The high-level control should in this case generate different generalized forces in order to amplify or reduce the vehicle response, or change its dynamics. The second approach consists of allocating differently the commands into the subsystems to generate different accelerations.

12.3.1 Reference Tuning

It should be noted that the MPC algorithm provided by Simcenter Amesim® is able generate a steering wheel angle and a velocity profile. The MPC can embody a driver model or a virtual driver. This work focuses more on the vehicle motion control in general after receiving the signals generated by the MPC without differentiating between a real or virtual driver.

The yaw rate reference needs to be generated using only the steering wheel angle value and the vehicle's speed value. The bicycle model can then be used to generate the yaw rate target. This simplified vehicle model represents the nominal lateral behavior of the car and is characterized by its fast computation to generate a reference, especially the static version of the model. Nevertheless, the dynamic bicycle model is used here to be able to not only generate an amplified yaw rate, but also to be able to control the transient behavior of the vehicle. The yaw rate

reference is then:

$$\dot{\psi}_{ref} = \frac{K_{tun}}{1+\tau_{tun}s} \frac{V_x}{L + \frac{MV_x^2}{LC_{\alpha_f}C_{\alpha_r}}\left(C_{\alpha_r}l_r - C_{\alpha_f}l_f\right)}\delta_f \tag{12.12}$$

Where K_{tun} and τ_{tun} are the tuning gain and tuning lag respectively. These latter can be then manually varied to see the influence on the vehicle behavior.

12.3.2 Tuned CA

It is claimed that motion sickness and discomfort are related to the vehicle's accelerations (Raimondi and Melluso, 2008). One could think of adding an additional objective to the CA problem to distribute differently the commands, and try to fulfill different objectives when it is possible as it was done in Chapter 10. However, in the CA problem, as we express tire forces with respect to generalized forces at the vehicle's center of gravity, we already link tire forces to accelerations. Adding another objective with almost the same effectiveness matrix leads to a rank deficiency. The optimization algorithm cannot then find a solution. This would not have been the case, if for example we want to penalize the lateral acceleration with another subsystem as the ARS system. This is why we present a different method in this chapter than the one shown in Chapter 10. The idea here is to amplify or reduce the accelerations directly by generating amplified or reduced generalized forces. The CA problem becomes then:

$$\mathbf{B_{eff}}\vec{\delta} = \mathbf{T}\vec{v}_{des} \tag{12.13}$$

Where $\mathbf{T}$ is a diagonal matrix with tuning parameters to amplify or reduce components of $\vec{v}_{des}$. $\mathbf{T}$ has been chosen to be diagonal to be able to influence each acceleration apart. This actually prevents from several difficulties. In this way, desired accelerations do not have to be predefined. And for good measure, there is no need to add an additional objective that may slow down the computation. However, this can lead to control imprecision. The tuning parameters should not reach large values. Again, this may need additional experimental tests. Indeed, these tuning parameters have a direct effect on how much the acceleration is amplified in a specific time. This comes with an influence on the jerk. Suitability of these parameters depends on the driver preference. The optimal control vector becomes:

$$\vec{\delta}_{opt} = arg \min_{\vec{\delta}_{min}\leq\vec{\delta}\leq\vec{\delta}_{max}} \left\| \mathbf{W_{ca}}\left(\mathbf{B_{eff}}\vec{\delta} - \mathbf{T}\vec{v}_{des}\right)\right\|^2 \tag{12.14}$$

The ASA is then used. The cost function is rewritten following the ASA formulation:

$$\vec{\delta}_{opt} = arg \min_{\vec{\delta}_{min}\leq\vec{\delta}\leq\vec{\delta}_{max}} \left\| \mathbf{A}\vec{\delta} - \vec{b}\right\| \tag{12.15}$$

So in case of a multi-objective problem, $\mathbf{A}$ and $\vec{b}$ represent vertical vectors with different specifications depending on the chosen objective. Here, to simplify, only CA precision is considered. No modifications is needed as the problem is naturally formulated as an ASA. The weighting matrix $\mathbf{W_{ca}}$ enables prioritizing the yaw rate control or the longitudinal speed control. Here, a matrix unity is considered as both controllable states are considered cardinal. For real-time maneuvers, number of iterations are limited to a finite value. A sub-optimal solution could then be generated rather than an optimal one.

12.4 Co-Simulation Results

Again, the high, middle, and low level control logic are implemented in Simulink, while the high-fidelity car model with 15 degrees of freedom is selected in Amesim®. The maneuver consists in a trajectory race tracking with high-speed values. The approved Magny-Cours area[2] has been reproduced in 3D by Amesim developers using softwares *Open Street Map* and *JOSM*. It should be noted that this track contains bridges, hills, slopes, and the curvatures are refined to make it look like the real one. For good measure, in the MPC controller, driver parameters have been identified using a learning procedure. The computed front steering angle respects then the driver constraints regarding the steering wheel amplitude and speed. The different PI controllers and control logics have been discretized considering a sampling time of only 10ms. We made all the necessary preparations to make the code work in real time.

12.4.1 Relevance of Advanced Chassis Systems

To show the relevance of the advanced chassis systems implemented, we simply carry the co-simulations with and without the TV system. We first present the results of a vehicle not equipped by in-wheel engines and pushing it to its limits, then we provide the same maneuver but with a vehicle equipped by the Torque Vectoring system to show how much these limits can be exceeded. We increase the speed of the vehicle in some specific turning to show the relevance of the advanced chassis systems embedded in this configuration. Secondly, we use this severe maneuver to evaluate the ability of generating different motion feelings while keeping the same trajectory using the different approaches exposed in this chapter.

Without Torque Vectoring

In this situation, the vehicle contains only one engine at the front axle. This engine acts equally on both front tires. Rear tires do not have any driving capabilities. Regarding the brakes, the command is only distributed between the front and rear axle by considering the static difference between the front and rear mass. As in this case the engine is located at the front axle, 60% of the brake command is allocated to the front wheels, and 40% to the rear wheels.

The maximum performance that we can get without destabilizing the vehicle is depicted in Figure 12.2.

The vehicle completes the Magny-Cours trajectory in about **124.2s**. Exceeding the velocity by 0.01m/s results on the situation illustrated in Figure 12.3.

[2] *Magny-Cours, Nevers, Niévre, Bourgogne, 58470, France.*

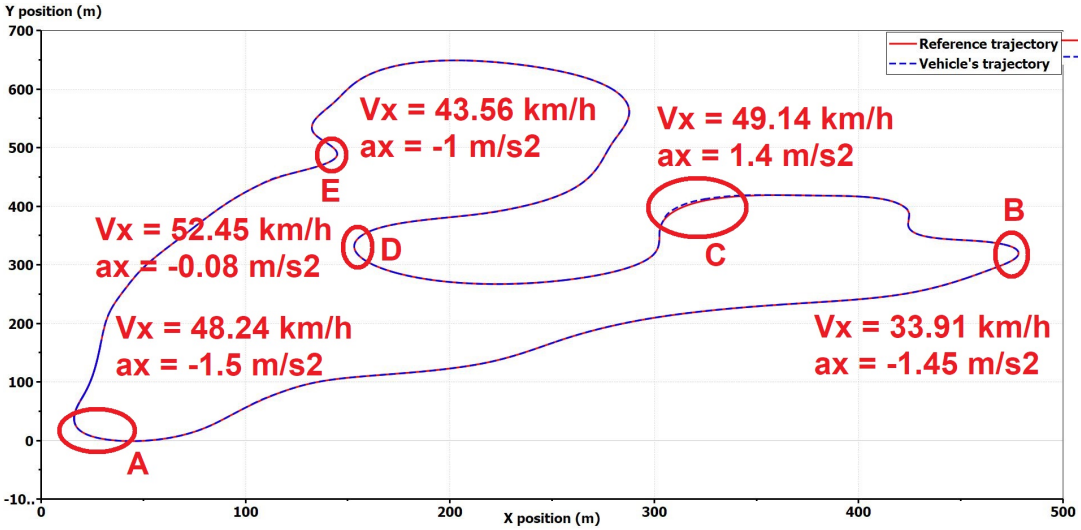

FIGURE 12.2: Magny-Cours trajectory with the maximum performance of a vehicle without torque vectoring.

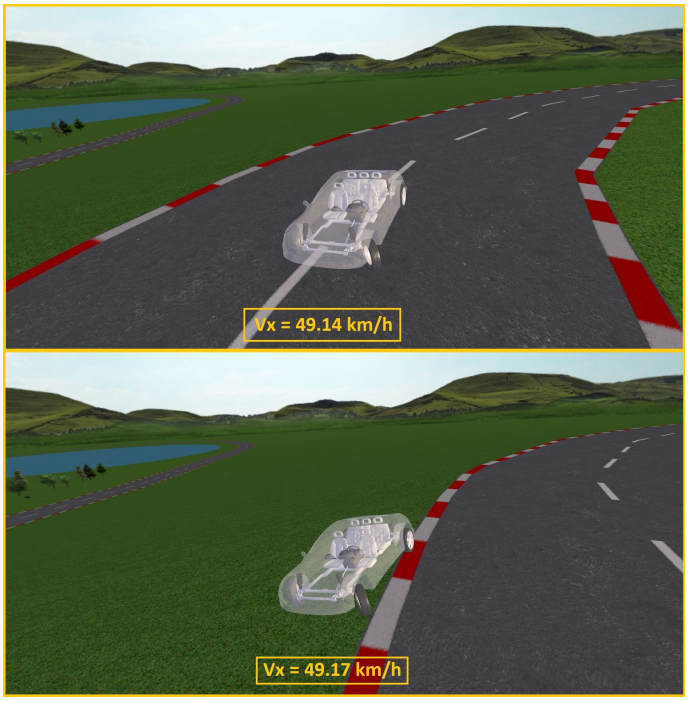

FIGURE 12.3: Case of vehicle's loss of control when no torque vectoring is ensured.

The loss of control happens in Section C. Among all the difficult sections, this is the only section where the vehicle was actually accelerating due to the presence of a slope. Here, the need for powertrain torque is too high for the grip capacity especially in this section. This causes front wheel spin, which leads to a global understeer behavior. This explains also the need of an important steering angle. The speed target is then reduced by the MPC which ask afterwards for braking torque. As the front wheel grip recovers, this leads to an important load transfer that causes rear wheel

blocking. As a consequence, the vehicle oversteers. Normally, a countersteering action is programmed in the MPC that consists in changing the steering wheel sign with respect to the sideslip when the latter increases too much. As this action allows the vehicle to recover its path for a maximum speed of 49.14 km/h, it remains insufficient for higher sped values. A video showing the loss of control of the vehicle in this case can be visualized following this link: Co-simulation without torque vectoring. Next, we demonstrate how an additional capability, namely the Torque Vectoring, enables exceeding this speed maximum and provides higher performance and safety.

With Torque Vectoring

Here, the vehicle is equipped by in-wheel engines and the brakes can be controlled separately. Figure 12.4 shows the maximum speed tracking before loosing control. We can see that the vehicle has been able to enter the severe Section C at a speed

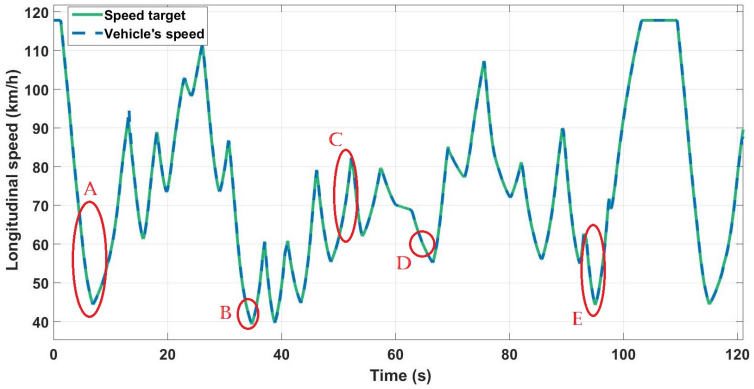

FIGURE 12.4: Maximum speed tracking with Torque Vectoring.

of almost 60 km/h. The Torque Vectoring enables supplementary yaw moment than the amount provided by only the front steering. The driving-based Torque Vectoring is especially pertinent when the vehicle is accelerating which makes it a suitable solution for the problem encountered in Section C (Figure 12.5). The braking-based VDC is more relevant when the vehicle is decelerating (Figure 12.6). Putting together both systems, larger values of yaw rate can be tracked (Figure 12.7).

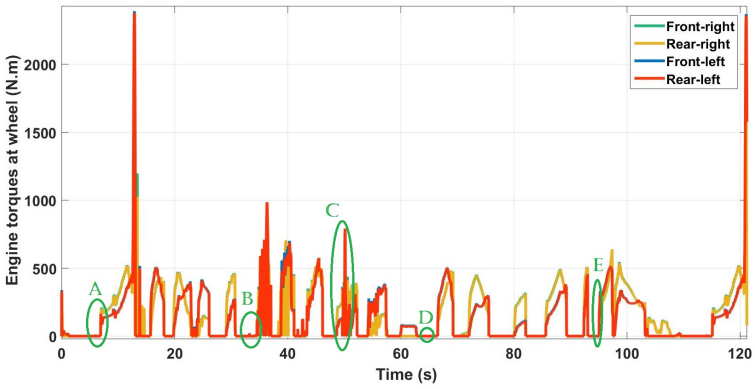

FIGURE 12.5: Engine torques distribution at Magny-cours.

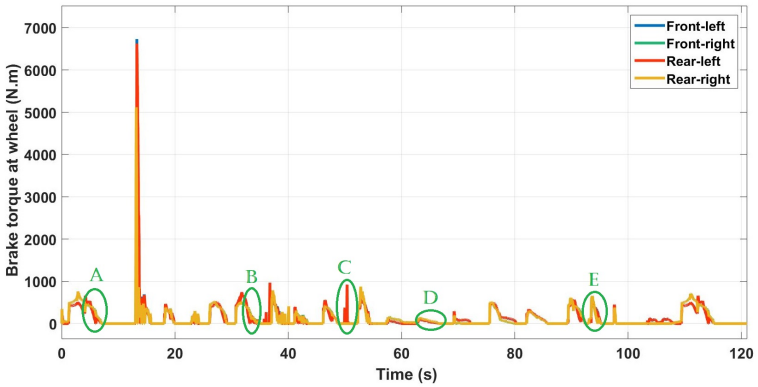

FIGURE 12.6: Braking torques distribution at Magny-cours.

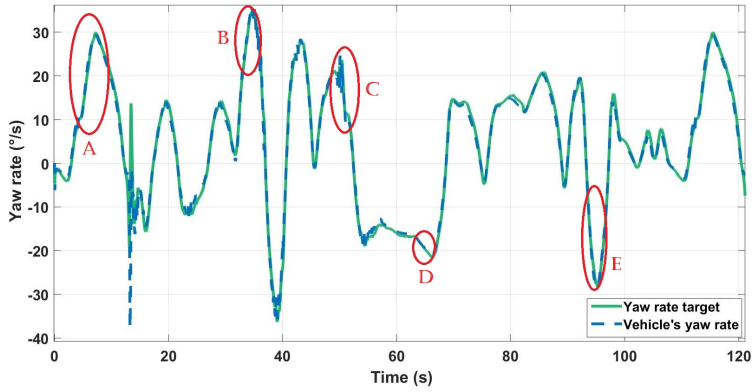

FIGURE 12.7: Maximum yaw rate tracking with Torque Vectoring.

Thanks to these additional subsystems, the equipped vehicle finished the Magny-Cours circuit at only **108.2s**, making a benefit of **16s**. The impressive vehicle behavior in this case, especially in Section C, can be visualized following this link: Co-simulation with torque vectoring. Additional chassis systems with an optimal coordination give simply expanded performances. This can include realizing difficult dynamic maneuvers or complex trajectories also by means of for example a ARS system.

12.4.2 Motion Feelings Tuning

It is important to keep the same trajectory in all simulations because we want to separate the effect of generating different trajectories for different feelings from achieving this with different accelerations. Figure12.8 shows the respect of the same trajectory in both approaches.

First Approach: Reference Tuning

First, we use equation (12.12) to change the yaw rate reference by means of K_{tun} for the response amplitude and τ_{tun} for the transient behavior. The yaw rate responses are illustrated in Figure 12.9.

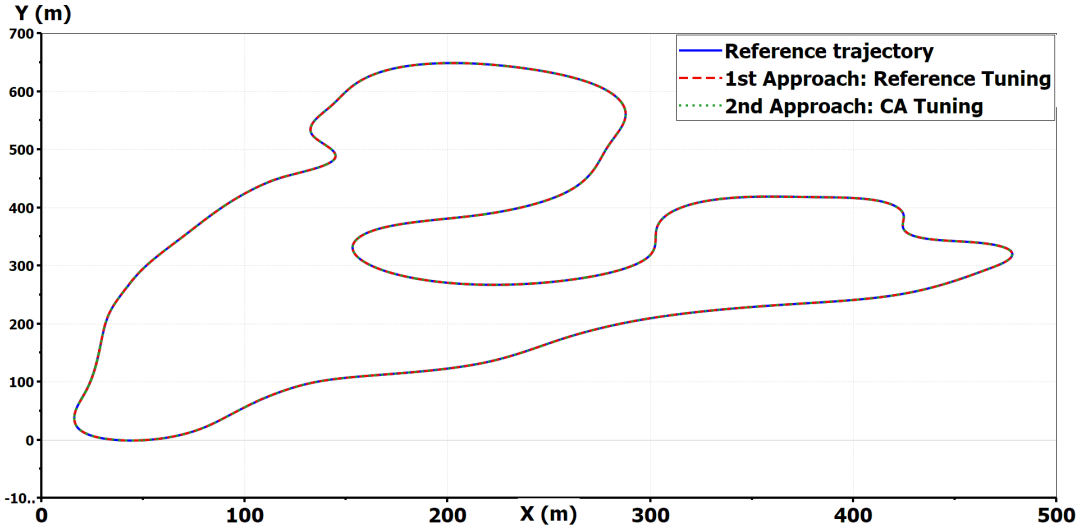

FIGURE 12.8: Trajectories in all simulations.

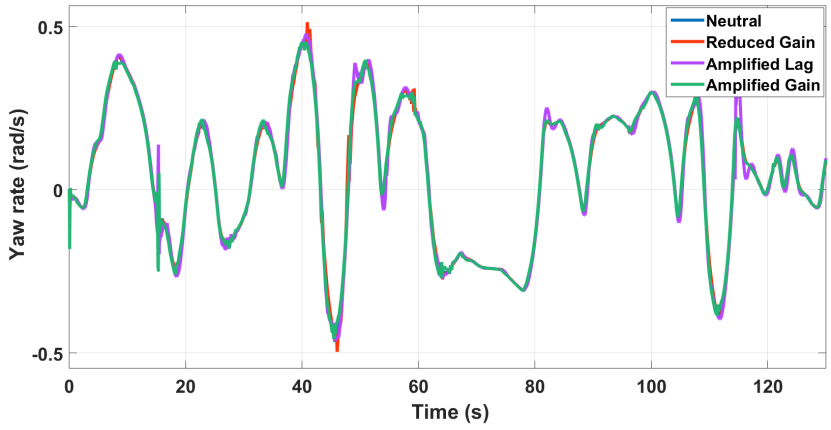

FIGURE 12.9: Yaw rate responses in case of reference tuning.

We notice that there is not much effect on the yaw rate response. In fact, when tracking the exact same trajectory with the same velocity, the yaw rate will always be the same. So when amplifying for example K_{tun}, to keep the same yaw rate, the MPC computes less front steering angle so the reference stay the same as Figure 12.10 shows.

In Figure 12.11 we can see that it is the difference between right and left tire forces that complements the influence of the front steering to turn the vehicle.

Therefore, this approach is not efficient regarding tuning accelerations for different feelings when there is a strict trajectory tracking along with a vehicle motion control (Figure 12.12).

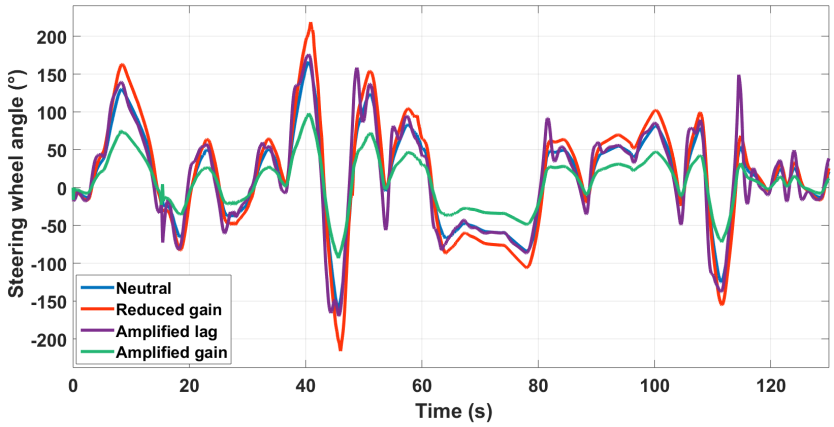

FIGURE 12.10: Steering wheel angle in case of reference tuning.

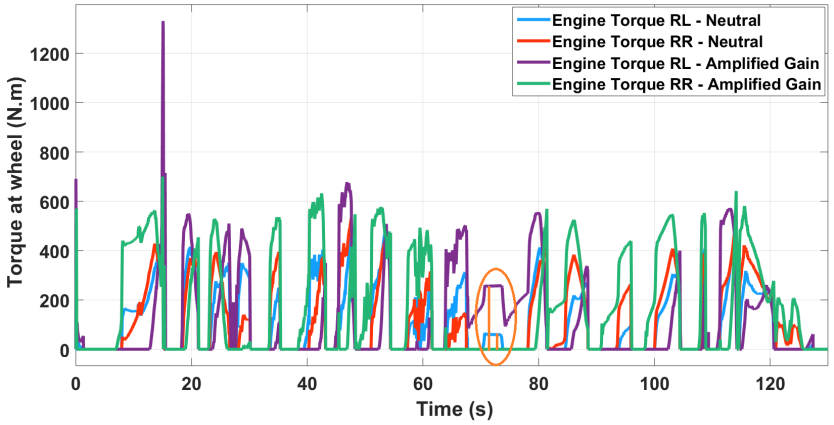

FIGURE 12.11: Engine torques in case of reference tuning.

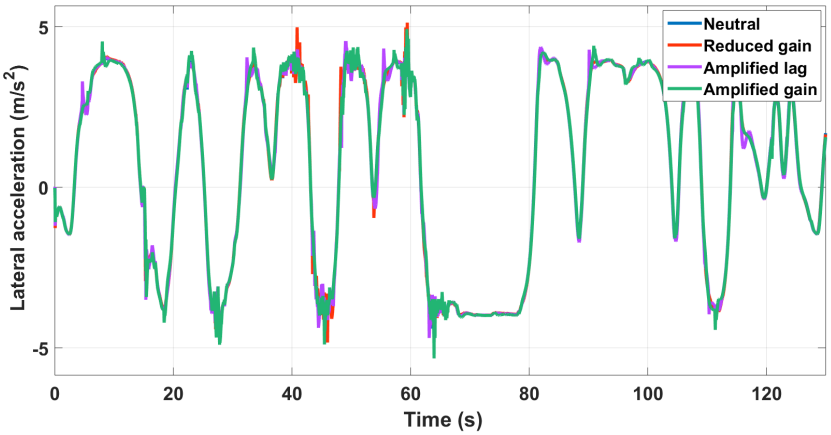

FIGURE 12.12: Lateral acceleration in case of reference tuning.

However, this can be relevant when there is a human driver as only few effort is needed to turn the vehicle. The TV and VDC act as assistance systems. This might be also more beneficial for automated emergency steering to avoid an obstacle for example, as even if the driver want to take back the control, the steering wheel does

not turn too much to hurt the driver's hands.

Second Approach: Tuned CA

Here, we penalize the forces allocation to influence directly the generated accelerations. As we can see in Figure 12.13, we can obtain different lateral accelerations.

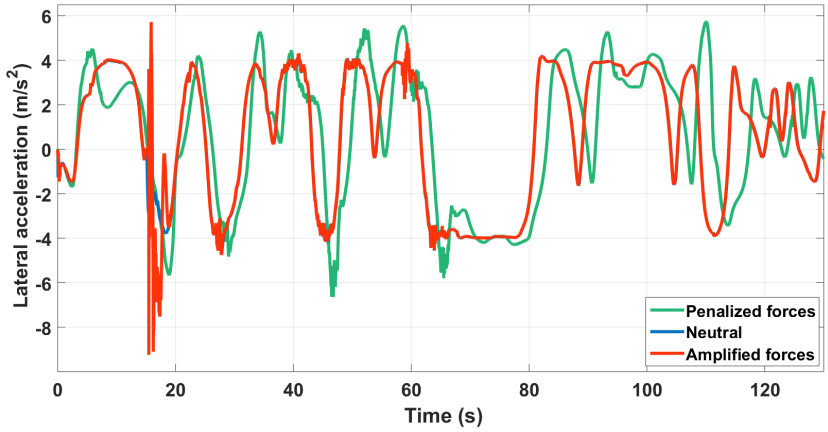

FIGURE 12.13: Lateral acceleration in case of CA tuning.

Which gives then different yaw rate responses while keeping the same trajectory (Figure 12.14).

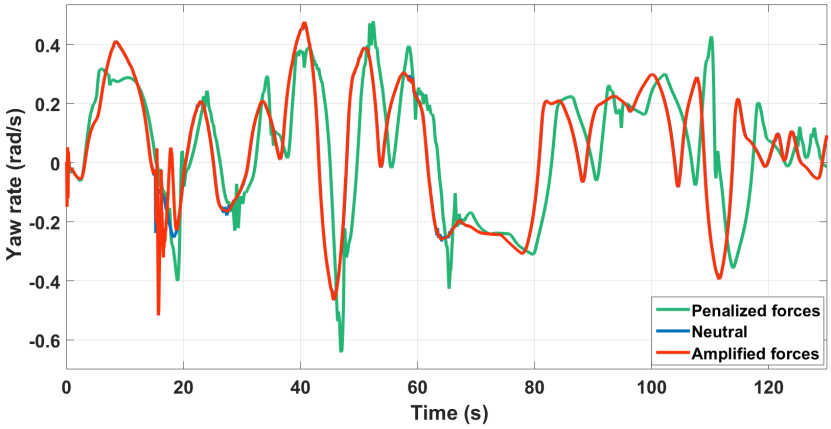

FIGURE 12.14: Yaw rate responses in case of CA tuning.

Regarding the front steering angle, this have little impact regarding the amplitude. Only the transient behavior is different as Figure 12.15 shows. In all Figures 12.13, 12.14 and 12.15, the "*neutral behavior*" and the behavior with "*amplified forces*" overlap. So to benefit from advantages of both approaches, a mixed approach is presented in the next paragraph.

Mixed Approach

Here, both the reference and the CA are tuned. This allows us the have different accelerations responses as Figure 12.16 shows.

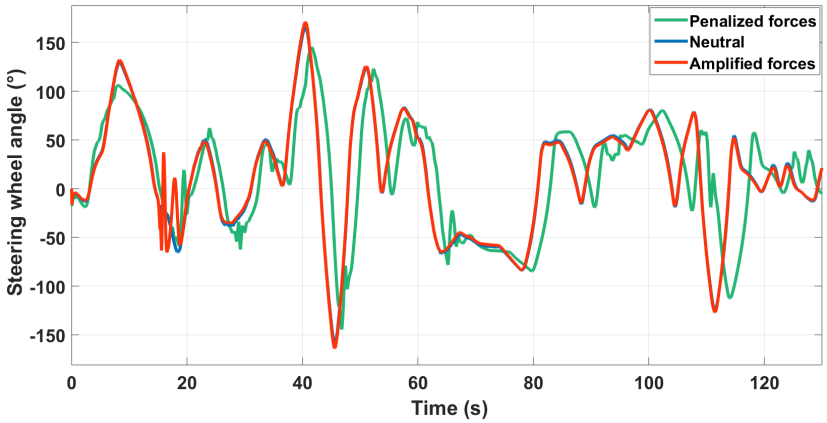

FIGURE 12.15: Steering wheel angle in case of CA tuning.

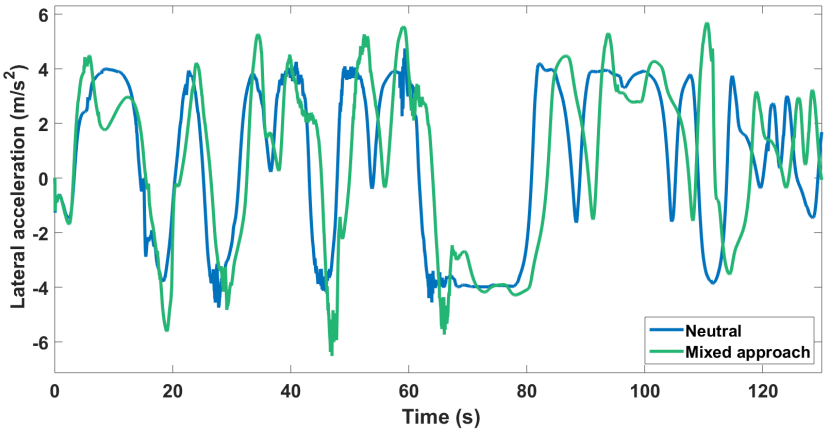

FIGURE 12.16: Lateral acceleration in case of mixed tuning.

This comes also with different steering wheel angles at the same time as Figure 12.17 shows.

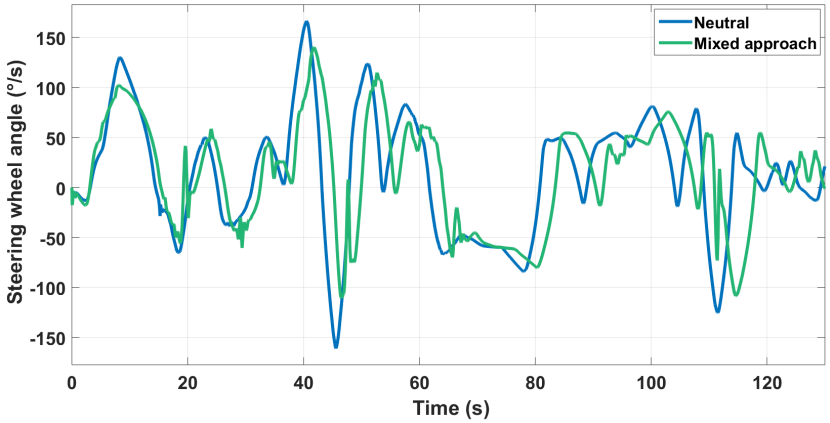

FIGURE 12.17: Steering wheel angle in case of mixed tuning.

And all of that while keeping the same trajectory. In this way, trajectory tracking can be decoupled from motion control, and both security and comfort can be ensured. But of course, with additional chassis systems, e.g. the ARS system, we can even allow different trajectory generation to have even more motion feelings as shown in Chapter 11.

12.5 Conclusion

In this chapter, we first compared two different vehicles. The first vehicle contains no Torque Vectoring features, while the second one is equipped by both a driving-based Torque Vectoring and a braking-based one. The additional chassis systems enabled the vehicle to deal with severe situations whereas the vehicle with no torque vectoring lost control at an earlier stage. Advanced chassis systems when optimally coordinated exhibit higher performances and safety. This represent additional opportunities when it comes to vehicle motion control. As we have separated trajectory tracking from dynamics control, this remains valid for both autonomous and non-autonomous vehicles. We believe that autonomous vehicles would have a big potential with an advanced intelligence, but a bigger one with additional systems to reduce the different constraints. We recognize the need of experimental results. Systems' operation in real time could add few technical limitations. These systems are also very expensive. The number of systems that can be implemented within the same vehicle will be limited especially for passenger cars.

Secondly, two approaches for tuning vehicle behavior have been compared. While the first one consists of changing motion references dynamics, the second one consists of distributing differently the commands into subsystems by means of a tuning matrix to amplify or reduce accelerations. Results showed that in the first approach, the use of TV and VDC is amplified to realize maneuvers with less front steering angle, and in the second approach, accelerations have been tuned to enable different motion feelings. A mixed approach have been proposed to benefit from both advantages. This demonstrates the need of implementing this kind of modern control algorithms in future cars. The more autonomous the vehicle will become, the more authority the driver should delegate, and the more the vehicle behavior should stay predictable to prevent drivers from taking back suddenly the control. The goal of this study is to prove that with a multi-layered architecture, control problems are separated from distribution problems. Therefore, by means of modern control techniques, additional objectives can be satisfied. For future autonomous vehicles, this represent an opportunity to exploit more the vehicle's potential to adapt its behavior to humans' expectations. More evidence should be provided however by means of real experiments before proposing any standards. We expect more collaboration from car manufacturers in order to prove our claims and participate in autonomous vehicles development.

12.6 Contributions

Our contributions in this chapter are focused on autonomous vehicles. Two major aspects are discussed: performance expansion while keeping the vehicle's safety, and motion feelings tuning. This can be summarized as follows:

1. Application of the upstream approach to an autonomous vehicle equipped with an EPAS, VDC, 4WD, and TV systems. The goal is to show first the relevance

of advanced chassis systems in terms of performance improvement, and second to show the ability of the upstream approach to keep the vehicle safe in sever scenarios. Both an over-actuated system with optimization-based control allocation algorithms offer new possibilities to autonomous vehicles to relax their constraints and make them able to handle more severe situations. This has been published in:

M. Kissai, X. Mouton, B. Monsuez, and A. Tapus, "Relevance of Advanced Chassis Systems for Vehicle Motion Control," *2018 7th International Conference on Mechatronics and Control Engineering (ICMCE 2018)* , Amsterdam, 2018. ***Accepted***.

2. Two additional motion behavior tuning strategies have been explored: reference motion tuning and CA tuning. In contrast to the method exposed in Chapter 10, no additional objective is needed here to avoid formalizing qualitative objectives. A mixed approach is also proposed to benefit from the advantages of each approach. This has been published in:

   M. Kissai, X. Mouton, B. Monsuez, D. Martinez and A. Tapus, "Optimizing Vehicle Motion Control for Generating Multiple Sensations," 2018 IEEE Intelligent Vehicles Symposium (IV), Changshu, 2018, pp. 928-935.
   DOI: 10.1109/IVS.2018.8500563.

Next, we present a first feedback from experimentation. We use the latest Renault Talisman equipped by only two conquering subsystems. Prototypes with higher over-actuation are still in construction unfortunately.

13 Experimental Results: A First Feedback of the ARS-VDC Case

Until now, only co-simulation results have been presented. Even though this gives more reliable results than classical simulations, the dynamics of each new advanced embedded system provided by a different equipment supplier are usually influenced by hidden control logic in black boxes, sometimes rule-based and hard to identify. The overall dynamics can be very uncertain, and even high-fidelity vehicle models can fail to depict the real behavior of the over-actuated vehicle.

In this chapter, we compare robust controllers applied on the latest Renault Talisman equipped by two uncertain chassis systems: the ARS and the VDC systems (Figure 13.1). Experiments were conducted on the Talisman to isolate the influence of each subsystem apart. Unfortunately, the controllers designed in Chapter 10 gave either stable controllers but with poor performances, or unstable controllers. This is mainly due to unexpected rule-based algorithms implemented within the most inner control logic provided by the supplier. An example of these unexpected rules is the fact that the saturation of the ARS actuator depends on the speed of the vehicle: the ARS system is saturated at $\pm 3.5^\circ$ at low speed, but only at $\pm 2.5^\circ$ at high speed for safety measures.

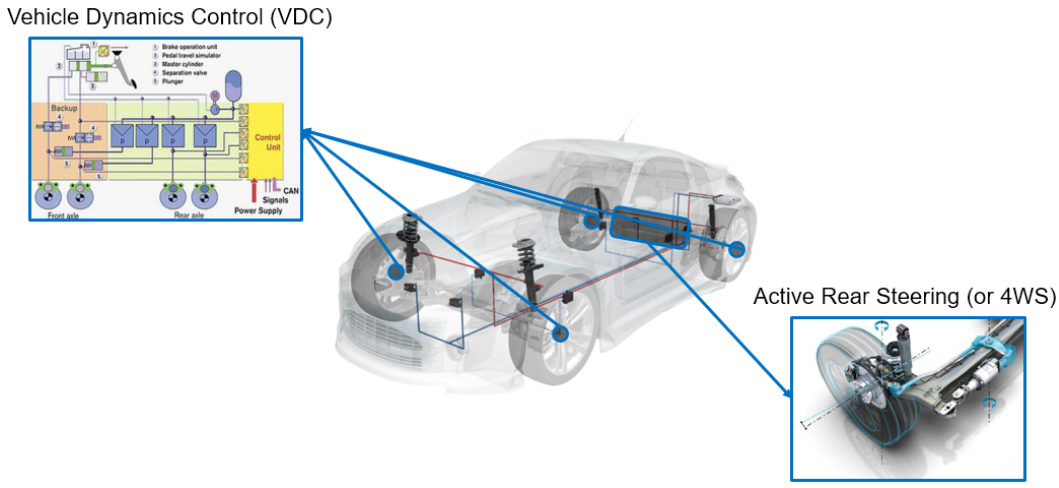

FIGURE 13.1: The prototype experimented.

Another limitation is the actuator speed limit. While this can be easily introduced in the CA problem, this may present few difficulties in the downstream approach. A single PI controller synthesized for the ARS system gave us the yaw rate response depicted in Figure 13.2. The large overshoot is of course unacceptable and generates undesired motion feelings. This is mainly due to the fact that the controller does not respect the real dynamics of the ARS actuator. The response of the actuator in Figure 13.3 shows that the controller does not respect the speed limits of the

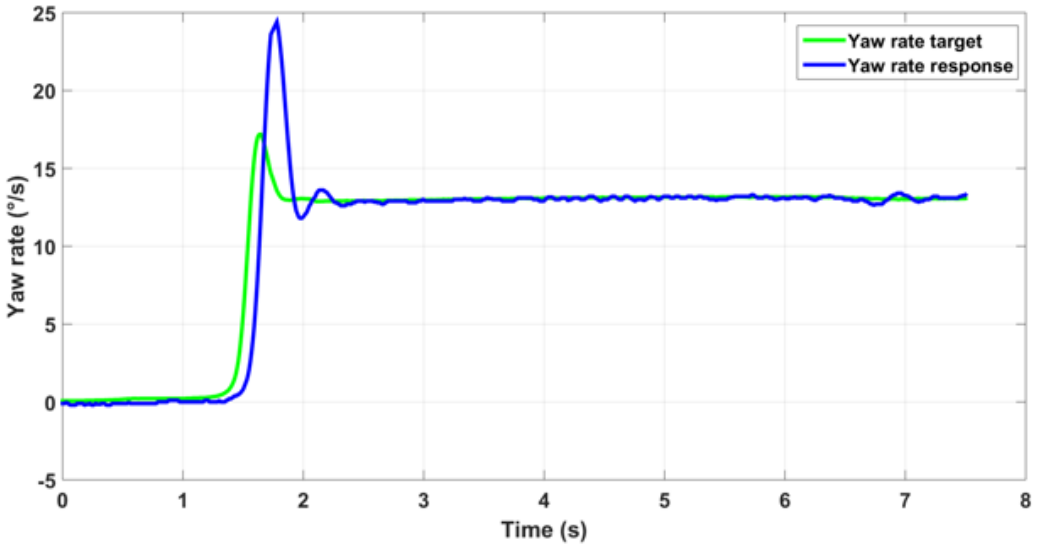

FIGURE 13.2: Real yaw rate response of the vehicle using only a PI for the ARS.

actuator and that a more sophisticated controller is needed to respect all the plant constraints.

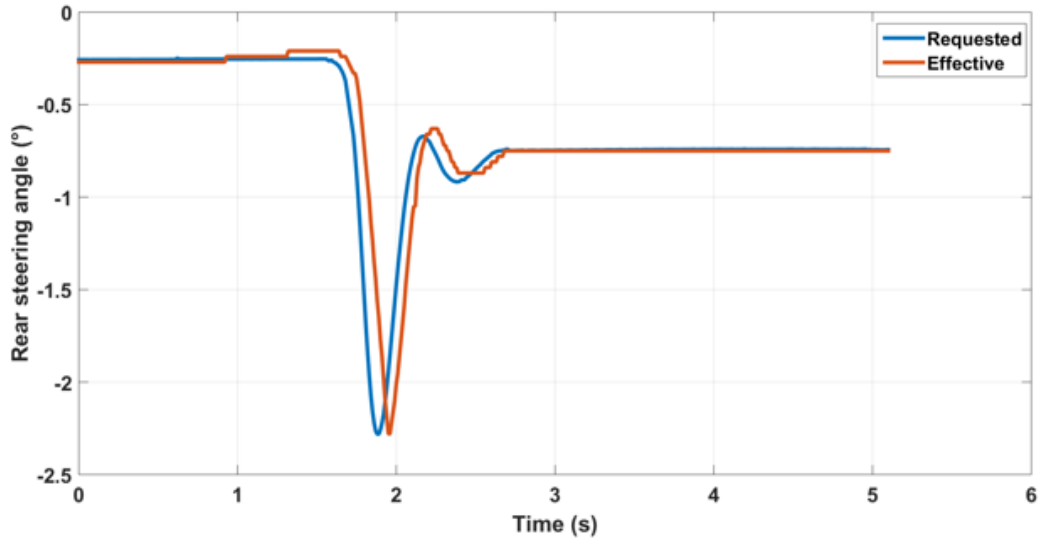

FIGURE 13.3: Real ARS actuator using only a PI.

In addition, the CA algorithm should be also adapted to fit the interfaces of each module. These technical difficulties are detailed in the following sections.

13.1 Modeling Methods

MBD methodology has proven its effectiveness in control system development (Nicolescu and Mosterman, 2010). This makes a comprehensive design approach possible by developing models to represent the behavior of the plant to be controlled.

However, the controller in this case is very related to the model. If the model is not accurate enough, the controller may fail to stabilize the plant. A proper way to proceed would be to first experimentally identify the dynamics involved, and then design a robust controller to guarantee the stability of the plant while keeping an acceptable level of performance.

The problem is that for the CA algorithm as we have seen (see Chapter 10), the commands have to be of the same unit, while the subsystems can be very different. In our case, the vehicle is equipped by both an ARS, which is called the 4WS system at Renault, and the braking-based VDC system. The first system can act on the yaw rate of the vehicle through the steering of the rear wheels. The VDC system can generate different brake torques at the right wheels than at the left wheels. This generates different longitudinal tire forces at the corners of the vehicle which create a yaw moment. Consequently, the VDC can also influence the yaw rate of the vehicle. The influence of each chassis system should be first identified in order to manage their interactions.

13.1.1 Experimental Identification

In order to synthesize a robust high-level controller, the first stop is to identify the vehicle dynamics and its subsystems whenever it is possible. Normally, any subsystem will influence the tire forces then the vehicle dynamics. A high-level controller would be synthesized in the base of the vehicle dynamics, the CA algorithm should distribute optimally tire forces, and then a low-level control layer should control each subsystem apart. Unfortunately, we do not have access to tire forces signals online in passenger cars. Figure 13.4 illustrates this problem where the accessible signals are depicted in green, and the inaccessible ones are depicted in red, where:

- $T_{b_{i,j_{req}}}$: requested brake torque at the $i-j$ wheel,
- $T_{b_{i,j_{eff}}}$: effective brake torque at the $i-j$ wheel,
- $\delta_{r_{req}}$: requested rear steering angle,
- $\delta_{r_{eff}}$: effective rear steering angle.

Note that also the effective brake torques cannot be measured. The good news is that we are able to measure both the input and output of the 4WS system. Therefore, by activating only the 4WS system we can isolate the vehicle dynamics from the 4WS actuator dynamics. Then, in the process of identifying the VDC dynamics, we can deduce the vehicle dynamics already identified to isolate the subsystem dynamics.

The 4WS system identification

From previous research on vehicle dynamics (Ono et al., 1994), (Brennan and Alleyne, 2001),we know that the vehicle dynamics depend on the speed. The experiments should be carried out using different speed values. Here, we apply a step to the 4WS actuator (same angle for both rear wheels), and we measure both the effective rear steering angle $\delta_{r_{eff}}$ and the yaw rate of the vehicle $\dot{\psi}$ to evaluate the influence of the 4WS actuator on the vehicle. We use afterwards the System Identification app of Matlab® to identify the dynamic models using input/output data. For a speed of $70km/h$ for example, we obtain the Figure 13.5.

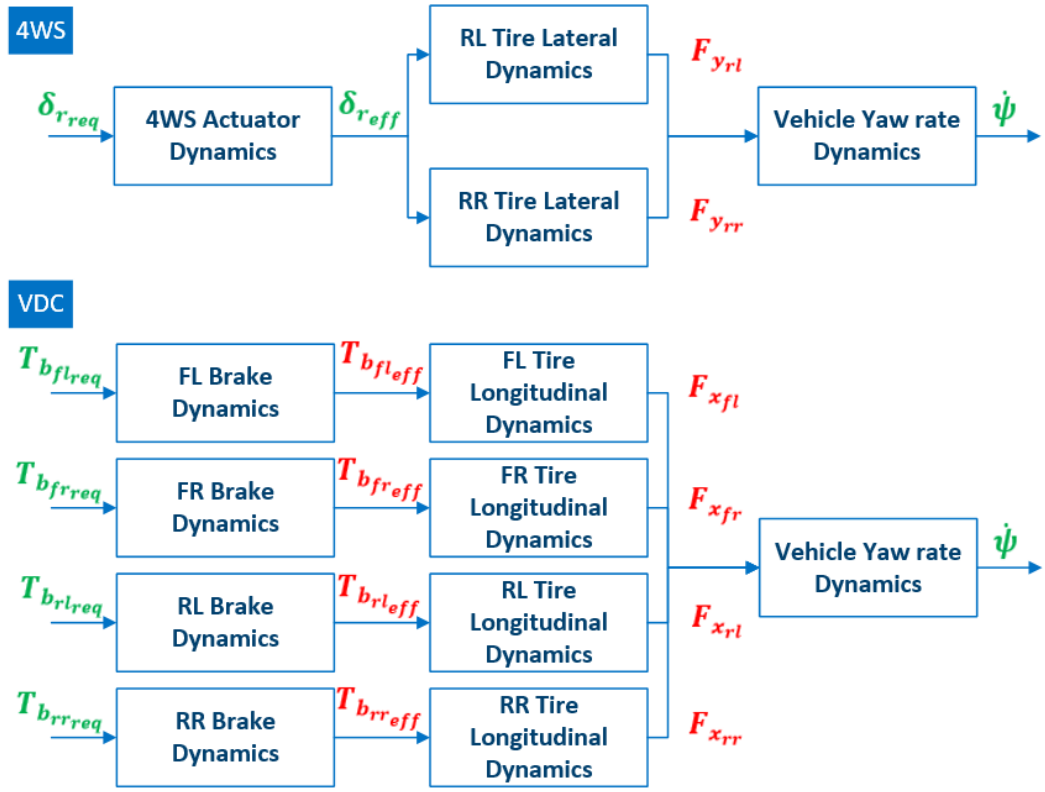

FIGURE 13.4: The identification problem in an over-actuated vehicle.

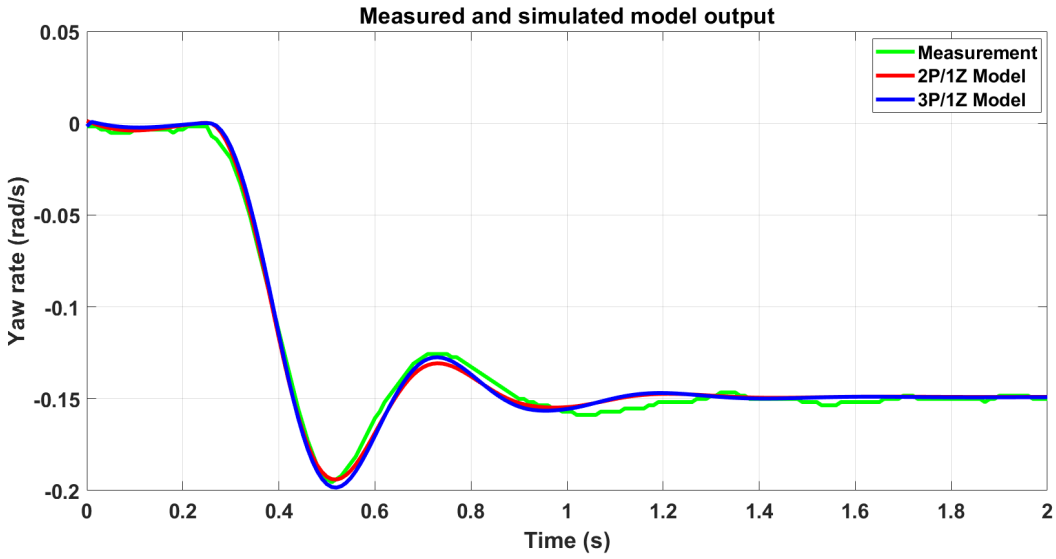

FIGURE 13.5: Comparison of the measured response and the estimated ones.

We use different transfer function shapes to approach the vehicle response. After several experiments we can conclude that two poles and one zero suffice to represent the vehicle dynamics influenced by the rear steering. Figure 13.5 shows that there is no need to add for example a third pole. Note that the zero characterize the

input. The real dynamics of the vehicle are therefore the two identified poles. The problem is that for the same speed value, we may obtain slightly different models as Bode diagrams in Figure 13.6 show. As long as we know that the diagram cor-

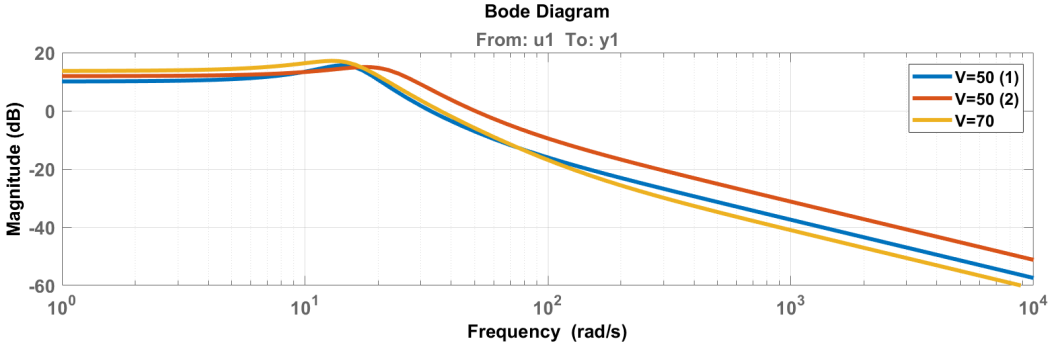

FIGURE 13.6: Comparison of bode diagrams for different speed values.

responding to the speed $70km/h$ has the highest gain in low frequencies because of the speed variance, for the remaining diagrams, the reason do not depend on the speed variance. Consequently, we develop a nominal model based on the experiments carried out for the same speed value, we add a dynamic uncertainty that covers all the model identified, and we isolate the varying parts depending on the speed using our knowledge on vehicle dynamics. The nominal model has the following shape:

$$G_{nom}(s) = K_{4WS}\frac{1 + Z_{4WS}(V)\,s}{1 + 2\dfrac{\zeta(V)}{\omega_c(V)} + \left(\dfrac{s}{\omega_c(V)}\right)^2} \tag{13.1}$$

Where:

- G_{nom} : the chosen nominal plant,
- $Z_{4WS}(V) = bV$: the zero induced by the 4WS system which depends on V, with b being a parameter characterizing the mass and cornering stiffness of the front axle (Soltani, 2014),
- $K_{4WS}(V) = -\dfrac{V}{L + aV^2}$: the gain generated by the 4WS system which depends on V, with a being a parameter characterizing the mass and cornering stiffness of the front and rear axles (Soltani, 2014),
- $\zeta(V) = \dfrac{\zeta_0}{\sqrt{1 + \left(\dfrac{V}{V_{ch}}\right)^2}}$: the damping of the vehicle, which depends on V, with ζ_0 is the natural damping and V_{ch} is the characteristic speed of the vehicle (Soltani, 2014),
- $\omega_c(V) = \omega_0\sqrt{1 + \left(\dfrac{V}{V_{ch}}\right)^2}$: the crossover frequency of the vehicle, which depends on V, with ω_0 being the natural one (Soltani, 2014).

We add a dynamic uncertainty so the set of identified models for the same speed fit into the set of uncertain models. We verify also the validity of this set for other speed values by changing it in the nominal model. Figure 13.7 shows that with a

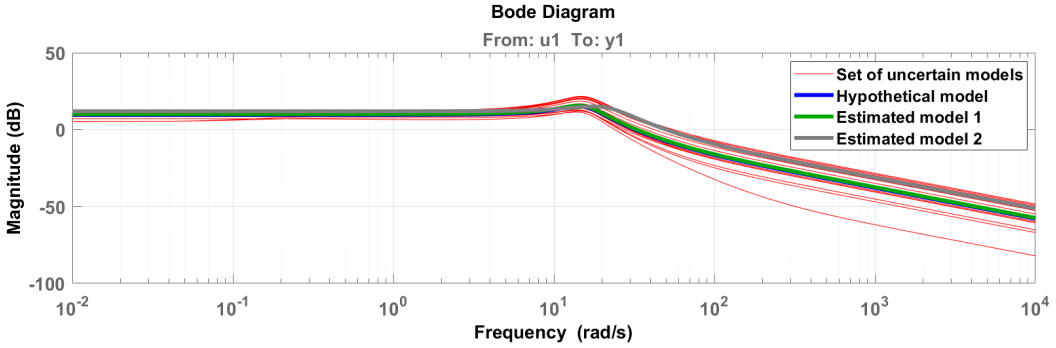

FIGURE 13.7: Set of uncertain models including the varying nominal model and identified experimental models.

proper dynamic frequency dependent uncertainty applied to the hypothetical speed-dependent nominal model, we can include the estimated models from experiments into a set of uncertain models.

Figure 13.8 shows that this approach remains valid even if we vary the speed value.

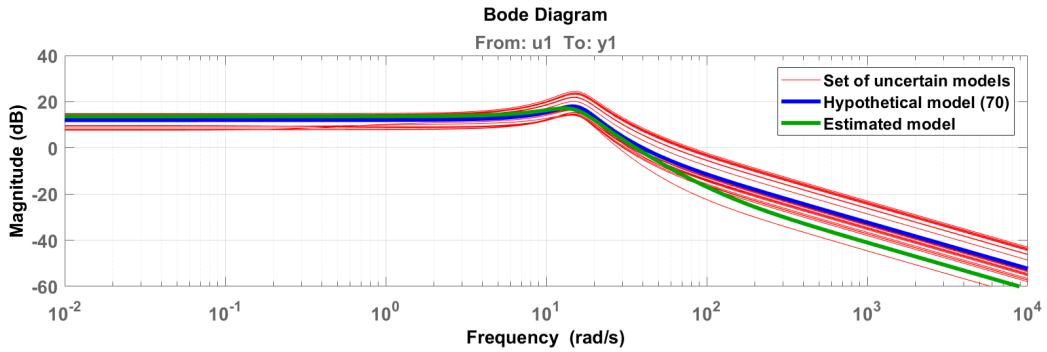

FIGURE 13.8: Set of uncertain models for a speed of $70km/h$.

The same procedure is carried out for the 4WS actuator only, by considering this time the input/output data at the actuator level only (see Figure 13.4). This time a small delay is needed to fit the real dynamics of the actuator as Figure 13.9 shows. The overall system is composed then of two poles characterizing the vehicle dynamics, one zero, one delay and two poles characterizing the 4WS system dynamics.

The VDC system identification

We follow the same procedure for the VDC also. However, as we have mentioned, we do not have access to the effective torques applied to the wheels. A series of torque values have been applied in the experimentations. Here, we present the results when applying a torque of $400N.m$ at each left wheel, and we measure the yaw rate response of the vehicle. We consider that all the four brakes have the same dynamics.

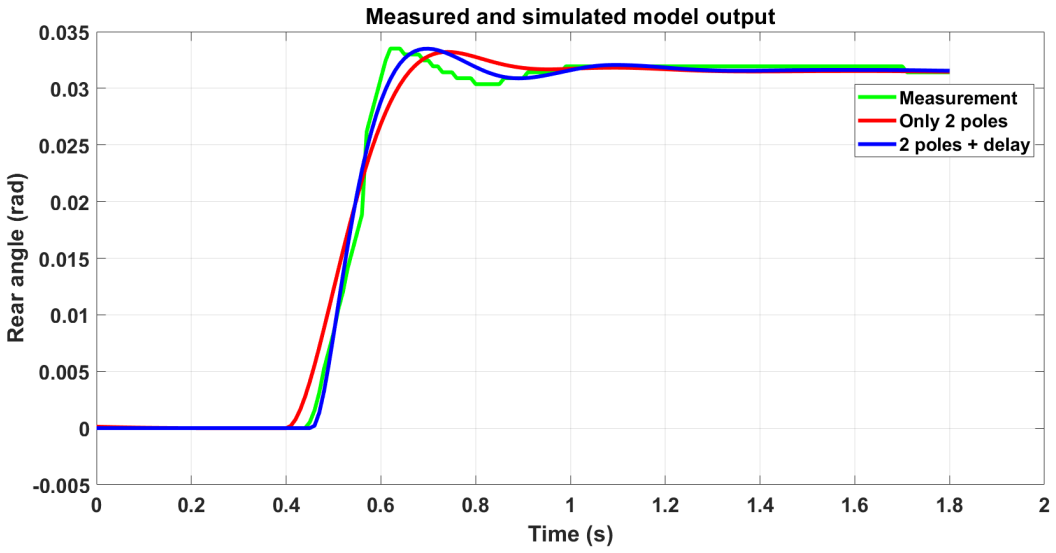

FIGURE 13.9: Comparison of the measured response and the estimated ones for the 4WS actuator.

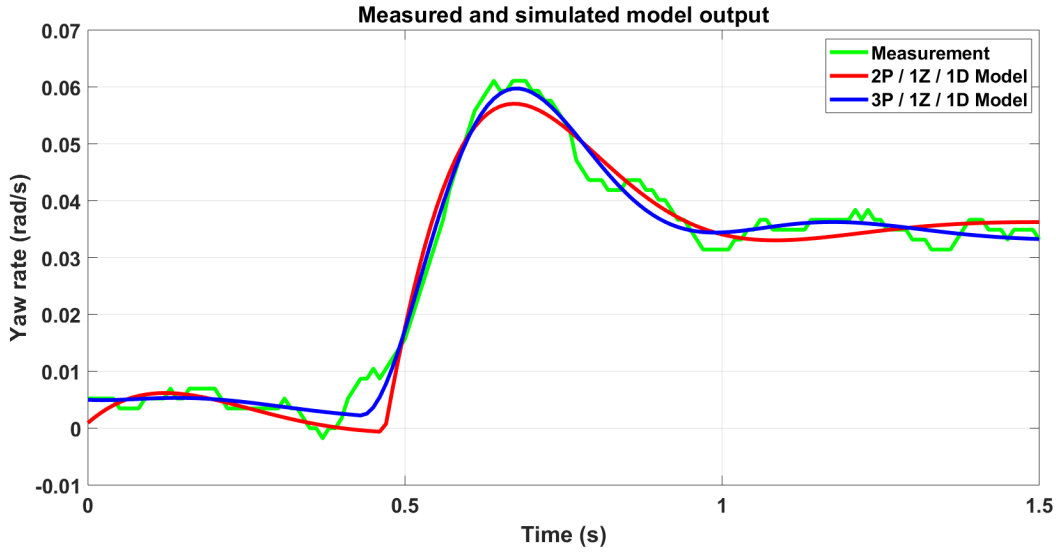

FIGURE 13.10: Comparison of the measured response and the estimated ones for the VDC.

Figure 13.10 shows that three poles, one zero, and one delay are needed to represent both the vehicle and the VDC system. Note that also non-linearities as delays[1] were also unexpected which leads us to redesign the controllers. The importance of the delay at the VDC level can be seen in Figure 13.11.

By analyzing the poles and zeros of the influence of the 4WS and the VDC system in Figure 13.12, we can see that the complex poles of both dynamic models are close enough.

We can conclude that the complex poles characterize the vehicle dynamics. The remaining pole, zero and pure delay characterize the VDC system. Following again

[1]We suspect that these delays originates from communications at the Controller Area Network (CAN).

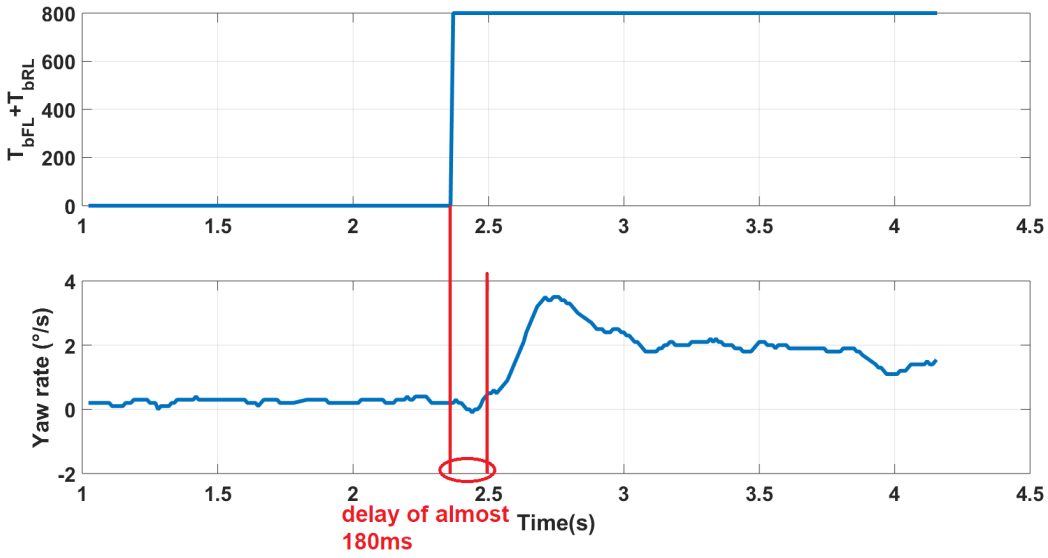

FIGURE 13.11: The amount of the VDC delay in an open-loop experimental test.

the same procedure, we can develop a hypothetical nominal model augmented by a dynamic uncertainty to cover all the experiments. A high-level controller can be synthesized relying on the uncertain complex poles of the vehicle, and two low-level controllers can be synthesized based on the uncertain dynamics of each embedded system and its influence (zeros) on the vehicle dynamics.

13.1.2 Analytic Modeling

Using an optimization-based CA method, the distribution depends closely on the coefficients contained in $\mathbf{B}$. This matrix expresses the influence of each control component on the overall system. It should contain therefore coefficients of the same unit for a right comparison. In our case, we should compare the influence of a steering angle and a braking torque. One could think of transforming the steering angle to an equivalent torque, or the torques to an equivalent steering angle. However, both systems generate first tire forces then a yaw moment. In addition, lateral tire forces and longitudinal ones are coupled and penalize each other according to the principle of the friction ellipse (Pacejka, 2005). Consequently, for a proper coordination, it is the tire forces that should be distributed optimally by taking into account the dynamic saturations caused by the friction ellipse. The distribution algorithm is then based on an analytic vehicle model showing the influence of tire forces. The problem is that we do not have access to tire forces in real time. The CA layer outputs will be then transformed to percentages to be applied to the control logic.

As we want to control the four brakes, a 4-wheeled vehicle model is needed. As only longitudinal and lateral forces are controllable, vertical motions were ignored making the model planar. However, vertical forces variations have significant influence on tire behavior (Pacejka, 2005). These should be taken into account in the tire model (Kissai et al., 2017). Reducing again the global vehicle model of Chapter

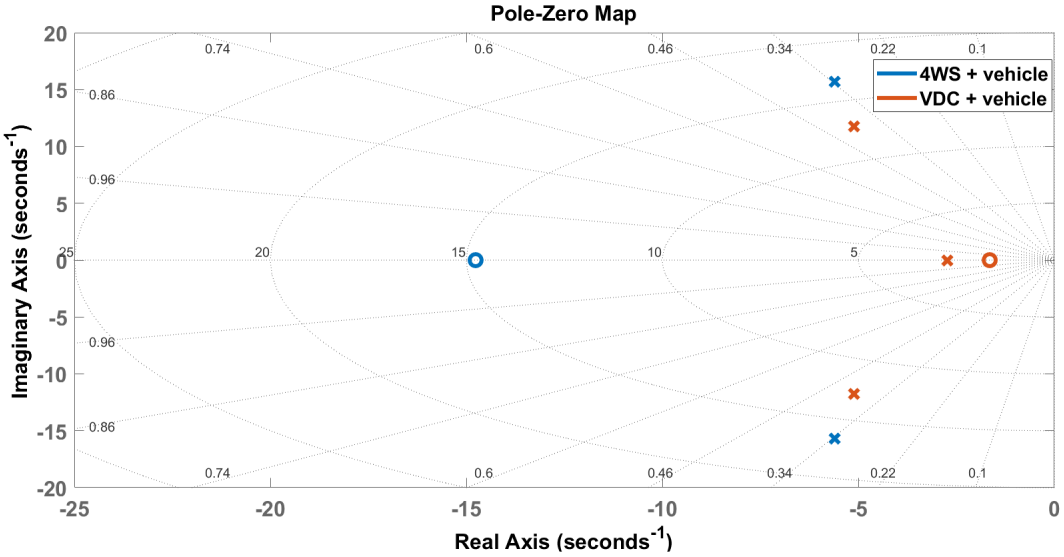

FIGURE 13.12: Poles-zeros analysis.

5, we can find the following equations:

$$\begin{cases} \dot{\psi}(s) = \dfrac{M_{z_{tot}}}{sI_z} & (13.2) \\ M_{z_{tot}} = \left(F_{x_{f,l}} + F_{x_{f,r}}\right) l_f \sin(\delta_f) + \left(F_{x_{f,r}} - F_{x_{f,l}}\right) \dfrac{t}{2} \cos(\delta_f) \\ \qquad + \left(F_{x_{r,r}} - F_{x_{r,l}}\right) \dfrac{t}{2} - F_{y_r} l_r & (13.3) \end{cases}$$

13.2 Robust Control Design

After several experiments, slightly different models have been obtained. As we have shown in Section 13.1, a dynamic uncertainty has been added to the nominal model to cover all experiments. The reason behind this methodology is to develop a robust controller able to stabilize all chosen uncertain models. In this chapter, we compare two well-known robust control design techniques: $\mathcal{H}_\infty$ synthesis and μ synthesis.

13.2.1 $\mathcal{H}_\infty$ Synthesis

As we have seen in Chapter 8, $\mathcal{H}_\infty$ synthesis is an optimization method to minimize the $\mathcal{H}_\infty$ norm of the augmented plant containing weight functions. Here, three weight functions are considered: $\mathbf{W_1}$, $\mathbf{W_2}$[2] and $\mathbf{W_3}$ penalizing the error signal, control signal and output signal respectively as Figure 13.13 shows.

Note that the $\mathcal{H}_\infty$ control design can only be applied to linear systems. However, the identified models in this chapter present delays. The delay T_d can be approximated using "*Padé approximant*" in order to use the $\mathcal{H}_\infty$ framework:

[2]The actuator limits are taken into account thanks to this weighting function.

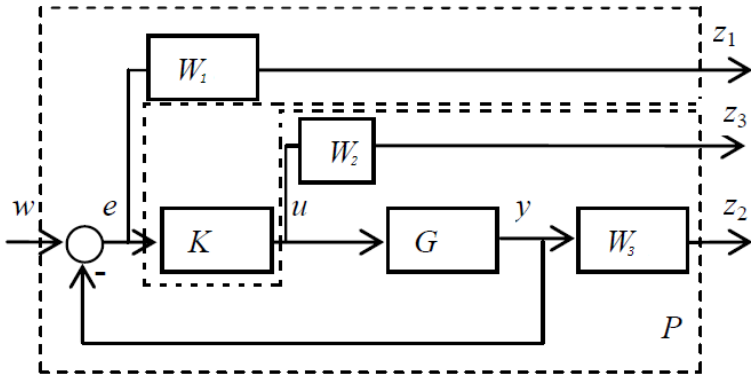

FIGURE 13.13: Augmented plant for $\mathcal{H}_\infty$ synthesis (adapted from (Vasičkanmová et al., 2015)).

$$e^{-T_d s} = e^{-\frac{T_d}{2}s} e^{-\frac{T_d}{2}s} = \frac{e^{-\frac{T_d}{2}s}}{e^{\frac{T_d}{2}s}} \approx \frac{1 - \frac{T_d}{2}s + \frac{(T_d s)^2}{8}}{1 + \frac{T_d}{2}s + \frac{(T_d s)^2}{8}} \tag{13.4}$$

13.2.2 μ Synthesis

As we have seen in Chapter 8, the uncertainty block may be structured (Wal, 1995). This led Doyle to propose in (Doyle, 1982) the concept of "*structured singular value*" commonly referred to "μ". The structured singular value $\mu_\Delta(T)$ is the inverse of the largest singular value of the smallest perturbation $\Delta \in \mathcal{D}$ that makes $(I - T\Delta)$ singular, with T is a complex-valued matrix. Thus, the larger is $\mu_\Delta(T)$, the smaller is the perturbation Δ which is needed to make $(I - T\Delta)$ singular. As there is no analytic method to calculate a μ-optimal controller due to computational difficulties (Vasičkanmová et al., 2015), the approximate solution, known as "*DK-iteration*", is used using Matlab® (Balas et al., 1998).

13.2.3 Comparison

Here, we keep the same weight functions and the same uncertainty modeling. We apply the $\mathcal{H}_\infty$ control design and then the μ control design to the synthesis of the high-level controller based on the uncertain poles of the vehicle dynamics. A step response of closed loops of both controllers applied to the set of identified models form experiments is illustrated in Figure 13.14.

It is clear that μ synthesis is more robust than the $\mathcal{H}_\infty$ synthesis as expected. However, the *DK-iteration* takes a greater amount of calculation time to synthesize the controller, and leads to much higher order than the $\mathcal{H}_\infty$ provides (Santos and Filho, 2012). Nevertheless, safety is our major goal in vehicle motion control. We rather prefer to be cautious and opt for the most robust controller. The μ-synthesis is therefore selected for the high-level controller, and both low-level controllers (4WS and VDC). Each controller is carefully reduced afterwards to avoid implementation issues. We redo the same procedure for different speed values. Controllers' parameters are then extrapolated. A gain-scheduling μ-robust controllers are applied in what follows. Note however the undershoot that some of the uncertain models present.

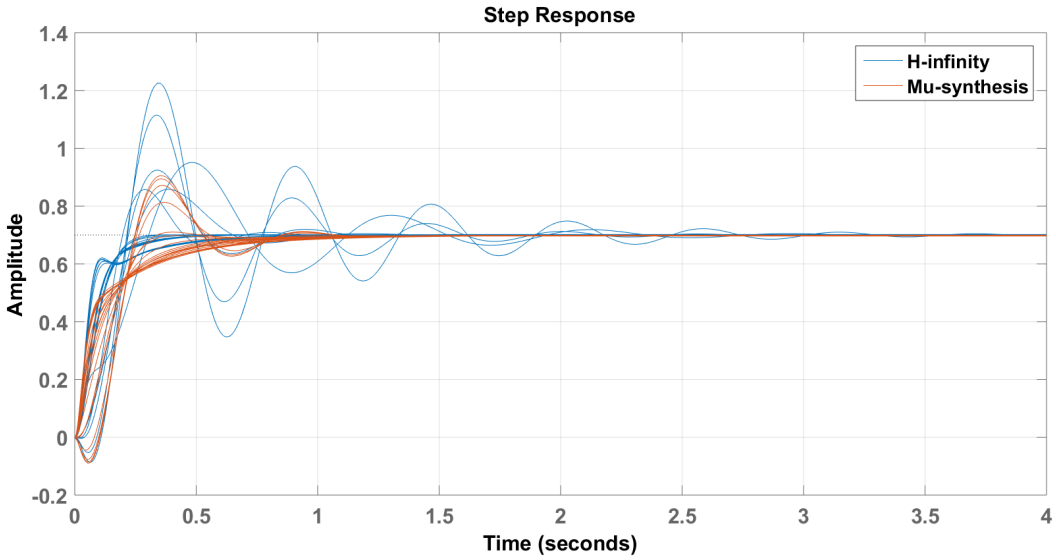

FIGURE 13.14: Comparison of $\mathcal{H}_\infty$ synthesis and μ synthesis.

This is mainly due to the "*Padé approximant*" that introduces a positive zero. This may generate unstable controllers in the real experiments. A better estimation of the pure delay is intended to be adopted in our future work.

Regarding the simplification process, we first compare the Bode diagram of the reduced controllers with the full order controller. The matching frequency range has been enforced to $[0.1, 100] rad/s$. Nichols diagram is then plotted for the selected reduced controllers applied to the set of uncertain systems. For the high-level controller, it would be only the isolated vehicle dynamics. Figure 13.15 shows that at least a controller of order 3 is needed as a high-level controller. The same process is

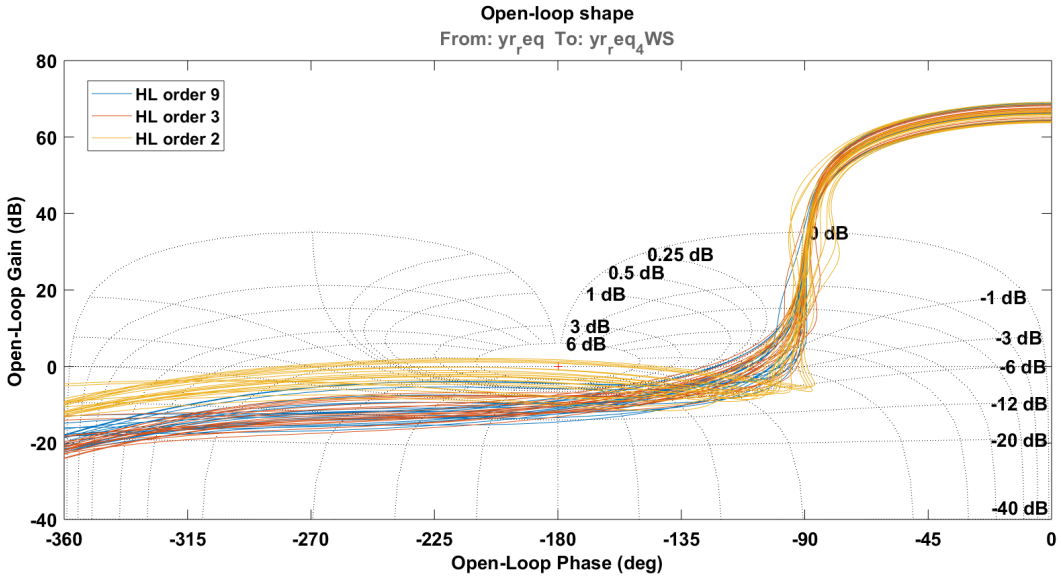

FIGURE 13.15: Nichols plots comparison of reduced high-level controllers applied to isolated uncertain vehicle dynamics.

adopted for the reduction of the low-level controllers. However, in this case, we take

into account the dynamics of the isolated vehicle dynamics, the actuator dynamics, and the reduced high-level controller. Figure 13.16 shows the performances of the high-level controller obtained with respect to the chosen weighting functions. The same performances are evaluated in Figure 13.17 with the corresponding weighting functions for the 4WS system combined with vehicle dynamics with both the high-level and low-level controllers.

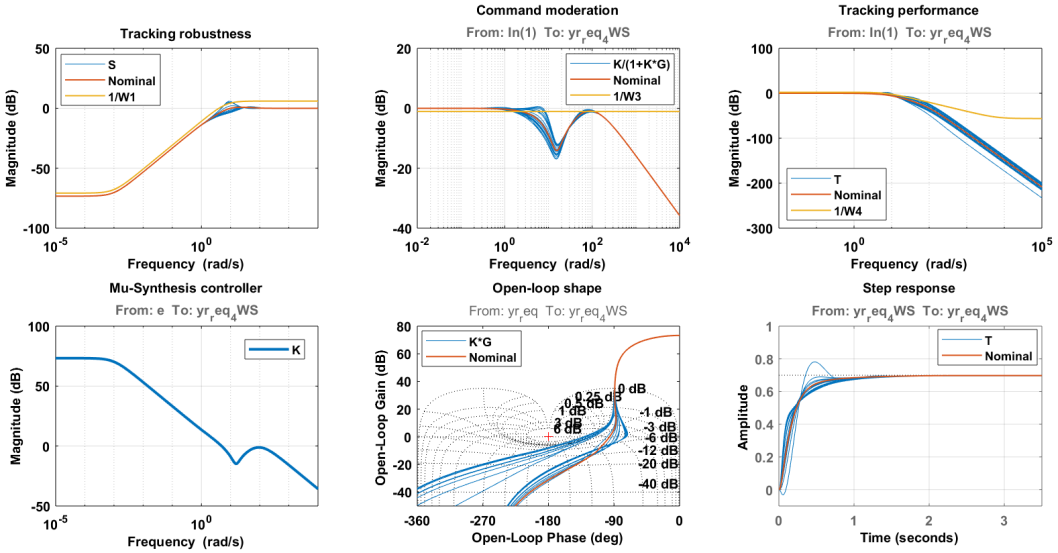

FIGURE 13.16: The high-level controller performances on the set of uncertain vehicle dynamics.

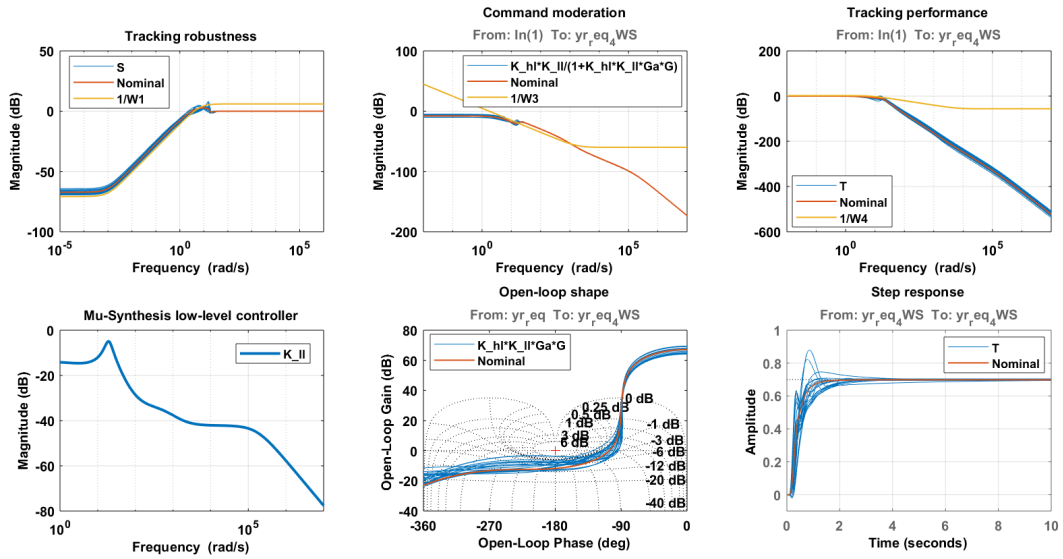

FIGURE 13.17: The low-level controller performances on the set of uncertain 4WS system dynamics plus the uncertain vehicle dynamics.

13.3 CA

The problem to be solved here is how to distribute the desired global control effort calculated by the high-level controller into the effectors. In our case, the control vector contains the controllable tire forces:

$$\vec{\delta} = \begin{bmatrix} F_{x_{fl}} \\ F_{x_{fr}} \\ F_{x_{rl}} \\ F_{x_{rr}} \\ F_{y_r} \end{bmatrix} \tag{13.5}$$

$\vec{\delta}_{min}$ and $\vec{\delta}_{max}$ reflect tire limits with respect to the friction ellipse concept (Kissai et al., 2017):

$$\begin{cases} F_x \leq \sqrt{(\mu F_z)^2 - F_y^2} & (13.6) \\ F_y \leq \sqrt{(\mu F_z)^2 - F_x^2} & (13.7) \end{cases}$$

We suppose that the friction coefficient and the vertical loads can be estimated using for example the methods detailed in (Kissai et al., 2018c) or Chapter 7. The longitudinal speed is constantly controller by the driver. This time, as a first step, the desired acceleration $\vec{v}$ contains only the global yaw moment $M_{z_{tot}}$. The effectiveness matrix $\mathbf{B}$ is filled by geometric relations between the vehicle and its tires using equation (13.3):

$$\mathbf{B} = \begin{bmatrix} b_{1,1} & b_{1,2} & -\frac{t}{2} & \frac{t}{2} & -l_r \end{bmatrix} \tag{13.8}$$

where:

- $b_{1,1} = l_f \sin(\delta_f) - \frac{t}{2}\cos(\delta_f)$,
- $b_{1,2} = l_f \sin(\delta_f) + \frac{t}{2}\cos(\delta_f)$.

Due to interfaces issues, the CA layer is not located between the high-level controller and the low-level controllers as in Chapter 10. Here, the CA algorithm acts more like a supervisor that quantifies the amount of effectiveness that each subsystem should satisfy. Therefore, a simple integrator has been added upstream the CA algorithm to transform the yaw rate error into the global yaw moment required to steer the vehicle. Downstream the CA, the fractions $\frac{\left|b_{i,j}F_{x_{i,j}}\right|}{|M_{z_{tot}}|}$ and $\frac{|b_{1,5}F_{y_r}|}{|M_{z_{tot}}|}$ are determined to evaluate the percentage that each actuator should satisfy to control to overall vehicle. Only these percentages are implemented between the high-level controller and the low-level controllers.

Regarding the online optimization solver, again according to the comparison given in paragraph 10.4.3, the WLS formulation based on ASA is chosen due to its rapidity to solve the problem with good precision and reach the optimum in a small finite number of iterations. This gives the following expression:

$$\vec{\delta}_{opt} = arg \min_{\vec{\delta}_{min} \leq \vec{\delta} \leq \vec{\delta}_{max}} \left\| \mathbf{W_u} \left(\vec{\delta} - \vec{\delta}_p \right) \right\|^2 + \gamma \left\| \mathbf{W_v} \left(\mathbf{B}\vec{\delta} - \vec{v} \right) \right\|^2 \tag{13.9}$$

13.4 Results

Two major features should be verified in this section: control robustness and CA benefits. Regarding control robustness, we compare controllers developed and validated by co-simulation using a high-fidelity software as in the previous chapters, and the controllers developed in this paper using an experimental maneuver. It should be noted that the controllers have been discretized according to the provided ECUs with a sampling time of $10ms$ using the method of "*Tustin*".

To show the benefits of CA algorithms, we only use simulation of the identified models by experiment. We did not carry experimental maneuvers due to lack of time and unavailability of prototypes for a long period of time.

13.4.1 Control Robustness

In chapters 10, 11 and 12, the control strategy has been tested using co-simulation of Matlab/Simulink® and Simcenter Amesim®. A high-fidelity vehicle model with 15 degrees of freedom provided by Amesim has been adapted to meet the nominal parameters of the real vehicle prototype. This has led us to synthesize a relatively simpler and structured $\mathcal{H}_\infty$ controller as a high-level controller, and adaptive gains as low-level controllers based on the LPV tire model (Kissai et al., 2017).

We carried an experiment of a slalom at a speed of $50km/h$. By applying the experimental input signals into the co-simulation platform, using the controller developed in Chapter 10 we obtain the Figure 13.18.

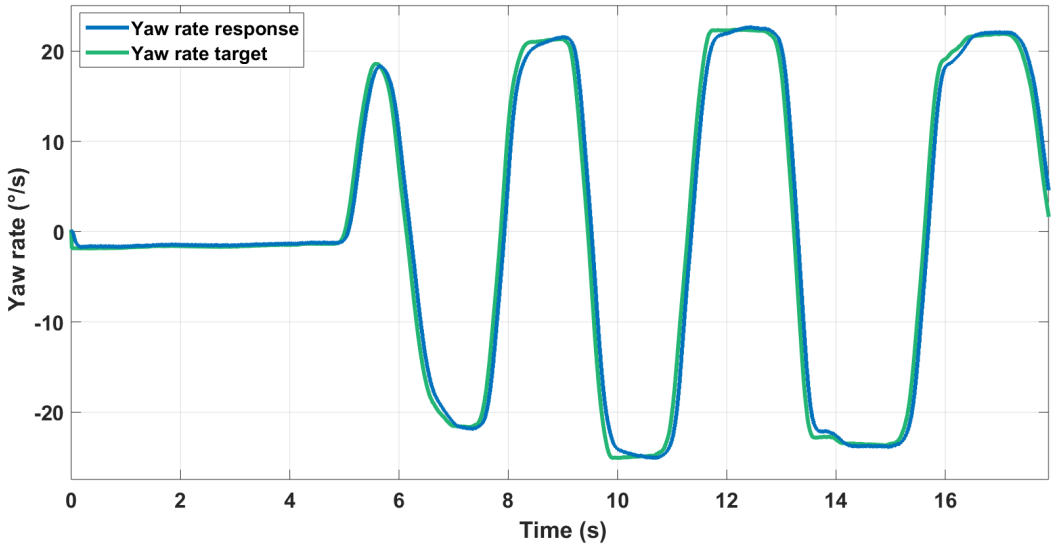

FIGURE 13.18: Co-simulation of the yaw rate control.

This suggests good performance of this simpler logic and may lead us to validate it. Now when we apply the same control logic to the identified models by experimentation, we obtain the Figure 13.19.

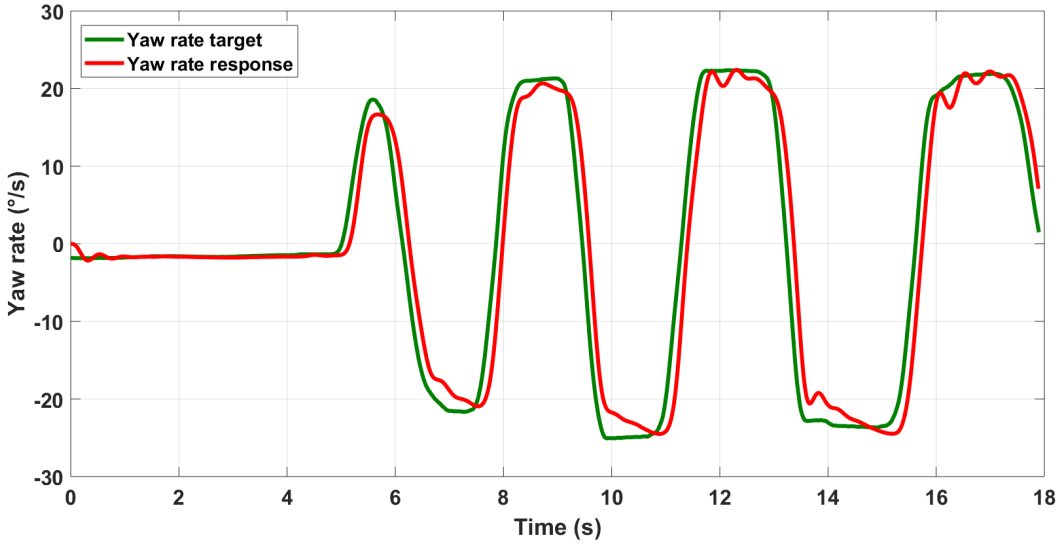

FIGURE 13.19: Yaw rate control using the identified model.

The control starts losing its precision even in this simple maneuver. Note also the fluctuations that start showing up which is an indication of the limit of stability. One could suggest that the identified models may be faulty or too restrictive. That is why we carried out the slalom maneuver once again by using the robust controllers developed in this Chapter. The comparison between the experimental response and the simulated one using the experimental identification is illustrated in Figure 13.20.

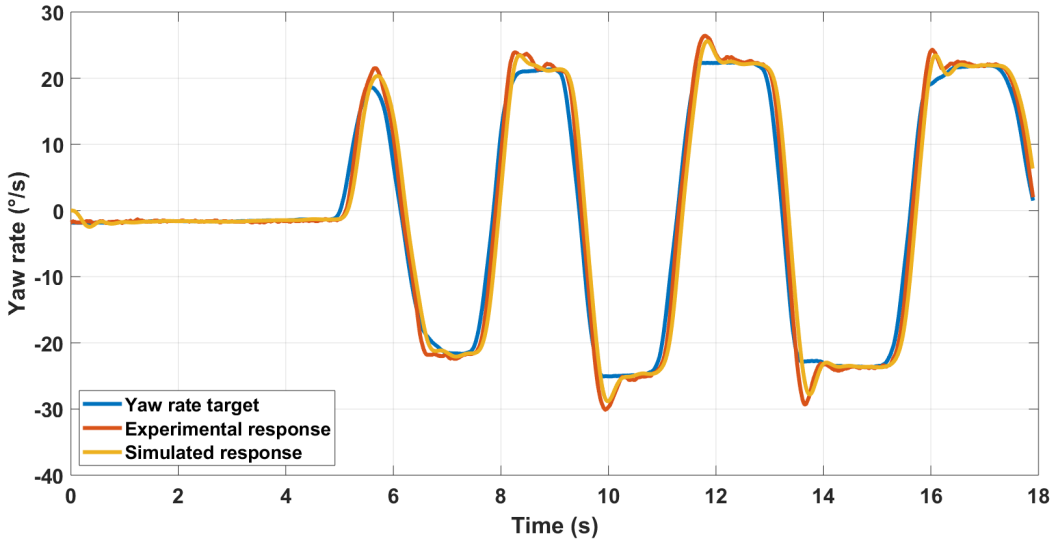

FIGURE 13.20: Comparison of the experimental response and the simulated one.

The simulated response using the identified models is almost identical to the experimental one. In addition, the control is more precise and stable. The overshoots are almost inevitable in order to obtain good performances. When using the new controller developed in this chapter, we obtain the Figure 13.21.

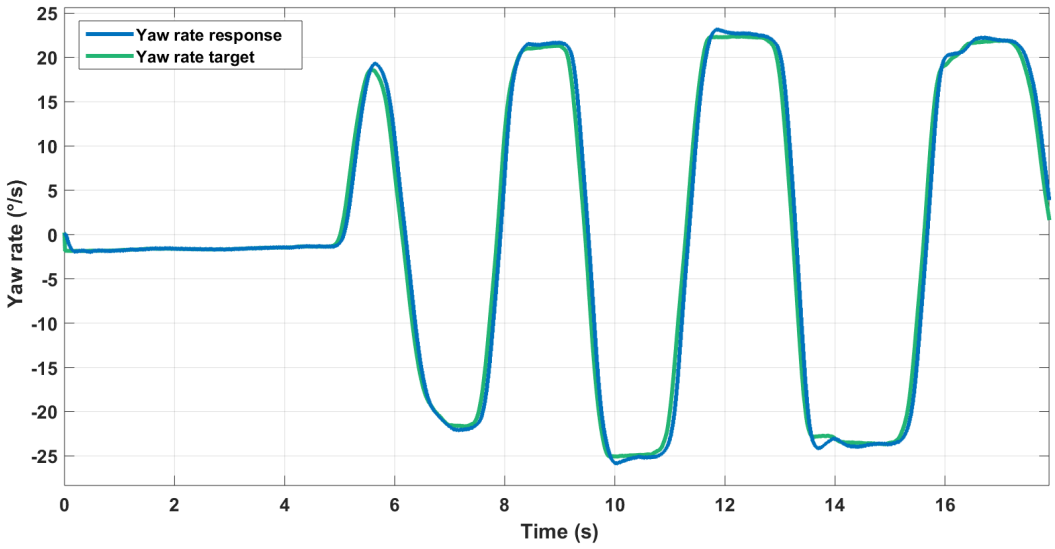

FIGURE 13.21: Response of Amesim model using the new controller.

Results in Figure 13.21 resemble those of Figure 13.18, because the real dynamics of the actuators are not precise enough in Amesim models. This proves that the identified models are more representative than the high-fidelity software, and therefore the need to develop new identified models for advanced chassis systems, especially in an MBD framework. These models can vary from an experiment to another. To overcome this, dynamic uncertainties can be applied to a chosen nominal model, and a robust controller can be developed based on the set of uncertain models identified to ensure successful real-life control applications. To verify that the controllers synthesized respect the speed limits of the actuators and overcome the problem described in Figure 13.2, the simulations are redone with and without taking into account the actuator speed limits in Figure 13.22.

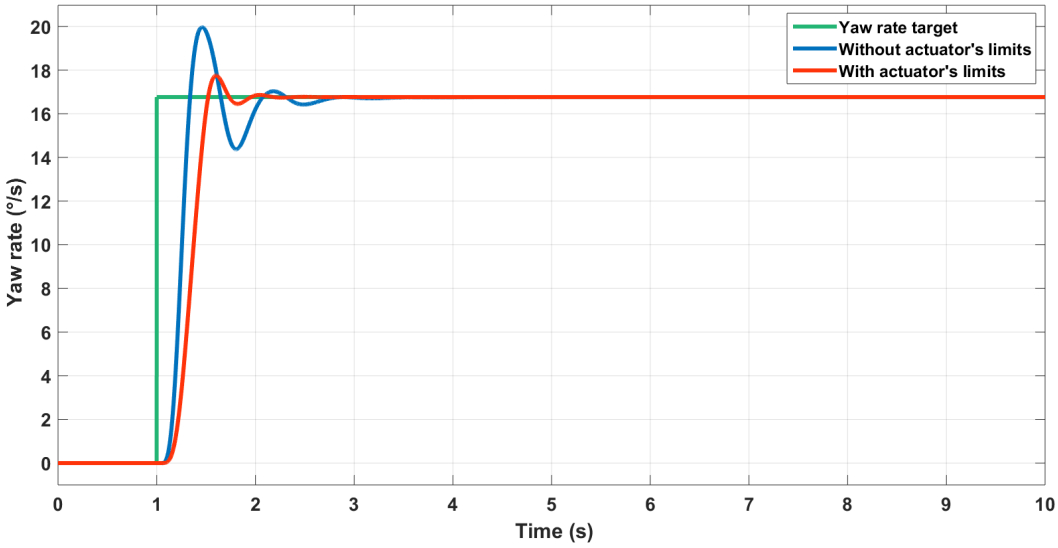

FIGURE 13.22: Comparison of the controllers with and without taking into account the actuator speed limits.

Taking into account the speed limits of the actuators prevent generating high overshoots. This is important as these overshoots induce undesirable motion feelings as a driver and as a passenger. It should be noted that the CA strategy has been optimized, and that the simulation time is now only 4s, which makes it suitable for real-time applications.

13.4.2 Benefits of Optimal CA

As the identified models have proven their precision with respect to the real behavior of the over-actuated vehicle, simulations can be conducted to foresee the performance of the CA layer. We plan in the future to test also severe situations as fault-tolerance, actuators' saturation and so on, once we figure out all the technical problems due to the different actuators.

In order to show the benefits of CA, we test the over-actuated vehicle in its limits of handling, but in realistic scenarios. Let us suppose for example a sporty vehicle going at a speed of $70km/h$. The vehicle encounter a progressive cornering where it should steer. The yaw rate target resembles then to a ramp. We first test the vehicle equipped by only the 4WS system. Then, we add the VDC with a simple downstream coordination strategy consisting in deactivating the 4WS system when the vehicle loses control and activating the VDC as an emergency backup. Finally, we add the CA layer to optimally coordinate both systems when they are activated at the same time. Figure 13.23 shows the results.

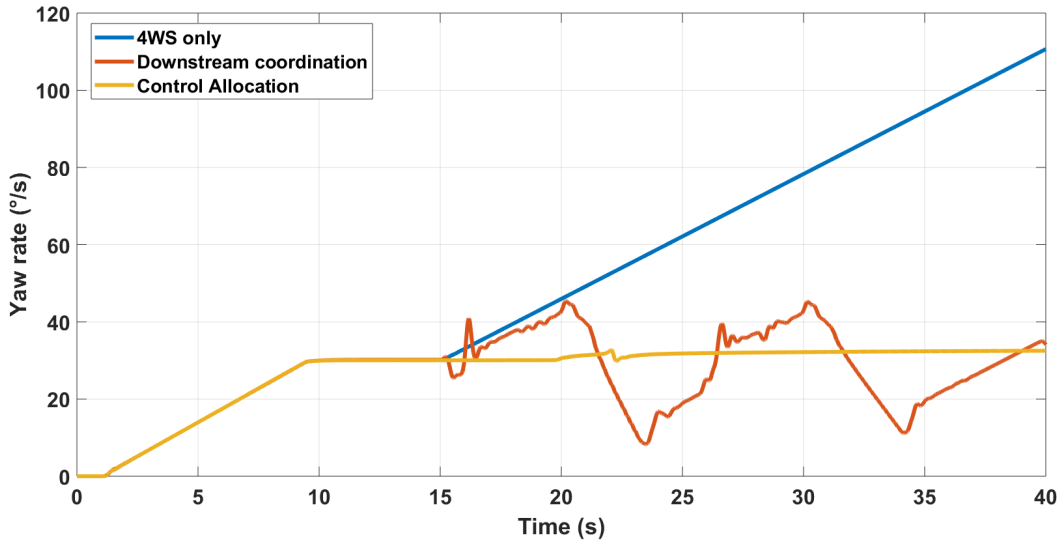

FIGURE 13.23: Comparison of systems coordination methods.

Note that in this situation we let the front steering angle continue growing to see if the chassis systems can detect the limit of handling and saturate the command. The 4WS system saturates around $t = 15s$. If only the 4WS system is activated, the front steering angle influence takes over which make the vehicle exceed the limits of handling. Regarding the simple downstream coordination, switching controllers in this severe maneuver can reduce the amount of yaw rate but destabilizes the vehicle as soon as the 4WS system is saturated. Thanks to the CA layer, these problems can be overcome. Both subsystems are activated at the same time. Optimal coordination

is ensured not only when actuators are saturated, but also when the friction circle limits are not respected.

13.5 Conclusion

In this chapter, two major aspects have been discussed regarding passenger cars motion control: robustness of the control especially when the subsystems provided by the suppliers come in a black-box, and the coordination strategy once the vehicle becomes over-actuated. Control synthesis have been carried using μ-robustness framework, and CA algorithms have been applied to optimally coordinate the embedded systems.

Contrary to previous chapters, controllers have been synthesized using identified models from experiments. Today's high-fidelity software fail to depict the real dynamics of advanced chassis systems. This proves the limits of co-simulation procedures for future vehicles and the need to upgrade high-fidelity softwares or adopt the design methodology presented in this chapter. Another solution could be tackling the "*openness*" problem by both manufacturers and suppliers to design open-boxes modules for an efficient overall vehicle motion control logic without jeopardizing the intellectual properties of each stakeholder.

CA algorithms also prove their benefits when it comes to expanding the potential of the vehicle. As we are advancing towards the full-autonomous driving, more systems are intended to be implemented. The more numerous the embedded systems within the same car will get, the more relevant these algorithms would become as the most important interface between the manufacturer and its suppliers. These algorithms need to be tested by experiments also to evaluate their real performances and limits. One of the already identified problems is the fact that subsystems have different delays and different time-responses. As mentioned in Chapter 9, only non-predictive C_α algorithms are investigated in this thesis. In the context of over-actuated systems with different delays, predictive C_α algorithms are worth investigating in the near future.

13.6 Contributions

Our contributions extend to experimental results. The overall control architecture have been simplified in order to be implemented in a real vehicle. Several experimentations have been carried to identify the remaining technical problems that should be overcome. To the best of our knowledge, this is the first attempt of implementing such complex solutions into a real vehicle. The farthest application of C_α algorithms in ground vehicles is in HIL (Heidrich et al., 2013), (Soltani, 2014). This first experimental feedback has been submitted to:

- M. Kissai, B. Monsuez, A. Tapus, D. Martinez and X. Mouton,"Robust Control for Over-Actuated vehicles," *2019 IEEE Conference on Control Technology and Applications (CCTA)*, Hong Kong, 2019. ***Accepted***.

- A more detailed discussion has been submitted to:

  Kissai, M., Monsuez, B., Martinez, M. and Tapus, A. "Optimal Coordination of Chassis Systems in Simultaneous Operations," SAE International Journal of Connected and Automated Vehicles, Special Issue on Revisiting Chassis and

Powertrain Design for Automated Vehicles, 2019. ***Submitted*** on April the 26th, ***Accepted*** on August the 18th.

In this part, both approaches have been first compared in the ARS-VDC coordination context. The downstream approach needs few modifications by adding only a coordination layer downstream the standalone subsystems. Less complexity is involved, and probably also less cost. We can understand the motivation of car manufacturers to adopt this approach as long as there are only few conflicting subsystems. Nevertheless, even in this simple configuration, the downstream approach can only satisfy a single objective. In contrast, the optimization-based CA algorithms offer already additional benefits by solving multi-objectives problems.

In addition, the upstream approach have been applied to configurations that are more complex by considering more than two implemented chassis systems. One major advantage should be highlighted is the fact that the same overall control architecture has been applied in all systems combination. The upstream approach offers an extensible control architecture that remains valid independently from the nature of the system implemented and how many systems are applied. Each new system can be integrated in a "*plug-and-play*" way without important modifications of the algorithms involved. This comes essentially from the fact that from the beginning we wanted to propose a standardization of integrated vehicle dynamics control architectures to suit best upcoming challenges of future automated vehicles. It should be noted that the thesis focus on the necessity of adopting the upstream approach, and not comparing the different chassis systems combination. The choice will depend also from cost constraints, energy consumption and other parameters. Be that as it may, the upstream approach can be adopted in most cases, and could be very beneficial for offline studies of each combination effectiveness.

However, as Chapter 13 shows, additional technical problems should be first solved before proposing any standardization. Each subsystem comes with its own unique dynamics. To top it all off, most of suppliers provide their embedded systems in black boxes. The development of any architecture should go along with field experiments to diagnose early enough any rule-based or internal control logic implemented by the supplier that may influence the overall dynamics of the vehicle and avoid redesigning the multiple complex layers of the control architecture. In spite of the fierce competition that exists in the automotive sector, we expect from car manufacturers and their suppliers to enable a degree of "*openness*" once they realize the benefits of developing an overall coordinated control architecture.

14 Relevance of Optimal Control Allocation for Future Vehicles

As we have previously mentioned, the number of integrated chassis systems is increasing. From ADAS to full autonomous driving, additional chassis systems are intended to be added to fulfil all driver maneuvers. Both longitudinal and lateral control have to be ensured at the same time. Dynamic couplings can no longer be ignored. More complex modelling is needed, and therefore more complex control strategies are required.

In this chapter, we will first focus on the relevance of the new classification of integrated automotive systems architectures. The proposal of only two antagonist approaches allowed us to identify rapidly the problem with the current approach and how to remedy it. The tire model is also put on the spotlight. A major difference between the two approaches is actually the omission of the real constraints of the tire, which becomes problematic in coupled maneuvers. The new tire model is implemented in the upstream approach and compared to the downstream approach to show the advantages of the proposed approach for future vehicles. The upstream approach is particularly relevant for autonomous vehicles when lateral and longitudinal control should be coordinated. A summary is given at the end of this chapter.

14.1 Relevance of the New Classification

Two enriching reviews of integrated architectures have been proposed in (Gordon, Howell, and Brandao, 2003) and (Ivanov and Savitski, 2015). In (Gordon, Howell, and Brandao, 2003), emphasis has been put on the architectures' topology. The authors pointed out two major extremes, *the fully decentralized control* and *the fully centralized control*, considering the *supervisory control* as an intermediate between them. This allowed the authors to highlight the benefits of a multi-layer architecture and to draw specific requirements related to the architecture topology: *modularity*, *simplicity*, *fault-tolerance*, and *openness*. However, no relations were proposed between the different structures and control objectives. The authors in (Ivanov and Savitski, 2015) focused rather on control objectives. Two classes have been proposed: *single-criterion* and *multi-criterion*. They studied a large amount of examples for both classes, but conclusions were limited to the control methods and challenges. They particularly highlighted that most *single-criterion* solutions are using rule-based methods (e.g. fuzzy logic control), while recent researches around *multi-criterion* control are switching their focus towards optimization methods, especially CA. Unlike (Gordon, Howell, and Brandao, 2003), no discussion about the architectures topology is provided. Fuzzy logic for example could be used downstream the stand-alone subsystems for single-objective control (Selby, 2003), or upstream the stand-alone subsystems for multi-objective control (Boada et al., 2006).

In order to gather the different stakeholders to start thinking on the standardization of integrated vehicle dynamics control architectures, we had to make a bridge

between the two types of classifications. For this reason, we believe that the architecture topology should be related to the control objective. As we are interested in subsystems coordination, classification of topologies should be linked to the coordination layer position with respect to stand-alone subsystems. The distinction of "*the downstream approach*" and "*the upstream approach*" and their suitability for control objectives could be more representative from an industrial point of view. The control designer would be able to choose automatically a standardized architecture depending on its objectives. *Upstream* or *downstream coordination* not only designate where, but also how the coordination is managed. This has allowed us to link each approach to control objectives. When the coordination is made downstream, rule-based control design is used. This technique can handle well single-objective control problems. As more interactions are added, it is hard to foresee the different couplings induced, so it is more complicated to formalize additional rules to achieve safe coordination. When the coordination is made upstream, the control design is based on a coupled vehicle model. Different interactions could be predicted. With an adapted optimization technique, multi-objective control problems can be handled.

14.2 Necessity of a More Accurate Tire Model

As tires are the sole effector for ground vehicles, commands distribution should focus on how to use optimally the four tires. The tire with the bigger potential to influence vehicle dynamics should be favored. This potential depends on mainly three criteria: combined slip, vertical load, and the interface rubber/ground state, which is represented by the friction coefficient. Not taking into account this criteria could saturate one or several tires and therefore destabilize the vehicle while other tires could be used to achieve the maneuver.

Tire potential manifests itself in its ability to adhere to the road. This can be represented by the tire stiffness. This stiffness should be therefore updated on-line to take into account the varying criteria mentioned. Moreover, the tire model should be suitable for control synthesis. Its complexity should be then reduced. A linear model is thus preferred. For all these reasons, the new LPV tire model is more suitable for GCC synthesis. It should be therefore implemented in autonomous vehicles.

14.3 Comparison of the two approaches

14.3.1 Complexity

The main advantage of the downstream approach is its low complexity. The design methodology consists in first studying the interactions between two or more systems and then establishing adequate rules to benefit from their potential synergies. This could be done for example by using a fuzzy logic approach or the β-phase plane control (Selby, 2003). These rule-based algorithms can be foreseen as long as few systems are implemented.

Regarding the upstream approach, complexity is rather the main drawback. The coordination lies on a coupled non-linear vehicle and tire models, and real-time optimization techniques. However, the more complex the interaction between the competing systems gets, the more this upstream approach is pertinent, and could even become necessary for future highly over-actuated vehicles.

14.3.2 Cost

The downstream approach has its own advantages in terms of cost. Without modifying the structure of the subsystem control logic, car manufacturers can proceed to bulk purchasing from their suppliers and take advantage from the economy of scale. The architecture does not require additional controllers, but simply a coordination strategy made downstream. Unfortunately, this is not the case for the upstream approach. Not only additional high-level controller(s) is(are) needed, but it may also require additional sensors or estimators (Heidrich et al., 2013). For these reasons, auto-makers are reluctant to implement this approach in real vehicles. However, the ECUs have became faster, less cumbersome, and cheaper through the years. And as pointed out in (Selby, 2003), adding a high-level controller allows exploiting the same information in several subsystems. Few sensors can then be reduced as well as computational overheads by not duplicating controller computations. A revaluation of the overall costs might be required.

Indeed, complementarity of systems could reduce considerably the overall cost. Smart actuators and new technologies are expensive. If autonomous vehicles rely on such systems, and if no complementarity is proposed, these systems should be redundant for safety requirements. Unlike this common practice, making integrated systems act as a backup for different other critical systems could reduce the number of necessary redundant systems. Calculators hosting online optimization algorithms may be more expensive, but the number of ECUs may be reduced (Wallentowitz, 1990). A deep safety study should however be carried out before taking any decision for commercial cars.

14.3.3 Safety

One of the most important criteria, if not the major one, that will make humans accept or refuse autonomous vehicles, is safety. Active chassis systems were invented to assist the driver in complex maneuvers to ensure passenger safety. The vehicle is becoming more and more automated, and it is expected that safety will increase with this practice. In this context, several researches are carried in different fields. Robotic vision is used to give the vehicle more information about its surrounding, data fusion is performed to make better decision taking into account all the information sensed, artificial intelligence enables the vehicle learning from the driver preferences and so on. Most of these researches are focused on the surrounding of the vehicle due to its complexity and uncertainty. However, the vehicle internal systems are also of major importance. These systems should be ready to operate safely at every possible situation. It is irrelevant to generate a robust decision if the vehicle cannot be controlled in such a way to satisfy this decision. Therefore, performance should be maximized while taking into account all physical limits.

In a downstream approach, rule-based algorithms are used to favor one system over another. These rules can be formulated when a small set of parameters are concerned. For example, in the simple example of ARS-VDC coordination, subsystems influence on the overall vehicle depends on longitudinal deceleration and actuators saturation. These criteria were chosen to coordinate between both subsystems. Other important parameters were ignored, as the vertical load dynamic variations and tire saturation. The reason is that these parameters should be taken into account before the command generation as the effector is influenced by the commands and not the opposite. Figure 14.1 illustrates the unsuitability of the downstream approach.

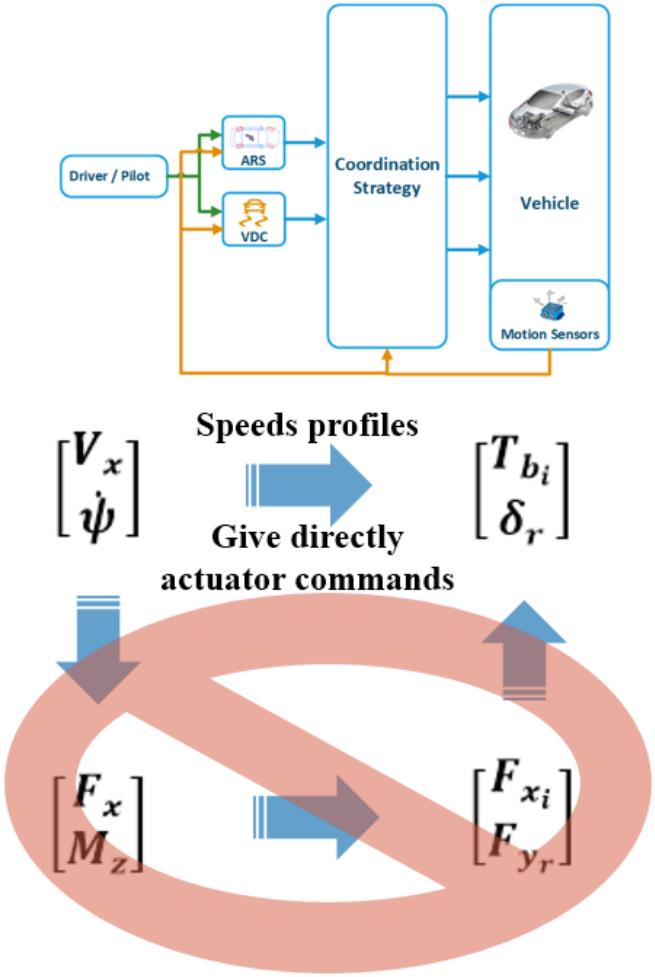

FIGURE 14.1: Unsuitability of the downstream approach.

A considerable effort has been made to make the downstream approach give good results, while actually in most commercial cars, this is not the case. Our mission extends to the proposal of a roadmap from the downstream approach to the upstream one. As only specific rules are proposed in a downstream configuration, we cannot prove if optimal solutions are provided. Therefore, the performance is not maximized. This is why this approach is used to handle single-objective problems while secondary objectives can be fulfilled. Due to costs constraints, a car manufacturer could not integrate a large number of chassis systems. To achieve bigger potential with the same set of chassis systems, the coordination approach should be reinvented.

Regarding the upstream approach, an optimization-based method is proposed. The algorithm enables knowing if best performances can be achieved, a sub-optimal solution can be proposed, or if there is no solution at all. Performances can be maximized. This is mainly due to the fact that interactions management has been brought up to a higher level of abstraction. In this configuration, tire limits, vertical load variation and so on can be taken into account before allocating the requests to the different subsystem. This, however, can only be done if a more complete description of tasks is ensured. This shows also the pertinence of the new tire model in this context, as it enables this description while keeping a simple formulation. With

the same number of chassis systems, better performances can be achieved, which gives the possibility of integrating additional features to improve the vehicle's safety.

Making subsystems complementary has the important advantage of improving safety. As it is shown in Chapter 10, fault-tolerance can be ensured by simply modifying the effectiveness matrix in order to take into account the actuators' state. When a fault occurs, the value of the effectiveness matrix is updated by representing the new situation. The control is then redistributed favoring healthy actuators. Co-simulations proved the effectiveness of this method in severe maneuvers as the double lane change.

14.3.4 Potential

The fact that the downstream approach is based on "expert knowledge", and because we cannot foresee all the possible use-cases, it is hard to measure this approach's potential. Another issue is the fact that the subsystems control laws may be based on different reduced vehicle models. As a result, putting together different systems based on different behavior models does not ensure proper operation of the overall vehicle system. In contrast, the upstream approach depicts mathematically the dynamic interactions, which is more suitable for numerical processes. Couplings can be quantified, so we can have some insights about the possibility of finding an optimum solution, a sub-optimal solution or no solution at all. The conflicts are rather prevented than mitigated. The upstream coordination techniques have more potential in terms of handling multi-objective control problems.

Actuators' faults and constraints are not the only reason for CA redistribution. Ground vehicles' performance is closely related to road friction. Coefficient of friction sudden changes are the cause of many accidents (Van-Zanten and Bosch-Gmbh, 2002). Even if it is said sometimes in the police jargon that 90% of accidents are due to driver errors, 50% of these accidents are actually due to the environment (Brown, 1971). Normal drivers' experience is limited largely to driving well within the physical limit of adhesion, and this should be taken into account. ADAS should be then effective beyond this limit. Redistribution of CA could be used to face this problem. As Chapter 11 shows, loss of potential due to friction change can be estimated. Weights related to the maximum potential of each tire can be added to the parameters φ_i. In this way, if a tire approaches saturation, weights will decrease to near zero making the control redistributed to other non-saturated tires. Consequently, the overall potential of the four tires can be used by the different integrated systems expanding the vehicle performance. Nevertheless, the estimation of the coefficient of friction still needs to be robustified. An ongoing work is carried out in order to overcome this challenge by means of closed-loop observation techniques.

Another reason why autonomous vehicles stakeholders should favor this approach, is the ability of solving multi-objectives problems. As it was shown in (Shyrokau et al., 2013), CA is able of not only preserving stability, but also favoring actuators with the least impact on energy consumption, which is very attractive for electric vehicles. This approach can also be used to generate different motion feelings. This is particularly very important for autonomous vehicles, because the challenge is not only following automatically a trajectory, but also how to follow this trajectory and which dynamics should be generated while following this trajectory. As motion feelings are related to vehicle's accelerations according to ISO 2631-1, CA can be executed by combining forces respecting this standards and generating more expected motions to make drivers trust their vehicles.

14.4 Relevance for Autonomous Vehicles

In the context of autonomous driving, dynamic couplings have to be considered. Until now, the driver ensures the longitudinal control by accelerating or braking. Most of ADAS are designed to stabilize one aspect of the vehicle. While controlling longitudinally the vehicle, the driver handles unconsciously the dynamic couplings. The virtual pilot has to take over and control the vehicle both longitudinally and laterally. A larger operation range is solicited in this case. More complex vehicle and tire modelling are required. As chassis systems are developed individually, they are generally based on different vehicle models. Their integration is not necessary uniform. Rule-based strategies can handle the problem only if most of the scenarios can be predicted. The more we approach to autonomous driving, the more numerous are chassis systems to be added in the same vehicle to replace the driver, and the more numerous are the scenarios that cannot be predicted in advance. Therefore, the upstream would become necessary despite its complexity.

CA methods express the problem as an optimization problem for an over-actuated system. This gives numerous solutions. Secondary objectives can be then satisfied. For example, the solution that consumes less energy or that gives more comfort can be favored. The upstream approach can then transform the problem in an opportunity. Choice of objectives and a supervisory (high-level control) strategy, gives the possibility for car manufacturers to tune their vehicles' behaviors. This is crucial for companies brand image. Indeed, the driver does not know which system coming from which supplier is integrated in his vehicle. All he judges is the vehicle performances and therefore the car manufacturer.

A major autonomous vehicles challenge is their acceptance by humans. Here, the feeling that generates the vehicle behavior plays a major role. The motion of the car should be done in a way to make drivers trust their vehicle. The difficulty is the fact that the definition of comfort or excitement differs from a driver to another. Current commercial vehicles enable you choose manually the driving mode. We could expect that future vehicles would learn and remember your preferences. However, the most suitable behavior may differ from the three main drive modes. Continuous behavior tuning would be preferred to make driving experience more personalized. This is one of the main innovations of the Group Renault[1]. This tuning is done at the reference calculation level. Again, the vehicle should be able to respond correctly and generate the expected feeling. A smart coordination between chassis systems should be ensured. This could be done by formalizing a multi-objective problem. Different weights could be affected to the objectives. These weights could be made variable and vary with the driving mode target to favor a set of subsystems over another. For example, if a more comfortable behavior is required, soft steering will be favored by means of the ARS system or the EPAS system. For people that prefer more sporty vehicles, allocation can be made so as to favor engine torque distribution based systems using the 4WD system or the TV system. Formalizing secondary objective can be done directly using variable weights. The solution will simply depends on these weights, and command distribution would be made so as to favor the feeling desired. Chapter 12 actually aims to prove the potential of CA to provide different motion feelings. This could be used to tune the vehicle behavior in order to make autonomous vehicles' motions predictable and then trustful (Hengstler, Enkel, and Duelli, 2016). This can facilitate the acceptance of such robots/autonomous vehicles in the society and then accelerate their development. However, each driver has its

[1] The Multi-Sense project already mentioned.

own perception of what a trustful motion means. The same vehicle motion behavior can therefore generate different feelings among humans, depending on their past experience with non-autonomous vehicles. Not only the CA should be weighted, but a learning algorithm should be added to enable adaptability of the overall control to each individual.

14.5 Summary

It appears that a compromise should be made between complexity, cost, and potential. To avoid complexity, the control designer may prefer a downstream approach as long as the problem consists in a single-objective control. As more interactions are added, upstream approach becomes necessary for safety matters. Although the upstream approach may seem expensive, with advances in electronics and computer science, a revaluation of the eventual cost of each architecture is needed. In addition, various algorithms have been developed and tested. According to (Tjønnås, 2008), (Chen and Wang, 2011), (Soltani, 2014), (Shuai et al., 2014), (Zhao et al., 2015), (Yim, S., 2015), CA methods are more suitable for this problem, especially for over-actuated vehicles. These methods have been reviewed and compared in (Bodson, 2002), (Johansen and Fossen, 2013). Linear Programming (LP) and Quadratic Programming (QP), could be executed in a few milliseconds with a limited number of iterations, which real-time computations require. These advances may finally convince car manufacturers to adopt this approach.

Autonomous vehicles requires from the virtual pilot to take into account multiple objectives at the same time. As we have mentioned, downstream coordination is more suitable for single objective control where the human pilot deals with the rest of his objectives. For example, in a high speed cornering maneuver, the driver controls the longitudinal acceleration while the active steering could be combined with the brake-based yaw control to control the lateral dynamics and stabilize the vehicle. In autonomous driving, these two objectives should be fulfilled at the same time by the virtual pilot. Interactions should be predicted, and conflicts should be avoided rather than mitigated. Consequently, as we are moving towards the autonomous driving, the upstream coordination approach will become necessary. Car manufacturers, equipment suppliers and the new mobility actors should prepare a common overall architecture. This architecture should have the following criteria:

- *Adaptability* to face environment changes and drivers behaviors. This makes the upstream approach with the new tire model particularly more relevant. A high-level control based on gain scheduled H_∞ controller satisfies an adaptive and robust control. Other modern methods as Model Reference Adaptive Control (MRAC) should be investigated (Alan, Yildiz, and Poyraz, 2018).

- *Fault-tolerance* to propose some degraded modes and keep ensuring safety even if one or a group of chassis systems fail. In the example of ARS-VDC coordination, the downstream approach managed to enable a certain degree of fault-tolerance with less performances when the ARS fails. This could be done by adding a rule that activates the VDC whenever there is a difference between the rear angle request and the rear angle command. This would become more complicated to formulate when a bigger set of subsystems is concerned. In contrast, in CA, this is naturally taken into account as command distribution is made depending on available subsystems. It is easily taken into account by adding in the matrix effectiveness the different systems' flags to

update this matrix when a failure is detected. Again, the upstream approach is expected to become more pertinent as we are heading to fully autonomous driving.

- *Dynamic reconfiguration* to ensure soft switching and prevent loss of stability. A way to add this feature is to tune the weighting functions used in CA. Switched control theory should be nevertheless revisited.
- *Extensibility* to insert rapidly additional technologies without redesigning the whole architecture. This is one of the major industrial concerns as autonomous vehicles needs are not frozen yet. The downstream approach is based on specific rules depending on the subsystems involved. This is one of its biggest drawbacks. CA methods are designed to handle over-actuated systems with a dimension of $\mathbb{R}^{m\times n}$. The same algorithm presented in this thesis could be applied to a bigger set, which makes it extensible.
- *Modularity* to ensure flexibility. This actually can be ensured in both architectures.
- *Openness* to support various systems from different sources without jeopardizing the intellectual property rights of the different stakeholders. This particularly constrains both approaches if unexpected rule-based algorithms are implemented within subsystems as seen in Chapter 13.

The multi-layer architecture with optimization-based CA methods presented in Part II seems to be a better choice to fulfill most of these criteria. We recommend therefore the adoption of the upstream approach as soon as possible by both manufacturers and suppliers in order to accelerate its standardization.

15 General Conclusion

15.1 Contributions

In this thesis, a new classification of integrated vehicle dynamics control architectures has been proposed. Two major classes related to the coordination logic have been outlined: the downstream coordination architecture and the upstream coordination architecture. These two classes have been compared. The downstream coordination which represent the state of the art, do not modify the subsystems provided by suppliers. These subsystems are integrated in parallel, which could lead to requests conflicts. Rule-based algorithms are added downstream these subsystems to prevent this risk. This approach is less cost and less complex but it is limited to single-objective control coordination. In contrast, the upstream coordination can handle multi-objective control coordination but it is more complex to design. This approach adds a high-level controller to specify the motion of the vehicle's CoG. Optimization-based CA techniques are added upstream the subsystems to distribute optimally the requests generated by the high-level controller. The literature shows that integrated vehicle dynamics control architectures are still an object of research. There is a clear lack of benchmark standards and common test procedures to validate the integrated subsystems coordination methods. This thesis aims to invite car manufacturers, equipment suppliers and new actors of mobility to adopt an upstream approach and standardize its structure. Car manufacturers and suppliers should join forces in order to establish new standards and a common framework to accelerate autonomous vehicle development. The different stakeholders have to show some degree of openness to avoid tragic conflicts at the vehicle level.

Furthermore, the modeling of vehicle dynamics has been revisited. A global vehicle model is proposed to serve as a starting model that may simplified depending on the controllable states. The tire modeling review led us to propose a new linear tire model with varying parameters has been developed. This model is particularly suitable for control problems and especially for global chassis control. Unlike other linear models, our model takes into account the combined slip in the tire's stable region. It depends also on physical parameters that can be estimated in real-time, which is necessary for online operations. In addition, every equation, as the definition of slip and side-slip, has been redefined. We showed that by considering the complete definition of vehicle's states, a good approximation of the friction circle can be obtained.

As a first step, the ARS system and the braking-based VDC system were chosen as an example to study both approaches. These systems can both influence the vehicle's yaw rate. Co-simulations of Matlab® and Amesim® was used to provide more realistic simulations. The results showed that the upstream approach enables, already with a small set of chassis systems, improvements in terms of safety, robustness, stability and mostly extensibility. The fault-tolerance criterion has been focused on to prove the safety improvement provided by control reallocation algorithms. The results showed that by making complementary different chassis systems, one system can take over another one in severe conditions, avoiding redundancy of the

same system. This gives the possibility of integrating additional systems without costs concerns.

The same configuration has been studied by experimentations using the Renault Talisman. Experiments showed us the problems of working by black boxes with poor communications with manufacturers and their suppliers. Rule-based algorithms can be implemented for safety measures, which hinder the benefit from using the full potential of each actuator. These uncertainties should be also taken into account when designing an overall vehicle motion control strategies. The low-level control is particularly influenced by these constraints. μ-robustness had to be employed in Chapter 13 instead of only direct transformations as in Chapter 10.

Another new problematic regarding motion feelings and vehicle dynamics control has been introduced. A solution using multi-objectives CA algorithm has been proposed in order to tune vehicle's motion. This method is based on amplifying or reducing the acceleration generated by tire forces to generate different feelings. Results by co-simulation showed different use of subsystem when it comes to motion feelings. This comes without jeopardizing the vehicle's stability ensured by the high-level control layer. This demonstrates the need of implementing such algorithms in future cars, especially for autonomous cars so their behavior stays predictable and fit best drivers' preferences.

Safety through fault-tolerance, and comfort through C_α and reference tuning have been employed in various configurations. In chapters 10, 11 and 12, different chassis systems combinations have been employed. Our goal was to prove how flexible and extensible the upstream coordination approach can be. The control architecture remains the same. The solutions for each block may vary from a scenario to another. The vehicle model and therefore the high-level controller depends on how many states can be controlled. As the number of vehicle's states to be controlled goes higher, the higher-level controller becomes more complex and should take into account the vehicle dynamics couplings in a MIMO framework. Regarding the CA problem, again, as the number of vehicle's states to be controlled goes higher, the number of the lines of the effectiveness matrix goes higher. And the more numerous the embedded systems become, the more numerous the number of columns of the effectiveness matrix become. The optimization problem becomes more complex. More effective ECUs should be implemented in this case. The low-level layer depends on the corresponding subsystems. This layer should handle specific features of each system, as pure delays, speed limits and so on. These information should be shared by the upper layer, namely the CA layer, so the control distribution takes into account not only the effectiveness of each actuator, but also its dynamic constraints. Nevertheless, the same overall approach can be applied each time. This thesis serve to prove its feasibility, efficacy and effectiveness to handle future vehicle control issues. We believe that the complexity added by the upstream approach is justified by the approach's numerous advantages.

All these contributions led to sixteen publications when we explained each problematic apart. A list of papers is provided at the end of this document. The authors recognize however that more evidence are required through experimentation. Our hypothesis must be solidified by real experiments before proposing any standards. More collaboration from car manufacturers are expected in the future.

15.2 Future Works

Our future works aims to carry first experimental campaigns of the multi-layer architecture with CA methods presented here. Its comparison with the downstream approach is cardinal to convince the different stakeholders to adapt the upstream approach. In addition, each solution adopted for each layer can still be improved as the following subsections show.

15.2.1 Real vehicle implementation

The first challenge is to be able to implement the overall multi-layered architecture in a real vehicle. Real-time computation of an optimization method is usually a challenging task. In Integrated Vehicle Dynamics Dynamics Control, the challenge gets bigger as the coordination technique is located in an inner loop. Consequently, a higher rate is required. CA with quadratic programming could be the solution where the computation is mush more faster (Bodson, 2002), (Johansen and Fossen, 2013). A first feedback from the experiments carried in this thesis have showed us an additional challenge related to the internal dynamics of each subsystem. The control should be robust regarding also the uncertainties of the black-boxes provided by the suppliers. Otherwise, the different stakeholders should opt for more open solutions. Indeed, integrated systems can be very different. As shown in Chapter 13, the 4WS and the VDC systems have different delays. When distributing the commands, the C_α layer should not take into account only the effectiveness of each subsystem, but also their latencies. In this context, predictive C_α algorithms should be also investigated.

Regarding friction estimation, the simulations presented in this thesis consider availability of accurate measurements. Additional difficulties are expected in case of real experiments that may need additional efforts to adapt this strategy. More specifically, two problems would arise. The first one is the fact that the Inertial Measurement Unit (IMU) gives noisy signals regarding the vehicle's acceleration measurement. These measurements may also contain few offsets. In addition, the IMU does not differentiate between variation in acceleration due to the vehicle motion or the variation due the standard gravitation orientation in slopes. A difference between the measured acceleration and the estimated one could lead to wrong friction coefficient estimation. Secondly, in the process of friction coefficient estimation, we considered a constant value of the mass, inertia ... etc. The estimation is not robust nor adaptive. More efficient and complex observers should be tested. The method presented in this thesis serves as a first step towards a better estimation. The goal is to show that the rigor in formulating vehicle dynamics could already bring few benefits in the estimation process.

15.2.2 Robustness-Performance Compromise

One of the most important features of control engineering is robustness. A big part of this thesis has been dedicated to this problem. If the plant model is well-known, the designer can aim for high performances using high gains. However, when the plant model presents important uncertainties, robust controllers should be designed for a set of uncertain models where the real model is guaranteed to be. A stationary controller can only stabilize a whole set of uncertain models for less attractive performances. This is actually a classic control engineering trade-off (Larminat, 1993). However, this concerns only stationary controllers. Adaptive controllers are being investigated and represent one of our future works. Particularly, the Model Reference

Adaptive Control (MRAC) commonly used for linear time-invariant systems with uncertain parameters has attracted our attention (Alan, Yildiz, and Poyraz, 2018). The idea is to be able to constantly identify online the plant model and reduce the uncertainty to be able to benefit from the full potential of the over-actuated vehicle.

15.2.3 Adaptability to Actuators' Aging

In this work, actuators' states were limited to faulty or healthy. However, the failure model can be classified into four different types (Yang, Kim, and Lee, 2010): *Lock-In-Place (LIP)*, *Hard-Over Failure (HOF)*, *Float*, and *Loss Of Effectiveness (LOF)*. While LIP, HOF, and Float failures can be considered as total failures to their independence from input commands, the LOE failure is rather a degradation of performance with respect to nominal input due to for example actuators' aging. This case can also be taken into account by making the parameters φ_i variable with respect to the actuator performance. However, aging should be quantified by evaluating the performance degradation. More investigations are needed for addressing this aspect.

15.2.4 Adaptability to Friction Change

As mentioned in paragraph 15.2.1, the aim of the method used in this thesis is to show that thanks to a better comprehension of vehicle dynamics, a better estimation of the friction circle can be provided. This can help to keep the vehicle controllable even in extreme and unpredictable situations. However, there is still some work to be done in this context not only due to the technical problems related to available sensors. The use of a threshold in the μ estimation algorithm shows that there are still some modeling errors that should be separated from environmental changes. Two different causes can be separated. The first one is the simplification of static nonlinear phenomena, e.g., camber angles, aerodynamics effects and so on. And the second one is more related to dynamic phenomena, e.g., tire wear, actuators degradation and so on. Even if a robust controller is used in the high-level layer to overcome parameter uncertainties, the estimation process makes use of the vehicle's initial parameters. Consequently, the additional phenomena would effect directly the precision of the estimation. The following possible solutions are worth investigating.

Machine Learning

In Chapter 7, we supposed that the lack of acceleration ability is due only to friction variation. In real life, accelerations can be affected by the wind velocity and slopes (Di Martino, 2005). In addition, slopes add the influence of the gravitational acceleration in the acceleration measurement. This makes the velocities estimation and the problem diagnosis more challenging. To top it all off, even the suspensions' spring stiffness and damper ratio are variable, axles' elastokinematics add additional nonlinearities, the mass varies with respect to the number of passengers and their objects which can change the position of the center of gravity, the wheels suffer from the camber effects that influence slip value (Pacejka, 2005) and so on.

One possible solution in this case is to consider the effect of the remaining not modeled phenomena as nonlinear unknown functions. The estimators presented in this paper can be separated into simple functions, where each function can represent a neuron. A Neural Network can be developed where its inputs could be the online measured variables, its output would be the global acceleration, and the different estimation layers would represent hidden layers (Hagan, Demuth, and De-Jesús,

2002). As the proposed inputs and outputs are measurable data, the neural network can be trained using real experimental data to estimate the remaining not modeled variations (Talebi et al., 2010).

As the previous method is more adapted to the static not modeled phenomena, a different method could be needed for the neglected dynamic variations. A model-based Monte Carlo method could fill the gap in this case. In (Cadini, Zio, and Avram, 2009), this method has been used for estimating failure probability of a component subject to degradation. Particularly, the fatigue degradation is modeled by the Paris-Erdogan law. The robustness of the results suggest applying these methods to estimate the remaining life of actuators and updating the prediction to avoid hazardous situations. Both methods can be combined for eventual better performances using Supervised Machine Learning as authors of (Panahandeh, Ek, and Mohammadiha, 2017) propose.

Robotic Vision

Most of autonomous vehicles researches are actually based on Model Predictive Control (MPC) (Funke et al., 2017). This approach does not need only an accurate vehicle model, but also some *prediction* of future events. In (Funke et al., 2017), a priori knowledge of μ is assumed. The problem that raises in this configuration is the fact that we do not need to know the friction coefficient at the current situation only, but future variations of the friction should also be known. This cannot be ensured by means of effect-based estimation techniques. Robotic Vision could give insights about friction changes in front of the vehicle. Recently, authors of (Tamura and Kambayashi, 2016) have proposed a method to estimate the coefficient of friction by analyzing photo images using at first a vertical camera, and then a front camera that could be used by a robot by applying a discriminant analysis. The method consists in taking preliminary pictures and measure the coefficient of friction, and then train the image processor in order to match new photos to a coefficient friction value. This was tested in twelve samples of the floor tiles that the authors have found on their campus at low velocities. Additional difficulties could be encountered for high velocities and for real roads going from icy to dry ones. We believe that a combination of effect-based methods and robotic vision could be needed. Robotic vision would warn of a potential friction change, and the effect-based method would give the right estimation of friction.

New Sensor Technology

For more accurate vertical dynamics signals, measured signals related to the wheel's load could provide better performances. In fact, load-sensing bearings and intelligent tires are capable of providing additional information regarding tire/road contact per wheel. In (Kerst, Shyrokau, and Holweg, 2016) for example, a novel model based on bearing load measurement approach is presented. Instead of strain filtering and in-situ mapping, the paper expose a model based reconstruction approach. An Unscented Kalman Filter (UKF) is used to reconstruct the unknown wheel loads by analysis of the bearing's outer-ring. Results showed good reconstruction of tire forces and moments signals. Therefore, the remaining states could be more accurate to ensure a better friction coefficient estimation.

Intelligent tires as in (Singh and Taheri, 2015) are developed by placing accelerometers on the inner liner of the tire. A noticeable difference has been shown regarding the acceleration response when the tire was tested on different surface

conditions. This variation may present an opportunity to characterize directly the friction coefficient.

15.2.5 Multi-Sense

As long as over-actuated systems are concerned, multiple solutions could be found for an optimization problem. Secondary objectives could be achieved. Allocation can be used to favour one solution over another according to the desired behaviour of the vehicle. Consequently, different "feelings" can be generated to realize the same manoeuvre. While controlling the yaw rate using the 4WD system could give the vehicle a sporty behaviour, using the 4WS system for the same manoeuvre could rather give a comfortable behaviour. This has a major importance for autonomous vehicles where the challenge is not only the trajectory following but also how the vehicle follows this trajectory. CA introduces new opportunities to make drivers accept autonomous vehicles. Using specific weighting functions to favour different subsystems combinations could be used to generate feelings of comfort and security, and therefore make drivers trust more their vehicles. However, the intra and inter-individual variability between the drivers is also a challenge. Motions that generate excitement for some people could generate fear among others. So allocation should be adaptable and change over time and maybe even learn from its driver's preferences. Evolutionary algorithms and artificial intelligence could be an interesting approach to investigate in this field too. In this thesis, two different approaches to prove the feasibility of motion tuning have been presented: Motion reference tuning and CA tuning.

Motion References

In the first approach, an addition tuning gain and tuning lag have been added in order to change the response amplitude but also its transient behavior. This enables to parameterize the vehicle response to commands generated by either a human driver or a virtual driver. In case of a human drive, starting from a steering wheel angle input, the generated yaw rate by the vehicle can be amplified, reduced, delayed and so on, thanks to activation of the other subsystems. This provides different sensations to the driver itself. The same logic can be applied for a virtual driver. If the MPC generates only a front steering angle to track a trajectory, the remaining systems can be used to change the dynamic responses of the vehicle. The driver can then choose among a sportive virtual driver, or a more careful virtual driver.

More complex reference models can be used to provide additional DOF. These additional parameters should be linked to motion feelings. Each parameter influence should be identified by experimental tests on humans. But these tests could be hard to interpret if results vary from a driver to another. A preliminary study could be necessary to classify first human drivers in order to be able to identify the influence of each parameter on generated sensations.

CA Tuning

Here, two simple approaches have been adopted for tuning CA algorithms. Either we add an secondary objective or we can directly amplify or reduce the vehicle's accelerations as these variables are directly related to motion feelings. However, these approaches face the same problem as the first one. The amount of accelerations to add or reduce or the objective to be added should be adapted to each driver. Only

experimental tests involving humans could give insights about the influence of tuning CA. Moreover, qualitative objectives as trust feelings, comfort and so one could be more sophisticated than only accelerations tuning. The feeling generated by differential braking is completely different from the one generated when steering the rear wheels. The CA problem could become a multi-objective problem with variable priorities depending on the situation. In this context, authors in (Funke and Gerdes, 2015) proposed an interesting approach regarding objectives priority variance. Their approach consists in defining stabilization and trajectory tracking envelopes in the MPC algorithm where the considered states should remain. But when an obstacle has to be avoided, these envelopes can be violated in a short amount of time to ensure passenger security, then stabilize the vehicle. These adaptability should be also permitted in CA optimization algorithms. Again, the considered qualitative objectives should be first identified and then formalized. Moreover, adaptability could also be needed not only to take account of the environment changes, but also depending on the driving styles. As authors of (Frison et al., 2017) have reported, passengers have different expectations from autonomous driving than manual driving, as in the first case, passengers get easily *bored*.

Also, more chassis systems should be integrated and studied. 4WS system for example could provide more comfortable and pleasant cornering maneuvers without influencing the vehicle's longitudinal speed as the brakes do (Harada, 1994). This shows the lack of researches in the literature about vehicle motion control and motion feelings. More support and is expected from car manufacturer for deeper investigations, and hopefully be able to develop an adaptive CA strategy for motion feelings tuning as Figure 15.1 shows.

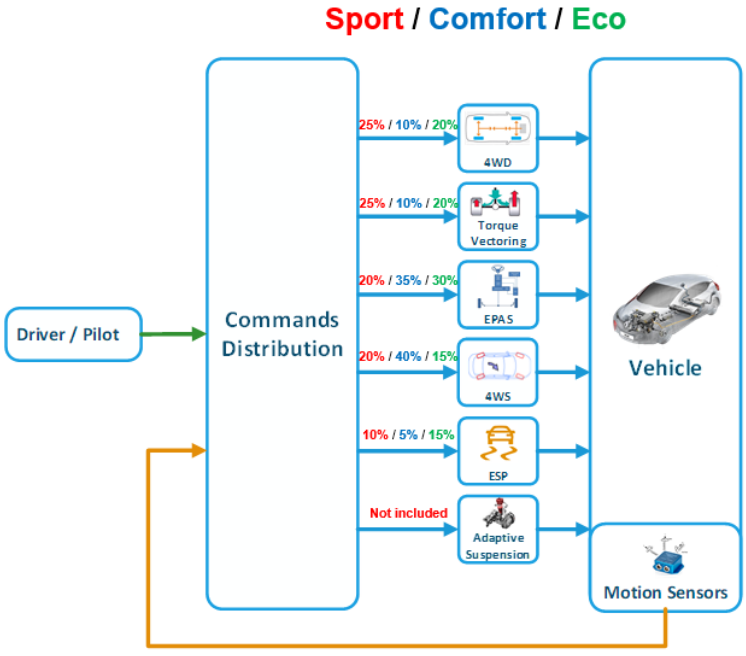

FIGURE 15.1: Future adaptive multi-objective CA architecture.

Motion Feelings Formalization

Knowing that the vehicle behavior influence the passengers' feelings, these motion feelings should be formalized in a way to make an autonomous vehicle behavior predictable and reliable. Research on motion sickness related discomfort to high acceleration values. ISO 2631-1 defines standards of the r.m.s. (road motion sickness) overall acceleration related to passengers comfort (Table 15.1) (Raimondi and Melluso, 2008):

TABLE 15.1: ISO 2631-1 standard

r.m.s. overall acceleration (m/s^2)	Passenger comfort level
$a_{rms} <$ 0.315	Not uncomfortable
0.315$< a_{rms} <$0.63	A little uncomfortable
0.5$< a_{rms} <$1	Fairly uncomfortable
0.8$< a_{rms} <$1.6	Uncomfortable
1.25$< a_{rms} <$2.5	Very uncomfortable
$a_{rms} >$2.5	Extremely uncomfortable

However, these researches concerned ground vehicles in general, without differentiating cars from buses for example. In a bus, passengers could be standing. One cannot generalize the comfort notion to any type of ground vehicles without taking into account the passengers' postures. Other researches have related ride quality to jerk, which is the time derivative of acceleration (Fuse, Kawabe, and Kawamoto, 2017). Unfortunately, it is hard to obtain good results by deriving the acceleration signal in real time, as this latter is already noisy and corrupted by the gravitational acceleration.

However, in hazardous situations, high acceleration values are often required to stabilize the vehicle. This does not go into contradiction with ISO 2631-1, as this latter concerns only the r.m.s. of the overall acceleration. In other words, high accelerations must not be maintained for a long period of time. Nevertheless, high values of acceleration or jerk can cause discomfort even during a short period of time (Svensson and Eriksson, 2015). Maximum allowable values of acceleration should be identified separately. According to (Kilinc and Baybura, 2012), discomfort threshold lies around $1 m/s^2$ to $1.47 m/s^2$. These values were set for different means of transport including buses and trains. Again, this has generalized the problem to both seated and standing passengers. Since we are interested in cars where passengers are always seated, it might be reasonable to set the maximum acceleration to higher values (Svensson and Eriksson, 2015). This shows the gap in the literature regarding motion feelings formalization. This field still should be investigated to facilitate autonomous vehicles introduction to the society.

15.2.6 Architecture Standardization and Openness

Because of unjustified complexity and cost, car manufacturers have been reluctant towards advanced control techniques as CA algorithms. This has already been experienced in flight-control systems (Bodson, 2002), (Oppenheimer, Doman, and Bolender, 2006), (Feng et al., 2014). While ganging has been preferred in many of these systems, CA methods have become necessary regarding advanced aircraft with more numerous actuators. Nevertheless, automotive and aerospace sectors do

not have the same cost constraints. Cheaper methods should be adopted for ground vehicles. Although the upstream approach may seem expensive, the ECUs have become faster, less cumbersome, and cheaper in the past years.

Regarding real-time computations, CA methods have been reviewed and extended in (Bodson, 2002), (Johansen and Fossen, 2013), (Oppenheimer, Doman, and Bolender, 2006), (Kissai et al., 2018a). For example, in (Bodson, 2002), several CA techniques have been transformed into a LP form to improve their execution time. Another technique is the limitation of the number of iterations (Soltani, 2014), (Johansen and Fossen, 2013). This puts a constraint in time of execution but could lead to a sub-optimal solution, which is still better in most of the situations. In (Heidrich et al., 2013), the architecture verification has been taken further through HIL procedure. However, this has not been implemented in a real commercial vehicle yet. There is still a clear lack of benchmark, standards and common test procedures to validate subsystems coordination methods. Experimentations should be conducted to deduce and normalize scenarios where combined manoeuvres are hazardous or uncomfortable. A standardized architecture should be provided to help car manufacturers and suppliers get prepared for autonomous driving challenges. A multi-layer architecture should be preferred, where modules can be easily "plugged and played" (Kissai, Monsuez, and Tapus, 2017).

The standardization can be especially relevant to tackle the critical issue of bringing together manufacturers and suppliers to collaborate. In this openness problem context, we have seen in Chapter 13 how even high-fidelity softwares fail to depict the real dynamics of advanced chassis systems. This is mainly due to the fact that suppliers provide their subsystems in a black-box, and most of the time containing few safety rule-based algorithms that cannot be identified by classical tools. The big drawback is the choice in this case of a too robust controller that may lead to conservatism and poor performances of an over-actuated vehicle presenting larger potential. We expect that the advantages provided in this thesis may convince the different stakeholders to start thinking about the design of open-boxes modules for an efficient overall vehicle motion control logic without jeopardizing the intellectual properties of each stakeholder. As you may notice, vertical motion control have been left out in this thesis. The reason is to show the existing challenges by only combining longitudinal and lateral control. Currently, the horizontal control and the vertical are two separated projects with different suppliers involved. We believe that by only a close collaboration of the different stakeholders that we can achieve an overall vehicle motion control as in Figure 15.2.

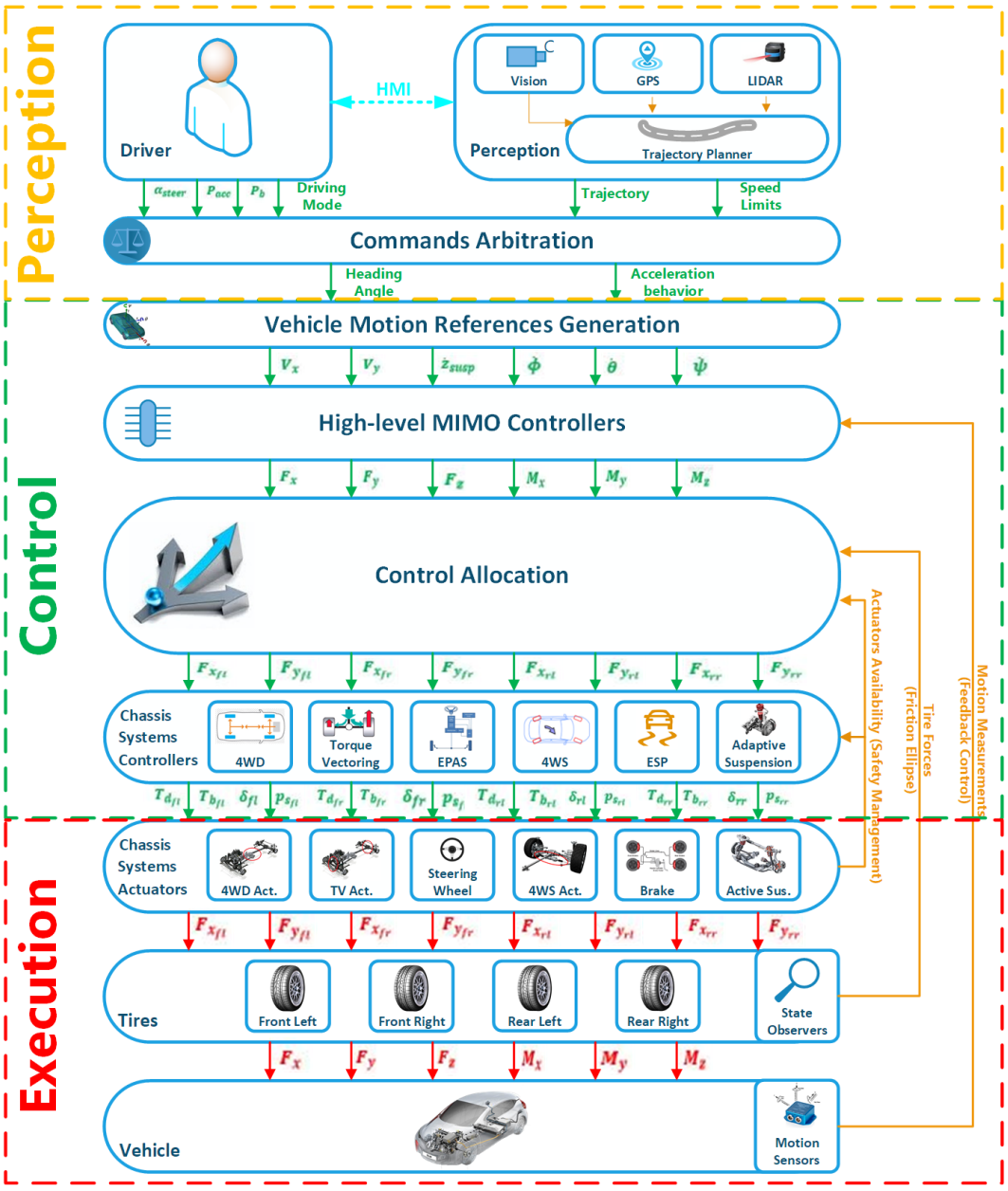

FIGURE 15.2: Future overall vehicle motion control architecture.

Publications

1. M. Kissai, B. Monsuez and A. Tapus, "Current and Future Architectures for Integrated Vehicle Dynamics Control," *2017 12th National Conference on Software and Hardware Architectures for Robots Control (SHARC17)* Toulouse, 2017. URL: https://sharc2017.sciencesconf.org/data/pages/SHARC2017_paper_7.pdf,

2. M. Kissai, B. Monsuez and A. Tapus, "Review of integrated vehicle dynamics control architectures," *2017 European Conference on Mobile Robots (ECMR)*, Paris, 2017, pp. 1-8. DOI: 10.1109/ECMR.2017.8098687,

3. M. Kissai, B. Monsuez, A. Tapus and D. Martinez, "A new linear tire model with varying parameters," *2017 2nd IEEE International Conference on Intelligent Transportation Engineering (ICITE)*, Singapore, 2017, pp. 108-115. DOI: 10.1109/ICITE.2017.8056891,

4. M. Kissai, B. Monsuez, A. Tapus, and D. Martinez, "Control Allocation of Active Rear Steering and Vehicle Dynamics Control Using a New Tire Model," *International Journal of Mechanical Engineering and Robotics Research*, Vol. 7, No. 6, pp. 608-616, November 2018. DOI: 10.18178/ijmerr.7.6.608-616,

5. M. Kissai, B. Monsuez, D. Martinez, X. Mouton and A. Tapus, "A Comprehensive Comparison of Chassis Systems Coordination Approaches," *2018 18th International Conference on Control, Automation and Systems (ICCAS)*, Daegwallyeong, 2018, pp. 351-356. URL: https://ieeexplore.ieee.org/document/8571569,

6. M. Kissai, X. Mouton, B. Monsuez, D. Martinez and A. Tapus, "Optimizing Vehicle Motion Control for Generating Multiple Sensations," 2018 IEEE Intelligent Vehicles Symposium (IV), Changshu, 2018, pp. 928-935. DOI: 10.1109/IVS.2018.8500563,

7. M. Kissai, X. Mouton, B. Monsuez, D. Martinez and A. Tapus, "Multi-Behavioural Control Allocation for Over-Actuated Vehicles," *the 14th International Symposium on Advanced Vehicle Control, AVEC'18*, Beijing, 2018,

8. M. Kissai, X. Mouton, B. Monsuez, D. Martinez and A. Tapus, "Complementary Chassis Systems for Ground Vehicles Safety," *2018 IEEE Conference on Control Technology and Applications (CCTA)*, Copenhagen, 2018, pp. 179-186. DOI: 10.1109/CCTA.2018.8511622,

9. M. Kissai, B. Monsuez, A. Tapus, X. Mouton, and D. Martinez, "Gain-Scheduled H_∞ for Vehicle High-Level Motion Control", in *Proceedings of the 6th International Conference on Control, Mechatronics and Automation (ICCMA 2018)*. ACM, Tokyo, Japan, pp. 97-104. DOI: https://doi.org/10.1145/3284516.3284544,

10. M. Kissai, B. Monsuez, X. Mouton, D. Martinez and A. Tapus, "Importance of Vertical Dynamics for Accurate Modelling, Friction Estimation and Vehicle Motion Control," *2018 21st International Conference on Intelligent Transportation Systems (ITSC)*, Maui, HI, 2018, pp. 1370-1377.
DOI: 10.1109/ITSC.2018.8569751,

11. M. Kissai, X. Mouton, B. Monsuez, and A. Tapus, "Relevance of Advanced Chassis Systems for Vehicle Motion Control," *2018 7th International Conference on Mechatronics and Control Engineering (ICMCE 2018)* , Amsterdam, 2018. ***Accepted***,

12. M. Kissai, B. Monsuez, A. Tapus, D. Martinez and X. Mouton, "Robust Control for Over-Actuated vehicles," *2019 IEEE Conference on Control Technology and Applications (CCTA)*, Hong Kong, 2019. ***Accepted***,

13. Kissai, M.; Monsuez, B.; Mouton, X.; Martinez, D.; Tapus, A. "Adaptive Robust Vehicle Motion Control for Future Over-Actuated Vehicles". *Machines* 2019, 7, 26. DOI: https://doi.org/10.3390/machines7020026,

14. M. Kissai, B. Monsuez, X. Mouton, D. Martinez and A. Tapus, "Model Predictive Control Allocation of Systems with Different Dynamics," *2019 22nd International Conference on Intelligent Transportation Systems (ITSC)*, Auckland, NZ, 2019. ***Submitted*** on April the 14th, ***Accepted*** on June the 24th,

15. Kissai, M., Monsuez, B., Martinez, M. and Tapus, A. "Optimal Coordination of Chassis Systems in Simultaneous Operations," SAE International Journal of Connected and Automated Vehicles, Special Issue on Revisiting Chassis and Powertrain Design for Automated Vehicles, 2019. ***Submitted*** on April the 26th, ***Accepted*** on August the 18th,

16. M. Kissai, B. Monsuez, D. Martinez and A. Tapus, "Review Update of Tire Behavior Models," *The International Journal of Automotive Technology*, 2019. ***Submitted***.

Bibliography

Abe, M. and O. Mokhiamar (2007). “An integration of vehicle motion controls for full drive-by-wire vehicle”. In: *Proceedings of the Institution of Mechanical Engineers, Part K: Journal of Multi-body Dynamics* 221.1, pp. 116–127. DOI: 10.1243/14644193JMBD72.

Alan, A., Y. Yildiz, and U. Poyraz (2018). “High-Performance Adaptive Pressure Control in the Presence of Time Delays: Pressure Control for Use in Variable-Thrust Rocket Development”. In: *IEEE Control Systems Magazine* 38.5, pp. 26–52. ISSN: 1066-033X. DOI: 10.1109/MCS.2018.2851009.

Antsaklis, P. J. and A. N. Michel (2007). *A Linear Systems Primer*. Birkhä user Basel. ISBN: 978-0-8176-4661-5. DOI: https://doi.org/10.1007/978-0-8176-4661-5.

Anwar, S. and L. Chen (2007). “An Analytical Redundancy-Based Fault Detection and Isolation Algorithm for a Road-Wheel Control Subsystem in a Steer-By-Wire System”. In: *IEEE Transactions on Vehicular Technology* 56.5, pp. 2859–2869. ISSN: 0018-9545. DOI: 10.1109/TVT.2007.900515.

Apkarian, P. and D. Noll (2006). “Nonsmooth $\mathcal{H}_\infty$ Synthesis”. In: *IEEE Transactions on Automatic Control* 51.1, pp. 71–86. ISSN: 0018-9286. DOI: 10.1109/TAC.2005.860290.

Balas, G. J., J. C. Doyle, K. Glover, A. Packard, and R. Smith (1998). *μ-analysis and synthesis toolbox: for use with Matlab®, user's guide version 3*. The MathWorks Inc.

Berg, E.H. (2016). “Optimal Control Allocation on Over-Actuated Vehicles”. PhD thesis. TU Delft.

Bhat, S. (2016). “An Investigation into the Optimal Control Methods in Over-actuated Vehicles : With focus on energy loss in electric vehicles”. MA thesis. KTH, Integrated Transport Research Lab, ITRL, p. 76.

Bian, M., L. Chen, Y. Luo, and K. Li (2014). “A Dynamic Model for Tire/Road Friction Estimation under Combined Longitudinal/Lateral Slip Situation”. In: *SAE Technical Paper*. SAE International. DOI: 10.4271/2014-01-0123.

Bianco, C. G. Lo and A. Piazzi (2000). “Optimal trajectory planning with quintic G2-splines”. In: *Proceedings of the IEEE Intelligent Vehicles Symposium 2000*, pp. 620 –625. ISBN: 0-7803-6363-9. DOI: 10.1109/IVS.2000.898417.

Biannic, J.-M. (2013). “Linear Parameter-Varying Control Strategies for Aero-space Applications”. In: *Robust Control and Linear Parameter Varying Approaches: Application to Vehicle Dynamics*. Ed. by O. Sename, P. Gaspar, and J. Bokor. Berlin, Heidelberg: Springer Berlin Heidelberg, pp. 347–373. ISBN: 978-3-642-36110-4. DOI: 10.1007/978-3-642-36110-4_14.

Biannic, J.-M., C. Roos, and A. Knauf (2006). “Design and Robustness Analysis of Fighter Aircraft Flight Control Laws”. In: *European Journal of Control* 12.1, pp. 71 –85. ISSN: 0947-3580. DOI: https://doi.org/10.3166/ejc.12.71-85.

Bishop, B. E. and M. W. Spong (1998). “Control of redundant manipulators using logic-based switching”. In: *Proceedings of the 37th IEEE Conference on Decision and Control (Cat. No.98CH36171)*. Vol. 2, 1488–1493 vol.2. DOI: 10.1109/CDC.1998.758498.

Boada, M. J. L., B. L. Boada, A. Muñoz, and V. Díaz (2006). "Integrated control of front-wheel steering and front braking forces on the basis of fuzzy logic". In: *Proceedings of the Institution of Mechanical Engineers, Part D: Journal of Automobile Engineering* 220.3, pp. 253–267. DOI: 10.1243/09544070JAUTO124.

Bodson, M. (2002). "Evaluation of Optimization Methods for Control Allocation". In: *Journal of Guidance Control and Dynamics* 25, pp. 703–711. DOI: 10.2514/2.4937.

Bordignon, K. A. (1996). "Constrained control allocation for systems with redundant control effectors". PhD thesis. Virginia Tech faculty.

Brach, R. Matthew and Raymond M. Brach (2000). "Modeling Combined Braking and Steering Tire Forces". In: *SAE Technical Paper*. SAE International. DOI: 10.4271/2000-01-0357.

Brach, Raymond M. and R. Matthew Brach (2009). "Tire Models for Vehicle Dynamic Simulation and Accident Reconstruction". In: *SAE Technical Paper*. SAE International. DOI: 10.4271/2009-01-0102.

Brennan, S. and A. Alleyne (2001). "Integrated vehicle control via coordinated steering and wheel torque inputs". In: *Proceedings of the 2001 American Control Conference. (Cat. No.01CH37148)*. Vol. 1, 7–12 vol.1. DOI: 10.1109/ACC.2001.945505.

Bristol, E. (1966). "On a new measure of interaction for multivariable process control". In: *IEEE Transactions on Automatic Control* 11.1, pp. 133–134. ISSN: 0018-9286. DOI: 10.1109/TAC.1966.1098266.

Brown, G.W. (1971). "Analysis of 104 Eastern Iowa Motor Vehicle Casualty Accidents". In: *Proceedings of the Third Triannial Congress on Medical and Related Aspects of Motor Vehicle Accidents*, pp. 216–218.

Burken, J. J., P. Lu, Z. Wu, and C. Bahm (2001). "Two Reconfigurable Flight-Control Design Methods: Robust Servomechanism and Control Allocation". In: *Journal of Guidance, Control, and Dynamics* 24.3, pp. 482 –493. DOI: https://doi.org/10.2514/2.4769.

Bächle, T., K. Graichen, M. Buchholz, and K. Dietmayer (2014). "Slip-Constrained Model Predictive Control Allocation for an All-Wheel Driven Electric Vehicle". In: *IFAC Proceedings Volumes* 47.3. 19th IFAC World Congress, pp. 12042 –12047. ISSN: 1474-6670. DOI: https://doi.org/10.3182/20140824-6-ZA-1003.01287.

Cadini, F., E. Zio, and D. Avram (2009). "Model-based Monte Carlo state estimation for condition-based component replacement". In: *Reliability Engineering & System Safety* 94.3, pp. 752 –758. ISSN: 0951-8320. DOI: https://doi.org/10.1016/j.ress.2008.08.003.

Canudas-de-Wit, C., C. Tsiotras, P. Tsiotras, and X. Claeys (2001). "Friction tire/road modeling, estimation and optimal braking control". In: *Lund NACO2 Workshop*.

Canudas-de-Wit, C., P. Tsiotras, E. Velenis, M. Basset, and G. Gissinger (2003). "Dynamic Friction Models for Road/Tire Longitudinal Interaction". In: *Vehicle System Dynamics* 39.3, pp. 189–226. DOI: 10.1076/vesd.39.3.189.14152.

Chang, S. and T. J. Gordon (2007). "Model-based predictive control of vehicle dynamics". In: *International Journal of Vehicle Autonomous Systems* 5.1-2, pp. 3 –27. ISSN: 1741-5306. DOI: https://doi.org/10.1504/IJVAS.2007.014945.

Chebly, A., R. Talj, and A. Charara (2017). "Coupled Longitudinal and Lateral Control for an Autonomous Vehicle Dynamics Modeled Using a Robotics Formalism". In: *IFAC-PapersOnLine* 50.1. 20th IFAC World Congress, pp. 12526 –12532. ISSN: 2405-8963. DOI: https://doi.org/10.1016/j.ifacol.2017.08.2190.

Chen, Y. and J. Wang (2011). “Energy-efficient control allocation with applications on planar motion control of electric ground vehicles”. In: *Proceedings of the 2011 American Control Conference*, pp. 2719–2724. DOI: 10.1109/ACC.2011.5991160.

Coelingh, E., P. Chaumette, and M. Andersson (2002). “Open-Interface Definitions for Automotive Systems Application to a Brake by Wire System”. In: *SAE Technical Paper*. SAE International. DOI: 10.4271/2002-01-0267.

Di Martino, R. (2005). “Modelling and simulation of the dynamic behaviour of the automobile”. Theses. Université de Haute Alsace - Mulhouse.

Dieter, A. (2005). “Vehicle dynamics analysis tasks and related tyre simulation challenges”. In: *Vehicle System Dynamics* 43.sup1, pp. 30–47.

Doumiati, M., O. Sename, L. Dugard, J.-J. Martinez-Molina, P. Gaspar, and Z. Szabo (2013). “Integrated vehicle dynamics control via coordination of active front steering and rear braking”. In: *European Journal of Control* 19.2, pp. 121 –143. ISSN: 0947-3580. DOI: https://doi.org/10.1016/j.ejcon.2013.03.004.

Doyle, J. C. (1982). “Analysis of feedback systems with structured uncertainties”. In: *IEE Proceedings D - Control Theory and Applications* 129.6, pp. 242–250. ISSN: 0143-7054. DOI: 10.1049/ip-d.1982.0053.

Doyle, J. C., K. Glover, P. P. Khargonekar, and B. A. Francis (1989). “State-space solutions to standard H/sub 2/ and H/sub infinity / control problems”. In: *IEEE Transactions on Automatic Control* 34.8, pp. 831–847. ISSN: 0018-9286. DOI: 10.1109/9.29425.

Duffie, N. A., R. Chitturi, and J.-I. Mou (1988). “Fault-tolerant heterarchical control of heterogeneous manufacturing system entities”. In: *Journal of Manufacturing Systems* 7.4, pp. 315 –328. ISSN: 0278-6125. DOI: https://doi.org/10.1016/0278-6125(88)90042-8.

Dugoff, H., P. Fancher, and L. Segel (1969). *Tire Performance Characteristics Affecting Vehicle Response to Steering and Braking Control Inputs: Final Report - May 1968-August 1969*. Highway Safety Research Institute, University of Michigan.

Dukkipati, R.V. (2010). *Road Vehicle Dynamics: Problems and Solutions*. Premiere Series Bks. SAE International. ISBN: 9780768020519.

Ellis, J. R. (1969). *Vehicle dynamics*. English. Includes bibliographical references. London : Business Books. ISBN: 0220992029.

Erdogan, G. (2009). “New Sensors and Estimation Systems for the Measurement of Tire-Road Friction Coefficient and Tire Slip Variables”. PhD thesis. University of Minnesota.

F. Borrelli A. Bemporad, M. Fodor and D. Hrovat (2006). “An mpc/hybrid system approach to traction control”. In: *IEEE Transactions on Control Systems Technology*. Vol. 14, pp. 541–552.

Falcone, P., H. E. Tseng, J. Asgari, F. Borrelli, and D. Hrovat (2007). “Iintegrated Braking and Steering Model Predictive Ccontrol Approach in Autonomous Vehicles”. In: *IFAC Proceedings Volumes* 40.10. 5th IFAC Symposium on Advances in Automotive Control, pp. 273 –278. ISSN: 1474-6670. DOI: https://doi.org/10.3182/20070820-3-US-2918.00038.

Feng, C., N.n Ding, Y. He, G. Xu, and F. Gao (2014). “Control allocation algorithm for over-actuated electric vehicles”. In: *Journal of Central South University* 21.10, pp. 3705–3712. ISSN: 2227-5223. DOI: 10.1007/s11771-014-2354-0.

Frison, A., P. Wintersberger, A. Riener, and C. Schartmüller (2017). “Driving Hotzenplotz: A Hybrid Interface for Vehicle Control Aiming to Maximize Pleasure in Highway Driving”. In: *Proceedings of the 9th International Conference on Automotive*

User Interfaces and Interactive Vehicular Applications. AutomotiveUI '17. Oldenburg, Germany: ACM, pp. 236–244. ISBN: 978-1-4503-5150-8. DOI: 10.1145/3122986.3123016.

Funke, J. and J. C. Gerdes (2015). "Simple Clothoid Lane Change Trajectories for Automated Vehicles Incorporating Friction Constraints". In: *ASME. J. Dyn. Sys., Meas., Control* 138(2), pp. 021002–021002–9. DOI: 10.1115/1.4032033.

Funke, J., M. Brown, S. M. Erlien, and J. C. Gerdes (2017). "Collision Avoidance and Stabilization for Autonomous Vehicles in Emergency Scenarios". In: *IEEE Transactions on Control Systems Technology* 25.4, pp. 1204–1216. ISSN: 1063-6536. DOI: 10.1109/TCST.2016.2599783.

Fuse, H., T. Kawabe, and M. Kawamoto (2017). "Speed Control Method of Electric Vehicle for Improving Passenger Ride Quality". In: *Intelligent Control and Automation*. 8, pp. 29–43.

Gaspar, P., Z. Szabo, and J. Bokor (2009). "Active Suspension in Integrated Vehicle Control". In: *Switched Systems*. Ed. by Janusz Kleban. Rijeka: IntechOpen. Chap. 5. DOI: 10.5772/7036.

Gerard, M.P. (2011). "Global Chassis Control and Braking Control using Tyre Forces Measurement". PhD thesis. TU Delft.

Gordon, T., M. Howell, and F. Brandao (2003). "Integrated Control Methodologies for Road Vehicles". In: *Vehicle System Dynamics* 40.1-3, pp. 157–190. DOI: 10.1076/vesd.40.1.157.15877.

Hagan, M. T., H. B. Demuth, and O. De-Jesús (2002). "An introduction to the use of neural networks in control systems". In: *International Journal of Robust and Nonlinear Control* 12.11, pp. 959–985. DOI: 10.1002/rnc.727.

Halconruy, T. (1995). *Les liaisons au sol*. ETAI. ISBN: 2726882501.

Harada, H. (1994). "Stability Criteria and Evaluation of Steering Maneuver in "Driver-Vehicle System"". In: *JSME Int. J. Ser. C, Dynamics, control, robotics, design and manufacturing* 37.1, pp. 115–122. DOI: 10.1299/jsmec1993.37.115.

Harada, M. and H. Harada (1999). "Analysis of lateral stability with integrated control of suspension and steering systems". In: *JSAE Review* 20.4, pp. 465 –470. ISSN: 0389-4304. DOI: https://doi.org/10.1016/S0389-4304(99)00040-5.

Harkegard, O. (2002). "Efficient active set algorithms for solving constrained least squares problems in aircraft control allocation". In: *Proceedings of the 41st IEEE Conference on Decision and Control, 2002.* Vol. 2, 1295–1300 vol.2. DOI: 10.1109/CDC.2002.1184694.

Heidrich, L., B. Shyrokau, D. Savitski, V. Ivanov, K. Augsburg, and D. Wang (2013). "Hardware-in-the-loop test rig for integrated vehicle control systems". In: *IFAC Proceedings Volumes* 46.21. 7th IFAC Symposium on Advances in Automotive Control, pp. 683 –688. ISSN: 1474-6670. DOI: https://doi.org/10.3182/20130904-4-JP-2042.00027.

Heißing, B. and M. Ersoy (2011). *Chassis Handbook: Fundamentals, Driving Dynamics, Components, Mechatronics, Perspectives*. ISBN: 978-3-8348-0994-0. DOI: 10.1007/978-3-8348-9789-3.

Hengstler, M., E. Enkel, and S. Duelli (2016). "Applied artificial intelligence and trust—The case of autonomous vehicles and medical assistance devices". In: *Technological Forecasting and Social Change* 105, pp. 105 –120. ISSN: 0040-1625. DOI: https://doi.org/10.1016/j.techfore.2015.12.014.

Heo, H., E. Joa, K. Yi, and K. Kim (2015). "Integrated Chassis Control for Enhancement of High Speed Cornering Performance". In: *SAE Int. J. Commer. Veh.* 8, pp. 102–109. DOI: 10.4271/2015-01-1568.

Holtmann, J., J. Meyer, and M. Meyer (2011). “A Seamless Model-Based Development Process for Automotive Systems”. In: *Software Engineering*.

Ivanov, V. and D. Savitski (2015). “Systematization of Integrated Motion Control Of Ground Vehicles”. In: *IEEE Access* 3, pp. 1–20. DOI: 10.1109/ACCESS.2015.2496108.

Jing, H., F. Jia, H. Liu, and J. Sun (2017). “Multi-objective optimal control allocation for a four-wheel-independent-drive electric vehicle”. In: *2017 36th Chinese Control Conference (CCC)*, pp. 9543–9547. DOI: 10.23919/ChiCC.2017.8028880.

Johansen, T. A. and T. I. Fossen (2013). “Control allocation—A survey”. In: *Automatica* 49.5, pp. 1087 –1103. ISSN: 0005-1098. DOI: https://doi.org/10.1016/j.automatica.2013.01.035.

Kelling, N. A. and W. Heck (2002). “The BRAKE Project - Centralized Versus Distributed Redundancy for Brake-by-Wire Systems”. In: *SAE Transactions* 111, pp. 141–150. ISSN: 0096736X, 25771531.

Kerst, S., B. Shyrokau, and E. Holweg (2016). “Wheel force measurement for vehicle dynamics control using an intelligent bearing”. In: *Proceedings of the 13th International Symposium on Advanced Vehicle Control (AVEC’ 16)*. Ed. by Johannes Edelmann, Manfred Plöchl, and Peter E. Pfeffer. CRC Press, pp. 547–552. ISBN: 978-1-138-02992-7. DOI: 10.1201/9781315265285-87.

Kiencke, U. and L. Nielsen (2000). *Automotive Control Systems: For Engine, Driveline and Vehicle*. 1st. Berlin, Heidelberg: Springer-Verlag. ISBN: 3540669221.

Kilinc, A. and A. Baybura (2012). “Determination of minimum horizontal curve radius used in the design of transportation structures, depending on the limit value of comfort criterion lateral jerk”. In: *Proceedings of Knowing to manage the territory, protect the environment, evaluate the cultural heritage*. 8.

Kissai, M., B. Monsuez, and A. Tapus (2017). “Review of integrated vehicle dynamics control architectures”. In: *2017 European Conference on Mobile Robots (ECMR)*, pp. 1–8. DOI: 10.1109/ECMR.2017.8098687.

Kissai, M., B. Monsuez, A. Tapus, and D. Martinez (2017). “A new linear tire model with varying parameters”. In: *2017 2nd IEEE International Conference on Intelligent Transportation Engineering (ICITE)*, pp. 108–115. DOI: 10.1109/ICITE.2017.8056891.

Kissai, M., X. Mouton, B. Monsuez, D. Martinez, and A. Tapus (2018a). “Complementary Chassis Systems for Ground Vehicles Safety”. In: *2018 IEEE Conference on Control Technology and Applications (CCTA)*, pp. 179–186. DOI: 10.1109/CCTA.2018.8511622.

Kissai, M., B. Monsuez, A. Tapus, and D. Martinez (2018b). “Control Allocation of Active Rear Steering and Vehicle Dynamics Control Using a New Tire Model”. In: *International Journal of Mechanical Engineering and Robotics Research* 7.6, pp. 608–616. DOI: 10.18178/ijmerr.7.6.608-616.

Kissai, M., B. Monsuez, X. Mouton, D. Martinez, and A. Tapus (2018c). “Importance of Vertical Dynamics for Accurate Modelling, Friction Estimation and Vehicle Motion Control”. In: *2018 21st International Conference on Intelligent Transportation Systems (ITSC)*, pp. 1370–1377. DOI: 10.1109/ITSC.2018.8569751.

Kissai, M., X. Mouton, B. Monsuez, D. Martinez, and A. Tapus (2018d). “Optimizing Vehicle Motion Control for Generating Multiple Sensations”. In: *2018 IEEE Intelligent Vehicles Symposium (IV)*, pp. 928–935. DOI: 10.1109/IVS.2018.8500563.

Klomp, M. and M. Lidberg (2006). *Safety Margin Estimation in Steady State Maneuvers*.

Knobel, C., A. Pruckner, and T. Bünte (2006). “Optimized Force Allocation: A General Approach to Control and to Investigate the Motion of Over-Actuated Vehicles”. In: *IFAC Proceedings Volumes* 39.16. 4th IFAC Symposium on Mechatronic Systems, pp. 366 –371. ISSN: 1474-6670. DOI: https://doi.org/10.3182/20060912-3-DE-2911.00065.

Kritayakirana, K. (2012). “Autonomous vehicle control at the limits of handling”. PhD thesis. Stanford University.

Kuisma, H. (2001). “Inertial Sensors for Automotive Applications”. In: *Transducers ’01 Eurosensors XV*. Ed. by Ernst Obermeier. Berlin, Heidelberg: Springer Berlin Heidelberg, pp. 430–433. ISBN: 978-3-642-59497-7.

Larminat, P. (1993). *Automatique : commande des systèmes linéaires*. HERMES. ISBN: 2-86601-359-X.

Li, L. and F.-Y. Wang (2007). *Advanced Motion Control and Sensing for Intelligent Vehicles*, p. 448. ISBN: 978-0-387-44407-9. DOI: 10.1007/978-0-387-44409-3.

Liebemann, E.K., K. Meder, J. Schuh, and G. Nenninger (2004). “Safety and Performance Enhancement: the Bosch Electronic Stability Control(ESP)”. In: *SAE Technical Paper*. SAE International, pp. 421–428.

Liu, Y.-H., T. Li, Y.-Y. Yang, X.-W. Ji, and J. Wu (2017). “Estimation of tire-road friction coefficient based on combined APF-IEKF and iteration algorithm”. In: *Mechanical Systems and Signal Processing* 88, pp. 25 –35. ISSN: 0888-3270. DOI: https://doi.org/10.1016/j.ymssp.2016.07.024.

Maakaroun, S. (2011). “Robotics modelling and tilting control of an innovative urban vehicle”. Theses. Ecole des Mines de Nantes.

Majdoub, K. El, F. Giri, H. Ouadi, L. Dugard, and F.Z. Chaoui (2012). “Vehicle longitudinal motion modeling for nonlinear control”. In: *Control Engineering Practice* 20.1. Special Section: IFAC Conference on Analysis and Design of Hybrid Systems (ADHS’09) in Zaragoza, Spain, 16th-18th September, 2009, pp. 69 –81. ISSN: 0967-0661. DOI: https://doi.org/10.1016/j.conengprac.2011.09.005.

Michelin (2001). *Le pneu: L’adhérence*. Michelin Clermont-Ferrand, France.

Moon, S., I. Moon, and K. Yi (2009). “Design, tuning, and evaluation of a full-range adaptive cruise control system with collision avoidance”. In: *Control Engineering Practice* 17.4, pp. 442 –455. ISSN: 0967-0661. DOI: https://doi.org/10.1016/j.conengprac.2008.09.006.

Moss and Darren (2015). “Renault Talisman revealed”. In: *Haymarket Media Group*. URL: autocar.co.uk.

M’sirdi, N. K., A. Rabhi, N. Zbiri, and Y. Delanne (2005). “Vehicle–road interaction modelling for estimation of contact forces”. In: *Vehicle System Dynamics* 43.sup1, pp. 403–411. DOI: 10.1080/00423110500109380.

Nagai, M., Y. Hirano, and S. Yamanaka (1998). “Integrated Robust Control of Active Rear Wheel Steering and Direct Yaw Moment Control”. In: *Vehicle System Dynamics* 29.sup1, pp. 416–421. DOI: 10.1080/00423119808969575.

Nagai, M., S. Yamanaka, and Y. Hirano (1998). “Integrated Control of Active Rear Wheel Steering and Yaw Moment Control Using Braking Forces”. In: *Transactions of the Japan Society of Mechanical Engineers Series C* 64.622, pp. 2132–2139. DOI: 10.1299/kikaic.64.2132.

Navet, N. and F. Simonot-Lion (2008). *Automotive Embedded Systems Handbook*. 1st. Boca Raton, FL, USA: CRC Press, Inc. ISBN: 9780849380266.

Nicolescu, G. and P. J. Mosterman (2010). *Model-Based Design for Embedded Systems*. CRC Press. ISBN: 9781138114722.

Noxon, N. (2012). “A Model Predictive Control Approach to Roll Stability of a Scaled Crash Avoidance Vehicle”. MA thesis. San Luis Obispo: The Faculty of California Polytechnic State University.

Nwagboso, C.O., X. Ouyang, and C. Morgan (2002). “Development of neural-network control of steer-by-wire system for intelligent vehicles”. In: *International Journal of Heavy Vehicle Systems* 9.1, pp. 1–26. DOI: 10.1504/IJHVS.2002.001167.

Ono, E., K. Takanami, N. Iwama, Y. Hayashi, Y. Hirano, and Y. Satoh (1994). “Vehicle integrated control for steering and traction systems by μ-synthesis”. In: *Automatica* 30.11, pp. 1639 –1647. ISSN: 0005-1098. DOI: https://doi.org/10.1016/0005-1098(94)90068-X.

Ono, E., S. Hosoe, H. D. Tuan, and S. Doi (1996). “Robust stabilization of vehicle dynamics by active front wheel steering control”. In: *Proceedings of 35th IEEE Conference on Decision and Control*. Vol. 2, 1777–1782 vol.2. DOI: 10.1109/CDC.1996.572823.

Oppenheimer, M. W., D. B. Doman, and M. A. Bolender (2006). “Control Allocation for Over-actuated Systems”. In: *2006 14th Mediterranean Conference on Control and Automation*, pp. 1–6. DOI: 10.1109/MED.2006.328750.

Pacejka, H. (2005). *Tire and Vehicle Dynamics*. Elsevier Science.

Panahandeh, G., E. Ek, and N. Mohammadiha (2017). “Road friction estimation for connected vehicles using supervised machine learning”. In: *2017 IEEE Intelligent Vehicles Symposium (IV)*, pp. 1262–1267. DOI: 10.1109/IVS.2017.7995885.

Papadimitriou, I. and M. Tomizuka (2003). “Fast lane changing computations using polynomials”. In: *Proceedings of the 2003 American Control Conference, 2003.* Vol. 1, 48–53 vol.1. DOI: 10.1109/ACC.2003.1238912.

Patra, N. and K. Datta (2012). “Observer Based Road-Tire Friction Estimation for Slip Control of Braking System”. In: *Procedia Engineering* 38. INTERNATIONAL CONFERENCE ON MODELLING OPTIMIZATION AND COMPUTING, pp. 1566 –1574. ISSN: 1877-7058. DOI: https://doi.org/10.1016/j.proeng.2012.06.192.

Petersen, J. A. M. and M. Bodson (2006). “Constrained quadratic programming techniques for control allocation”. In: *IEEE Transactions on Control Systems Technology* 14.1, pp. 91–98. ISSN: 1063-6536. DOI: 10.1109/TCST.2005.860516.

Phillips, A. M. (2002). “Functional decomposition in a vehicle control system”. In: *Proceedings of the 2002 American Control Conference (IEEE Cat. No.CH37301)*. Vol. 5, 3713–3718 vol.5. DOI: 10.1109/ACC.2002.1024505.

Pita-Gil, G. (2011). “Applications of advanced control techniques in the automotive field”. Theses. Supélec.

Pommier, S. and Y. Berthaud (2010). *Mécanique Générale*. DUNOD. ISBN: 978-2-10-054820-0.

Raimondi, F. M. and M. Melluso (2008). “Fuzzy motion control strategy for cooperation of multiple automated vehicles with passengers comfort”. In: *Automatica* 44.11, pp. 2804 –2816. ISSN: 0005-1098. DOI: https://doi.org/10.1016/j.automatica.2008.04.012.

Rath, J. J., K. C. Veluvolu, and M. Defoort (2015). “Simultaneous Estimation of Road Profile and Tire Road Friction for Automotive Vehicle”. In: *IEEE Transactions on Vehicular Technology* 64.10, pp. 4461–4471. ISSN: 0018-9545. DOI: 10.1109/TVT.2014.2373434.

Reinold, P. and A. Traechtler (2013). “Closed-loop control with optimal tire-force distribution for the horizontal dynamics of an electric vehicle with single-wheel chassis actuators”. In: *2013 American Control Conference*, pp. 2159–2164. DOI: 10.1109/ACC.2013.6580155.

Rugh, W. J. and J. S. Shamma (2000). “Research on gain scheduling”. In: *Automatica* 36.10, pp. 1401–1425. ISSN: 0005-1098. DOI: https://doi.org/10.1016/S0005-1098(00)00058-3.

Santos, F. L. and A. A. Filho (2012). “Comparison Of Robust Control Techniques for Use in Active Suspension Systems”. In: *ABCM Symposium Series in Mechatronics*. Vol. 5, pp. 270–279.

Schofield, B. (2008). “Model-Based Vehicle Dynamics Control for Active Safety”. eng. PhD thesis. Lund University, p. 186.

Scorletti, G. and V. Fromion (2009). “Automatique fréquentielle avancée”. Lecture. Ecole Centrale de Lyon, France.

Seddiki, L., A. Rabhi, N.K. M’Sirdi, and Y. Delanne (2006). “Analyse comparative des modèles de contact pneu chaussée”. In: *e-STA*. Vol. 3. 1.

Selby, M. A. (2003). “Intelligent vehicle motion control”. PhD thesis. University of Leeds.

Shaout, A. and K. Mcgirr (2013). “Real-Time Systems in Automotive Applications: Vehicle Stability Control”. In: *Electrical Engineering Research,* vol. 1. 4, pp. 83–95.

Shi, W., M. B. Alawieh, X. Li, H. Yu, N. Arechiga, and N. Tomatsu (2016). “Efficient statistical validation of machine learning systems for autonomous driving”. In: *2016 IEEE/ACM International Conference on Computer-Aided Design (ICCAD)*, pp. 1–8. DOI: 10.1145/2966986.2980077.

Shi, W., M. B. Alawieh, X. Li, and H. Yu (2017). “Algorithm and hardware implementation for visual perception system in autonomous vehicle: A survey”. In: *Integration* 59, pp. 148 –156. ISSN: 0167-9260. DOI: https://doi.org/10.1016/j.vlsi.2017.07.007.

Shuai, Z., H. Zhang, J. Wang, J. Li, and M. Ouyang (2014). “Lateral motion control for four-wheel-independent-drive electric vehicles using optimal torque allocation and dynamic message priority scheduling”. In: *Control Engineering Practice* 24, pp. 55 –66. ISSN: 0967-0661. DOI: https://doi.org/10.1016/j.conengprac.2013.11.012.

Shyrokau, B. and D. Wang (2012). “Control Allocation with Dynamic Weight Scheduling for Two-task Integrated Vehicle Control”. In: *12th International Symposium on Advanced Vehicle Control*, p. 6.

Shyrokau, B., D. Wang, and M. Lienkamp (2013). “Integrated Vehicle Dynamics Control Based on Control Allocation With Subsystem Coordination”. In: *23rd International Symposium on Dynamics of Vehicles on Roads and Tracks*.

Shyrokau, B., D. Wang, L. Heidrich, and K. Höpping (2013). “Analysis of subsystems coordination for electric vehicle during straight-line braking and brake-in-turn”. In: *2013 IEEE Symposium on Computational Intelligence for Engineering Solutions (CIES)*, pp. 61–67. DOI: 10.1109/CIES.2013.6611730.

Shyrokau, B., D. Wang, D. Savitski, K. Hoepping, and V. Ivanov (2015). “Vehicle motion control with subsystem prioritization”. In: *Mechatronics* 30, pp. 297 –315. ISSN: 0957-4158. DOI: https://doi.org/10.1016/j.mechatronics.2014.11.004.

Shyrokau, B. and Wang, D. (2013). “Coordination of Steer Angles, Tyre Inflation Pressure, Brake and Drive Torques for Vehicle Dynamics Control”. In: *SAE Int. J. Passeng. Cars - Mech. Syst.* 6, pp. 241–251. DOI: 10.4271/2013-01-0712.

Siampis, E., M. Massaro, and E. Velenis (2013). “Electric rear axle torque vectoring for combined yaw stability and velocity control near the limit of handling”. In: *52nd IEEE Conference on Decision and Control*, pp. 1552–1557. DOI: 10.1109/CDC.2013.6760103.

Sill, J. and B. Ayalew (2012). “Vehicle Stability Control Through Predictive and Optimal Tire Saturation Management”. In: vol. 6, pp. 407–416. DOI: 10.1115/DETC2012-71182.

Singh, K. B. and S. Taheri (2015). “Estimation of tire–road friction coefficient and its application in chassis control systems”. In: *Systems Science & Control Engineering* 3.1, pp. 39–61. DOI: 10.1080/21642583.2014.985804.

Skogestad, S. and I. Postlethwaite (2005). *Multivariable Feedback Control: Analysis and Design*. Vol. 2. JOHN WILEY & SONS.

Soltani, A. (2014). “Low cost integration of Electric Power-Assisted Steering (EPAS) with Enhanced Stability Program (ESP)”. PhD thesis. Cranfield University.

Svendenius, J. (2003). *Tire Models for Use in Braking Applications*. eng. Licentiate Thesis.

Svendenius, J. and B. Wittenmark (2003). “Brush tire model with increased flexibility”. In: *2003 European Control Conference (ECC)*, pp. 1863–1868. DOI: 10.23919/ECC.2003.7085237.

Svendenius, J. (2007). “Tire Modeling and Friction Estimation”. PhD thesis. Lund University, p. 194.

Svensson, L. and J. Eriksson (2015). *Tuning for Ride Quality in Autonomous Vehicle : Application to Linear Quadratic Path Planning Algorithm*. Independent thesis Advanced level (professional degree).

Talebi, H. A., F. Abdollahi, R. V. Patel, and K. Khorasani (2010). *Neural Network-Based State Estimation of Nonlinear Systems, Application to Fault Detection and Isolation*. Springer-Verlag New York. ISBN: 978-1-4419-1438-5. DOI: 10.1007/978-1-4419-1438-5.

Tamura, H. and Y. Kambayashi (2016). “Estimation of Coefficient of Static Friction of Surface by Analyzing Photo Images”. In: *Intelligent Decision Technologies 2016*. Ed. by Ireneusz Czarnowski, Alfonso Mateos Caballero, Robert J. Howlett, and Lakhmi C. Jain. Cham: Springer International Publishing, pp. 15–26. ISBN: 978-3-319-39627-9.

Tanaka, H., H. Inoue, and H. Iwata (1992). “Development of a Vehicle Integrated Control System”. In: *Proceedings of the XXIV FISITA Congress, London*. Vol. 1, pp. 63–74. ISBN: 0-85298-834-6.

Tjønnås, J. (2008). “Nonlinear and Adaptive Dynamic Control Allocation”. PhD thesis. Norway: NTNU, Trondheim.

Van-Zanten, A. T. and R. Bosch-Gmbh (2002). “Evolution of electronic control systems for improving the vehicle dynamic behavior”. In: *Proceedings of the International Symposium on Advanced Vehicle Control (AVEC)*.

Vasičkanmová, A., M. Bakošová, E. Čirka, and M. Kalúz (2015). “Comparison of Robust Control Techniques for Use in Continuous Stirred Tank Reactor Control”. In: *IFAC-PapersOnLine* 48.14. 8th IFAC Symposium on Robust Control Design ROCOND 2015, pp. 284 –289. ISSN: 2405-8963. DOI: https://doi.org/10.1016/j.ifacol.2015.09.471.

Velardocchia, M. (2013). “Control Systems Integration for Enhanced Vehicle Dynamics”. In: *The Open Mechanical Engineering Journal* 7, pp. 58–69. DOI: 10.2174/1874155X01307010058.

Vermillion, C., J. Sun, and K. Butts (2007). “Model predictive control allocation for overactuated systems - stability and performance”. In: *2007 46th IEEE Conference on Decision and Control*, pp. 1251–1256. DOI: 10.1109/CDC.2007.4434722.

Villagra, J., B. d'Andréa Novel, M. Fliess, and H. Mounier (2011). "A diagnosis-based approach for tire–road forces and maximum friction estimation". In: *Control Engineering Practice* 19.2, pp. 174 –184. ISSN: 0967-0661. DOI: https://doi.org/10.1016/j.conengprac.2010.11.005.

Vivas-Lopez, C. A., J. C. Tudon-Martinez, D. Hernandez-Alcantara, and R. Morales-Menendez (2015). "Global Chassis Control System Using Suspension, Steering, and Braking Subsystems". In: *Mathematical Problems in Engineering* 2015. DOI: http://dx.doi.org/10.1155/2015/263424.

Wal, M.M.J. (1995). *Actuator control with H-infinity and mu-synthesis*. English. DCT rapporten. WFW 1995.062. Technische Universiteit Eindhoven.

Wallentowitz, H. (1990). "Scope for the Integration of Powertrain and Chassis Control Systems: Traction Control - All-Wheel Drive - Active Suspension". In: *Vehicle Electronics in the 90's: Proceedings of the International Congress on Transportation Electronics*, pp. 439–453. DOI: 10.1109/ICTE.1990.713041.

Wang, J. and R. G. Longoria (2009). "Coordinated and Reconfigurable Vehicle Dynamics Control". In: *IEEE Transactions on Control Systems Technology* 17.3, pp. 723–732. ISSN: 1063-6536. DOI: 10.1109/TCST.2008.2002264.

Wang, J.-X., N. Chen, D.-W. Pi, and G.-D. Yin (2009). "Agent-based coordination framework for integrated vehicle chassis control". In: *Proceedings of the Institution of Mechanical Engineers, Part D: Journal of Automobile Engineering* 223.5, pp. 601–621. DOI: 10.1243/09544070JAUTO1015.

Wang, Z., Y. Wang, L. Zhang, and M. Liu (2017). "Vehicle Stability Enhancement through Hierarchical Control for a Four-Wheel-Independently-Actuated Electric Vehicle". In: *Energies* 10.7. ISSN: 1996-1073. DOI: 10.3390/en10070947.

Will, A. B., M. C. M. Teixeira, and S. H. Zak (1997). "Four wheel steering control system design using fuzzy models". In: *Proceedings of the 1997 IEEE International Conference on Control Applications*, pp. 73–78. DOI: 10.1109/CCA.1997.627476.

Wong, J. Y. (2001). *Theory of Ground Vehicles, 3rd Edition*. John Wiley & Sons.

Xiong, L. and Z. Yu (2011). "Research on Robust Control for longitudinal Impact of 4 Wheel-Drive Hybrid Electric Vehicle". In: *Procedia Engineering* 15. CEIS 2011, pp. 293 –297. ISSN: 1877-7058. DOI: https://doi.org/10.1016/j.proeng.2011.08.057.

Yang, I., D. Kim, and D. Lee (2010). "Fault-tolerant control strategy based on control allocation using smart actuators". In: *2010 Conference on Control and Fault-Tolerant Systems (SysTol)*, pp. 377–381. DOI: 10.1109/SYSTOL.2010.5675961.

Yim, S. (2012). "Design of a robust controller for rollover prevention with active suspension and differential braking". In: *Journal of Mechanical Science and Technology* 26.1, pp. 213–222. ISSN: 1976-3824. DOI: 10.1007/s12206-011-0915-9.

Yim, S. (2015). "Coordinated control with electronic stability control and active steering devices". In: *Journal of Mechanical Science and Technology* 29.12, pp. 5409–5416. ISSN: 1976-3824. DOI: 10.1007/s12206-015-1142-6.

Zhang, X. and D. Göhlich (2018). "Improvement in the vehicle stability of distributed-drive electric vehicles based on integrated model-matching control". In: *Proceedings of the Institution of Mechanical Engineers, Part D: Journal of Automobile Engineering* 232.3, pp. 341–356. DOI: 10.1177/0954407017701284.

Zhang, Y. and J. Jiang (2008). "Bibliographical review on reconfigurable fault-tolerant control systems". In: *Annual Reviews in Control* 32.2, pp. 229 –252. ISSN: 1367-5788. DOI: https://doi.org/10.1016/j.arcontrol.2008.03.008.

Zhao, H., B. Ren, H. Chen, and W. Deng (2015). "Model predictive control allocation for stability improvement of four-wheel drive electric vehicles in critical driving

condition". In: *IET Control Theory Applications* 9.18, pp. 2688–2696. ISSN: 1751-8644. DOI: 10.1049/iet-cta.2015.0437.

Zhao, S., Y. Li, and X. Qu (2014). "Vehicle Chassis Integrated Control Based on Multimodel and Multilevel Hierarchical Control". In: *Mathematical Problems in Engineering* 2014, pp. 1–13. DOI: 10.1155/2014/248676.

Zhao, Y.-Q., H.-Q. Li, F. Lin, J. Wang, and X.-W. Ji (2017). "Estimation of Road Friction Coefficient in Different Road Conditions Based on Vehicle Braking Dynamics". In: *Chinese Journal of Mechanical Engineering* 30.4, pp. 982–990. ISSN: 2192-8258. DOI: 10.1007/s10033-017-0143-z.

Åström, K. J. (2000). "Model uncertainty and robust control". In: *Lecture Notes on Iterative Identification and Control Design*, pp. 63–100.

Titre:COORDINATION OPTIMALE DES SYSTÈMES CHÂSSIS POUR LE CONTRÔLE DU MOUVEMENT DES VOITURES

Mots clés: Dynamique du Véhicule, Systèmes Châssis, Contrôle Robuste, Distribution Optimale de Commande.

Résumé: Un grand intérêt a été porté récemment au contrôle global du châssis. Un véhicule automatisé devrait être capable de gérer des situations couplées impliquant le contrôle longitudinal, latéral et vertical. Le constructeur automobile doit coordonner différents sous-systèmes provenant de différents fournisseurs. Jusqu'à présent, des solutions consistant à hiérarchiser un système par rapport à un autre en fonction des scénarios étaient privilégiées. Les véhicules autonomes ont besoin de sous-systèmes supplémentaires pour fonctionner en toute sécurité. Les interactions entre ces sous-systèmes pourraient devenir imprévisibles. Cette thèse focalise sur l'approche de coordination qui devrait être adoptée dans ce cas. La couche de coordination est déplacée en amont des sous-systèmes en tant que superviseur, assurant une distribution de commande optimale. Les résultats ont montré que cette approche permet de coordonner un plus grand nombre de sous-systèmes, que la tolérance aux panne peut être garantie entre différents systèmes de châssis et que des objectifs qualitatifs peuvent être satisfaits. Plus les sous-systèmes seront nombreux à l'avenir, plus l'approche en amont deviendra pertinente.

Title: OPTIMAL COORDINATION OF CHASSIS SYSTEMS FOR VEHICLE MOTION CONTROL

Keywords: Vehicle Dynamics, Chassis Systems, Robust Control, Optimal Control Allocation.

Abstract: A large interest has been given recently to global chassis control. An automated vehicle should be able to manage coupled situations involving longitudinal, lateral and vertical control. The car manufacturer has to coordinate different subsystems originated from different suppliers. Until these days, simple solutions consisting of prioritizing one system over another depending on few use-cases were favored. Autonomous vehicles need additional subsystems to operate safely. Subsystems interactions would become unpredictable. This thesis focus on the coordination approach that should be adopted by future vehicles. Particularly, the coordination layer is moved upstream the standalone subsystems as a supervisor ensuring an optimal control distribution. Results showed that this approach is able to coordinate a larger set of subsystems, fault-tolerance can be ensured between different chassis systems, and qualitative objectives can be satisfied. The more numerous subsystems will get in the future, the more relevant the upstream approach would become.

Université Paris-Saclay
Espace Technologique / Immeuble Discovery
Route de l'Orme aux Merisiers RD 128 / 91190 Saint-Aubin, France